HIGH-RESOLUTION STRATIGRAPHY, RESERVOIR GEOMETRY, AND FACIES
CHARACTERIZATION OF CRETACEOUS AND TERTIARY TURBIDITES FROM
BRAZILIAN PASSIVE MARGIN BASINS.

HIGH-RESOLUTION STRATIGRAPHY, RESERVOIR GEOMETRY, AND FACIES

CHARACTERIZATION OF CRETACEOUS AND TERTIARY TURBIDITES FROM

BRAZILIAN PASSIVE MARGIN BASINS.


By

CARLOS HENRIQUE LIMA BRUHN, B.Sc., M.Sc.


A Thesis Submitted to the

School of Graduate Studies in

Partial Fulfillment of the Requirements

for the Degree

Doctor of Philosophy


McMaster University

1993

DOCTOR OF PHILOSOPHY (1993)　　　　　　　McMASTER UNIVERSITY

(Geology)　　　　　　　　　　　　　　　　　Hamilton, Ontario


TITLE:　　High-resolution stratigraphy, reservoir geometry,

　　　　　and facies characterization of Cretaceous and

　　　　　Tertiary turbidites from Brazilian passive margin

　　　　　basins.


AUTHOR:　　Carlos Henrique Lima Bruhn, B.Sc. (Universidade

　　　　　Federal da Bahia, Brazil), M.Sc. (Universidade

　　　　　Federal de Ouro Preto, Brazil)


SUPERVISOR: Dr. R.G. Walker


NUMBER OF PAGES: xix, 433

## ABSTRACT

Two canyon-filling, coarse-grained turbidite systems have been studied, essentially at the oil-field scale, in immature passive margin basins of eastern Brazil. Three oil fields were chosen for detailed study from a group of over 120 turbidite oil fields distributed along the eastern Brazilian margin; Carapeba and Pargo fields (tabular or lobate reservoirs, Coniacian/Santonian to early Maastrichtian, Campos basin), and Lagoa Parda field (channelized reservoirs, early Eocene, Espírito Santo basin). The three oil fields combined contain 162 wells (20 cored), with average spacing of 200 - 500 m.

The Carapeba/Pargo turbidite system contains 181 - 198 coarse-grained turbidites, each with a thickness in the 0.5 - 12 m range. There are eight facies successions, 27 - 140 m thick. Each succession contains between 7 and 58 turbidites. Most of these successions become finer-grained upward and downcanyon, and their younger or more distal turbidites tend to become thinner-bedded and more discontinuous. The Carapeba/Pargo turbidite successions form 1 - 12 km wide, non-channelized, tabular or lobate sandstone bodies. They were stacked in an overall retrogradational pattern for at least 20 km, recording the backfilling of the Carapeba/Pargo canyon.

The Lagoa Parda turbidite system contains unstratified, coarse-grained turbidites up to 6 m thick, with interbedded bioturbated mudstones and thin-bedded (< 70 cm), stratified, fine-grained sandstones. The coarse-grained facies fill 38 deeply-incised channels; these channel fills are 9 - > 50 m thick, 210 - > 1,050 m wide, and > 1 km long. The finer-grained facies build asymmetrical levees that are higher and thicker on the left side (looking downstream) of their associated channels. Nine levee successions (up to 50 m thick) are associated with the 20 youngest channels. The overall Lagoa Parda turbidite system is characterized by channel fills that become narrower, thinner, and finer-grained upward. As a result of the common amalgamation of channel fills, and the partial preservation of levee deposits between channel fills, Lagoa Parda reservoirs show a complicated, multi-storied sand body geometry.

Coarse-grained turbidite successions that fill canyons were developed in the eastern Brazilian margin during relative sea level falls that punctuated the overall transgressive setting of the late Cretaceous and early Tertiary. Only a few of the turbidite successions studied here can be correlated with global, eustatic sea level curves. Most of the relative sea level falls probably resulted from increased sediment supply, which, in turn, would have responded to tectonic reactivation in the source area and basin margin, and/or to climatically-controlled denudation rates in the source area.

## ACKNOWLEDGEMENTS

Raychaudhuri, and Elaine Bishop helped me to identify the trace fossils of the studied rocks. Elizabeth Bruhn patiently coloured most of the geological sections and maps included in this thesis. Jack Whorwood provided prompt and expert photographical services. My office mates (past and present) Charle Gamba, Bruce Ainsworth, Elaine Bishop, Terry Wiseman, Zuwena Al-Rawahi, and Richard Rouble provided countless good times. To all of them I extend my utmost gratitude.

I would like to thank my parents, Karl Heinz and Eunice for supporting me in obtaining my education, and for the continuous example of integrity and hard work; without them, I could not have gone this far.

Finally, I would like to dedicate this thesis to my wife, Elizabeth, and my daughters, Caroline and Christiane; their love and encouragement over the years have been the best gift I have ever gotten.

# TABLE OF CONTENTS

**LIST OF FIGURES**

# LIST OF TABLES

# 1. INTRODUCTION


## 1.1. TURBIDITY CURRENTS AND TURBIDITES: A BRIEF HISTORICAL BACKGROUND


Density underflows were originally recognized in Swiss lakes more than a century ago (e.g. Forel, 1885, 1892). However, turbidity currents and their deposits have been extensively studied only since the publication in the early 1950's of three benchmark papers; "Turbidity currents as a cause of graded bedding" (Kuenen and Migliorini, 1950), "Sedimentary history of the Ventura basin, California, and the action of turbidity currents" (Natland and Kuenen, 1951), and "Turbidity currents and submarine slumps, and the 1929 Grand Banks earthquake" (Heezen and Ewing, 1952). These three papers combined flume experiments, outcrop studies, foraminiferal paleontology and paleoecology, and oceanographic data, to demonstrate that coarse-grained sands can be transported into deep water by turbidity currents and be deposited as graded beds.

Bouma (1962) elegantly grouped the most important turbidite sedimentary structures into the "Bouma sequence".

1

Harms and Fahnestock (1965), and Walker (1965) recognized the hydrodynamic significance of the individual sedimentary structures that comprise the Bouma sequence; this, in turn, became a widely-used facies model. The 60's also record important advances in the experimental modelling of turbidity currents, particularly regarding their movement and deposition (e.g. Middleton 1966a, 1966b, 1967).

Some important depositional models for submarine fans were published in the literature during the 70's. These models were based on descriptions of outcrops (Mutti and Ricci Lucchi, 1972, 1974, 1975; Mutti and Ghibaudo, 1972), on the acoustic and seismic characterization of recent fans (Normark, 1970, 1978), and also on the integration of both sources of information (Walker and Mutti, 1973; Walker, 1978). Despite their differences, all of these channel-feeding-lobe models typically have three major morphologic divisions (Fig. 1.1). These models are described briefly below, although they have now been replaced by larger-scale models based on seismic studies of modern fans.

The upper fan portion comprises one single, large channel or fan valley, characterized by prominent levees, where lenticular conglomerates and massive sandstones tend to accumulate. The middle fan is typified by depositional lobes (named "suprafan lobes" by Normark, 1978). In the upper parts of the depositional lobes turbidity currents flow through many channels, which are narrower and shallower than the single

Fig. 1.1 - Walker's (1978) submarine fan model.
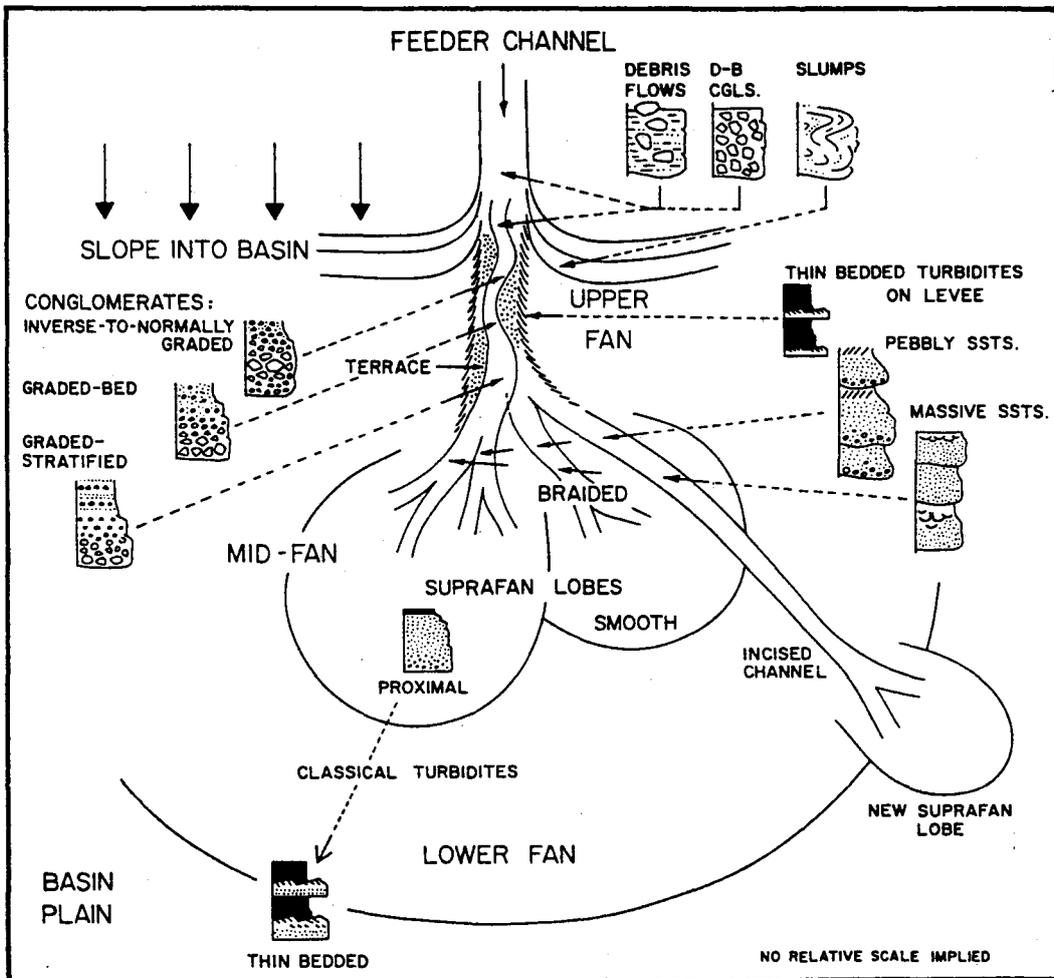
FEEDER CHANNEL

DEBRIS FLOWS

D-B CGLS.

SLUMPS

SLOPE INTO BASIN

CONGLOMERATES:
INVERSE-TO-NORMALLY GRADED

GRADED-BED

GRADED-STRATIFIED

TERRACE

UPPER FAN

THIN BEDDED TURBIDITES ON LEVEE

PEBBLY SSTS.

MASSIVE SSTS.

BRAIDED

MID-FAN

SUPRAFAN LOBES

SMOOTH

INCISED CHANNEL

PROXIMAL

CLASSICAL TURBIDITES

LOWER FAN

NEW SUPRAFAN LOBE

BASIN PLAIN

THIN BEDDED

NO RELATIVE SCALE IMPLIED

leveed-channel of the upper fan; they also have poorly developed levees. Massive and stratified sandstones tend to be deposited within the smaller channels of the middle fan, whereas thick-bedded turbidites with Bouma sequences accumulate preferentially on the unchannelized outer portions of the middle fan. The lower fan is a topographically smooth, low-gradient area, characterized by the accumulation of hemipelagic muds and thin-bedded turbidites.

During the 80's, significant improvements in the acoustic and seismic characterization of recent fans have changed the ideas about the internal composition of submarine fans, and their growth patterns. The best-studied recent fans are the Amazon (Damuth et al., 1983a, 1983b, 1988; Manley and Flood, 1988; Flood et al., 1991), Indus (McHargue and Webb, 1986; Kolla and Coumes, 1987; McHargue, 1991), Mississippi (Bouma et al., 1985b, 1989; Weimer and Buffler, 1988; Weimer, 1989, 1990), and Rhone (Droz and Bellaiche, 1985). The data show that the upper and middle portions of these submarine fans consist of mud-rich, channel-levee systems (Fig. 1.2). The terminology "channel-levee system" was introduced by Damuth et al. (1983b, p.470) to designate "a depositional-erosional channel perched atop a wide natural levee ... that builds upward and laterally through time by overbank spilling" (Fig. 1.2). Equivalent terms provided by the literature are "lenticular acoustic unit" (Droz and Bellaiche, 1985), and "fanlobe" (Bouma et al., 1985b). The channel-levee systems

Fig. 1.2 - Watergun seismic profile and line-drawing interpretation of upper (ULC) and lower (LLC) levee complexes of the Amazon fan (Manley and Flood, 1988). Individual channel-levee systems are identified within these levee (or channel-levee) complexes. Units R and DF represent widespread mass transport complexes. Typical seismic facies of channel fills (**cf**), levees (**lev**), non-channelized turbidites (**nct**), and mass transport complexes (**mtc**) are indicated.

W                                                   E
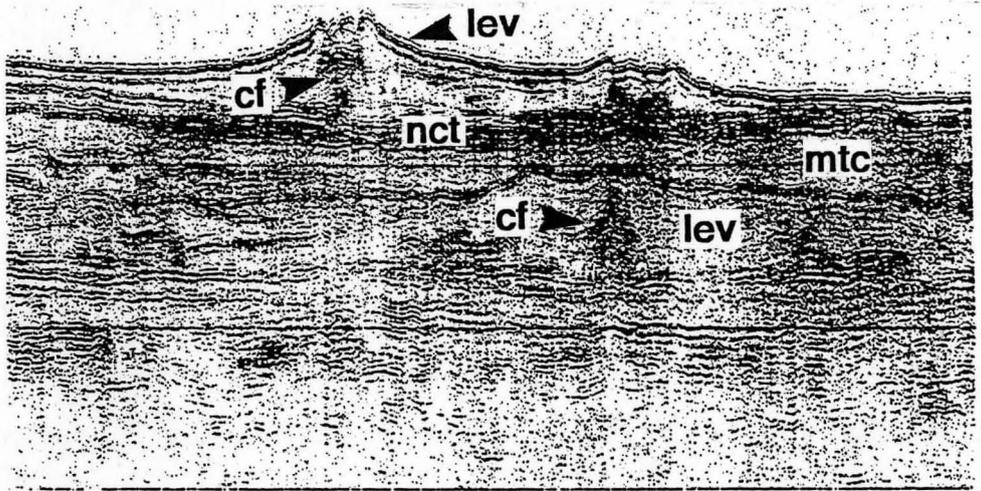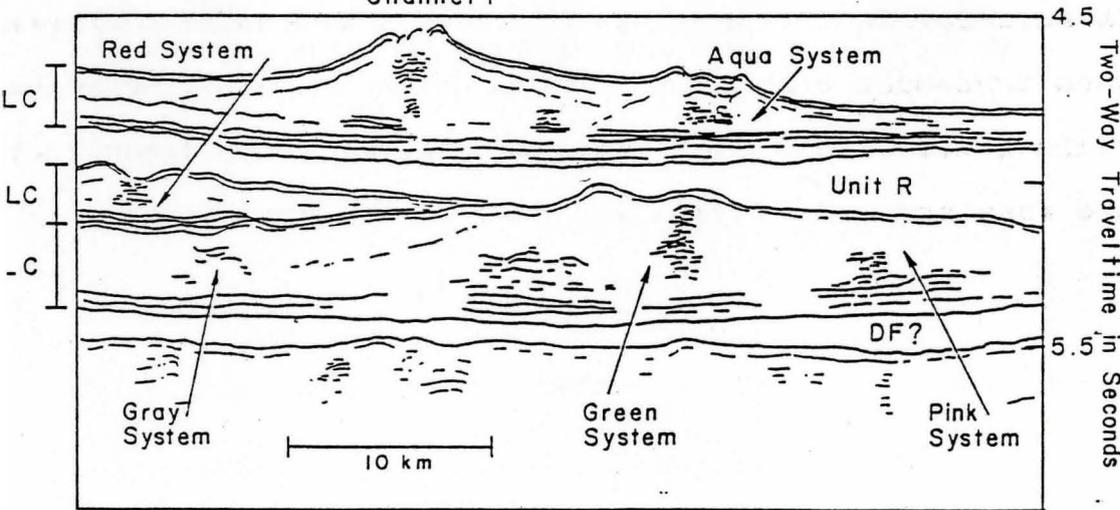
Channel 1

frequently overlap, coalesce, or interfinger laterally, forming large tongue-like or elongate bodies named "channel-levee complexes" (Figs. 1.3 and 1.4). Observations from these recent fans contrast with the emphasis on lobe deposits given by the channel-feeding-lobe models.

The decade of 1980 was also characterized by criticism of the channel-feeding-lobe models (e.g. Nilsen, 1980; Walker, 1980, 1984; Shanmugam and Moiola, 1985, 1988; Mutti and Normark, 1987), leading to proposals of alternative models or facies schemes (e.g. Hsü et al., 1980; Stow et al., 1982; Chan and Dott, 1983; Heller and Dickinson, 1985; Mitchum, 1985; Mutti, 1985; Bruhn and Moraes, 1988; Nelson et al., 1991; Peres, 1993). Some of the major points raised by these studies concern: (1) the longitudinal distribution of turbidites along the axis of tilted, elongated basins (e.g. Hsü et al., 1980); and (2) the almost continuous turbidite accumulation along the base of the slope in basins characterized by a line source. In this situation, the turbidite successions can form (1) thick, basin-margin wedges or aprons (e.g. Stow et al., 1982; Nelson et al., 1991), or (2) aggrading ramplike features fed by a network of deltaic channels (e.g. Chan and Dott, 1983; Heller and Dickinson, 1985). These models provided an important alternative to the submarine fans fed by discrete submarine canyons (point source), commonly oriented perpendicularly to the basin margin (e.g. Mutti and Ricci Lucchi, 1972; Walker, 1978; Fig. 1.1).

Fig. 1.3 - Major morphologic features and physiographic boundaries of the Amazon fan (Damuth et al., 1988). Sinuous distributary channels on upper and middle fan were mapped from sonographs. Successive channel-levee formation and abandonment built two broad channel-levee complexes composed of overlapping, coalescing segments of channel-levee systems across the present fan surface. The western and eastern channel-levee complexes defined by Damuth et al. (1983b, 1988) are included in the upper channel-levee complex of Manley and Flood (1988) (Fig. 1.4).

DEMERARA ABYSSAL PLAIN

VEMA F.Z.

LOWER FAN

4500

CONTINENTAL RISE

4000

MIDDLE

WESTERN LEVEE COMPLEX

EASTERN LEVEE COMPLEX

CEARA RISE

FAN

3000

DEBRIS FLOW

SLUMP DEBRIS FLOW

2000

UPPER

1000

SHELF

KEY

CANYON WALLS AND SCARPS

CHANNELS MAPPED FROM GLORIA AND PDR

CHANNEL AXES FROM PDR ONLY

CHANNEL LEVEE COMPLEXES

SLUMP
DEBRIS FLOW } MASS-TRANSPORT DEPOSITS

CENTRAL CHANNEL

AMAZON CANYON

BREAK

FAN

MID-ATLANTIC RIDGE

CONTINENTAL

DEMERARA ABYSSAL

AMAZON CONE

CEARA RISE

CONTINENTAL

SOUTH AMERICA

CONTINENTAL SHELF

RISE

ABYSSAL PLAIN

AMAZON R.

**200 km**

Fig. 1.4 - Schematic diagram across the Amazon fan at the upper to middle fan transition, showing a cyclic growth pattern of channel-levee complexes (Manley and Flood, 1988). DF is debris flow.
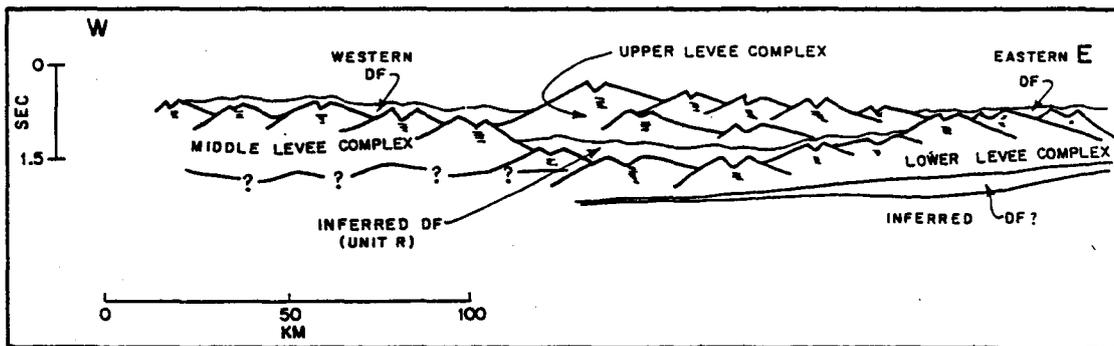
However, the major contribution from the debate of the 80's was the recognition that the development and internal architecture of turbidite systems may be controlled allocyclically, particularly by tectonics, sediment supply, and sea level fluctuations (e.g. Mutti, 1985; Stow et al., 1985; Mutti and Normark, 1987; Posamentier and Vail, 1988; Vail et al., 1991). This new perspective contrasts with the purely autocyclic and sedimentological view represented by the channel-feeding-lobe models (e.g. Normark, 1970, 1978; Mutti and Ricci Lucchi, 1972; Walker, 1978). The allocyclic perspective can be exemplified by Mutti's (1985) model (Fig. 1.5), and Exxon's sequence stratigraphy (e.g. Posamentier and Vail, 1988; Haq, 1991; Vail et al., 1991; Fig. 1.6), which rely heavily on sea level fluctuations to explain the development of submarine fans. On the other hand, the influence of tectonics and sediment supply on turbidite sedimentation has been under-emphasized, despite the fact that tectonic effects can be well-illustrated in many basins (e.g. Prosser, 1993; Silva, 1993).

In recent years, research on turbidites has been more intense than ever, largely due to technological advances in the tools for oceanographic studies (e.g. high-resolution, continuous seismic-reflection profiling, side-looking-sonar imaging, and industry-quality coring techniques), and the growing economic importance of turbidite systems as petroleum reservoirs. Syntheses of the most important recent advances on

Fig. 1.5 - Mutti's (1985) fan types. Three types of submarine fans (**a**) are related to three stages of fan evolution (**b**). The different scales of turbidity currents are related to the size of slope failures, which is thought to be related to the position of relative sea level (**b**).

MARGIN OF DEEP-WATER BASIN

CHANNEL-LEVEE DEPOSITS

BASINAL MUDSTONE

TYPE III

THIN-BEDDED LOBE FRINGE

THICK-BEDDED SANDSTONE LOBES

**a**

THICK-BEDDED CHANNEL-FILL SANDSTONE FACIES

TYPE II

THICK-BEDDED SANDSTONE LOBES

COARSE-GRAINED LAG DEPOSITS
INFILLING EROSIONAL DEPRESSIONS

SUBMARINE EROSION

SLOPE FAILURE

approx. 20 km

TYPE I

TYPE III SYSTEM OR
STAGE III DEPOSITS

STAGE III

CHANNEL-LEVEE
COMPLEX

Medium-   to small-volume
mud-loaden turbidity currents

SHALLOW SLUMP

TYPE II SYSTEM OR
STAGE II DEPOSITS

STAGE II

sea level

**b**

CHANNEL-ATTACHED
SAND LOBE

Medium-   to small-volume
sand-loaden turbidity currents

TYPE I SYSTEM OR
STAGE I DEPOSITS

STAGE I

Large-volume  sand-loaden
turbidity currents

TURBIDITY CURRENT ——— SLIDE

CHANNEL-DETACHED SAND LOBE

LARGE-SCALE
SLOPE FAILURE

UNDERCONSOLIDATED
SHELFAL MUD AND
SAND

Fig. 1.6 - Exxon's sequence stratigraphy, summarized in conceptual cross sections in relation to depth (**a**) and geological time (**b**). The sections show stratal geometry, systems tracts, and the distribution of siliciclastic facies within unconformity-bounded depositional sequences (modified from Vail, 1987, by Christie-Blick, 1991). Systems tracts: **LST** = lowstand systems tract; **TST** = transgressive systems tract; **HST** = highstand systems tract; and **SMST** = shelf margin systems tract. Sequence boundaries: **sb1** = type 1; and **sb2** = type 2. Other abbreviations: **iss** = interval of sediment starvation; **ts** = transgressive surface (corresponding to the time of maximum regression); **iv** = incised valley; **sf** = slope fan; **bff** = basin floor fan.

EXPLANATION

- FLUVIAL AND COASTAL PLAIN
- SHOREFACE AND DELTAIC
- SHELF AND SLOPE
- SUBMARINE "FAN"
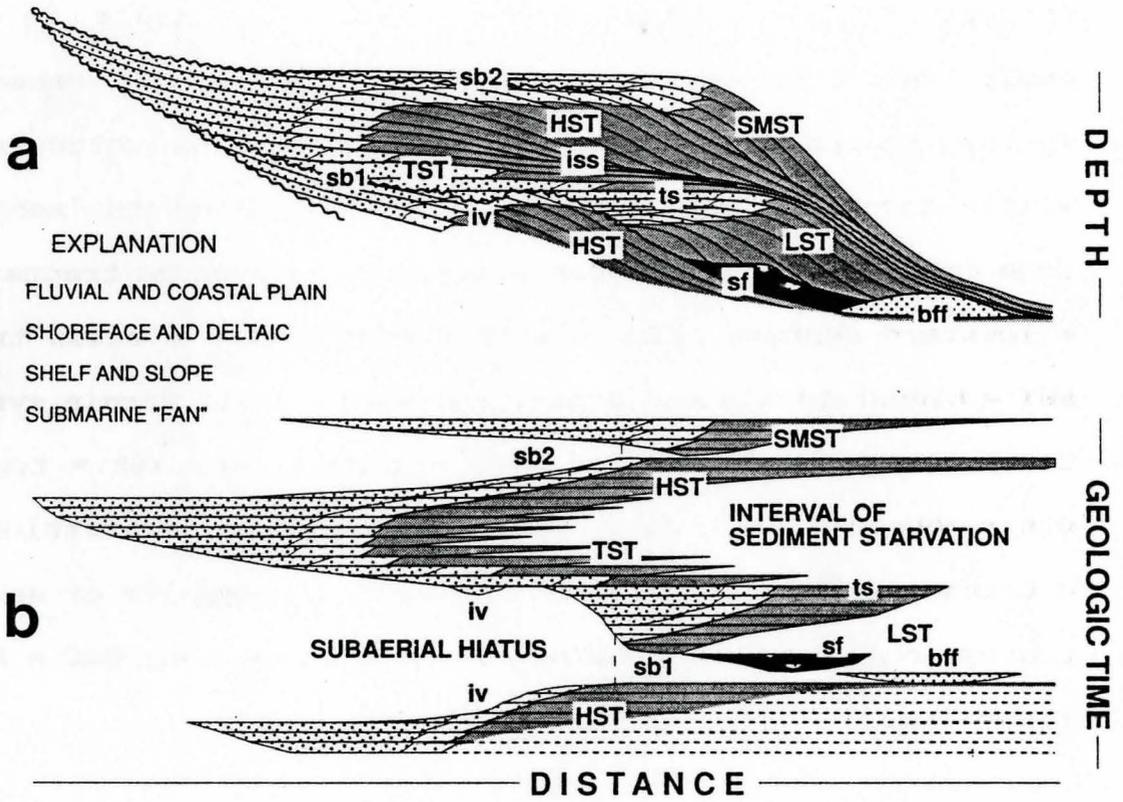
turbidite studies have been presented in many books, including those by Nelson and Nilsen (1984), Bouma et al. (1985a), Wilgus et al. (1988), Pickering et al. (1989), Brown et al. (1990), Weimer and Link (1991a), Mutti (1992), and Walker and James (1992). However, after more than 40 years of research on turbidity currents and turbidites, it is clear that there is no general model available for the description, interpretation, and prediction of the variety of turbidite systems observed in modern and ancient basins. Future models, in order to have a wide applicability, will have to combine the effects of allocyclic and autocyclic controls. It also seems inevitable that any attempt at synthesis will have to be supported by a large number of case-histories, which in turn must be derived from seismic, well-log, core, and outcrop studies.

## 1.2. DEFINING THE SCIENTIFIC PROBLEM AND THE DATA BASE

This section is intended to present and justify the main scientific aims of this thesis, and characterize its supporting data, particularly in terms of general geological setting, type of turbidites studied, and scale of approach.

Turbidites are major petroleum reservoirs in more than 80 sedimentary basins worldwide; in the North Sea, California, and eastern Brazil combined they contain a volume of

recoverable oil exceeding 25 billion barrels (Weimer and Link, 1991b). Divergent margins represent one of the most important future frontiers for oil exploration in turbidite reservoirs. Potential discoveries in these settings are expected in syn-rift, lacustrine or marine turbidites, or in turbidites deposited in post-rift, intracratonic sags or passive margins. Therefore, there is an increasing need for models in the exploration of turbidite reservoirs in divergent margin basins. On the other hand, the large number of oil fields already found requires a detailed geometrical characterization of turbidite reservoirs to guide oil production.

Besides their economic importance, immature passive margin basins provide scientifically interesting situations to understand the combined effects of allocyclic controls on turbidite sedimentation. These basins commonly have proximal sediment sources, narrow and steep coastal plains and shelves, and intense tectonic activity contemporaneous with sedimentation. Therefore, turbidite sedimentation in these geological settings is very sensitive not only to sea level fluctuations, but also to variations in sediment supply and tectonic activity.

Immature passive margin basins also contain many examples of turbidite types that have received little attention in the literature, particularly coarse-grained channel-levee complexes and coarse-grained canyon fills. Mud-rich channel-levee complexes have been extensively studied in many modern

submarine fans (e.g. Damuth et al., 1988; Weimer, 1989, 1990; Droz and Bellaiche, 1985). In ancient rocks they have been termed "type III systems" (Mutti, 1985; Fig. 1.5), or "slope fans" (e.g. Vail et al., 1991; Fig. 1.6). However, there are very few examples of coarse-grained channel-levee complexes in the literature, most of them from the ancient record (e.g. Winn and Dott, 1979; Walker, 1985; Bruhn and Moraes, 1988, 1989; Morris and Busby-Spera, 1990).

Although many submarine canyons may be filled essentially with fine-grained sediments (e.g. Cohen, 1976; Goodwin and Prior, 1989; Galloway et al., 1991), there are also others that may include a thick succession of coarse, commonly conglomeratic turbidites (e.g. May et al., 1983; Morris and Busby-Spera, 1988; Bruhn and Moraes, 1989). Despite the economic importance of coarse-grained canyon fills as petroleum reservoirs (Weimer and Link, 1991b), these deposits are virtually ignored by the channel-feeding-lobe models (e.g. Mutti and Ricci-Lucchi, 1972; Walker, 1978; Fig. 1.1), and also by the eustatically-driven model of Mutti (1985; Fig. 1.5) and sequence stratigraphic scheme of Exxon (e.g. Posamentier and Vail, 1988; Van Wagoner et al., 1990; Posamentier and Erskine, 1991; Fig. 1.6).

Turbidite systems in general tend to be only partially preserved in outcrop (especially mud-rich successions), making the geometrical characterization of these deposits very difficult. The recognition of turbidite environments

(particularly channels and lobes) in many outcropping systems has been influenced by the presence of fining (or coarsening) upward and thinning (or thickening) upward successions (e.g. Ghibaudo, 1980; Link and Nilsen, 1980; Link and Welton, 1982), rather than by the external geometry of these deposits. This procedure may be subjective and lead to misinterpretations (Hiscott, 1981; Walker, 1984, 1992; Heller and Dickinson, 1985). On the other hand, although recent submarine fans may provide entire systems to be studied, they are still poorly cored and dated. Thus, the geometrical characterization of turbidite systems using subsurface data can be a very efficient approach, especially if developed at the "oil-field scale". Oil fields showing a large number of closely-spaced wells, a comprehensive production/pressure history, and extensive coring of the reservoirs permit a detailed geometry and facies characterization of the turbidite reservoirs.

**The main purpose of this thesis is the detailed characterization, essentially at the oil-field scale, of the internal stratigraphy, reservoir geometry, and facies associations of turbidite systems deposited in ancient immature passive margin basins.** The study is mostly based on two turbidite systems, which were selected from a group of over 120 turbidite oil fields discovered by PETROBRÁS (the Brazilian national oil company). Brazilian petroleum-bearing turbidites occur in Neocomian to Barremian, lacustrine rift basins, and in Albian to Miocene, marine passive margin

basins; most of these accumulations are distributed along the eastern Brazilian margin (Fig. 1.7). The turbidite systems discussed in this thesis were chosen in order to represent two types of turbidite reservoirs still poorly described in the literature, namely **coarse-grained channel-levee complexes**, and **coarse-grained canyon fills**. The selected oil fields are (Fig. 1.8):

**(1) CARAPEBA AND PARGO FIELDS (CONIACIAN/SANTONIAN TO EARLY MAASTRICHTIAN, OFFSHORE CAMPOS BASIN): coarse-grained, non-channelized turbidites filling a submarine canyon.**

**(2) LAGOA PARDA FIELD (EARLY EOCENE, ONSHORE ESPÍRITO SANTO BASIN): coarse-grained, channel-levee complexes, also filling a submarine canyon.**

Other important criteria for the selection of these oil fields include the large number of closely-spaced wells, the extensive coring of the reservoirs, the quality of the well logs, and the detailed production/pressure history. The three oil fields combined contain 162 wells, with spacing averaging 200 - 500 m. These wells have a comprehensive suite of high-quality well logs, including gamma-ray, spontaneous potential, resistivity, density, neutron, caliper, sonic, and dipmeter logs. The studied reservoirs were cored in 20 wells, permitting the description of a cumulative 901 m thick

Fig. 1.7 - Location map for the most important Brazilian sedimentary basins. Eastern Brazilian marginal basins are named.

80°W        60°W        40°W

ATLANTIC OCEAN

0°

BRAZIL

PARAÍBA-PERNAMBUCO BASIN

SERGIPE-ALAGOAS BASIN

BAHIA NORTE BASIN

RECÔNCAVO BASIN

BAHIA SUL BASIN

Serra da Mantiqueira

ESPÍRITO SANTO BASIN

20°S

Serra do Mar

CAMPOS BASIN

20°S

SANTOS BASIN

PACIFIC OCEAN

PELOTAS BASIN

1000 km

40°S

STUDIED MESOZOIC-CENOZOIC BASINS

MESOZOIC-CENOZOIC BASINS

PALEOZOIC BASINS

PROTEROZOIC BASINS

80°W        60°W        40°W        40°S

Fig. 1.8 - Generalized geological section for the eastern Brazilian marginal basins. Turbidites are highlighted in yellow. Geology of the different megasequences is largely supported on data from the following basins: continental pre-rift megasequence - Recôncavo basin; continental rift megasequence - Recôncavo and Campos basins; transitional evaporitic megasequence - Sergipe-Alagoas and Campos basins; and marine transgressive and marine regressive megasequences - Campos and Espírito Santo basins.

W     Sea level     E

MR
MT
SC
T
PR
R
R
LP
CRP/PG
sd

−10 km

0

0     30 km
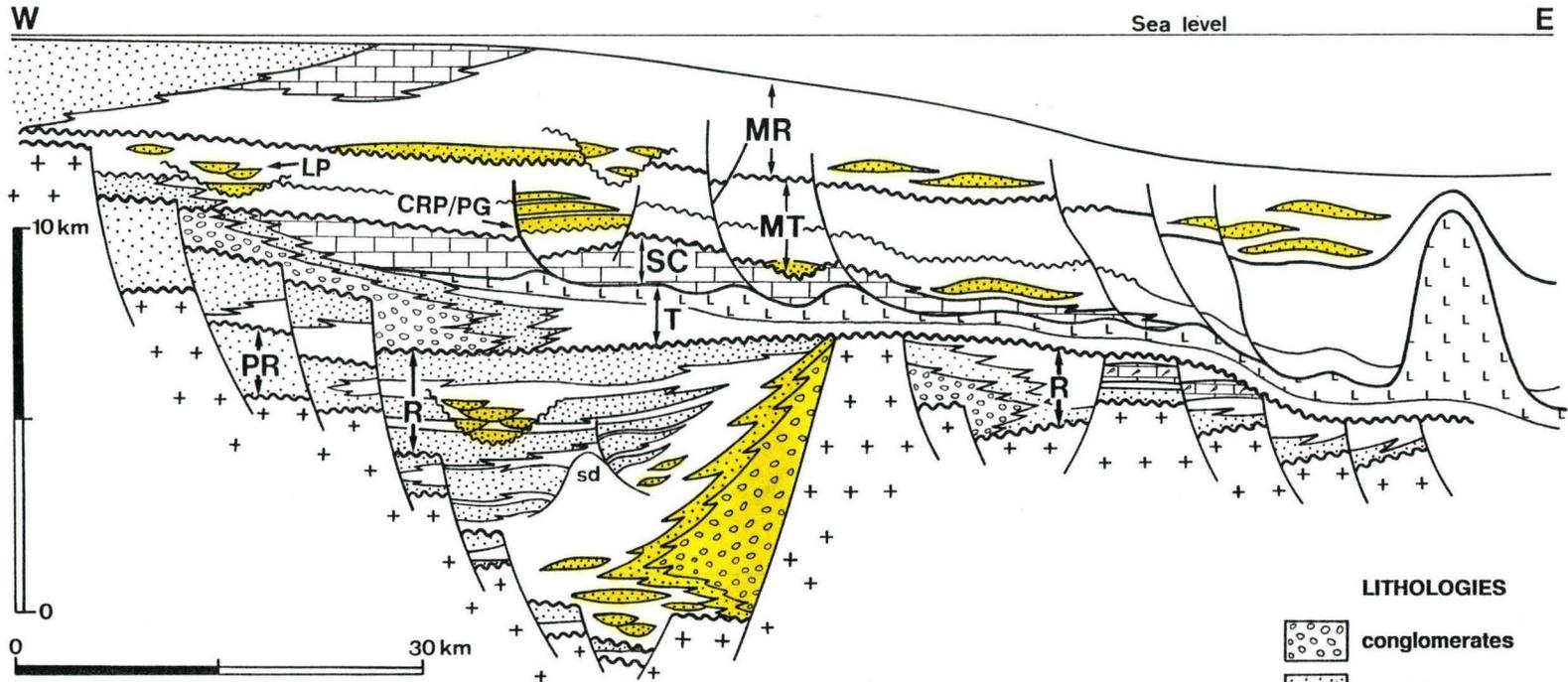
**MEGASEQUENCES:**

PR - Continental pre-rift megasequence
(late Jurassic to early Neocomian)

R - Continental rift megasequence
(early Neocomian to early Aptian)

T - Transitional evaporitic megasequence
(mid Aptian to early Albian)

SC - Shallow carbonate platform megasequence
(early- to mid-Albian)

MT - Marine transgressive megasequence
(late Albian to early Tertiary)

MR - Marine regressive megasequence
(early Tertiary to present)

**STUDIED TURBIDITES**

CRP/PG - Carapeba and Pargo oil fields,
Campos basin

LP - Lagoa Parda oil field,
Espírito Santo basin

**LITHOLOGIES**

conglomerates

sandstones

shales, siltstones,
and marls

carbonate rocks

evaporites

coquinas

metamorphic and
igneous basement

sd = shale diapirs

succession of rocks.


## 1.3. THESIS LAYOUT


Chapter 1 defines the scientific problems investigated in this research, and the criteria used to select the data base.

Chapter 2 comprises an overview of the geology of the eastern Brazilian marginal basins, where the studied turbidites are located. The chapter discusses age, lateral distribution, thickness, and depositional environments of the sediments, and also major controlling factors on sedimentation, as tectonic setting, sea level fluctuations, sediment supply, and climate. Therefore, Chapter 2 represents an integrated view of the general geological setting of the studied turbidites, which is related to the Neocomian breakup of Gondwana, and the subsequent opening of the South Atlantic Ocean (Fig. 1.8).

The two studied turbidite systems are described and interpreted separately, in chapters 3 (Carapeba and Pargo fields), and 4 (Lagoa Parda field). Each of these chapters follows the same organization; location and data base, general geological setting, facies characterization, high-resolution stratigraphy and reservoir geometry, and sedimentation evolution and controls. Readers who do not need the descriptive details and sedimentological interpretation of the

individual facies, and also the detailed stratigraphy and geometrical characterization of the reservoirs, will find a summary of these aspects, respectively in **pages 152** (Carapeba and Pargo fields), and **268** (Lagoa Parda field).

The main purpose of chapter 5 (synthesis) is to present a tentative depositional model for transgressive turbidites from immature passive margin basins. Chapter 5 also contains a comparative analysis of the two studied turbidite systems and widely-used submarine fan models (e.g. Mutti and Ricci-Lucchi, 1972; Walker, 1978; Mutti, 1985), concepts derived from the study of modern submarine fans (e.g. Bouma et al., 1985a; Weimer and Link, 1991a; and references therein), Exxon's sequence stratigraphy (e.g. Posamentier and Vail, 1988; Van Wagoner et al., 1990; Vail et al., 1991), and an outcropping turbidite system showing the same age of the early Maastrichtian Carapeba/Pargo turbidite successions, but comprising similar facies to those of the early Eocene Lagoa Parda turbidite system (Almada basin; Bruhn and Moraes, 1989). This chapter also presents how the major contributions of this thesis can be applied to oil exploration and production from similar turbidite systems.

Finally, chapter 6 (conclusions) summarizes the most important descriptive aspects, interpretations, and potential applications of this research.

# 2. GEOLOGY OF THE EASTERN BRAZILIAN MARGINAL BASINS: AN OVERVIEW

## 2.1. GENERAL GEOLOGICAL SETTING

The eastern Brazilian marginal basins lie beneath the present day coastal plain, continental shelf and slope of the western portion of the South Atlantic Ocean. Their tectonic and sedimentary evolution is linked to the Neocomian breakup of Gondwana, and the subsequent opening of the South Atlantic Ocean (e.g. Asmus and Porto, 1972; Ponte and Asmus, 1978).

Eight major eastern Brazilian marginal basins have been recognized in an area of about 650,000 km$^2$, including the Klemme's (1980) Type III (intracontinental rift) Recôncavo basin, and also the Type III evolved into Type V (pull-apart, divergent/passive margin) basins of Pernambuco-Paraíba, Sergipe-Alagoas, Bahia Sul, Espírito Santo, Campos, Santos and Pelotas (Fig. 1.7). A large amount of geological information about the Sergipe-Alagoas, Recôncavo, Espírito Santo, Campos, and Santos basins has been collected by PETROBRÁS (the Brazilian national oil company), particularly after 1968, when offshore exploration for hydrocarbons started. Over 12,000

21

wells have been drilled, and about 700,000 km of reflection seismic profiles have been obtained in these 5 basins, which contain 91 % of the total Brazilian oil-in-place.

Since the early 1970's (e.g. Asmus and Ponte, 1973), four major tectonic and sedimentary stages have been recognized in the eastern Brazilian marginal basins: pre-rift, rift, proto-oceanic, and continental margin. During the last 20 years, understanding of the stages has improved due to extensive petroleum exploration conducted by PETROBRÁS. Comprehensive reviews of the geology of eastern Brazilian marginal basins have been provided by Ponte and Asmus (1978), Ponte et al. (1980), Ojeda (1982), Asmus and Baisch (1983), Bruhn et al. (1988), Chang et al. (1988, 1992), Guardado et al. (1990), and Figueiredo et al. (1993).

The general late Jurassic to recent stratigraphy of the eastern Brazilian marginal basins can now be subdivided into six megasequences (Fig. 1.8):

(1) **continental pre-rift megasequence (late Jurassic to early Neocomian);**

(2) **continental rift megasequence (early Neocomian to early Aptian);**

(3) **transitional evaporitic megasequence (mid Aptian to early Albian);**

(4) **shallow carbonate platform megasequence (early to mid Albian);**

**(5) marine transgressive megasequence (late Albian to early Tertiary); and,**

**(6) marine regressive megasequence (early Tertiary to present).**

These megasequences are bounded by regional unconformities that, in the case of the marine successions, may become correlative conformities basinwards (Fig. 1.8). The only exception is the boundary between the transitional evaporitic and the shallow carbonate platform megasequence, which so far appears to be gradational (e.g. Guardado et al., 1990; Koutsoukos et al., 1991). Each megasequence may be composed of one or several sequences [using this term as defined by Mitchum (1977), and Van Wagoner et al. (1988, 1990)]. The age span for each megasequence may vary along the eastern Brazilian marginal basins, but significant differences are recorded only for the change from a marine transgressive to a marine regressive pattern of sedimentation.

## 2.2. LITHOSTRATIGRAPHIC, CHRONOSTRATIGRAPHIC, AND BIOSTRATIGRAPHIC FRAMEWORK

Several lithostratigraphic units have been formally recognized within the six major sedimentary megasequences of the eastern Brazilian marginal basins. Despite the widespread

distribution and striking facies similarities presented by these lithostratigraphic units, their formal names may change from one basin to other. In order to keep this overview clear and short, no specific stratigraphic names that make up the long (over 120) and complicated list of Mezosoic and Cenozoic Brazilian lithostratigraphic units will be mentioned.

The formal biostratigraphy for the non-marine pre-rift, rift, and transitional megasequesences (Fig. 2.1) is based on studies of ostracods (11 zones, 26 subzones) and palynomorphs (11 zones) (e.g. Schaller, 1969; Viana et al., 1971; Moura, 1987; Arai et al. 1989; Regali and Viana, 1989). These zones bear no similarities to the fauna and flora in early Cretaceous type-sections around the world. The difficulties in identifying stages of the standard international chronostratigraphy led to the formal definition of six local stages (Schaller, 1969; Viana et al., 1971): Dom João Stage including late(?) Jurassic sediments (pre-rift megasequence), and the Rio da Serra, Aratu, Buracica, Jiquiá, and Alagoas stages, embracing successions from the Neocomian to early Albian (rift and transitional megasequences) (Fig. 2.1). Some attempts have been made to correlate the local Brazilian stages to the international standard stages (e.g. Arai et al., 1989; Regali and Viana, 1989), but the results obtained are still considered preliminary, requiring further investigation. Despite these uncertainties, the combined use of the ostracod subzones and palynomorph zones permits the breaking of the

Fig. 2.1 - Chronostratigraphy and biostratigraphy for the early Cretaceous, non-marine successions of the eastern Brazilian marginal basins. Sources for the different columns are indicated at the bottom.

| STANDARD STAGES | LOCAL STAGES | OSTRACOD ZONES | OSTRACOD SUBZONES | PALYNOMORPH ZONES |
|---|---|---|---|---|
| 112 ALBIAN<br>113 | 112 | 112 | 112 (hachured) | 112 *Complicatisaccus cearensis* P-280<br>113 |
| APTIAN | ALAGOAS | "*Cytheridea*" (?) spp. | | *Sergipea variverrucata* P-270<br>114.5<br>*Inaperturopollenites turbatus* P-260<br>115.6<br>*Inaperturopollenites curvimuratus* P-240<br>116.7 |
| | | NRT-011<br>NRT-010 | | *Clavatipollenites crisopolensis* P-230 / P-220 |
| 118 | 118 JIQUIÁ | 118 *Limnocythere troelsoni*<br>118.3 | 118.3 *Cypridea (P.) faveolata* 009.3<br>118.6 *Cypridea (S.) devexa* 009.2 | 118 *Aequitriradites spinulosus*<br>118.3 *Stellatopollis bituberensis* P-190<br>119 |
| 119 | | *Petrobrasia diversicostata* | 119 *Bisulcocypris p. postangularis* 009.1 | |
| 120 | BURACICA | 120 NRT-009<br>*Cypridea (Sebastianites) fida minor* NRT-008<br>120.8 | 120<br>120.3 *Cypridea (S.) mira* 008.3<br>120.5 *Petrobrasia capivarensis* 008.2<br>120.8 *Cypridea (S.) s. sostensis* 008.1<br>121.1 *Paracypridea q. weberi* 007.4<br>121.4 *Metacypris sp.* 007.3<br>121.7 *Petrobrasia martinsensis* 007.2<br>*Cypridea eminens* 007.1 | *Dicheiropollis etruscus* |
| BARREMIAN<br>122 | 122 ARATU | *Coriacina coriacea*<br>122 NRT-007 | 122 | 121.8 P-180 |
| | | *Cypridea (Morinina?) bibullata bibullata* | *Cypridea (Morinina?) bibullata tribullata* 006.2<br>123.3 *Reconcavona triebelli* 006.1<br>124.5 | |
| 125 | | 124.5 NRT-006 | *Reconcavona gastracantha* 005.5<br>125.5 *Reconcavona uniacantha* 005.4<br>126.6 *Reconcavona uncinata* 005.3<br>127.8 *Paracypridea elegans elegans* 005.2<br>128.9 *Ilhasina remanei cuneiformis* 005.1 | *Caytonipollenites pallidus* |
| HAUTERIVIAN | | *Paracypridea obovata obovata* | | |
| 130 | | 130 NRT-005 | 130 | 130 P-160 |
| 131 | RIO DA SERRA | | *Cypridea ventronodata* 004.5<br>131.6 *Paracypridea maacki* 004.4<br>133.1 *Paracypridea bicallosa* 004.3<br>134.6 *Reconcavona polita* 004.2<br>136.1 *Cypridea salvadorensis nodifer* 004.1<br>137.5 | *Leptolepidites major* |
| VALANGINIAN | | *Paracypridea brasiliensis* | | |
| 137.5 | | 137.5 NRT-004 | 137.5 | 137.5 P-140 |
| 138 | | *Cypridea (Morininoides) candeiensis* | *Cypridea (Morininoides) hadronodosa* 003.2<br>139 *Cypridea sellata* 003.1<br>140.5 | |
| BERRIASIAN | | 140.5 NRT-003 | | *Alisporites (?) sp.* |
| | | *Theriosynoecum varietuberatum* | *Cypridea cf. C. primaria* 002.1<br>142.2 *Cypridea kegeli* 002.2 | |
| 144 | 144 | 144 NRT-002 | 144 | 144.5 P-120 |

N E O C O M I A N (vertical, left)

Ma

Harland et al. (1982) | Schaller (1969), Viana et al. (1971), Arai et al. (1989) | Schaller (1969), Viana et al. (1971) | Schaller (1969), Viana et al. (1971) | Regali et al. (1974a, 1974b), Regali and Viana (1989)

Neocomian to Aptian sedimentary succession into chronostratigraphic units with average duration of 1.0 m.y. (Fig. 2.1).

The formal biostratigraphy for the three younger marine megasequences (Albian to recent) is supported by studies of planktonic calcareous nannofossils (52 zones), planktonic foraminifera (37 zones), and palynomorphs (31 zones) (e.g. Troelsen and Quadros, 1971; Noguti and Santos, 1972; Quadros and Gomide, 1972; Regali et al., 1974a, 1974b; Beurlen, 1982; Antunes, 1984, 1990a; Shimabukuro et al., 1985; Azevedo et al., 1987b). In contrast with the biozones defined for the non-marine megasequences, most of the marine biozones can be correlated with confidence to worldwide accepted biostratigraphic zonations (e.g. Martini, 1971; Sissingh, 1977; Berggren et al., 1985; Caron, 1985). The calcareous nannofossil biozones are particularly useful, permitting the discrimination of chronostratigraphic units with an average duration of 2.2 m.y. Figures 2.2 and 2.3 present the Albian to recent chronostratigraphy and biostratigraphy for the Campos basin, which contains most of the marine biozones defined in the eastern Brazilian marginal basins.

## 2.3. MAJOR CONTROLS ON MEGASEQUENCE DEVELOPMENT

The eastern Brazilian marginal basins are typical

Fig. 2.2 - Chronostratigraphy and biostratigraphy for the marine, Albian to Maastrichtian successions of the Campos basin. Sources for the different columns are indicated at the bottom.

| STAGE | PLANKTONIC FORAMINIFERA | CALCAREOUS NANNOFOSSILS | PALYNOMORPHS |
|---|---|---|---|
| 66.4 | 66.4 | 66.4 | 66.4 |
| | *Abathomphalus mayaroensis* 67 F-150.2 | | 67 |
| MAASTRICHTIAN | *Globotruncana gansseri* | *Arkhangelskiella cymbiformis* | *Tricornites elongatus* |
| | 72.2 F-150.1 *Globotruncana fornicata* 73 F-140 | 72.2 N-290 *Tetralithus trifidus* 73 N-280 | 72.2 73 P-470 |
| 73 | | | |
| CAMPANIAN | *Globotruncana lapparenti* | *Eiffellithus eximius* | *Retiperiporites piacabucuensis* |
| 83 | 83 F-130 | 83 N-265 | 83 P-460 |
| SANTONIAN | *Dicarinella concavata* | *Marthasterites furcatus* | *Confossia vulgaris* |
| 87.5 | 87.7 F-120.5 | | 87.5 P-425 |
| CONIACIAN | | | *Anacolosidites sp.* |
| 88.5 | *Dicarinella imbricata* | 88.5 N-260 | 88.5 P-423 |
| TURONIAN | 90.2 F-120.4 | | *Steevesipollenites nativensis* |
| 91 | *Whiteinella spp.* | | 91 |
| | 93.2 F-120.2 | | *Classopollis major* |
| CENOMANIAN | | | |
| 97.5 | 97.5 | 97.5 | 97.5 γ |
| | *Ticinella raynaudi* | | *Oligosphaeridium complex* |
| | 103 F-110.2 | | |
| ALBIAN | *Favusella washitensis* | *Nannoconus truitti truitti* | 108.1 β |
| | | | *Cyclopsiella sp.* |
| | 112 F-110.1 | 112 N-250 | 112 α |
| 113 | | | |

Harland et al. (1982)    Azevedo et al. (1987b)    Richter (1987)    Uesugui (1976)

↑
Ma

Fig. 2.3 - Chronostratigraphy and biostratigraphy for the marine, Tertiary successions of the Campos basin. Sources for the different columns are indicated at the bottom.

| EPOCH | STAGE | PLANKTONIC FORAMINIFERA | CALCAREOUS NANNOFOSSILS | PALYNOMORPHS |
|---|---|---|---|---|

PLEISTOCENE — 0.8
—1.6— CALABRIAN

PLIO —3.4— PIACENZIAN

ZANCLEAN
—5.3—
MESSINIAN
—6.5—

M I O C E N E

TORTONIAN
—10.5—

SERRAVALLIAN
—13.1— — — —

LANGHIAN
—15.1—
—16.3—

BURDIGALIAN

—21.8—

AQUITANIAN
—23.7—

O L I G O C E N E

CHATTIAN

RUPELIAN
—36.6—

E O C E N E

PRIABONIAN
—40—

BARTONIAN
—43.6—

LUTETIAN

—52—

YPRESIAN

—57.8—

P A L E O C E N E

SELANDIAN
—62.3—

DANIAN
—66.4—

**PLANKTONIC FORAMINIFERA**

*Globorotalia truncatulinoides*
3 — F-700
*Globoquadrina altispira altispira*
—10.5— F-600
*Globorotalia mayeri*
F-560
—13.9— F-550
—14.4— G. fohsi peripheroacuta
—15 G. fohsi peripheroronda F-540
*Praeorbulina glomerosa*
19 — F-530
*Globigerina rohri*
—21.8— F-520
*Globorotalia kugleri*
—23.7— F-510
*Globigerina ciperoensis ciperoensis*
—28.2— F-430
*Globorotalia opima opima*
—32.6— F-420
*Globigerina ampliapertura*
—36.6— F-410
—37.6 Globorotalia cerroazulensis F-380
*Globigerinatheka semiinvoluta*
—40.6— F-370
*Truncorotalinoides rohri*
—42.6— F-360
*Orbulinoides beckmani*
—46— F-350
*Globigerinoides higginsi*
—52.4— F-340
*Globorotalia palmerae*
*Globorotalia quetra*
—55.2— F-320 / F-330
*Globorotalia wilcoxensis*
F-310
—57.8— F-250
—58.8 Globorotalia velascoensis
—59.8 Globorotalia pseudomenardii F-240
*Globorotalia pusilla pusilla*
—61.7— F-230
*Globorotalia pseudobulloides*
—64— F-220
*Globoconusa daubjergensis*
—66.4— F-210

**CALCAREOUS NANNOFOSSILS**

—0.5 Geophyrocapsa oceanica
Pseudoemiliania lacunosa N-720
—1.9 N-710
—2.4 Discoaster brouweri N-670
—3.4 Discoaster surculus N-660
Reticulofenestra pseudoumbilica
—5.6 N-650
Discoaster quinqueramus
—7.8 N-640
—8.8 Discoaster neorectus N-635
Discoaster hamatus
—10.8 N-630
Discoaster kugleri
—13.1 N-620
Cyclicargolithus floridanus N-590
—14.4 Sphenolithus heteromorphus
—16.2 N-580
Helicosphaera ampliaperta N-570
—17.4 Sphenolithus belemnos N-560
—18.9 Triquetrorhabdulus carinatus
—22.8 N-550
—23.4 Discoaster calculosus N-547
Helicosphaera recta
—25.2 N-545
Sphenolithus ciperoensis
—28.5 N-540
Sphenolithus predistentus
—31.5 N-530
Sphenolithus pseudoradians
N-520
—34.6 N-510
—35.1 Reticulofenestra umbilica
Ericsonia formosa N-505
—36.6 N-505
Discoaster barbadiensis
—39 N-470
—40 Micrantholithus procerus N-460
Chiasmolithus grandis
—42.3 N-450
Chiasmolithus solitus
—47 N-447
—48.1 Chiasmolithus gigas N-440
Discoaster sublodoensis
—52 N-437
Discoaster lodoensis
—53.7 N-430
Tribrachiatus orthostylus
N-420
—56.5 N-410
Tribrachiatus bramlettei
—57.8 Fasciculithus tympaniformis
—58.8 N-350
Heliolithus kleinpellii
—61.6 N-340
Fasciculithus janii N-330
—62 Lanternithus duocavus
—65 N-307
Cruciplacolithus primus N-305
—66.4

**PALYNOMORPHS**

—16.1
Crassoretitriletes vanraadshooveni
—20 P-760
—21.5
Tuberculodinium vancampoae
—23.7 P-720
Scyadopityspollenites quintus
—30 P-680
Scabraperiporites nativensis
—36.6 P-660
Retibrevitricolpites triangulatus
—40 P-630
—45.5
Areosphaeridium diktyoplokus
—52 P-610
—54
Homotriblium tenuispinosum
—57.8 P-520
—66.4

Ma
Berggren et al. (1985)    Noguti and Santos (1972)    Richter et al. (in prep.)    Regali et al. (1974a, 1974b)

examples of passive margin basins, as characterized, for example, by McKenzie (1978); they ultimately represent the result of a succession of thermo-mecanical processes including continental rifting, crustal extension and rupture, and subsequent sea-floor spreading. Neocomian to Barremian mechanical (rift) subsidence, followed by Aptian to recent thermal-contraction subsidence (enhanced by flexural loading of sediments), were able to accommodate Mezosoic-Cenozoic sedimentary successions over 10,000 m thick.

The integrated analysis of tectonic subsidence, eustatic sea level fluctuations, climate, and sediment supply is critical for the understanding of the evolution of the eastern Brazilian marginal basins. Chang and Kowsmann (1987), and Chang et al. (1988) provided a composite subsidence curve for the eastern Brazilian marginal basins (excluding the aborted rift of the Recôncavo basin), where they described the development of the Neocomian to recent stratigraphy in terms of the interaction of tectonic subsidence (extensional and thermal) and first-order eustatic sea level fluctuations (Fig. 2.4). Their tectonic subsidence curve is theoretical, based on McKenzie's (1978) model. It describes the behavior of the lithosphere when extended by 100 % ($\beta$ = 2.0) or thinned to 50 % ($\gamma$ = 0.5), which represents a typical situation beyond the basin hinge-line, where the stratigraphic succession tends to be complete. The syn-rift tectonic subsidence curve was simplified, being considered linear (constant rate of about

Fig. 2.4 - Composite subsidence curve and its relationships to the stratigraphic megasequences of the eastern Brazilian marginal basins (after Chang et al., 1988).

| TECTONIC STAGES | | |
|---|---|---|
| RIFT | POST-RIFT THERMAL CONTRACTION SUBSIDENCE | |

MEGASEQUENCES

| CONTINENTAL RIFT | | | |
|---|---|---|---|
| TRANSITIONAL | | | |
| CARBONATE PLATFORM | RISING | | |
| TRANSGRESSIVE | | | |
| TRANSGRESSIVE TO REGRESSIVE | HIGHSTAND | MARINE | |
| REGRESSIVE | FALLING SEA LEVEL | | |

SUBSIDENCE (km)

COMPOSITE SUBSIDENCE

TECTONIC SUBSIDENCE

SEA LEVEL

NEOCOMIAN
BARREMIAN
APTIAN
ALBIAN
CENOMANIAN
TURONIAN
CONIACIAN/SANTONIAN
CAMPANIAN
MAASTRICHTIAN
PALEOCENE
EOCENE
OLIGOCENE
MIOCENE
PLIOCENE/QUATERNARY

(Ma)

SEA LEVEL FLUCTUATION (m)
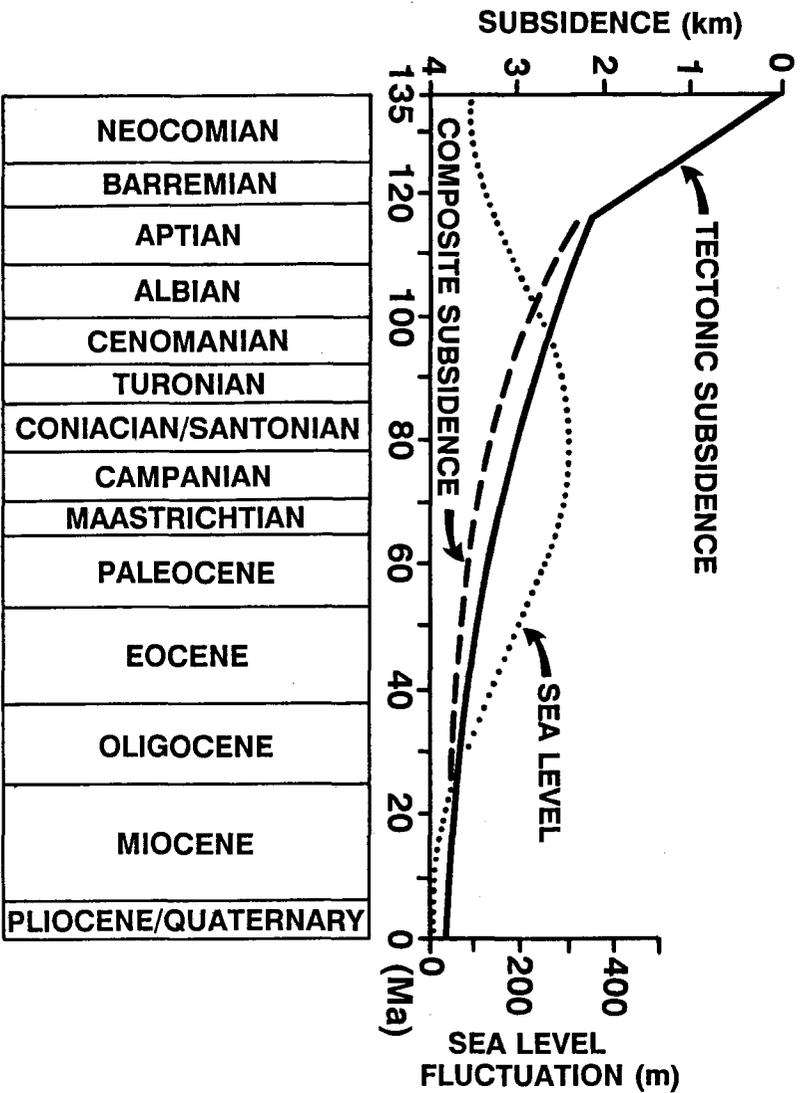
110m/m.y.). The subsidence produced by thermal contraction (cooling) of the lithosphere follows an exponential decrease. Considering the rifting age (135 to 120 Ma), the subsidence is almost insignificant for the last 60 m.y. (Fig. 2.4). The first-order eustatic sea level fluctuations are described by the combined use of the curves published by Vail et al. (1977), and Pitman (1978), respectively for the time intervals before and after 85 Ma. Chang and Kowsmann (1987) insisted on using Pitman's (1978) curve, despite the fact that it embraces only the last 85 m.y., because it results directly from estimates of volumetric variations in the ocean basins.

In the following sections of this chapter, the six major megasequences of the eastern Brazilian marginal basins will be described. Each megasequence will be characterized by age, lateral distribution, thickness, depositional environments, facies associations, and major controlling factors of sedimentation, including where possible, tectonic setting, sea level fluctuations, climate and sediment supply. The composite subsidence curve of figure 2.4 is particularly important for the description of the three marine megasequences.

## 2.4. CONTINENTAL PRE-RIFT MEGASEQUENCE

The continental pre-rift megasequence includes a late Jurassic, eastward prograding, succession of continental red

beds (fluvial, aeolian and shallow lacustrine sediments) (Netto, 1978; Bruhn and De Ros, 1987; Garcia et al., 1990), overlain by an early Neocomian, southward prograding, succession of fluvial, aeolian, and anoxic, shallow lacustrine deposits (Netto, 1974; Negreiros, 1990). These rocks overlie Precambrian igneous and low- to high-grade metamorphic rocks, and also scattered remnants of Paleozoic sedimentary rocks, within a large (> 500,000 km$^2$) intracratonic sag located to the north of the Espírito Santo basin (Fig. 1.7).

Pre-rift sediments reach a maximum thickness of about 1,200 m in the southern Recôncavo basin, but they average less than 600 m. No evidence of syn-depositional faulting has been recorded in the pre-rift megasequence. Its thickness variation is believed to reflect differential subsidence in a basin developed by ductile deformation of the subcrustal lithosphere, a process that may indicate an early stage of rifting (Conceição et al., 1988). Also, Netto (1978) points out that the radical change in direction of progradation recorded by the early Neocomian pre-rift rocks seems to herald the onset of rifting between South America and Africa.

## 2.5. CONTINENTAL RIFT MEGASEQUENCE

Syn-rift sedimentation took place along the entire eastern Brazilian margin, in response to fault-controlled

subsidence related to the stretching of continental crust that preceeded the emplacement of oceanic crust. The continental rift megasequence contains a large and diverse group of siliciclastic, carbonate, and volcanic rocks, formed from early Neocomian to early Aptian. These rocks were emplaced in several depositional environments, including fresh-water to saline, deep to shallow lakes, and also deltas, alluvial plains and alluvial fans.

Continental drift between South America and Africa started between 135 and 120 Ma, with most age determinations clustering around 125 Ma. These ages are estimated by the study of M-series paleomagnetic anomalies in the southern South Atlantic Ocean (e.g. Larson and Ladd, 1973; Rabinowitz and La Brecque, 1979; Austin and Uchupi, 1982), by K-Ar dating of rift-related volcanic-sedimentary successions (Fodor et al., 1983; Mizusaki, 1986), and also by the recognition of the earliest marine sediments accumulated in the new-born South Atlantic basins (e.g. Ponte and Asmus, 1978; Koutsoukos et al., 1991).

The continental rift megasequence typically accumulated in rapidly subsiding, asymmetric half-grabens, which are defined by antithetic- and synthetic normal faults involving the Precambrian basement (Fig. 1.8). These extensional faults commonly can be traced for tens of kilometers, and show cumulative throws of as much as 6,000 m. The rift-phase half-grabens are typically a few tens of kilometers wide, NE-

trending (roughly perpendicular to the main extension direction during the early Neocomian), and they may be separated by basement highs, NW-trending transfer faults, and/or accommodation zones.

The composition and structural framework of the Precambrian basement exerted a large influence on the position and evolution of the eastern Brazilian rifts. The spatial distribution of Precambrian provinces with different rheological behavior (e.g. cratonic shield areas, polycyclic mobile belts and suture zones) was able to control the location and orientation of internal and basin-bounding faults (Cordani et al., 1984; Milani et al., 1988). Extensional rift-phase faults are preferentially NE-oriented, which is the major weakness trend present in the eastern Brazilian Precambrian basement.

The rifting between South America and Africa had an important bifurcation at the latitude of 13°S (Fig. 1.7), that gave rise to two branches: (1) a 450-km long, northward trending branch (Recôncavo-Tucano rift), that terminates in an ENE-trending graben at its northern end (Jatobá rift); and, (2) a NE-trending branch that includes the Sergipe-Alagoas basin, and which subsequently became the continental margin of South America. The triangular east Brazilian microplate (Szatmari et al., 1985) is located between these two branches. It was detached from South America and rotated anticlockwise by the adjacent African continent during Neocomian and

Barremian times (local Rio da Serra, Aratu, and Buracica stages). As a consequence of this rotation, the easternmost rift branch started to develop as a left-lateral transform margin with northward-trending, en échelon pull-apart grabens (Milani et al., 1988).

During the Neocomian and Barremian, the westernmost rift branch (Recôncavo-Tucano rift) was the major site of extension and subsidence: its southernmost portion, the Recôncavo basin (Fig. 1.7), contains a syn-rift sedimentary succession as thick as 6,000 m. However, by late Barremian and early Aptian times (local Jiquiá and Alagoas stages), rifting was aborted in the Recôncavo-Tucano rift, and the east Brazilian microplate stopped its rotation and became part of the South American plate. Meanwhile, the major site of subsidence was transferred to the transform Sergipe-Alagoas basin, which had previously been undergoing transform motion, but evolved into a purely extensional passive margin basin (Milani et al., 1988).

Active and passive rifting styles (Keen, 1985) can be recognized among the eastern Brazilian marginal basins. The northernmost basins (Pernambuco-Paraíba, Sergipe-Alagoas, Recôncavo, and Bahia Sul; Fig. 1.7) contain relatively thick pre-rift sediments and do not record volcanic rocks, indicating a passive rifting. Conversely, the southernmost basins (Espírito Santo, Campos, Santos, and Pelotas; Fig. 1.7) record no pre-rift sedimentation, but had a very active, 130-

120m.y.-old basaltic volcanism (Mizusaki, 1986), typical of active rifting.

During the early and mid Neocomian (local Rio da Serra Stage), a series of deep lakes developed in the northernmost eastern Brazilian rifts. They were filled mainly by a thick succession of dark-coloured organic-rich shales and turbidites (Fig. 1.8), and also by subordinate, marginal (shallower) oncolitic calcarenites and ostracod coquinas (e.g. Bruhn, 1985; Bruhn et al., 1985; Carozzi and Fonseca, 1989). At the end of the Rio da Serra Stage, deltas and closely-related turbidites and debris-flow deposits prograded over the shallowing lacustrine basins (Klein et al., 1972; Caixeta, 1988). The intense seismicity associated with syn-depositional faulting seemed to be able to liquefy and modify the original sedimentary structures of thick successions of siltstones and very-fine- to fine-grained sandstones (Raja Gabaglia, 1991). The Recôncavo basin contains up to 3,000 m of deep lacustrine sediments, accumulated at rates as high as 680 mm/1,000 yr. (Silva and Picarelli, 1990). Along the rapidly and extensively subsiding eastern margin of the Recôncavo basin a thick (up to 2,000 m) wedge of conglomerates and sandstones was deposited by high-density turbidity currents and debris flows (Carozzi et al., 1976; Bruhn and Moraes, 1988) (Fig. 1.8). The sedimentation of this syntectonic, coarse-grained facies assemblage took place continuously from the early Neocomian up to the Barremian (Rio da Serra to Buracica local stages).

Palynological studies suggest climatic modifications during the Rio da Serra Stage, from warm and humid to cold and arid (Regali, 1966). Ostracod studies agree with the sedimentological observations, and indicate deep water with low oxygen content for the early Rio da Serra Stage, and shallow and aerobic environments for the late Rio da Serra Stage (Tölderer-Farmer et al., 1989; Silva and Picarelli, 1990).

In the southernmost Brazilian rifts, the Neocomian record (Rio da Serra and early Aratu stages) is restricted to alkaline basalts with thin intercalations of volcaniclastic and sedimentary rocks. Mizusaki (1986) recognized episodes of subaerial volcanism in the Campos basin, characterized by explosive red volcanic tuffs, and also subaqueous volcanism indicated by an association of basic lavas and lacustrine sediments.

During the late Neocomian and early Barremian (local Aratu and Buracica stages) the northernmost lacustrine basins became even shallower, and recorded cyclic fluvial-deltaic sedimentation (Fig. 1.8) controlled by rapid base-level changes in response to climatic variations (Horschutz et al., 1973; Anjos and Carozzi, 1988). Frequent flooding episodes are recorded by widely distributed beds of ostracod coquinas overlying delta plain facies. In the western Recôncavo basin, a fault-controlled sublacustrine canyon was eroded and filled with channelized turbidites (Fig. 1.8), contemporaneously with

sedimentation in adjacent shallower deltaic systems (Bueno, 1987; Bruhn and Moraes, 1988). The accumulation of thick deltaic sequences in the Recôncavo basin triggered the development of large shale diapirs, by the mobilization of late Rio da Serra muddy facies (Fig. 1.8).

In the southernmost Brazilian rifts the volcanic events became less frequent, and the accumulation of volcaniclastic rocks interbedded with mudstones and carbonate rocks took place in shallow lakes during the Barremian and early Aptian (Bertani and Carozzi, 1985a, 1985b; Abrahão and Warme, 1990). In the Campos basin this lacustrine succession contains stevensite peloids and talc oolites, which characterize chemical precipitation in magnesium-rich alkaline lakes (Rehim et al., 1986). Bertani and Carozzi (1985a, 1985b) also recognize cyclic oscillations in lake salinity, as indicated by the interbedding of a high salinity (dolomite/evaporite flats and matrix-supported ostracod calcarenites) and a lower salinity (grain-supported pelecypod calcarenites) facies assemblage. At the edge of these lacustrine basins, and adjacent to intrabasinal active highs, a continuous coarser-grained alluvial fan sedimentation took place (Fig. 1.8).

The latest stages of rift sedimentation (late Barremian to early Aptian, or local Jiquiá Stage), record different facies assemblages along the eastern Brazilian marginal basins. In the Sergipe-Alagoas basin, sedimentation is characterized by a mixed siliclastic-carbonate succession,

comprising lacustrine pelecypod-carbonate banks associated with fan delta, fluvial-deltaic, and slope-basin deposits (Figueiredo, 1981). The aborted rift of the Recôncavo basin records a thick, sand-rich fluvial succession (Netto, 1978; Figueiredo et al., 1993) (Fig. 1.8). Farther south, sedimentation of coquina beds (bioaccumulated calcarenites and calcirudites composed of pelecypods, ostracods, and gastropods) became more important in the Campos basin. High energy, matrix-free coquinas tend to be found on syndepositional structural highs, while organic-rich marls and shales occupy adjacent lower areas (Dias et al., 1988) (Fig. 1.8).

Rift-phase mudstones and marls, ranging in age from early Neocomian to early Aptian (Rio da Serra to Jiquiá stages) represent the most important hydrocarbon source rocks in Brazil (e.g. Estrella et al., 1984; Mello and Maxwell, 1990; Figueiredo et al., 1993). Organic geochemistry studies discriminate two lacustrine systems for the rift megasequence hydrocarbon source rocks: early Neocomian to early Aptian, deep, fresh-water lakes (Bahia Sul, Recôncavo, and Sergipe-Alagoas basins), and late Neocomian, shallow, saline lakes (Campos and Espírito Santo basins) (Mello and Maxwell, 1990).

## 2.6. TRANSITIONAL EVAPORITIC MEGASEQUENCE

The transitional evaporitic megasequence was deposited from mid Aptian to early Albian (local Alagoas Stage). It spreads widely over the post-rift unconformity, which was an essentially flat-lying surface covering the tilted and block-faulted rift megasequence (Fig. 1.8).

Sedimentation in the transitional megasequence started with the accumulation of alluvial fan complexes derived from adjacent, faulted highlands (Azambuja et al., 1980; Cândido and Wardlaw, 1985; Dias et al., 1988). These coarse-grained deposits are distally associated with lacustrine, finer clastic and carbonate facies (Fig. 1.8), including euxinic, saline, organic-rich shales (Mello and Maxwell, 1990), and stromatolitic and nodular limestones (Dias et al., 1988). Aptian shales of the transitional megasequence represent the second most important oil-source rock for the eastern Brazilian marginal basins, being particularly important in the Sergipe-Alagoas basin (Babinski and Santos, 1987; Mello and Maxwell, 1990). The siliciclastic succession of the transitional megasequence has a maximum thickness of 50 m (aborted rift of Recôncavo basin) to 1,400 m (southern Sergipe-Alagoas basin). However, an impressive exception occurs at the northern Sergipe-Alagoas basin, where important faults were active during the entire Aptian. These faults allowed the development of a 5,000 m-thick succession, which includes the shallow water facies described above, and also turbidite aprons (Bruhn and Moraes, 1988; Abreu and Potter,

1990).

A thick evaporitic succession overlies the basal clastic sediments of the transitional megasequence. The basal contact is mostly smooth, and gently dipping to the east (Fig. 1.8). Pereira et al. (1986) estimate an original (pre-halokinesis) thickness of up to 2,500 m for the Santos basin evaporite succession, probably the thickest along the entire eastern Brazilian margin. These evaporites were deposited in a narrow evaporitic seaway (about 3,000 km long, and 400 km wide), developed in between South America and Africa, to the north of the Pelotas basin (Fig. 1.7), immediately before the opening of the South Atlantic Ocean (Leyden et al., 1976). Restricted sea-water incursions from the southern South Atlantic Ocean (Leyden et al., 1976), and possibly also from the central North Atlantic Ocean (Koutsoukos et al., 1991), allowed the precipitation of a complete suite of evaporites (anhydrite, halite, sylvite, carnallite, and tachyhydrite) under hot, arid climatic conditions (e.g. Szatmari et al., 1979).

The sedimentation of the transitional megasequence occurred simultaneously with the early stages of thermal subsidence along the eastern Brazilian margin (Fig. 2.4). However, evaporite accumulation rates are very high, commonly exceeding the combined effects of tectonic subsidence and sea-level rise. For example, these rates may reach 1,000 cm/1,000 yr. in the Zechstein basin, 100 cm/1,000 yr. in the Mediterranean basin, and 60 cm/1,000 yr. in the Elk Point

basin, Canada (Kendall, 1984). On the other hand, the maximum rate of tectonic subsidence is around 25 cm/1,000 yr., which is achieved by the oceanic crust during early cooling stages (Sclater et al. 1971), and the maximum rate of sea-level rise due to volume variations in the mid-ocean ridges reach about 1 cm/1,000 yr. (Pitman, 1978). Thus, evaporite sedimentation seems to be controlled essentially by high evaporation rates (climate) and restricted influx of brines (paleogeography) (Kendall, 1992).


## 2.7. SHALLOW CARBONATE PLATFORM MEGASEQUENCE

The establishment of truly marine conditions along the proto-South Atlantic Ocean took place gradually during the early Albian, as indicated by paleoecological and sedimentological studies (e.g. Spadini et al., 1988; Koutsoukos et al., 1991). Basin subsidence by crustal thermal contraction associated with a very important eustatic sea-level rise during the early to mid Albian (Fig. 2.4) permitted the vertical aggradation of a thick (up to 2,500 m in the Santos basin) carbonate platform along the eastern Brazilian margin (Fig. 1.8).

Immediately overlying the transitional evaporitic megasequence is a succession of laminated carbonate mudstones, bioturbated pelletoidal mudstones, and subordinated oolitic

grainstones and fine-grained sandstones, recording the sedimentation on tidal flat-lagoon systems (Spadini et al., 1988). However, with the evolution of the Albian carbonate ramp, higher-energy facies tended to accumulate preferentially, particularly oncolitic calcarenites. Elongated, NE-trending shoals are recognized in the Campos basin, which are composed mostly of grainstones and packstones containing oncolites, peloids, oolites, and rare bioclasts (Esteves et al., 1987; Spadini et al., 1988). Shoaling-upward cycles, starting with peloidal wackestones, and followed by oncolitic/oolitic packstones and oncolitic/oolitic grainstones represent very common facies associations recorded at the Santos (Carvalho et al., 1990) and Campos (Spadini et al., 1988) basins. In between the shoals, lower-energy, finer-grained carbonates, particularly peloidal calcisiltites, were deposited. On the other hand, in the most proximal (westernmost) portions of the basins, the deposition of siliciclastic, very coarse-grained fan deltas took place continuously during the early to mid Albian. This clastic wedge represents a continuation of the sedimentation of the marginal coarser facies recorded in the transitional megasequence (Fig. 1.8).

During the Albian, the eastern Brazilian marginal basins started to undergo a generalized eastward (seaward) tilting, which induced the downslope creep of Aptian evaporites by gravitational instability (e.g. Dauzacker, 1981; Figueiredo

and Mohriak, 1984; Pereira et al., 1986). The salt flowage triggered the development of listric faults soling out on evaporite beds, rollover structures, and also salt pillows and diapirs, which define the typical structural style for the post-rift megasequences (Fig. 1.8). Such listric faults already influenced the sedimentation on the early to mid Albian carbonate platform, with the shallower carbonate facies (shoal calcarenites) tending to accumulate preferentially on faulted anticlines and rollover crests (Esteves et al., 1987).

The Albian carbonate platform was mostly developed in shallow neritic (< 50 m) waters, as indicated by studies of planktonic foraminifera (e.g. Azevedo et al., 1987a; Dias-Brito, 1987). However, its calcarenites are replaced seawards by calcilutites formed in average water depths of about 100 m, but never exceeding 300-400 m, as suggested by benthic foraminifera recovered by the DSDP Legs 26, 36 and 40 (Scheibnevorá, 1981). The climate during carbonate platform deposition was warm and arid, as recorded by the presence of xerophytic palynomorphs (Lima, 1983), oolites, peloids and micrite-coated grains (Leonard et al., 1981), and very negative oxygen isotopes ($\delta^{18}O$ = -4 to -5 ‰) (Rodrigues and Takaki, 1987; Spadini et al., 1988). Also, the intense bioturbation, the light colour of carbonate grains, and the low organic carbon content of the finer-grained carbonates characterize the early to mid Albian sea as an oxygen-rich basin (Dias-Brito, 1987). Hypersalinity prevailed at that

time, as suggested by the poorly diversified and stunted biota (Dias-Brito, 1987; Spadini et al., 1988), as also by high values of carbon isotopes ($\delta^{13}C$ = +3 to +4 ‰) (Rodrigues and Takaki, 1987; Spadini et al., 1988).

## 2.8. MARINE TRANSGRESSIVE MEGASEQUENCE

During the late Albian the shallow carbonate platform started to be covered by an increasingly deep succession of calcilutites, marls, shales, and sandy and conglomeratic turbidites, which comprise the marine transgressive megasequence (Fig. 1.8). Marine transgressive sedimentation took place in response to the combined effects of thermal-contraction subsidence (amplified by sedimentary loading) and a general tendency for eustatic sea level rise (Fig. 2.4), which allowed the accumulation of a sedimentary pile as thick as 2,400 m (Santos basin). **The two turbidite systems detailed in this thesis are included in the marine transgressive megasequence; i.e. the Coniacian/Santonian to early Maastrichtian Carapeba/Pargo turbidite system (Campos basin), and the early Eocene Lagoa Parda turbidite system (Espírito Santo basin) (Fig. 1.8).**

Marine transgressive sedimentation started with the deposition of calcilutites and marls, mostly under deep neritic to upper bathyal (100 - 300 m) depths (e.g. Azevedo et

al., 1987a; Koutsoukos and Hart, 1990). The progressive sea level rise and the increasing water exchange between the South Atlantic and North Atlantic oceans lowered the salinity of the late Albian sea, allowing biotic diversity and abundance (Dias-Brito, 1987; Spadini et al., 1988). The establishment of a subtropical high pressure cell over the enlarged South Atlantic watermass (Parrish and Curtis, 1982) seems to have induced a very important climatic change during the late Albian and Cenomanian, from warm and dry to warm and humid conditions. This climatic transformation appears to have occurred through alternating dry and humid climatic cycles, as suggested by rhythmic interbeddings of calcilutites and marls (Spadini et al., 1988). Isotopic data for the early Albian to early Turonian succession of Campos basin (Rodrigues and Takaki, 1987; Spadini et al., 1988) show $\delta^{18}O$ values increasing from -6.0 to -3.0 ‰. These suggest warm waters for the entire period, but also a trend of decreasing temperatures. Also, a sharp increase in the $\delta^{13}C$ values, from +4 to -2 ‰, indicates an enhanced continental runoff ($^{12}C$-rich waters) due to the late Cenomanian/early Turonian wetter climate.

The increasing sea level rise and the larger clastic supply by continental runoff suppressed carbonate sedimentation along the eastern Brazilian margin, whereas the transgressive megasequence became an essentially siliciclastic, muddy succession. In the late Turonian the South Atlantic Ocean was fully connected to the North Atlantic

and Indian oceans, with the establishment of environmental stability under truly oceanic conditions (Dias-Brito, 1987). Great biological diversity took place, including the development of a benthic foraminifera assemblage typical of lower bathyal (1,000 to 2,000 m) depths (Azevedo et al., 1987a; Koutsoukos and Hart, 1990). These very deep water depths are a function of large basement subsidence. For example, seismic data from the Santos basin show a total basement downwarping of about 12 km (at a position 200 km offshore); of this, little more than 2 km was accommodated by normal faulting (Hubbard, 1988).

The marine transgressive megasequence is characterized by sediment starvation, due the combined effects of high composite subsidence (Fig. 2.4) and relatively low influx of terrigenous sediments. In the Campos basin undecompacted sedimentation rates are as low as 0.5 cm/1,000 yr. for the succession between 100 and 50 Ma (Mohriak et al., 1990). However, increasing salt tectonics created important low areas for the accumulation of turbidites. These were emplaced during shorter-term sea-level falls within the overall transgressive event (e.g. Figueiredo and Mohriak, 1984; Guardado et al., 1990).

Several turbidite systems are recognized within the transgressive marine megasequence. They can best be studied in the Campos basin, where over 900 wells and abundant high-quality seismic data (113,000 km of 2-D seismic profiles, and

126,000 km of 3-D seismic profiles; Figueiredo and Martins, 1990) permitted the detailed mapping of turbidite systems from the late Albian, late Cenomanian/early Turonian, Coniacian/Santonian, and Maastrichtian (e.g. Guardado et al., 1990; Martins et al., 1990). Late Albian turbidites comprise sandy accumulations as thick as 100 m, spreaded over areas exceeding 200 $km^2$ (Cândido, 1990b; Martins et al., 1990). On the other hand, the late Cenomanian/early Turonian, Coniacian/Santonian, and Maastrichtian systems tend to be confined to narrow (< 15 km), fault-controlled troughs which subsided differentially in response to halokinesis (Figueiredo and Mohriak, 1984; Becker et al., 1988; Cândido, 1990a; Martins et al., 1990). The prolonged subsidence along these troughs allowed the accumulation of thick successions of coarse-grained turbidites, with a maximum thickness of 262 m being found in the Coniacian/Santonian system.

Along the western margin of the Espírito Santo and Bahia Sul basins, several large (up to 25 km wide and 100 km long), deeply-incised submarine canyons were excavated after the Albian (Fig. 2.5). The position of these canyons was controlled by the reactivation of rift-phase faults involving the Precambrian basement. Each canyon records many phases of erosion and filling, largely influenced by sea level fluctuations (Antunes, 1984, 1990a, 1990b; Rangel, 1984; Bruhn and Moraes, 1989). These canyon-filling sections, which also make part of the transgressive megasequence, were deposited in

Fig. 2.5 - Location map for the major late Cretaceous and early Tertiary submarine canyons in the Espírito Santo and Bahia Sul basins.
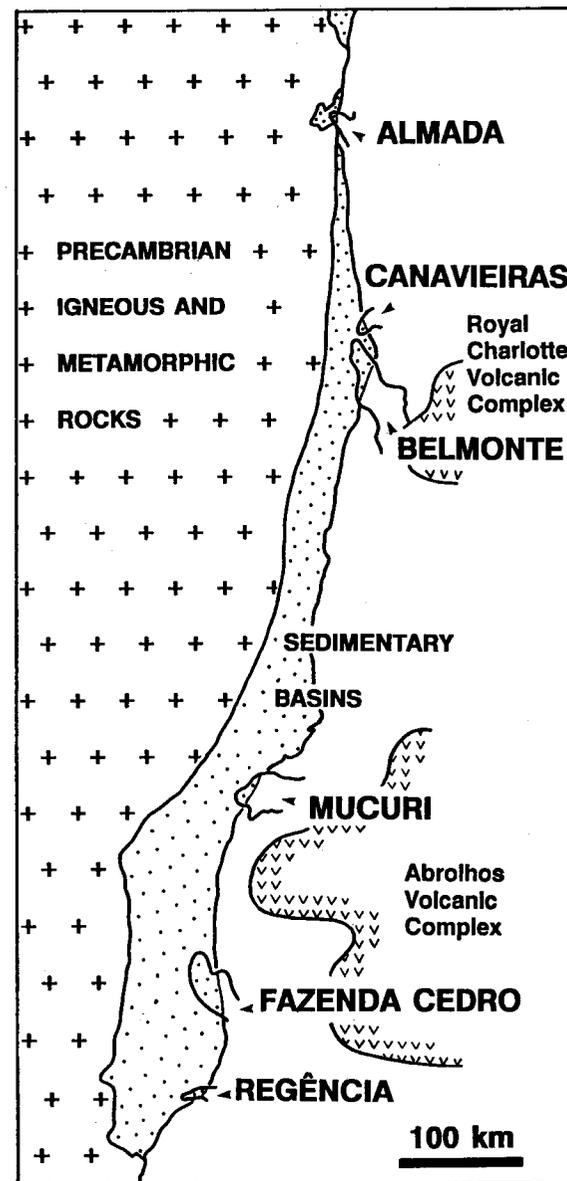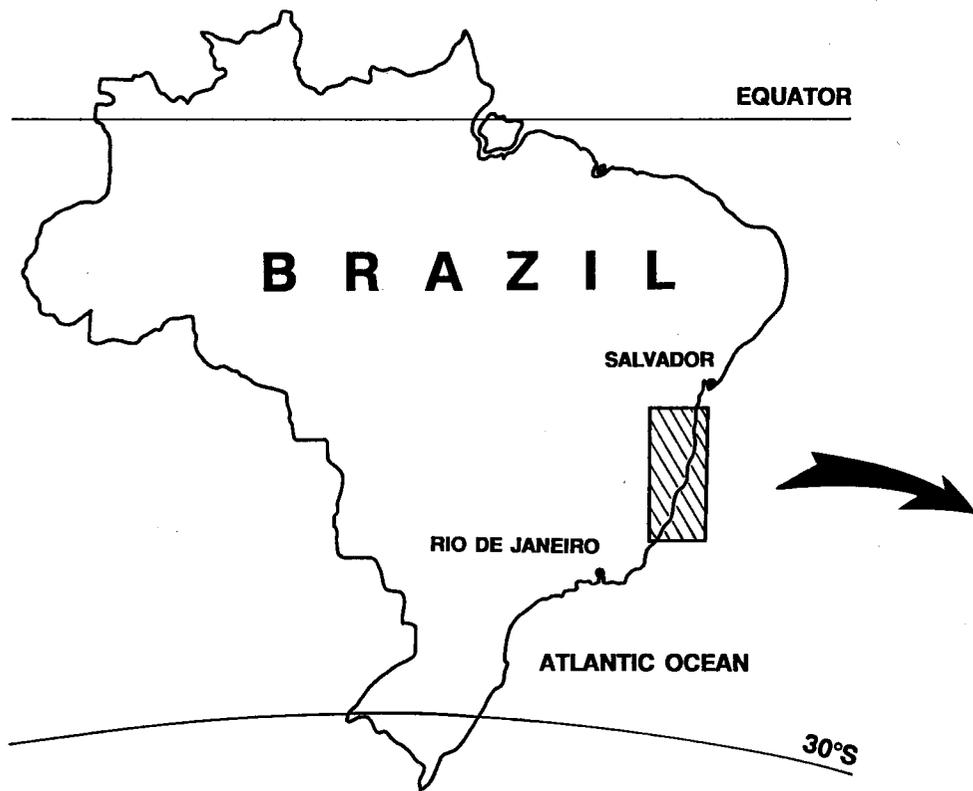
deep neritic to upper bathyal (200 - 600 m) water depths (Azevedo, 1985; Bruhn and Moraes, 1989), from the Coniacian/Santonian to the early Eocene. Antunes (1990a) recognized at least 9 major phases of erosion within the Regência Canyon (Fig. 2.5), which can be correlated to some of the third-order sea level falls suggested by Haq et al. (1987, 1988).

During the late Cretaceous and early Tertiary, very important magmatic and tectonic activity took place in the southernmost eastern Brazilian marginal basins, and also in the adjacent craton. Recurrent magmatic activity, from the Coniacian to the Eocene, is recorded by alkali basalt intrusions and volcanic tuffs in the Santos, Campos, Espírito Santo and Bahia Sul basins (e.g. Ponte and Asmus, 1978; Asmus and Porto, 1980), and by alkaline rocks intruding the Precambrian craton onshore (Almeida, 1983). Large volcanic complexes were developed in the Espírito Santo and Bahia Sul basins (Fig. 2.5). The reactivation of basement-attached faults led to the uplift (> 2,000 m) of coastal mountain ranges in southeastern Brazil (e.g. the Serra do Mar and Serra da Mantiqueira; Fig. 1.7), which are supported essentially by Precambrian high-grade metamorphic rocks. The Serra do Mar became an important source of coarse-grained sediments not only for the proximal, shallow-water systems, but also for the widely-distributed, deep-water turbidite systems of the Santos and Campos basins (e.g. Figueiredo and Mohriak, 1984; Guardado

et al., 1990). Macedo (1987) suggests that opposing isostatic forces may have kept the Serra do Mar uplifting during the development of the entire transgressive megasequence and part of the following regressive megasequence: the uplifting force was due to the load released by erosion onshore, and the downwarping force was produced by sediment load offshore.


## 2.9. MARINE REGRESSIVE MEGASEQUENCE


The marine regressive megasequence is composed of a group of synchronous depositional systems (strand plain, fluvial-deltaic, fan delta, siliciclastic shelf, carbonate platform, slope, and deep-basin systems), typically displaying a progradational pattern (Fig. 1.8). This succession of rocks may attain maximum thickness exceeding 3,600 m (Campos basin), and is mostly Miocene in age.

The change from a bathyal, transgressive onlapping, to a shallowing, regressive offlapping style of sedimentation took place at different times along the eastern Brazilian margin. Starting in the Santos basin (late Turonian), the onset of the regressive megasequence became younger northwards; Paleocene in the Campos Basin, early Eocene in the Espírito Santo basin, and late Eocene in the Sergipe-Alagoas basin.

The development of the regressive megasequence was controlled by the combined effects of the pronounced first-

order eustatic sea level fall following the late Cretaceous, the negligible rates of thermal subsidence in the basins that formed about 135-120 Ma (Fig. 2.4), and the increasing sediment supply (particularly from the uplifted Serra do Mar and Serra da Mantiqueira). Along the most proximal portions of the basins, the falling sea level was followed by intense erosion, which was sufficiently deep in the Campos basin to remove the coarser-grained, proximal facies of the transgressive megasequence. Differential sediment supply may explain the older age of the regressive megasequence in the northernmost eastern Brazilian marginal basins (Chang et al., 1988); high coastal ranges similar to the Serra do Mar and Serra da Mantiqueira were not developed in areas north of the southern Espírito Santo basins (Fig. 1.7). A lower supply of sediment, from topographically lower and more distant areas, may explain why the widely distributed, coarse-grained turbidite systems of Santos and Campos basins have not been found to the north, except for the canyon-confined, coarse-grained turbidites of the Espírito Santo and Bahia Sul basins.

The continuity of the halokinesis, particularly the collapse and evacuation of salt ridges, was responsible for the development of depressed catchment areas for turbidite systems (e.g. Figueiredo and Mohriak, 1984; Guardado et al., 1990). Peres (1993) also believes that salt flowage would have been capable of increasing the outer shelf slope, triggering the development of high-density turbidity currents. However,

the most important turbidite systems of the regressive megasequence seem to be related to well-known sea level lowstands (e.g. Souza Cruz et al., 1987; Azambuja, 1990; Guardado et al., 1990; Carminatti and Scarton, 1991). The exposure of large areas of the shelf during periods of sea-level fall not only was responsible for removing large amount of sand from the shelf to basin, but also for carving several submarine canyons along the entire eastern Brazilian margin (Gamboa et al., 1986; Antunes et al., 1988; Viana et al., 1990; Cainelli, 1992; Carminatti and Scarton, 1991). Cainelli (1992) recognizes the importance of canyon-truncation of carbonate-rimmed shelves on creating pathways for turbidity currents. In the Sergipe-Alagoas basin, carbonate-rich turbidites and debris flows are related to canyons reaching only the upper slope or shelf edge, whereas sand-rich turbidites are associated with deeply-incised canyons into the shelf (Cainelli, 1992).

In the Campos basin, three major turbidite systems are recognized in the regressive megasequence: mid Eocene, Oligocene, and Miocene (Guardado et al., 1990; Martins et al., 1990). Mid Eocene turbidites occur as thick, trough-confined sand bodies or younger, widely distributed blankets of coarse-grained turbidites. Cumulative isopach maps for the mid Eocene turbidites show maximum thickness exceeding 500 m (Martins et al., 1990). Three type-I sequences (Van Wagoner et al., 1988) are recognized within the Oligocene succession of the Campos

basin, with boundaries defined at about 35, 30, and 25 Ma (Carminatti and Scarton, 1991). Each one of these sequences is characterized by deep erosion on the shelf and slope, and the accumulation of lowstand fans on the continental rise and abyssal plain. Oligocene turbidites show cumulative thickness around 200 m (Martins et al., 1990), and can be seismically traced for over 6,000 km$^2$ (Peres, 1993). Miocene turbidites are still poorly known, but the available isopach maps suggest maximum thickness over 175 m, and a wide lateral distribution toward the northeastern portion of the basin, where present water depth exceeds 1,000 m (Martins et al., 1990).

# 3. CARAPEBA AND PARGO FIELDS, CAMPOS BASIN

## 3.1. LOCATION AND DATA BASE

The Carapeba and Pargo fields are located in the northeastern Campos basin, offshore eastern Brazil, in an area with a present bathymetry of about 100 m. They comprise two independent oil accumulations, 55 to 75 km from the Brazilian coast (Fig. 3.1).

The most important reservoirs of the Carapeba and Pargo fields are contained within a thick (up to 286 m) succession of late Cretaceous, coarse-grained turbidites, deposited in a 150 km long, NW- to WNW-oriented canyon (Fig. 3.1). Subsidence along listric faults with different orientation and variable activity represented the major control on the variable orientation and width of the Carapeba/Pargo canyon and its successive filling sections (Fig. 3.2), which show lateral extent ranging from 1 to 12 km in the studied area.

Pargo field was discovered in 1975 by the wildcat RJS-12, which was followed by the drilling of 12 step-out wells, and also 21 exploitation wells. The reservoirs cover an area of 10 km$^2$ (Fig. 3.3), and contain an original oil-in-place volume of

Fig. 3.1 - Net sand map for the Coniacian to Maastrichtian, coarse-grained turbidites of the northern Campos basin (after Martins et al., 1990).

N

Isobaths

City of Campos

Lake Feia

ATLANTIC OCEAN

7 600 000

CARAPEBA FIELD

PARGO FIELD

7 500 000

Limit of occurrence of late Cretaceous rocks

20 km

C.I. = 100 m

300 000

400 000

100 m

400 m

1000 m

2000 m
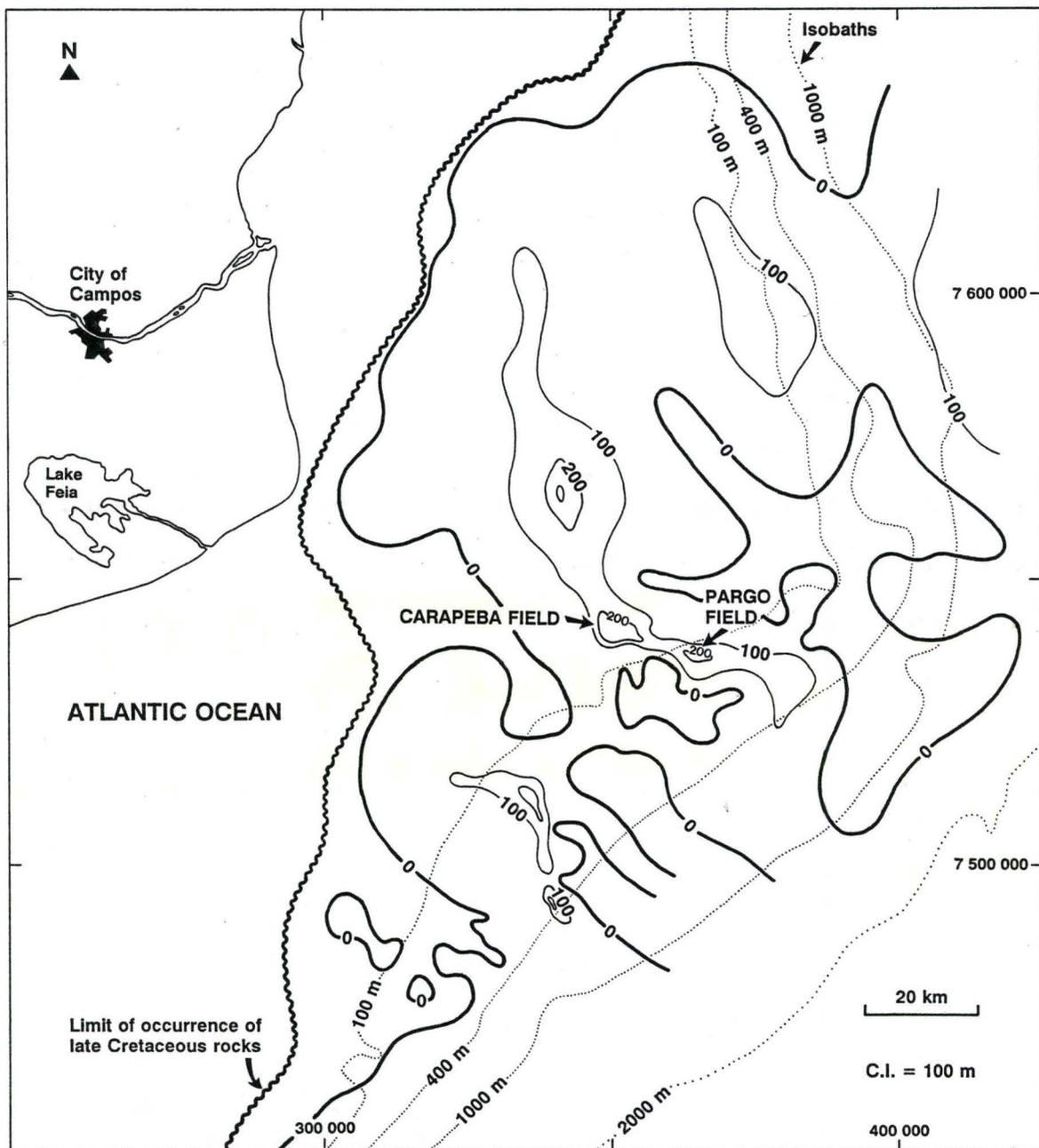
Fig. 3.2 - Typical geological cross section for the Carapeba field, showing the Coniacian/Santonian (CRP/PG-S3 to CRP/PG-S6) and early Maastrichtian (CRP/PG-S7 and CRP/PG-S8), coarse-grained turbidite successions. Section is transverse to the Carapeba/Pargo fault-controlled canyon. Datum is the radioactive S/C log marker (approximate boundary between Santonian and Campanian). Several radioactive log markers are correlated within the late Cenomanian/early Turonian (CT), Coniacian/Santonian (C/S-1, C/S-2, and C/S-3), and Maastrichtian (M-1 and M-2) mudstone successions. The uppermost turbidite succession (CRP/PG-S8) dates from the early Maastrichtian, but there is no log response that can be correlated to the boundary between early and late Maastrichtian. Well logs used to construct the section: gamma-ray, resistivity, and density. Vertical scale = 5.8 x horizontal scale.

S
CRP - 26D    CRP - 8    CRP - 3D    CRP - 18D    CRP - 11    RJS - 221    CRP - 14    RJS - 193A    CRP - 6    N

MARINE REGRESSIVE MEGASEQUENCE
MARINE TRANSGRESSIVE MEGASEQUENCE

CRP/PG - S8
CRP/PG - S7

CRP/PG - S6
CRP/PG - S5
CRP/PG - S4
CRP/PG - S3

MID EOCENE
EARLY PALEOCENE
LATE MAASTRICHTIAN    Gamma-ray log
LATE MAASTRICHTIAN    Resistivity log
EARLY MAASTRICHTIAN
M-1
CAMPANIAN    DATUM
Density log

CONIACIAN/SANTONIAN

EARLY TURONIAN
LATE CENOMANIAN

EARLY TURONIAN
LATE CENOMANIAN

CONIACIAN/SANTONIAN

LATE CENOMANIAN/EARLY TURONIAN

LATE ALBIAN

Late Cenomanian/early Turonian
turbidites (Namorado Sandstone)

CAMPOS
FORMATION
MACAÉ
FORMATION

TURBIDITE SUCCESSIONS: SANDSTONES

Early Maastrichtian
CRP/PG - S8: W
CRP/PG - S7: V

Coniacian/Santonian
CRP/PG - S6: Q, R, S, T
CRP/PG - S5: M, N, O, P
CRP/PG - S4: D, E, F, G, H, I, J, K, L
CRP/PG - S3: C

CARAPEBA FIELD
PARGO FIELD

5 km

0    1    2 km

200 m

100

0

BRUHN (1993)

Fig. 3.3 - Location map of wells and detailed geological cross sections in the Carapeba and Pargo fields. Four of these cross sections are reproduced in figures 3.21 to 3.24. Dashed lines indicate the maximum areal extent of oil accumulations in both fields.

CARAPEBA FIELD

PARGO FIELD

345 000    350 000    355 000    360 000

N

Fig. 3.23

Fig. 3.24

6

222

193A

14

224

145A

7 540 000

221
11

5A

9

8

7A

282A

Fig. 3.21

Fig. 3.22

27A

52
228
4
209

2

12

3

0        3 km

o Well control

▲ Cored well
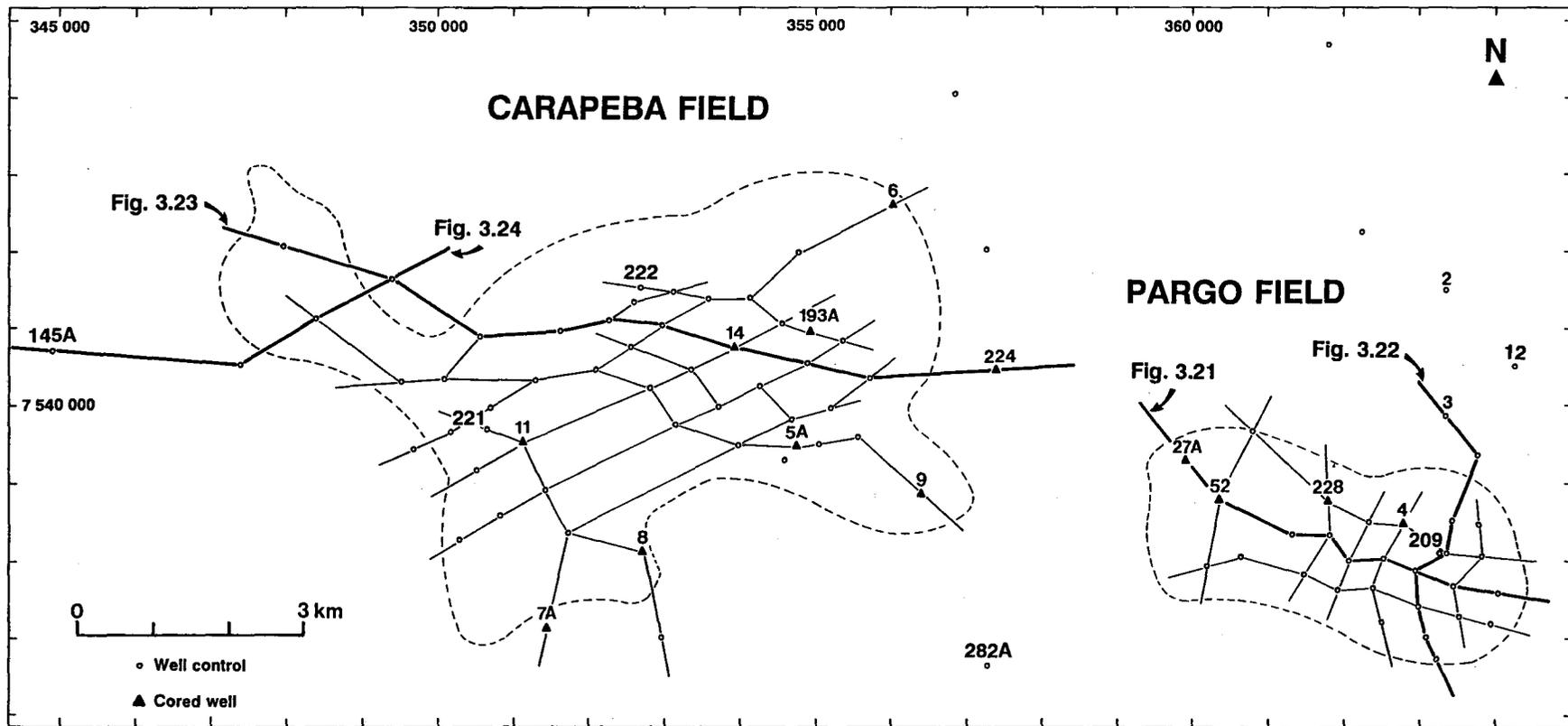
34 x 10$^6$ m$^3$ (214 million bbl), and ultimate recoverable reserves of 10 x 10$^6$ m$^3$ (63 million bbl) (Becker et al., 1988). The 21 producing wells have a typical spacing of 400 to 500 m. The reservoirs were cored in four wells (PG-4, PG-27A, RJS-52, and RJS-228; Fig. 3.3), which permit the study of a cumulative 155 m thick succession of rocks.

Carapeba field was discovered in 1982 by the wildcat RJS-193A. Subsequent drilling of 18 step-out- and 35 exploitation wells permitted the mapping of a giant oil accumulation, covering 35 km$^2$ (Fig. 3.3). Carapeba field contains an original oil-in-place volume of 99 x 10$^6$ m$^3$ (620 million bbl), and ultimate recoverable reserves of 29 x 10$^6$ m$^3$ (182 million bbl) (Horschutz et al., 1992). There are 36 oil-producing wells in Carapeba, drilled with an average spacing of 500 to 700 m. A total of 422 m of rocks were recovered from 9 cored wells (CRP-5A, CRP-6, CRP-7A, CRP-8, CRP-9, CRP-11, CRP-14, RJS-193A, and RJS-224; Fig. 3.3).

Carapeba and Pargo oil accumulations occur mostly in different reservoirs, and both fields present distinct oil/water contacts, respectively 3,025 and 3,039 m below sea level. However, their reservoirs are part of the same turbidite system, where several sandstone bodies or even individual turbidites can be traced up to 20 km, from the western portion of Carapeba to the eastern boundaries of Pargo (Fig. 3.4). The present configuration of the oil accumulations was defined not only by the facies distribution within the

Fig. 3.4 - Geological cross section longitudinal to the Carapeba/Pargo canyon. Datum is the base of the widely distributed K sandstone. S-1, S/C, M-1 and M-3 are radioactive (mudstone) log markers. S/C indicates the approximate boundary between Santonian and Campanian. The uppermost turbidite succession (CRP/PG-S8) dates from the early Maastrichtian, but there is no well log response that can be correlated to the boundary between early and late Maastrichtian. Arrows (fu) indicate major fining upward successions as defined by density logs. Well logs used to construct the section: gamma-ray, resistivity, and density. Vertical scale = 14 x horizontal scale.

WNW CRP-25 ... RJS-222

CARAPEBA FIELD

CRP-35D

MARINE REGRESSIVE MEGASEQUENCE
MARINE TRANSGRESSIVE MEGASEQUENCE

RJS-52

PARGO FIELD

PG-8D    ESE

Gamma-ray log

Resistivity log

Density log

CRP/PG-S8
CRP/PG-S7

W
V
U
S
T
CRP/PG-S6 R
P O
CRP/PG-S5

Q
N
M

MID EOCENE
EARLY PALEOCENE
M-1
M-3
S/C
LATE MAASTRICHTIAN
CAMPANIAN
LATE MAASTRICHTIAN/
EARLY MAASTRICHTIAN
CONIACIAN/SANTONIAN
S-1

fu

-3000

-3000

-3000

-3000

-3200

-3200

-3200

-3200

200 m

DATUM

L
K
J I H G
F
E
D

CRP/PG-S4

100

CRP/PG-S3

Coniacian/Santonian
Late Cenomanian/Early Turonian

Campos Formation
Macaé Formation

CRP/PG-S2

fu

C

fu

B

0

CRP/PG-S1

A

SANTONIAN/
CONIACIAN

EARLY TURONIAN/
LATE CENOMANIAN

TURBIDITE SUCCESSIONS: SANDSTONES

Early Maastrichtian

Coniacian/Santonian:

CRP/PG-S8: W          CRP/PG-S6: Q, R, S, T, U
CRP/PG-S7: V          CRP/PG-S5: M, N, O, P
                      CRP/PG-S4: D, E, F, G, H, I, J, K, L
                      CRP/PG-S3: C
                      CRP/PG-S2: B
                      CRP/PG-S1: A

BRUHN (1993)

0    1    2    3 km

CARAPEBA FIELD        N
CRP-25  RJS-222
        CRP-35D    PARGO FIELD
              RJS-52
              PG-8D
        5km

turbidite system, but also by a fault system reactivated during the Maastrichtian and early Tertiary. These faults had a limited influence on the sedimentation of the late Cretaceous reservoir sandstones.

The turbidite system sampled in the Carapeba and Pargo fields was studied along a 20-km-long, 8-km-wide area, where 92 wells were drilled between 1973 and 1987 (Fig. 3.3). These wells present a comprehensive suite of high-quality well-logs, including gamma-ray, resistivity, density, neutron, caliper, sonic, and dipmeter logs. The facies defined in the 13 cored wells can be calibrated with well log responses, and hence recognized in the non-cored wells.

Unpublished biostratigraphic reports from the Research Center of PETROBRÁS are available for 15 wells: calcareous nannofossil zones for the wells CRP-11, CRP-14, PG-2, PG-3, PG-4, PG-27A, RJS-12, RJS-52, RJS-145A, RJS-193A, RJS-209, RJS-221, RJS-222, RJS-228, and RJS-282A; palynomorph zones for the wells PG-2, RJS-145A, RJS-193A, RJS-209, RJS-221, and RJS-222; and foraminifera zones for the wells RJS-12, RJS-52, RJS-145A, and RJS-193A (Fig. 3.3).

Seismic profiles do not form part of the data set for this study. Because of the large thickness of amalgamated coarse-grained rocks, and also their great burial depth (2,900 to 3,350 m), seismic data still do not achieve sufficient resolution for high-resolution stratigraphic analysis and detailed geometrical characterization of the late Cretaceous

turbidite successions in the Campos basin. Nevertheless, seismic data published by Figueiredo and Mohriak (1984), Dias et al. (1990), Figueiredo and Martins (1990), Guardado et al. (1990), and Mohriak et al. (1990) helped to place the studied fields in a regional geological context.

Detailed descriptions of the development of the Carapeba and Pargo fields, including the breaking of the reservoir succession into distinct oil-producing zones, are presented by Becker et al. (1988), Tigre et al. (1988), Cândido (1990a), and Horschutz et al. (1992).

A few sedimentological and petrographic studies have been made of the Carapeba and Pargo reservoirs, including those by Moraes (1985), Freitas (1987), Becker et al. (1988), and Bruhn and Moraes (1988). This study is the first to provide an integrated description of the late Cretaceous turbidite system present in both fields, embracing also the non-oil-bearing turbidites.

## 3.2. GENERAL GEOLOGICAL SETTING

## 3.2.1. Stratigraphy

The Carapeba and Pargo reservoirs consist of sandy and conglomeratic turbidites, which make part of the marine transgressive megasequence recognized throughout the eastern

Brazilian marginal basins (Fig. 1.8). These mostly coarse-grained rocks are included in the Carapebus Member of the Campos Formation, which comprises not only the Coniacian/Santonian and Maastrichtian turbidites of the marine transgressive megasequence, but also the Eocene, Oligocene and Miocene counterparts of the marine regressive megasequence.

The mudstones that occur interbedded with the coarser-grained facies of the Carapebus Member are formally named Ubatuba Member of the Campos Formation. Calcareous nannofossil studies of the mudstones of the Ubatuba Member (Fig. 2.2) allow the recognition of two major turbidite successions in the Carapeba/Pargo system (Fig. 3.4): (1) a Coniacian/Santonian succession, up to 262 m thick, and (2) an early Maastrichtian sucession, with a maximum thickness of only 24 m. These coarse-grained successions are separated by an up to 24 m thick, Campanian mudstone package.

The Coniacian/Santonian and Maastrichtian coarse-grained turbidites of the Campos basin are largely confined to NNW to WNW-oriented troughs, which were established mostly in base-of-slope settings. At least four major sites for turbidite deposition have been recognized in the basin, with the northernmost of them being identified only by its westernmost marginal portion (Fig. 3.1). The Carapeba/Pargo turbidite system is located along the best defined trend of turbidite deposition (Fig. 3.1). The troughs containing late Cretaceous turbidites were eroded into Coniacian/Santonian mudstones of

the Campos Formation, or even deeper, into late Cenomanian/
early Turonian marls and mudstones of the Macaé Formation
(Fig. 3.2). The Coniacian/Santonian turbidite succession may
overlie a regional unconformity (Fig. 3.4), which is related
to the erosion of late Turonian sediments. This unconformity
was carved stratigraphically deeper along the late Cretaceous
troughs, but it can be largely recognized in the Campos basin,
even outside these large erosional features.

Early and late Maastrichtian, and early Paleocene
mudstones overlie the early Maastrichtian coarse-grained
succession in the Carapeba and Pargo fields (Fig. 3.4). They
represent the uppermost section of the marine transgressive
megasequence in the Campos basin.

The basal part of the marine regressive megasequence is
represented in the studied area by late mid Eocene mudstones
and sandstones, which were deposited over a widespread
unconformity (Fig. 1.8). A large amount of erosion is related
to this unconformity, which was responsible for eliminating
the entire record of the proximal, shallower facies of the
Coniacian to early Paleocene portion of the marine
transgressive megasequence. Fig. 3.1 shows the westernmost
limit of occurrence of the late Cretaceous rocks of the Campos
Formation.

### 3.2.2. Tectonics and magmatism

A dense system of listric normal faults influenced sedimentation in the Campos basin from the early Albian onwards (e.g. Figueiredo and Mohriak, 1984; Esteves at al., 1987; Peres, 1993). They also controlled the development of the large troughs that contain coarse-grained, late Cretaceous turbidites (Fig. 3.1). Some of the faults that exerted major influence on the sedimentation along the Carapeba/Pargo trough are shown in figure 3.2. These faults sole out on Aptian evaporitic beds of the transitional megasequence (Fig. 1.8), and their establishment as well as episodic reactivation seem to be related to evaporite flowage (Figueiredo and Mohriak, 1984; Guardado et al., 1990). A detailed map for the basement-detached, post-rift fault system is provided by Guardado et al. (1990, their figure 39). Most of these faults strike northeast, as basement-attached, rift-phase faults. However, subordinate modes of N-, NW-, or even E-W trending faults can be recognized.

In contrast to the offshore area, the tectonism operating in the adjacent, onshore Precambrian craton was characterized by NE-trending faults that deeply penetrated the basement. The continuous reactivation of these faults led to the uplift (over 2,000 m) of a coastal mountain range (the Serra do Mar; Fig. 1.7), and also to the opening of a series of elongated pull-apart basins filled with up to 850 m of late Cretaceous (?) and Tertiary sediments (Melo et al., 1985; Marques, 1990).

Recurrent magmatic activity from the Coniacian to the

Eocene is recorded in the Campos basin, particularly in its southernmost portion, where alkali basalts and volcaniclastic rocks cover an area of more than 10,000 km$^2$ (Dias et al., 1990). A laterally restricted, 96 m thick basalt intrusion was drilled about 20 km southeast of the Pargo field, along the Carapeba/Pargo trough. This volcanic intrusion is surrounded by Coniacian/Santonian rocks, which comprise a 150 m thick turbidite succession. Alkaline intrusions, also recurrent from the Coniacian to the Eocene, are recorded in the adjacent, onshore Precambrian craton (Almeida, 1983).

### 3.2.3. Paleoenvironment

The fauna described from the Coniacian/Santonian and Maastrichtian mudstones of the Campos Formation is very diversified, and is typical of open oceanic environments. Agglutinated benthic foraminifera characteristic of bathyal environments have been described in the Carapeba/Pargo area (Azevedo et al., 1987a).

A mid to lower bathyal (500 - 2,000 m) association of benthic foraminifera has been described in the Coniacian/Santonian mudstones. It includes the following genera and species: *Bathysiphon*, *Gavelinella beccariformis*, *Gyroidinoides*, *Haplophragmoides*, *Glomospira corona*, *Glomospira charoides*, *Trochammina globigeriformis*, *Ammodiscus*, *Rzeakina epigona*, *Lenticulina*, *Gaudryina*, *Hormosina*, *Dorothia bulleta*,

*Cyclammina cancellata*, *Spiroplectamina*, and *Quinqueloculina lamarkina*.

The Maastrichtian mudstones contain a lower bathyal (1,000 - 2,000 m) association, including the following genera and species: *Bathysiphon*, *Ammodiscus*, *Haplophragmoides*, *Trochammina globigeriniformis*, *Spiroplectammina*, *Glomospira charoides*, and *Cyclammina cancellata*.

Paleobathymetric maps presented by Azevedo et al. (1987a) suggest paleodepths between 1,000 and 1,500 m for the Carapeba/Pargo area during the Coniacian/Santonian and Maastrichtian. These estimates differ from the deep neritic to upper bathyal (100 - 300 m) environment indicated for the late Cenomanian/early Turonian marls and mudstones, which underlie the Coniacian/Santonian turbidites along most of the studied area.

Organic geochemistry studies of the Coniacian to early Paleocene mudstones in the Campos basin have measured low values for total organic carbon content (typically less than 1 % by weight), which suggest deposition in a highly oxygenated environment (Guardado et al., 1990).

Palynomorph studies suggest a warm and humid climate for Coniacian to Maastrichtian time (Lima, 1983), which is also indicated by the common occurrence of plant debris in the cores of the Carapeba and Pargo fields. These local observations agree with global paleoclimatic reconstructions, which suggest a relatively warm and humid climate for the

Campos basin during most of the late Cretaceous (e.g. Parrish
and Curtis, 1982; Parrish et al., 1982).


## 3.3. FACIES CHARACTERIZATION


The description of 577 m of core recovered from 13 wells
(Fig. 3.3) permitted the recognition of five major facies in
the Coniacian/Santonian, Campanian and early Maastrichtian
successions of the Carapeba and Pargo fields. These facies
were distinguished chiefly on the basis of texture, physical
sedimentary structures, bioturbation, and soft-sediment
deformation. The facies are given the following names:


(1) **Facies CRP/PG-F1: UNSTRATIFIED, GRADED CONGLOMERATES
    AND SANDSTONES;**

(2) **Facies CRP/PG-F2: STRATIFIED SANDSTONES;**

(3) **Facies CRP/PG-F3: BIOTURBATED MUDSTONES;**

(4) **Facies CRP/PG-F4: DEFORMED, INTERBEDDED MUDSTONES AND
    FINE-GRAINED SANDSTONES;**

(5) **Facies CRP/PG-F5: DISORGANIZED, INTRACLASTIC
    MUDSTONES AND SANDSTONES.**


The abbreviations **CRP** and **PG** come from the names Carapeba
and Pargo respectively, and also have been used by PETROBRÁS
to designate most of the wells drilled in these two fields.

The facies identified in the Carapeba and Pargo fields are named CRP/PG-F1 to CRP/PG-F5, in order to differentiate them from those described in the Lagoa Parda field (**LP**; Chapter 4).

Figures 3.5 and 3.6 present the facies distribution in three extensively cored wells, which were selected in order to illustrate most of the facies recognized in the Carapeba/Pargo turbidite system. CRP/PG-F1 (unstratified, graded conglomerates and sandstones) is by far the volumetrically most important among all of the sandstone-bearing facies (CRP/PG-F1, CRP/PG-F2, CRP/PG-F4, and CRP/PG-F5), comprising 95 % of the cores of these rocks.

**Readers who do not need the descriptive details, sedimentological interpretation, well log response, and reservoir properties of each of the five facies can proceed to section 3.4 (High-resolution stratigraphy and reservoir geometry) or section 3.5 (Sedimentation evolution and controls).**

## 3.3.1. Facies CRP/PG-F1: unstratified, graded conglomerates and sandstones

**Description:**

CRP/PG-F1 includes essentially unstratified conglomerates, conglomeratic sandstones, and very-coarse- to medium-grained sanstones (Fig. 3.7), which typically comprise normally graded beds ranging in thickness from 0.5 to 12 m

LEGEND OF LITHOLOGY, SEDIMENTARY STRUCTURES, TRACE FOSSILS, AND OTHER SYMBOLS USED IN FIGURES 3.5, 3.6, 4.6, 4.7, AND 5.7:

## Lithology

■ Mudstone

▦ Siltstone

▦ Medium- to very fine-grained sandstone

▦ Very coarse- to coarse-grained sandstone

▦ Pebble- to granule-rich conglomerate

▦ Boulder- to cobble-rich conglomerate

■ Intraclastic mudstone

## Sedimentary structures

▦ Unstratified

▦ Parallel-stratification

▦ Ripple cross-stratification

▦ Dish structure

▦ Pillar structure

▦ Flame structure

Median grain-size: **p** = pebble, **g** = granule, **vc** = very coarse sand, **c** = coarse sand,

**m** = medium sand, **f** = fine sand, **vf** = very fine sand, **s** = silt, **c** = clay

## Dominant trace fossils

**Zo** = *Zoophycos*

**He** = *Helminthopsis*

**Th** = *Thalassinoides*

**Pl** = *Planolites*

**Op** = *Ophiomorpha*

## Other symbols

▦ Boulder- to cobble-sized, mud intraclasts

▦ Pebble- to granule-sized, mud intraclasts

◁▱▷ Lenticular, discontinuous conglomerates

—— Sharp contact

⌒ Erosional contact

⌒ Loaded contact

—? Poorly-defined contact

⊐⊔⊏ Contact disrupted by fluid escape

〜 Slumps

*θ* Burrows

Fig. 3.5 - Typical facies and respective well log responses of the Carapeba/Pargo turbidite system. Explanation of symbols used in this figure is provided in page 70.

# PG - 4
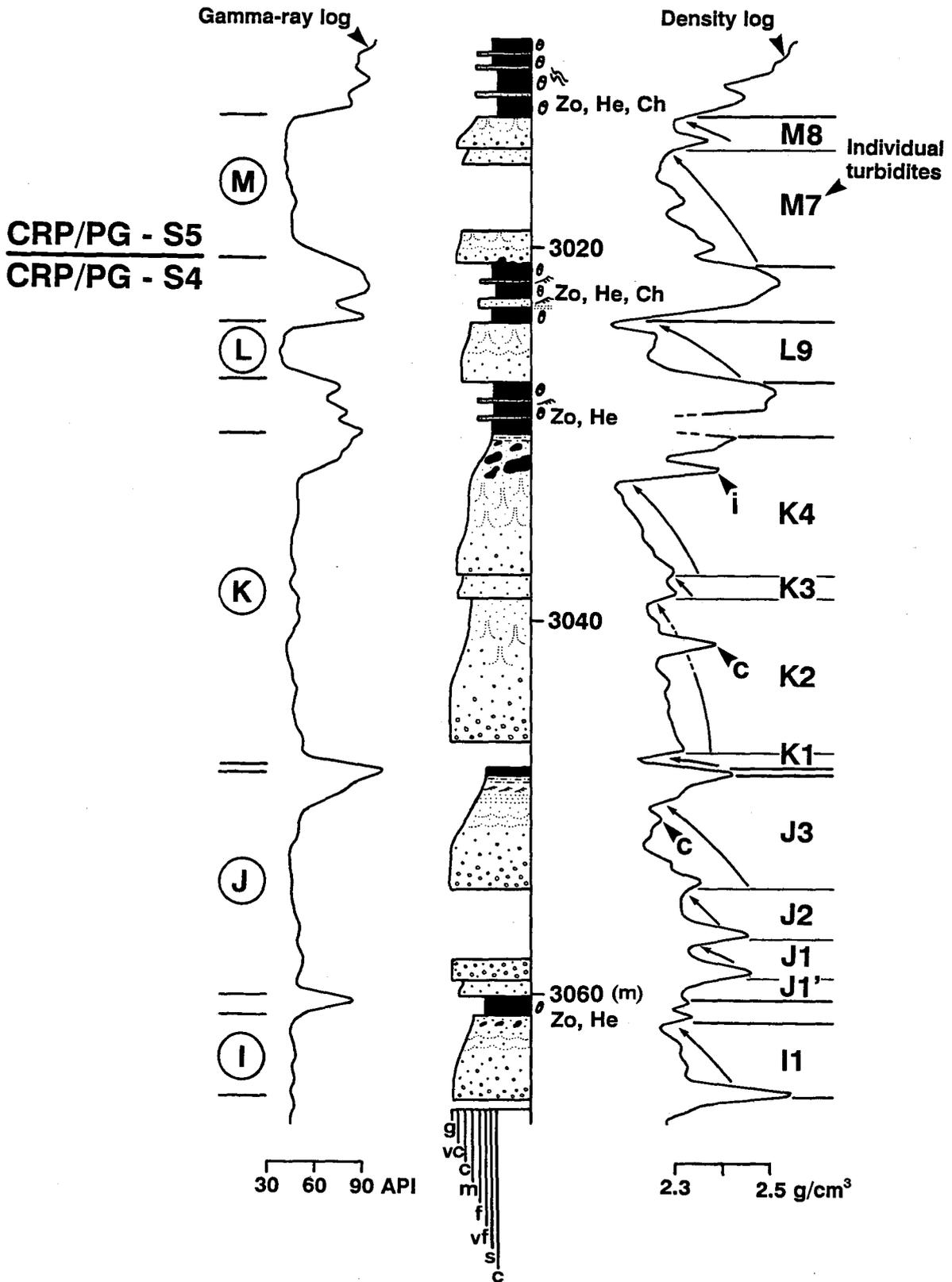
Fig. 3.6 - Typical facies and respective well log responses of the Carapeba/Pargo turbidite system. Explanation of symbols used in this figure is provided in page 70.

# CRP - 14

Gamma-ray log

CAMPANIAN

CONIACIAN/SANTONIAN

S/C ►

Density log

Zo, He, Th, Pl

(T)

Zo, He, Th, Pl

T2

3000

(S)

Individual
turbidites ◄

S3 ◄

S2

(R)

Zo, He

R3

R2

3020

R1

(Q)

Q3

Q1

CRP/PG - S6

CRP/PG - S5

Zo, He

Zo, He

P8

◄C

P7

(P)

Zo, He

P3

3040

P2

Zo, He

O5

(O)

O4

O3

Zo, He

N5

◄C

N4

(N)

3060
(m)

N3

30   60   90 API

p
g
vc
c
m
f
vf
s
c

2.3      2.5 g/cm³
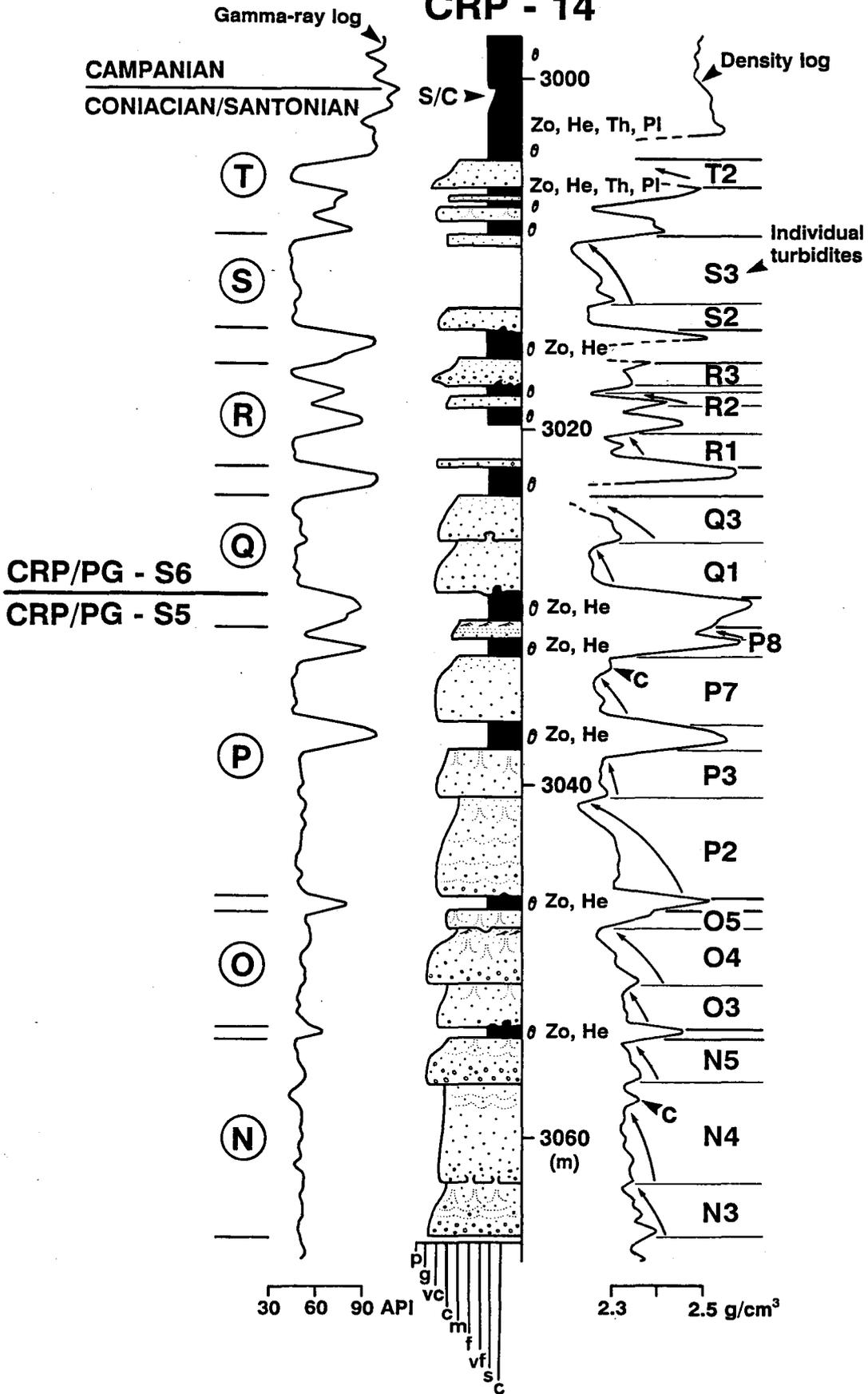
Fig. 3.7 - **FACIES CRP/PG-F1:** Unstratified conglomerates and sandstones.


(a) Pebble- to granule-rich conglomerate (pebble diameter < 1 cm). Turbidite P2; well CRP-11; depth: 3,016.8 m.


(b) Very coarse-grained sandstone. Turbidite Q1; well CRP-11; depth: 2,995.0 m.


(c) Coarse-grained sandstone with pillar structures (**p**). Sediment comprising pillars is coarser-grained and better-sorted. Turbidite R1; well CRP-11; depth: 2,986.5 m.


(d) Medium-grained sandstone with pillar structures (**p**). Sediment comprising pillars is coarser-grained and better-sorted. Turbidite K4; well PG-4; depth: 3,034.8 m.

a     1 cm

b     1 cm

c  p→     1 cm

d  ←p     1 cm
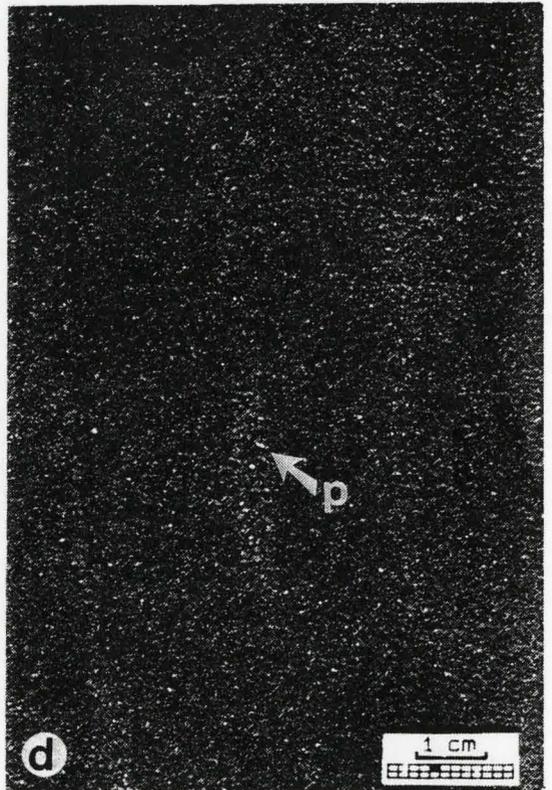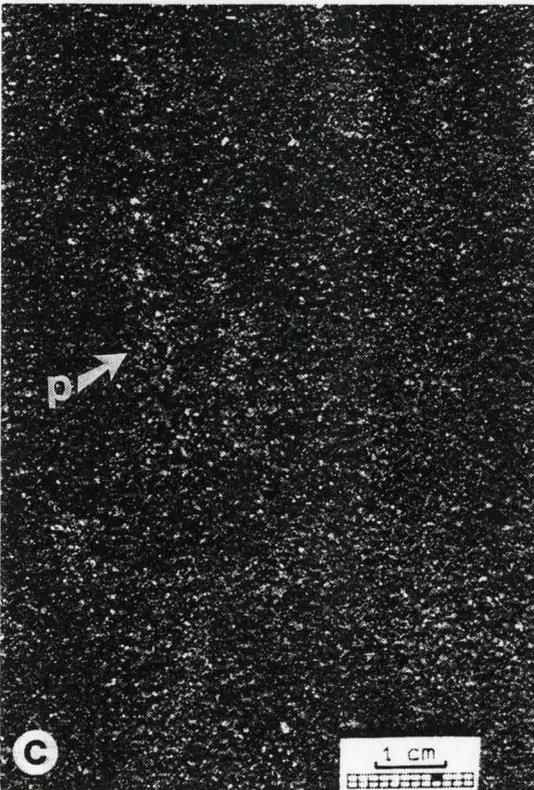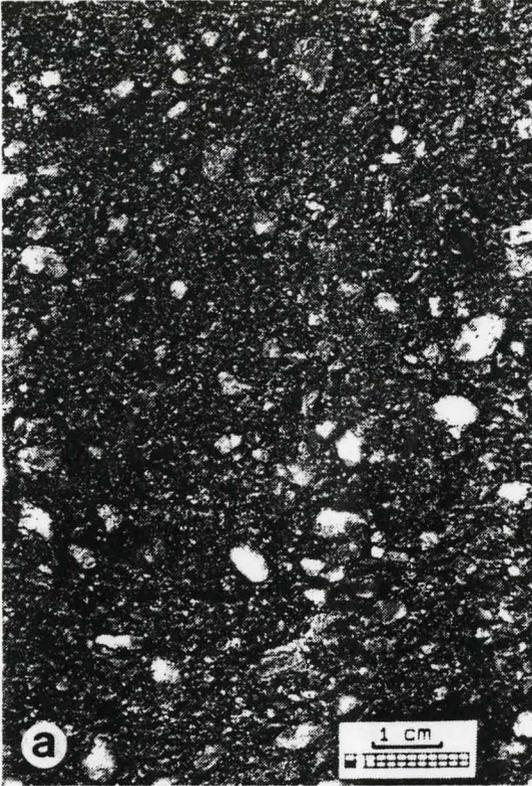
(Figs. 3.5, 3.6, 3.8, 3.9 and 3.10). Most of the cored graded beds are 2 to 4 m thick, starting at the base with conglomeratic sandstones or very coarse-grained sandstones, and grading upward to coarse- and medium-grained sandstones. CRP/PG-F1 also includes thin (mostly < 1 m) interbeddings of bioturbated mudstones, which are similar to the mudstones described for the facies CRP/PG-F3. A few graded beds of CRP/PG-F1 are capped by thin (< 1 m) parallel- and ripple cross-stratified, fine- to very fine-grained sandstones and siltstones (Fig. 3.10).

The conglomerates recorded in CRP/PG-F1 are 0.1 to 3.5 m thick, and are characterized by a gravel content of at least 30 %, which includes granules and pebbles up to 2 cm diameter (Fig. 3.7a). Conglomeratic sandstones contain 5 to 30 % granules and small pebbles (< 1 cm), supported by a matrix of very-coarse- to coarse-grained sand. They tend to be thicker than the conglomerates, with a maximum of 6 m. Most of the graded beds consist of very coarse- to medium-grained sandstones, characterized by a gravel content smaller than 5 % (Figs. 3.7b, 3.7c and 3.7d). Mudstone and marl intraclasts, typically 1 - 3 cm diameter (but sometimes exceeding 10 cm), are found in a few graded beds, preferentially in their uppermost part (medium to coarse-grained sandstones) (Fig. 3.8).

The rocks that comprise CRP/PG-F1 are also characterized by poor sorting ($\sigma_I$ = 1.3 - 1.7; Folk and Ward, 1957);

Fig. 3.8 - **FACIES CRP/PG-F1:** Sandstone composed of three amalgamated turbidites; their bases are indicated by **K2**, **K3**, and **K4**. The lowermost turbidite (K2; at least 7.5 m thick) shows a gradation from granule-rich conglomerate to medium-grained sandstone. Zones strongly cemented by calcite are indicated by **c**. Turbidite K3 (1.3 m thick) comprises very coarse- to coarse-grained sandstone. Turbidite K4 (8.0 m thick) shows a continuous gradation from conglomeratic sandstone to finely-laminated mudstone (**m**). Most of turbidite K4 is composed of medium- to fine-grained sandstone showing pillar (**p**) and stress pillar (**s**) structures, and also large (up to 30 cm diameter) mudstone and marl intraclasts (**i**). Sandstone K; well PG-4; depth: 3,029.1 - 3,046.4 m.
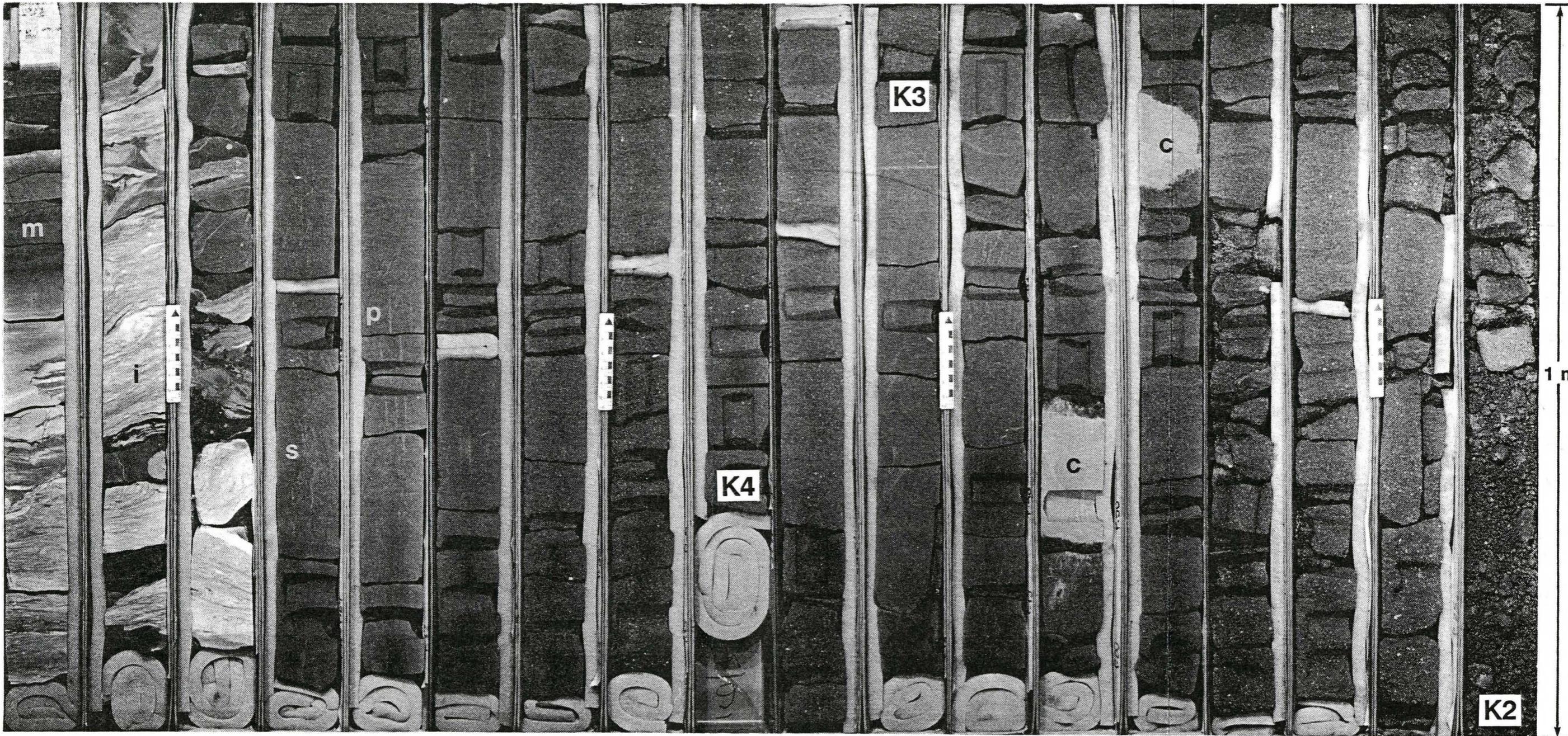
Fig. 3.9 - **FACIES CRP/PG-F1 AND CRP/PG-F4:** Sandstone composed of two amalgamated turbidites (their bases are indicated by **Q1** and **Q3**), which overlies a 4.8 m succession of deformed mudstones and thin-bedded sandstones. Turbidite Q1 (6.2 m thick) comprises a gradation from unstratified, conglomeratic sandstone to parallel-laminated, medium-grained sandstone. Zones strongly cemented by calcite are indicated by **c**. Turbidite Q3 (1.6 m thick) is composed of unstratified coarse- to medium-grained sandstone with mud intraclasts, and parallel-stratified, fine-grained sandstone. The contact between Q1 and Q3 is loaded. The mudstones show convoluted sand injection structures. Well CRP-11; depth: 2,988.8 - 3,001.1 m.

TOP

Q1

C

Q3

C
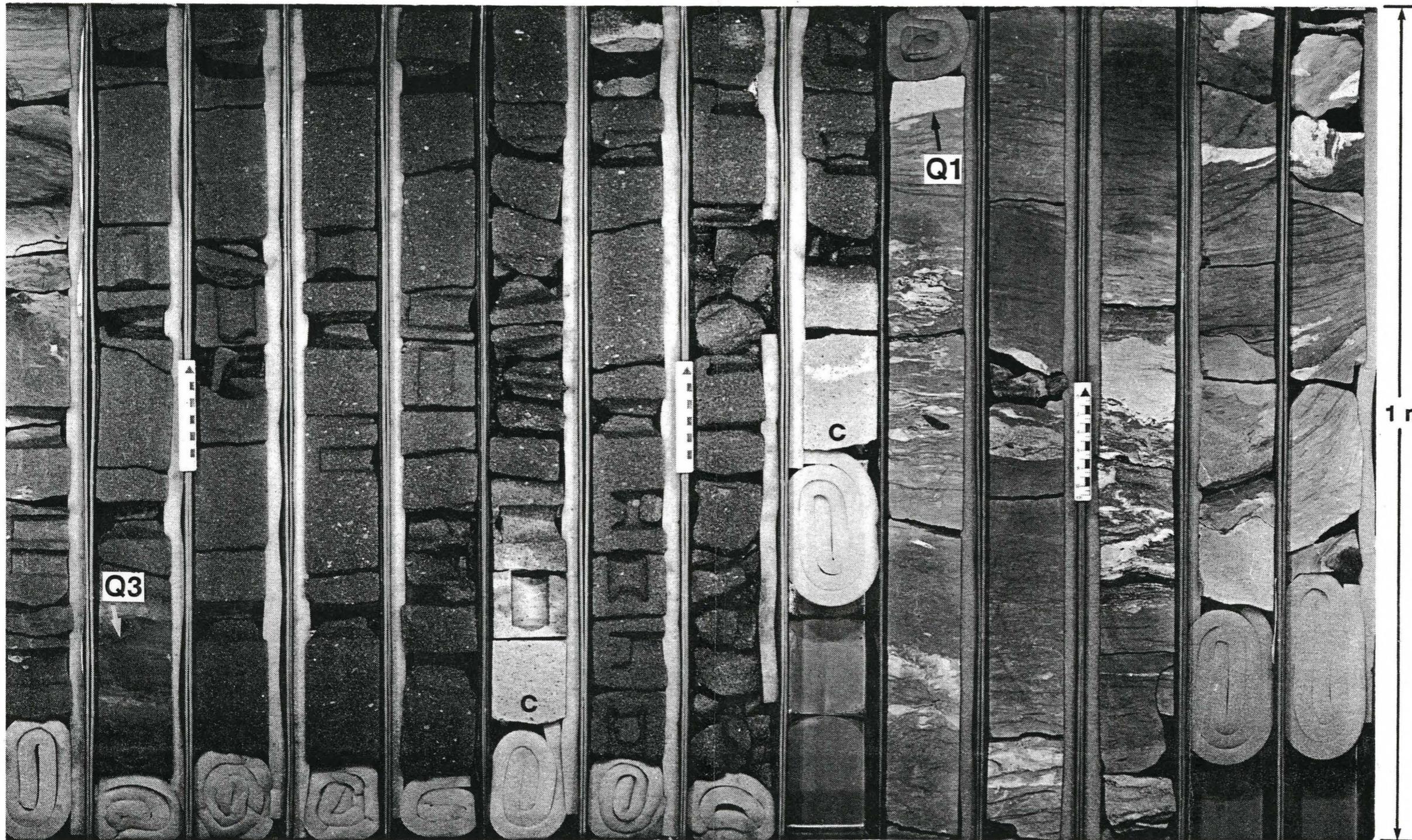
1 m

BASE

Fig. 3.10 - **FACIES CRP/PG-F1:** Individual turbidite J3 (7 m thick) composed of (from bottom to top): unstratified, granule-rich conglomerate to medium-grained sandstone; parallel-stratified, fine-grained sandstone (**p**); ripple cross-stratified, very fine-grained sandstone (**r**); parallel-laminated siltstone (**s**); and blocky mudstone (**m**). Dish structures (**d**) occur in a zone strongly cemented by calcite, which is located in the upper part of the unstratified sandstone (medium-grained sand). Well PG-4; depth: 3,048.0 - 3,055.0 m.
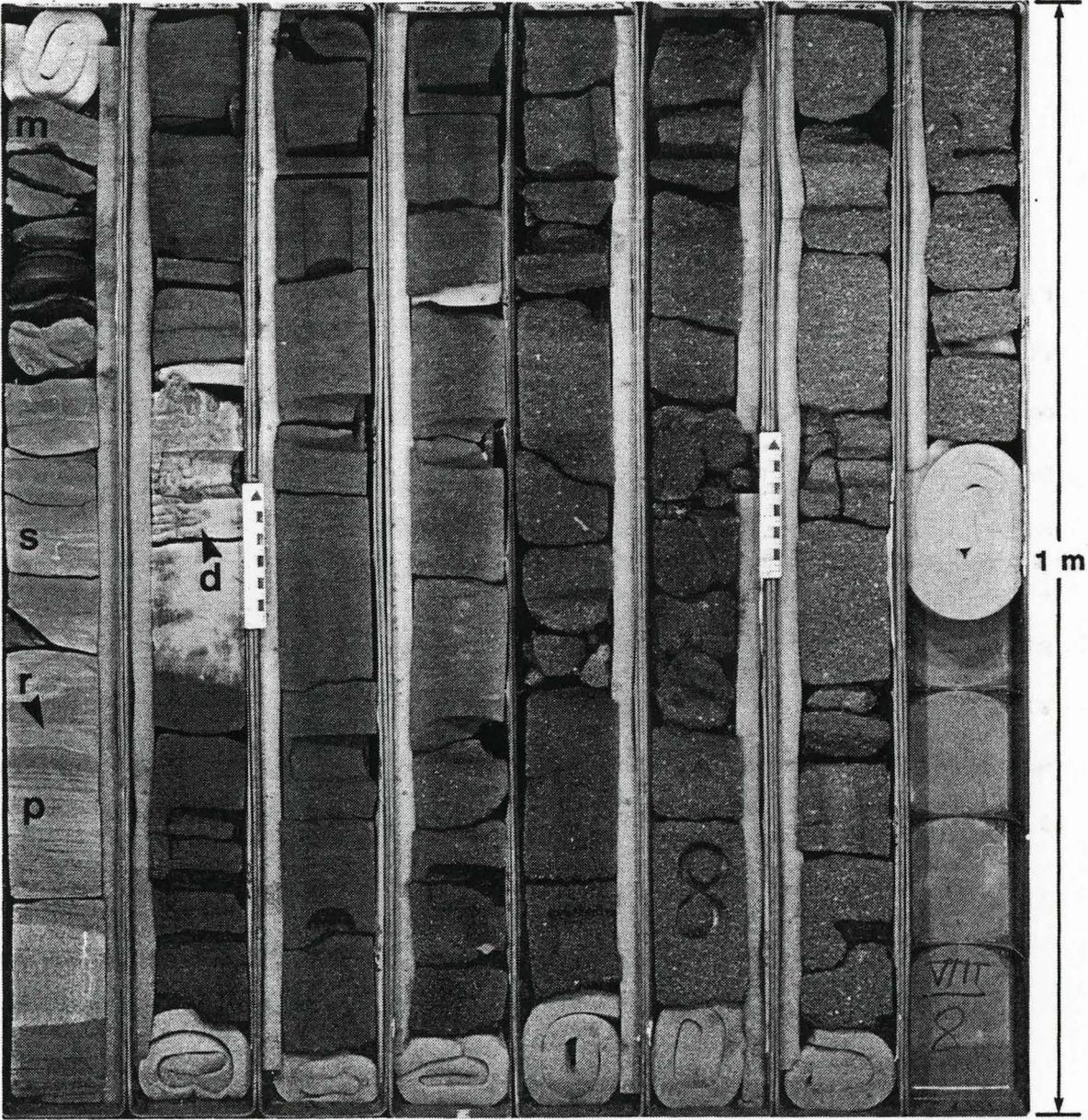
subangular to angular grains (Powers, 1953); and low mud matrix content (2 - 5 % for conglomerates and conglomeratic sandstones, and 4 - 8 % for very coarse- to medium-grained sandstones).

The contacts between graded beds and underlying mudstones are typically sharp (e.g. Fig. 3.9), but they may be deformed by loading, including the development of flame structures (Fig. 3.11a) and centimeter-sized, ball-and-pillow structures. The graded beds capped by stratified, finer-grained sandstones and siltstones may grade continuously to mudstones (Fig. 3.10), or be truncated by the coarser-grained base of the next graded bed (Fig. 3.11b). However, the most common case is represented by graded beds containing unstratified, coarse- to medium-grained sandstones at the top, which are truncated by the subsequent graded bed, or present a sharp contact with the overlying mudstones (Figs. 3.5 and 3.6). The amalgamation of successive graded beds results in the development of sandstone packages up to 78 m thick without interbedded mudstones (Fig. 3.4).

The graded beds of CRP/PG-F1 are almost exclusively normally graded (Figs. 3.5 and 3.6). Two types of normal grading are recognized: content grading and coarse-tail grading (Middleton, 1967). Content grading, characterized by the upward reduction of the mean grain size, occurs preferentially in graded beds starting at the base with very-coarse grained sandstone. The graded beds containing

Fig. 3.11 - **FACIES CRP/PG-F1:** (a) Inverse grading from coarse-grained sandstone to granule-rich conglomerate in a basal zone up to 5 cm thick. Flame structure occurs at the loaded contact with underlying mudstone. Turbidite R3; well CRP-14; depth: 3,017.4 m.

(b) Loaded contact between unstratified, very coarse-grained sandstone, and thin (4 cm thick), ripple cross-stratified, fine-grained sandstone. Contact between turbidites O4 and O5; well CRP-14; depth: 3,048.0 m.
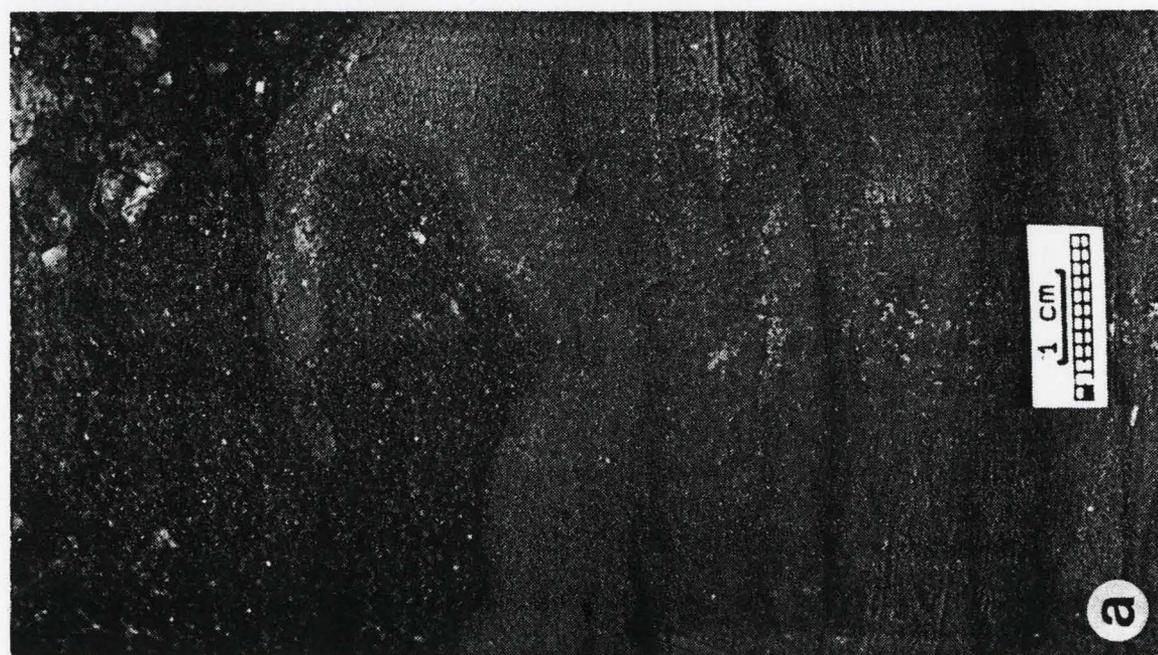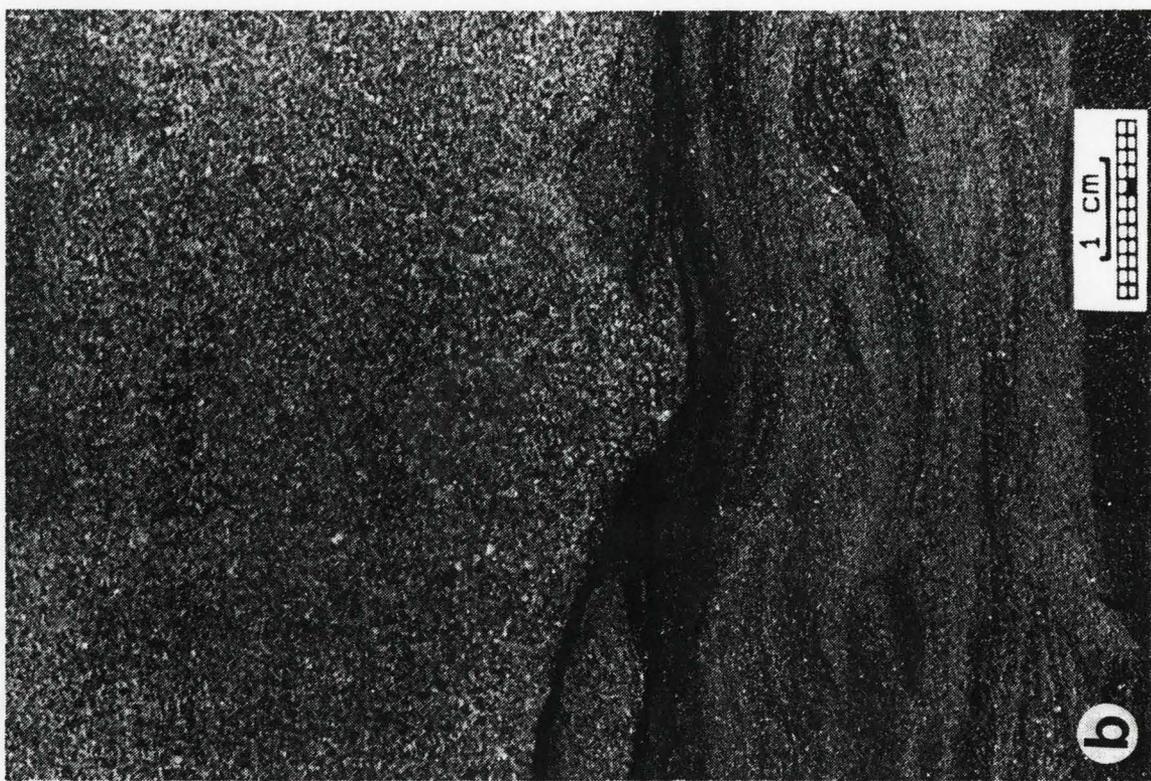
conglomerates and conglomeratic sandstones typically show coarse-tail grading in their lowermost portions, where the size (and proportion) of the coarsest grains (gravel grade) diminishes upwards, while the rest of the population remains roughly constant. Very few examples of inverse grading were recognized; where present, there is a gradation from coarse-grained sandstone to conglomerate in a basal zone up to 5 cm thick (Fig. 3.11a). Inverse grading occurs at the base of graded beds that become normally graded upwards (e.g. sandstone R3; Fig. 3.6).

Fluid escape structures are very common in this facies, including mostly pillar and dish structures (Figs. 3.12 and 3.13). Flat to strongly concave-upward dish structures tend to be abundant in graded beds that are thicker than 3 m, and contain a high proportion of poorly-sorted very coarse-grained and conglomeratic sandstones (Figs. 3.12 and 3.13a). Pillar structures are more widespread than dish structures, occurring both in the coarser- and finer-grained portions of the graded beds (Fig. 3.7c, 3.7d, 3.8, 3.12, and 3.13b). They range from small (< 2 cm wide) pillars located between the upward-curving margins of dish structures (Fig. 3.12) to large (up to 3 cm wide and 30 cm long) vertical or steeply inclined fluid escape channels (Figs. 3.8 and 3.13b). The longer (> 10 cm) pillar structures occur preferentially in better-sorted medium- to coarse-grained sandstones (Fig. 3.8). The sediments comprising the pillars are composed of coarser sand grains and have a

Fig. 3.12 - **FACIES CRP/PG-F1:** Granule-rich conglomerates, and very coarse- to coarse-grained sandstones containing abundant fluid escape structures. The larger-scale picture shows that fluid escape structures may affect two juxtaposed turbidites (N3 and N4). Well CRP-14; depth: 3,062.0 - 3,065.8 m.

TOP

N4

N3
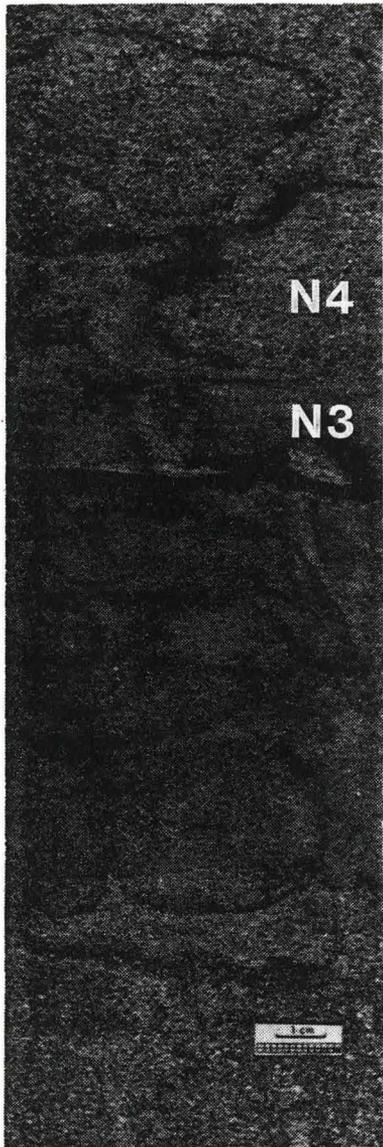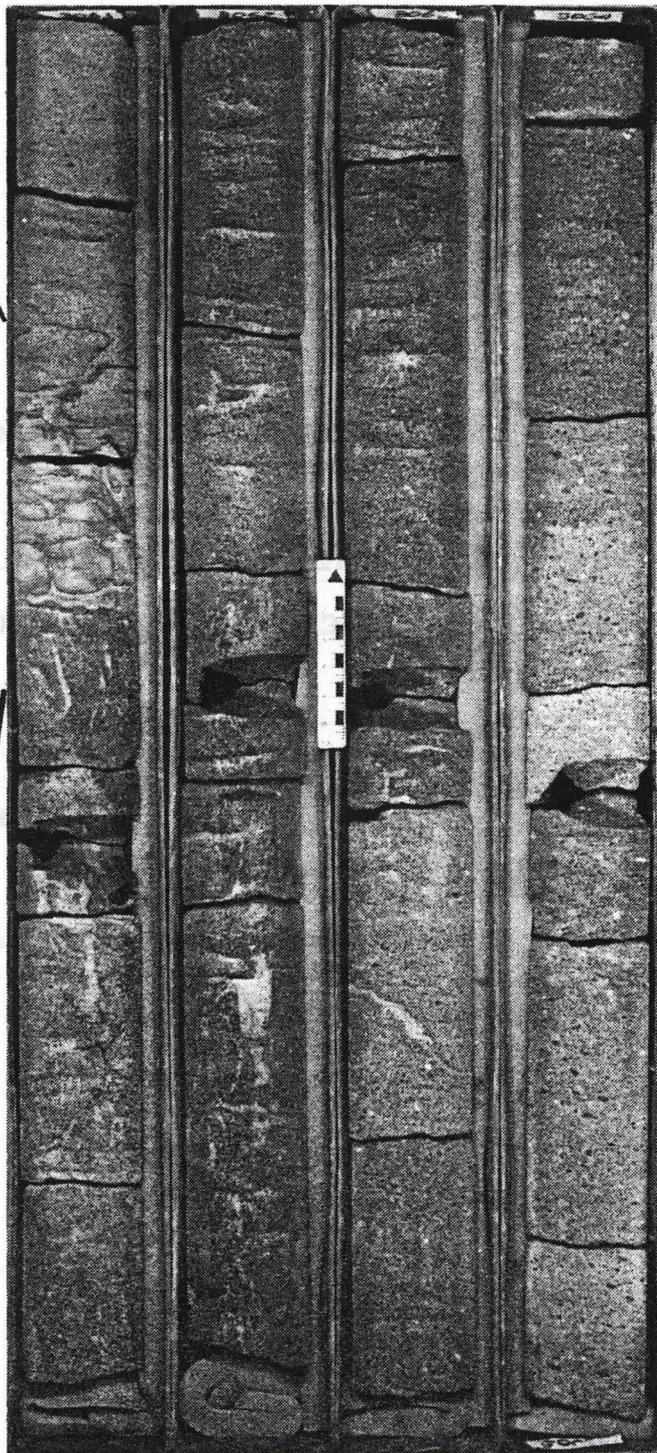
1 m

BASE

Fig. 3.13 - **FACIES CRP/PG-F1:** Fluid escape structures.


(a) Very coarse-grained sandstone with dish structures (**d**).
Turbidite N4; well CRP-11; depth: 3,024.0 m.


(b) Coarse-grained sandstone with pillars (**p**) strongly
cemented by calcite. Differential cementation by calcite is
also observed in the surrounding, undisturbed sediment.
Turbidite O5; well CRP-14; depth 3,048.0 m.
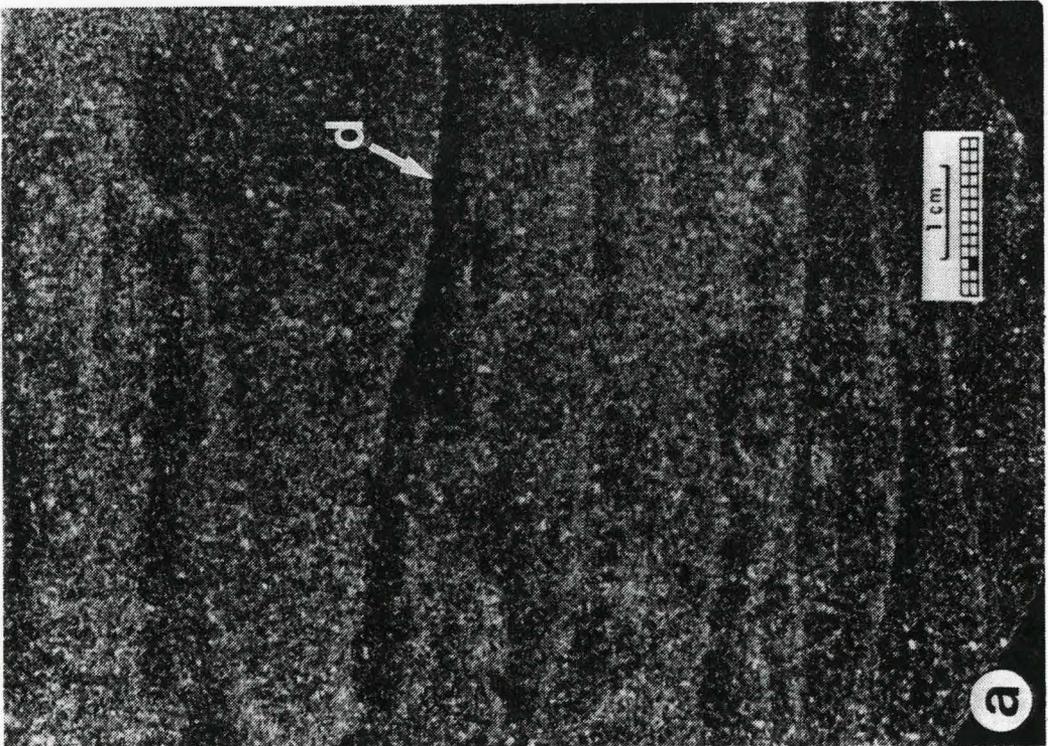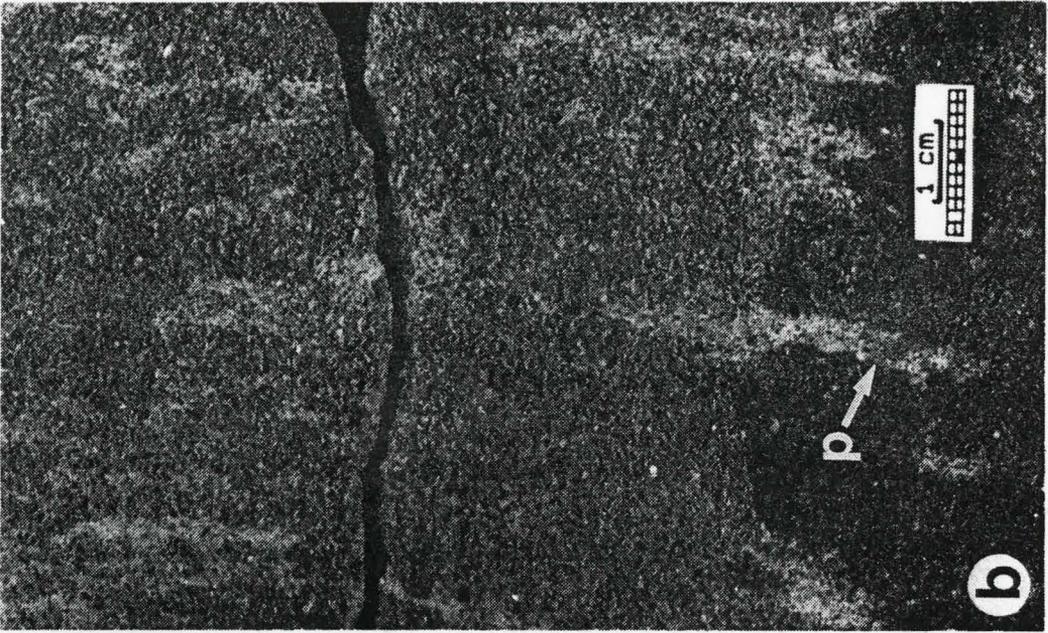
much lower mud content than the surrounding undisturbed sediments (Figs. 3.7c and 3.7d). "Stress" pillars (Lowe, 1975), characterized by sets of narrow, irregularly-shaped, light-coloured streaks of sand also have been recognized (Fig. 3.8).

Petrographic studies of typical rocks of the facies CRP/PG-F1 (Freitas, 1987; Becker et al., 1988; Moraes, 1989) have described the framework of sandstones and conglomerates as composed mainly of quartz (monocrystalline and polycrystalline grains), feldspar (chiefly microcline, with subordinate plagioclase, orthoclase and perthite), and fragments of quartzo-feldspathic, high grade metamorphic rocks. The average content of quartz (Q), feldspars (F) and lithic fragments (L) vary according to the grain size distribution (Freitas, 1987): $Q_{54}F_{32}L_{14}$ for conglomerates, conglomeratic sandstones, and very coarse-grained sandstones; $Q_{56}F_{34}L_{10}$ for coarse-grained sandstones; and $Q_{56}F_{37}L_{07}$ for medium-grained sanstones. According to McBride's (1963) classification, these are arkoses and lithic arkoses, which suggest a continental block provenance (Dickinson and Suczek, 1979).

Accessory components are represented by sand-sized mud intraclasts, biotite, muscovite, bioclasts (planktonic and benthic foraminifera, pelecypods, coccoliths, and radiolaria), glauconite, garnet, tourmaline, zircon, and epidote. Except for the mud intraclasts (up to 30 %), the accessory minerals

represent less than 1 % of the rocks. There is less than 10 % of sand-sized mud intraclasts in the conglomerates and sandstones, with the exception of the uppermost graded beds cored in the Pargo field (sandstones L, M, N, O, and P; Fig. 3.4), which have a mud intraclast content averaging 20 % (range 15 - 30 %) (Becker et al., 1988).

The diagenetic mineral assemblage includes mostly opal/microquartz and calcite cements, and also very subordinate (< 1 %) amounts of quartz, feldspar, anatase and pyrite cement (Freitas, 1987; Becker et al., 1988; Moraes, 1989). The opal and microquartz cements were formed by the silicification of mud intraclasts, which have undergone strong mechanical compaction, thus producing large amounts (up to 30 %) of compaction matrix in the uppermost sandstones beds of the Pargo field. The calcite cement content averages 5 %, but may reach 32 % (Freitas, 1987). Intense cementation by calcite is more common along the contacts between the conglomerates or sandstones and the interbedded mudstones (Fig. 3.9). However, zones with strong calcite cementation (up to 30 cm thick) also may occur within graded beds, usually showing sub-spherical shapes (Figs. 3.8). These restricted, randomly distributed calcite-rich zones represent remnants of an original widespread calcite cement, which was partially dissolved by organic acids in deep burial conditions (Moraes, 1989).

**Interpretation:**

The thick, unstratified, coarse-grained graded beds of CRP/PG-F1 probably were formed by the rapid deposition of suspended load carried by high-concentration (or high-density, > 1.1 g/cm$^3$) turbidity currents (Kuenen and Migliorini, 1950; Middleton, 1967, 1970; Lowe, 1982). Concentration has a bearing on flow velocity (as demonstrated experimentally by Middleton, 1966a, 1966b), and therefore competence on basin slopes. High-density turbidity currents would be able to transport coarse-grained sediments on both steep and gentle slopes (Lowe, 1982).

Except for a very crude stratification suggested by concentrations of dish structures in some conglomeratic and very coarse-grained sandstones (Figs. 3.12 and 3.13a), the only organization displayed by CRP/PG-F1 is grading. This localized crude stratification is probably related to different rates of deposition from the suspended load. Thus, the deposition of CRP/PG-F1 took place mostly at high suspended-load fallout rates, which did not allow a sufficient time for the development of bed traction (Walker, 1978; Lowe, 1982).

Normal grading is well-defined throughout most of the turbidites of the Carapeba/Pargo turbidite system. Two types of grading are recognized: distribution grading, suggesting that late-stage turbulence may have retarded deposition of the finer grains (coarse- to medium-grained sand); and coarse-tail grading, indicating that at least the coarser fraction of the

sediment cloud (very coarse-grained sand, granules and small pebbles) may have settled as a non-turbulent suspension (Middleton, 1967). The thin (< 5 cm) inverse-graded deposits at the base of a few graded beds (Fig. 3.11a) record the very localized development of traction carpets (Hein, 1982; Lowe, 1982), where concentrated mixtures of coarse sediments are maintained at the base of the turbidity current by grain collisions (dispersive pressure; Bagnold, 1956).

The higher content of sand-sized mud intraclasts in some thinner-bedded and more distal turbidites in the Pargo field (sandstones L, M, N, O, and P; Fig. 3.4) suggests a trend of dilution in the high-density turbidity currents responsible for the deposition of the graded beds of CRP/PG-F1. Fragments of mudstones and marls eroded from the margins and bottom of the trough where the turbidites are confined were incorporated into the flows and gradually broken into smaller pieces. These finer muddy grains would better survive abrasion in turbidity currents of lower concentration, but still dense enough to transport granules and very coarse-grained sand. On the other hand, the larger pebble- to boulder-sized mud and marl intraclasts found in the uppermost part of some graded beds (Fig. 3.8) probably were derived from the erosion and collapse of the canyon margins, and were deposited within a very short distance. These large intraclasts could eventually be incorporated into the deposits of the same turbidity current that induced canyon wall collapse.

Fluid escape structures (dish and pillar structures; Figs. 3.12 and 3.13) were generated by the expulsion of fluids from the rapidly deposited turbidites (Lowe and LoPiccolo, 1974; Lowe, 1975; Hein, 1982). They are particularly abundant in the thicker (> 3 m) graded beds, where a larger volume of water permeated through unstable, loosely-packed sediments. The dominance of dish structures over pillars in some graded beds suggests the presence of a crude stratification in these rocks (Figs. 3.12 and 3.13a), which made the escaping fluid follow a tortuous pathway. On the other hand, the exclusive development of long pillars (Fig. 3.8) characterizes a very homogeneous fabric, which allowed quick, vertical dewatering. The absence of fluid escape structures in the uppermost portion of some graded beds, both in unstratified- and stratified sandstones, suggests that dewatering may have taken place simultaneously with sedimentation. However, fluid escape structures affecting two juxtaposed depositional units also have been identified, indicating that dewatering may have occurred during and after the deposition of some graded beds (Fig. 3.12).

## 3.3.2. Facies CRP/PG-F2: stratified sandstones

**Description:**

CRP/PG-F2 comprises thin-bedded, parallel- and ripple cross-stratified, fine- to very fine-grained sandstones and

siltstones (Fig. 3.14), which occur interbedded with bioturbated mudstones (Fig. 3.5). Most of the sandstone beds are thinner than 10 cm, but thicker (up to 80 cm) successions also can be recognized. Their basal and top contacts with the interbedded mudstones are typically sharp (Fig. 3.14).

The fine- and very fine-grained sandstones in this facies are characterized by poor sorting ($\sigma_I > 1.2$), relatively high silt (> 10 %) and clay (> 5 %) content, and intense calcite cementation (> 10 %). The common occurrence of sand-sized mud intraclasts, organic matter, and mica flakes help to define the sandstone stratification. Convolute lamination is largely found in parallel- and cross-laminated sandstones (Fig. 3.14c). Petrographic studies of the fine-grained sandstones in the Carapeba field indicate an average composition of $Q_{64}F_{33}L_{03}$ (Freitas, 1987).

Bioturbation is common in the sandstones of CRP/PG-F2, but is not as pervasive as in the interbedded mudstones. Resting (*Conichnus* ?) and escape trace fossils occur in the uppermost portion of the sandstones (Fig. 3.14d), along the contacts with mudstones. Also *Thalassinoides* and *Planolites* may be found in the top portion of sandstones or in the interior of siltstones (Fig. 3.14c).

## Interpretation:

CRP/PG-F2 contains Bouma's (1962) divisions, mainly $T_{bcde}$, $T_{bc}$, $T_{cd}$ (Fig. 3.14a), and $T_c$ (Fig. 3.14d). They were probably

Fig. 3.14 - **FACIES CRP/PG-F2**: Stratified sandstones.


(a) Ripple cross-stratified, fine-grained sandstone (**c**), and parallel-laminated siltstone (**d**) ($T_{cd}$ turbidite) overlying bioturbated mudstone containg *Zoophycos* (**Zo**). Well PG-4; depth: 3,021.5 m.


(b) Parallel- and ripple cross-laminated siltstone. Well RJS-228; depth: 3,059.5 m.


(c) Fine-grained sandstone with convolute lamination, overlain by parallel-laminated siltstone. Bioturbation by *Thalassinoides* (**Th**) and *Planolites* (**Pl**) in the top portion of the sandstone, and in the siltstone. Well RJS-228; depth: 3,046.4 m.


(d) Ripple cross-stratified, fine-grained sandstone overlain by bioturbated mudstone. Escape (**e**) and resting (**r**) trace fossils occur in the top portion of the sandstone. Well RJS-228; depth: 3,067.4 m.
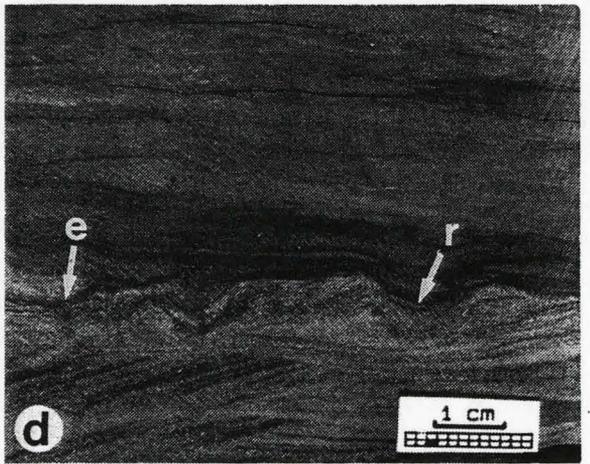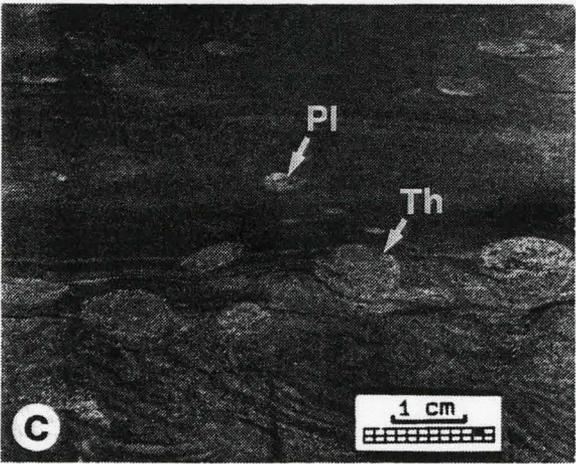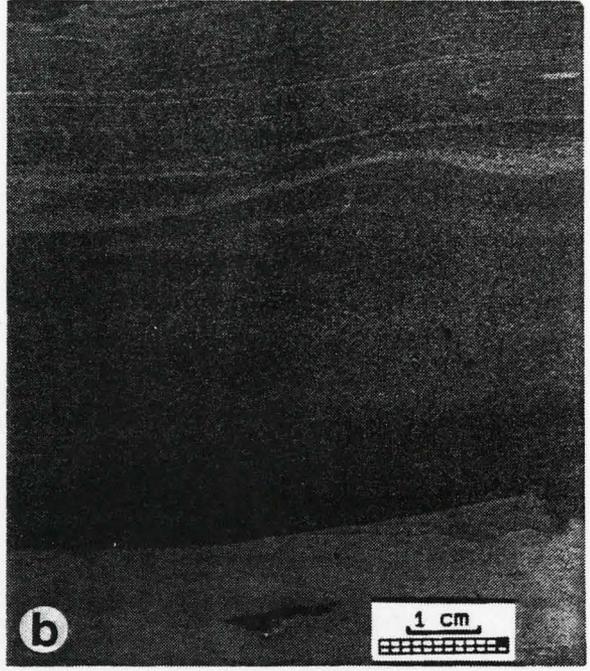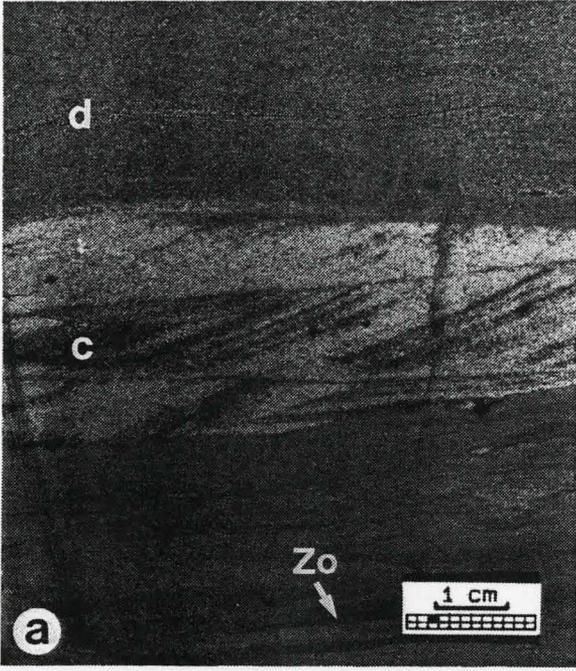
deposited by low-density turbidity currents (Lowe, 1982), with slow deceleration permitting the transfer of sediment from suspended to bed load, followed by traction sedimentation of the Bouma $T_b$ (parallel-laminated) and $T_c$ (ripple cross-laminated; Figs. 3.14a and 3.14d) divisions (Walker, 1965). The overlying parallel-laminated, silty $T_d$ division (Fig. 3.14a) reflects the effects of some traction or near-bed shear sorting during deposition, and the laminated to homogeneous, muddy $T_e$ division is formed by direct suspension sedimentation of the finest sediment transported by the turbidity current (Walker, 1965).

Low-density turbidity currents may continue as residual currents following the deposition of the coarse-grained load of high-density turbidity currents (Lowe, 1982). The resulting low-density turbidity current would be able to deposit its finer load immediately above coarser-grained turbidites (Fig. 3.10), or to bypass areas of high-density turbidity current sedimentation.

### 3.3.3. Facies CRP/PG-F3: bioturbated mudstones

**Description:**

CRP/PG-F3 embraces a group of fine-grained rocks, including mainly mudstones (silt/clay ratio between 1/3 and 2/3) and siltstones, and also subordinate shales. Most of these rocks are light to dark greenish-gray, but the siltier

deposits contain more calcite and are paler in colour. The most important feature exhibited by this facies is the pervasive bioturbation (Fig. 3.15). The degree of bioturbation ranges between 30 and 90 % by volume in most of the cores.

The trace fossil assemblage is largely dominated by the ichnogenus *Zoophycos*, characterized by delicate and well-preserved, 1 to 8 mm wide, mostly horizontal to gently inclined spreiten structures (Figs. 3.16 to 3.18). The *Zoophycos*-making organisms seem to be the first colonizers of the fine-grained sediments in the Carapeba and Pargo areas. The *Zoophycos* ichnogenus is extremely abundant in the entire Coniacian/Santonian and Campanian successions, and is recorded in most of the early Maastrichtian cores.

*Helminthopsis* is the second most widespread ichnogenus. The distribution of its tiny, vermicularly-tangled dark fills is mostly patchy (Fig. 3.16a). *Helminthopsis*-makers occupied mainly unburrowed muddy facies (Fig. 3.16a and 3.17a), but also frequently reburrowed *Zoophycos* (Fig. 3.17b) and *Thalassinoides* (Fig. 3.18a) traces.

*Thalassinoides* is a widespread ichnogenus, but almost always subordinate to *Zoophycos* and *Helminthopsis*. However, the colonization by *Thalassinoides* is particularly pervasive in the some intervals in the uppermost Santonian, Campanian and early Maastrichtian successions (Fig. 3.18). Two major types of *Thalassinoides* are recognized: (1) robust, mud-filled types that are frequently reburrowed by *Helminthopsis* (Fig.

Fig. 3.15 - **FACIES CRP/PG-F3 AND CRP/PG-F5:** Bioturbated mudstones and thin-bedded, disorganized intraclastic sandstones (**is**). The intraclastic sandstones show sharp basal contacts, and poorly-defined upper contacts due to the intense bioturbation. **S/C** is a clay-rich, dark mudstone, located at the boundary between Santonian and Campanian; it makes a high-radioactivity well log marker, which can be correlated across most of the study area. Well CRP-11; depth: 2,961.0 - 2,966.0 m.
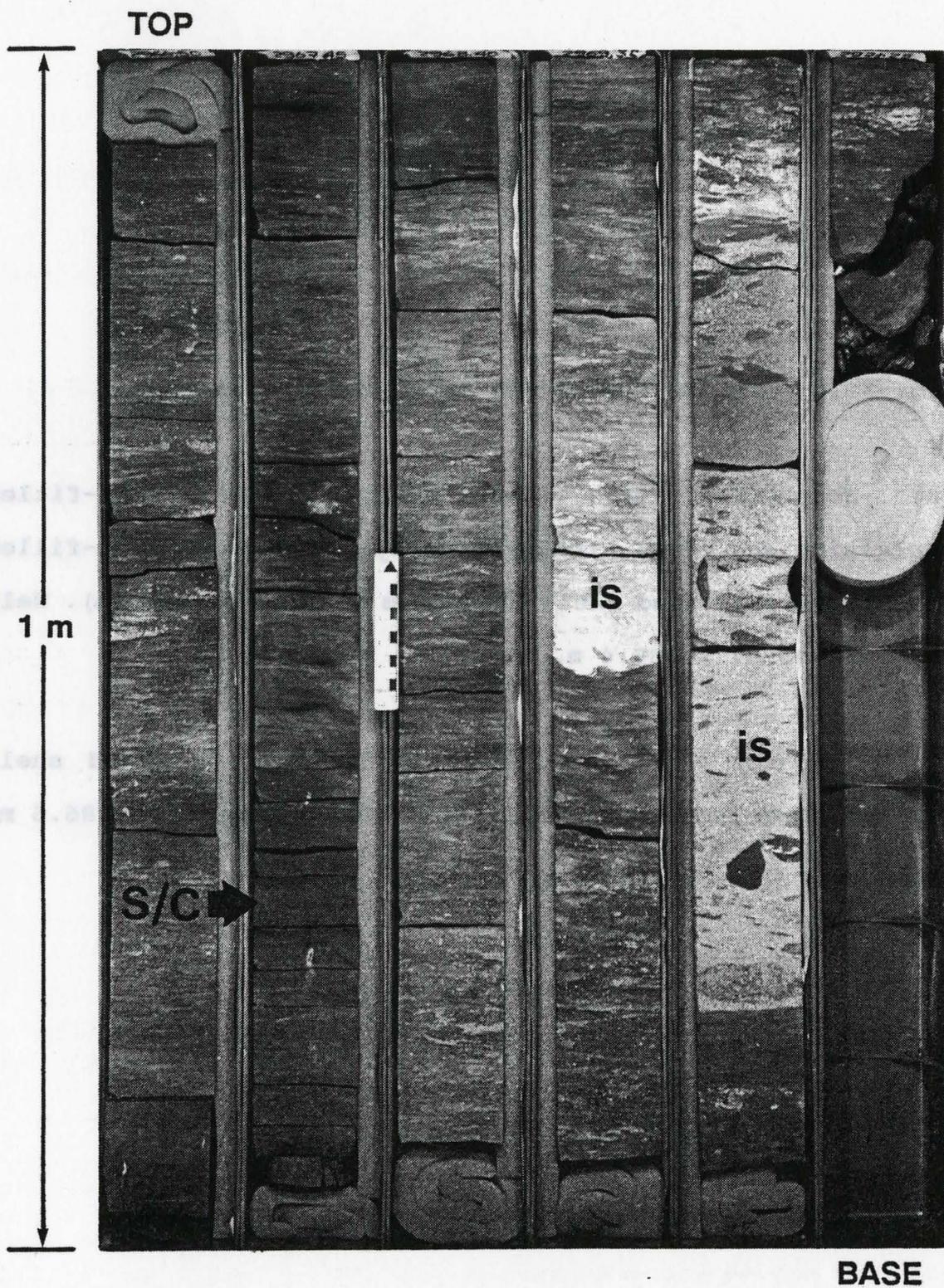
Fig. 3.16 - **FACIES CRP/PG-F3**: Bioturbated mudstones.


(a) *Zoophycos* (**Zo**); *Helminthopsis* (**He**); mud-filled *Thalassinoides* (**Th**) reburrowed by *Zoophycos*; mud-filled *Planolites* (**Pl**); and shell fragments of *Inoceramus* (**In**). Well CRP-14; depth: 2,989.4 m.


(b) *Zoophycos* (**Zo**); mud-filled *Chondrites* (**Ch**); and shell fragments of *Inoceramus* (**In**). Well CRP-14; depth: 2,986.6 m.
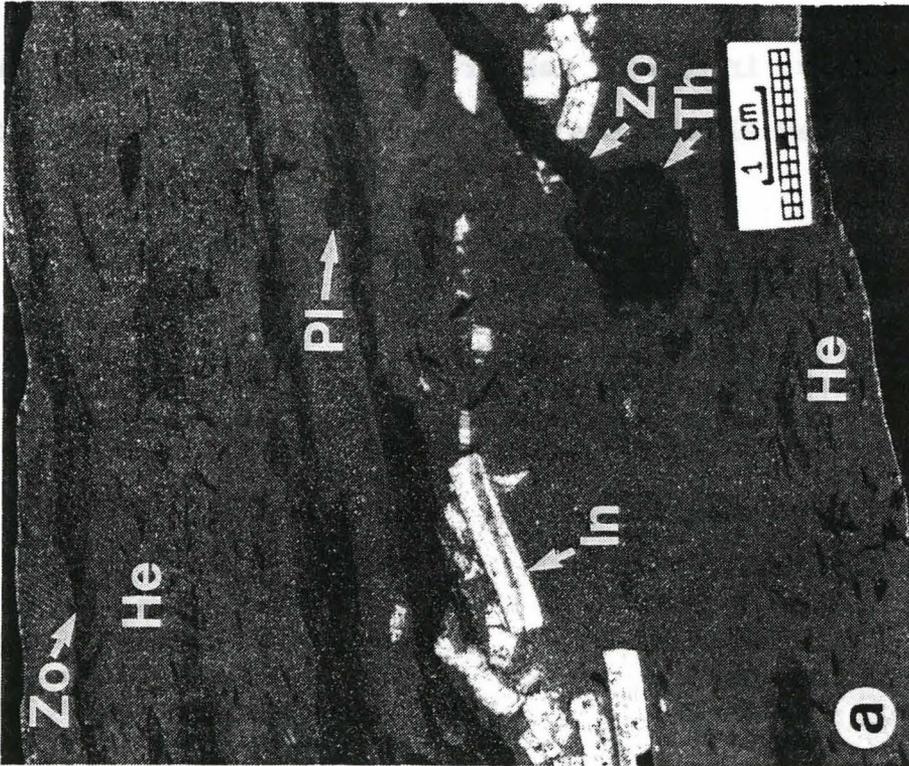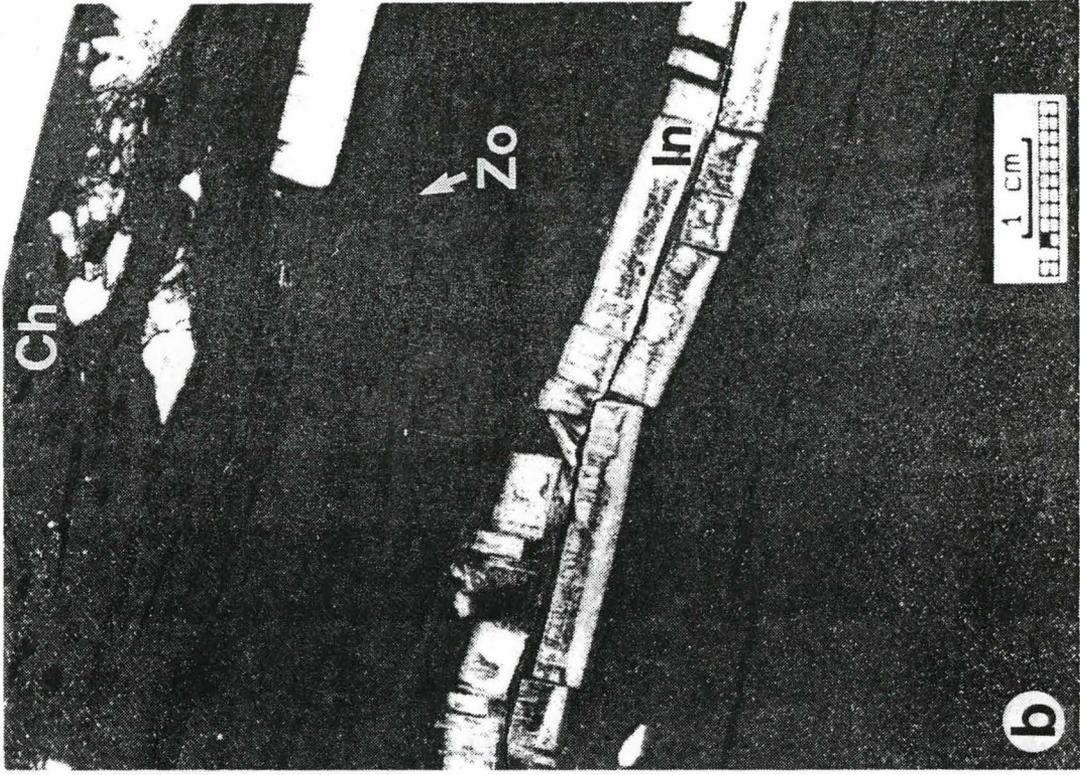
Fig. 3.17 - **FACIES CRP/PG-F3**: Bioturbated mudstones.


(a) *Zoophycos* (**Zo**); and *Helminthopsis* (**He**). Well CRP-14; depth: 3,046.9 m.


(b) *Zoophycos*, in places reburrowed by *Helminthopsis* (**Zo, He**); and mud-filled *Planolites* (**Pl**). Well CRP-14; depth: 3,022.6 m.
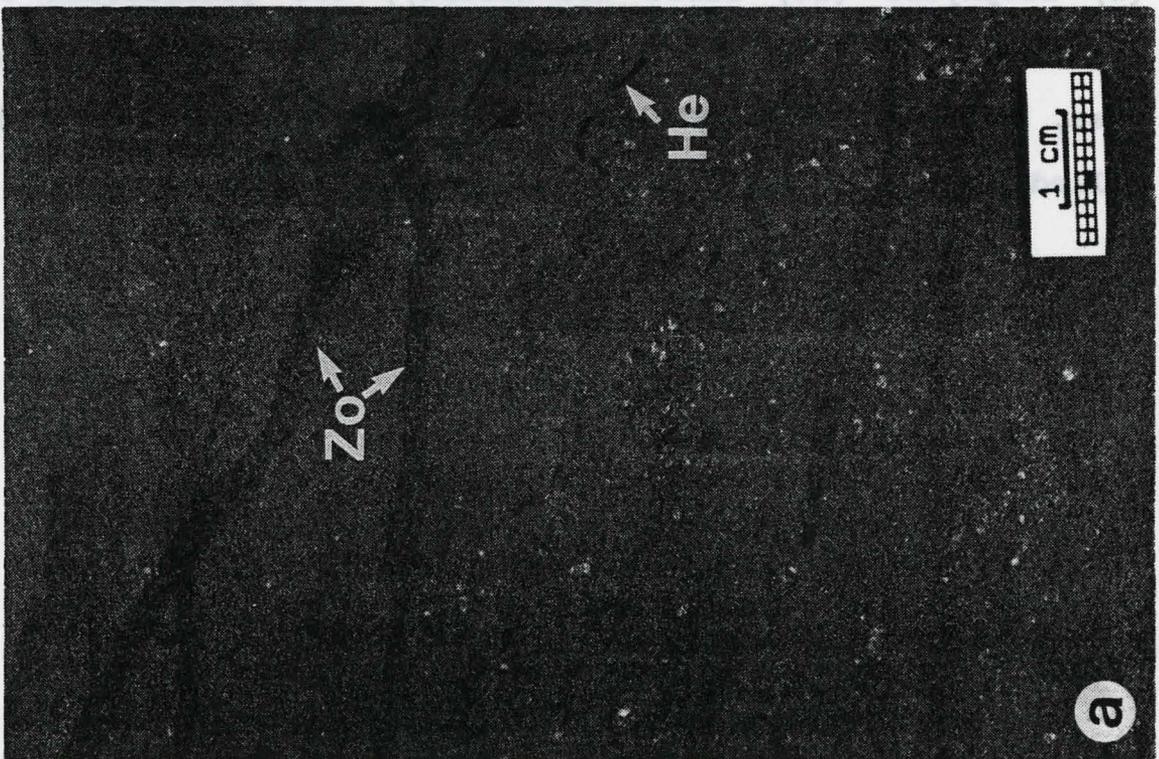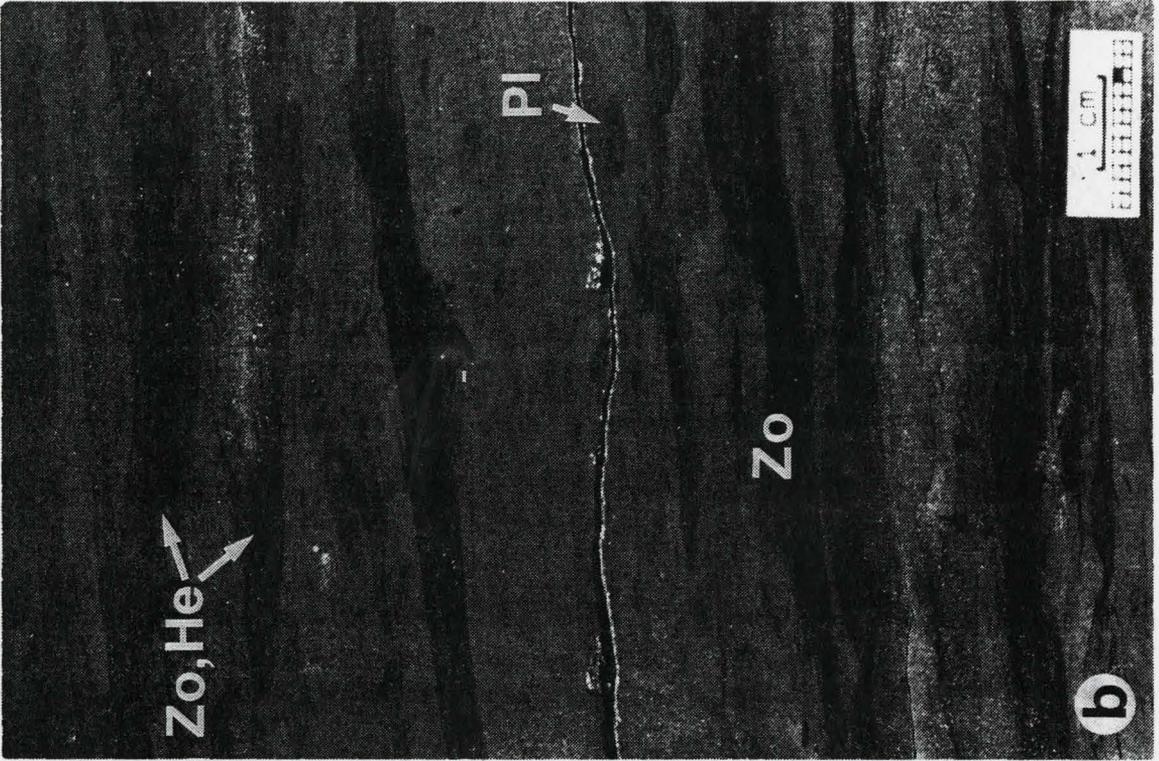
Fig. 3.18 - **FACIES CRP/PG-F3**: Bioturbated mudstones.


(a) *Zoophycos* (**Zo**); *Helminthopsis* (**He**); robust, mud-filled *Thalassinoides* (**Th**) reburrowed by *Helminthopsis*; mud-filled *Planolites* (**Pl**); *Skolithos* (**Sk**); and *Arenicolites* (**Ar**). Well CRP-14; depth: 2,999.5 m.


(b) *Zoophycos* (**Zo**; first colonizers); two generations of *Thalassinoides* (**Th**), i.e. a finer sand-filled suite at the base, and a coarser sand-filled suite at the top; and sand-filled *Planolites* (**Pl**). Well CRP-11; depth: 2,970.7 m.
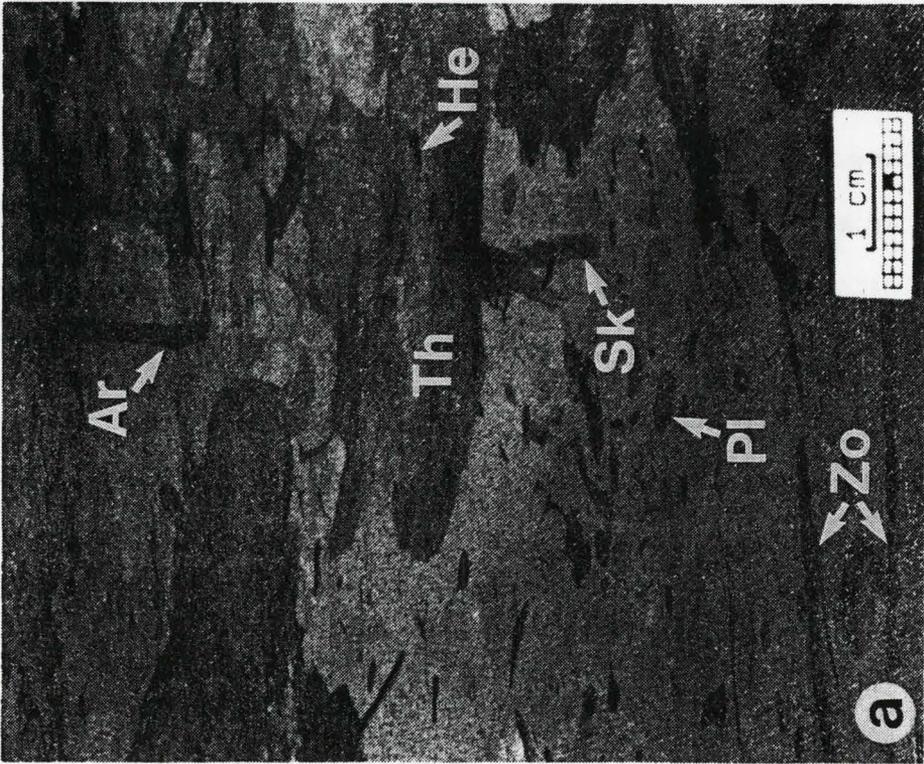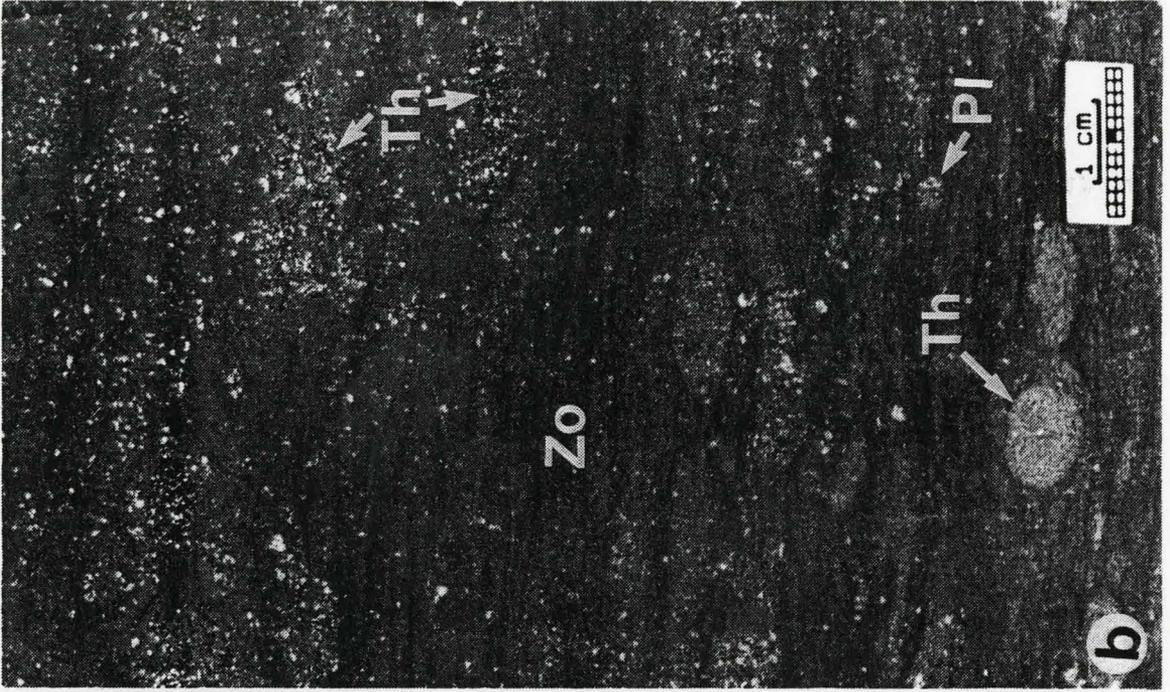
3.18a); and (2) 1 to 2 cm diameter burrows, filled with very fine- to very coarse-grained sand, reburrowing thin (< 3 mm) *Zoophycos* spreiten (Fig. 3.18b).

The ichnogenus *Planolites* also may be important, particularly in some *Thalassinoides*-rich horizons. It comprises mainly mud-filled tubes (Figs. 3.16a, 3.17b, and 3.18a), with subordinate sand-filled forms (Fig. 3.18b).

*Chondrites* occurs in very localized thin-bedded (< 20 cm thick), dark gray to black mudstones, which may produce high radioactivity/low resistivity well-log markers (e.g. marker S-1; Fig. 3.4). *Chondrites* usually represents the only trace fossil in these rocks, but a few *Zoophycos* and *Helminthopsis* may also be preserved (Fig. 3.16b).

Much less common traces are *Palaeophycus*, *Anconichnus*, *Skolithos* (mud-filled, vertical shafts; Fig. 3.18a), *Arenicolites* (mud-filled, J-shaped and U-shaped shafts; Fig. 3.18a), *Terebellina*, and poorly-structured *Asterosoma*.

The mineralogical composition of the fine-grained rocks of CRP/PG-F3, expressed in terms of major components, is presented in tables 3.1 and 3.2. The variations in the contents of clay minerals (all types together), quartz, K-feldspar, plagioclase, and calcite are primarily a function of the facies sampled. The coarser-grained facies (siltstones) tend to be poorer in clay minerals and richer in quartz, feldspars, and calcite; the finer-grained facies (shales) contain a higher content of clay minerals and lower proportion

**Table 3.1 - Mineralogical composition of the fine-grained rocks of the facies CRP/PG-F3[a].**

| | DISTRIBUTION RANGE, % (AVERAGE, %) | |
|---|---|---|
| MAJOR COMPONENTS | CONIACIAN/SANTONIAN | MAASTRICHTIAN |
| Clay minerals | 30 - 50  (37) | 25 - 40  (33) |
| Quartz | 15 - 35  (25) | 20 - 35  (26) |
| K-Feldspar | 5 - 15  (8) | 5 - 10  (9) |
| Plagioclase | 10 - 25  (14) | 10 - 30  (16) |
| Calcite | 10 - 20  (13) | 0 - 15  (8) |

[a] Based on 22 X-ray diffraction analysis (16 samples of Coniacian/ Santonian rocks, 6 samples of Maastrichtian rocks). Source: Anjos et al. (1991).

**Table 3.2 - Clay mineralogy of the fine-grained rocks of the facies CRP/PG-F3[a].**

| | DISTRIBUTION RANGE, % (AVERAGE, %) | |
|---|---|---|
| MAJOR COMPONENTS | CONIACIAN/SANTONIAN | MAASTRICHTIAN |
| Illite/smectite interlayerings[b] | 35 - 60  (47) | 55 - 65  (60) |
| Illite | 25 - 40  (33) | 25 - 30  (28) |
| Chlorite | 10 - 35  (18) | 10 - 15  (12) |
| Kaolinite | ≤ 5 | ≤ 5 |

[a] Based on 22 X-ray diffraction analysis (16 samples of Coniacian/ Santonian rocks, 6 samples of Maastrichtian rocks). Source: Anjos et al. (1991).
[b] Ordered interlayerings in the Coniacian/Santonian succession, with illite content of 75 to 85 %. Both ordered and random illite/smectite interlayerings occur in the Maastrichtian succession, with average illite content of 75 - 85 %, and 55 - 60 %, respectively.

of quartz, feldspars and calcite. The intensity of bioturbation, particularly by *Thalassinoides*, also may influence the mineralogical composition of the mudstones (this term will be used henceforth to designate all rocks of CRP/PG-F3), by concentrating coarser quartz and feldspar-rich grains (Fig. 3.18b).

The contents of clay minerals, quartz, and feldspars are very similar for the Coniacian/Santonian and Maastrichtian successions (Table 3.1). However, important contrasts exist in the amounts of calcite (Table 3.1) and different types of clay minerals (Table 3.2). The Maastrichtian mudstones show a higher mean calcite content probably due to the common occurrence of shell fragments of *Inoceramus*, which are typically under 1 cm long, but may exceed 10 cm (Fig. 3.16). The lower content of illite/smectite mixed layers, and the higher proportions of nonmixed-layered illite and chlorite suggest that the Coniacian/Santonian mudstones are diagenetically more mature than the Maastrichtian counterparts. Illite and chlorite have been considered common products of the thermally-induced diagenesis of illite/ smectite interlayerings (e.g. Hower et al., 1976; Boles and Franks, 1979). The occurrence of random interlayerings of illite/smectite only in the Maastrichtian mudstones also indicates that these younger rocks are not as diagenetically mature as the Coniacian/Santonian mudstones.

A few thin (< 20 cm) horizons of CRP/PG-F3 mudstones show

a reddish-brown colour due to high (> 20 %) content of siderite and rhodochrocite; this colour contrasts with the gray colour shown by most of the CRP/PG-F3 rocks.

**Interpretation:**

CRP/PG-F3 documents the sedimentary processes operating in the Campos basin during most of the time from the Coniacian to the early Paleocene (between 88.5 and 65 Ma). These fine-grained rocks suggest low sedimentation rates (< 0.5 cm/1,000 yr.; Mohriak et al., 1990) in a relatively quiet environment, with these conditions being episodically disturbed by high- to low-density turbidity currents carrying coarser-grained sediments. The mudstones contain a relatively abundant, benthic foraminifera fauna typical of mid to lower bathyal (1,000 - 1,500 m) depositional settings (Azevedo, 1987a).

The ubiquitous presence of *Zoophycos* places the entire facies CRP/PG-F3 within the Seilacher's (1964, 1967) *Zoophycos* ichnofacies, which is thought to represent outer neritic to bathyal depths. Although there are reported occurrences of the *Zoophycos* ichnofacies in shallower-water environments, they are restricted to Paleozoic rocks (e.g. Osgood and Szmuc, 1972; Marintsch and Finks, 1982). Shallow-water *Zoophycos* ichnofacies is uncommon in Mesozoic rocks and virtually absent in Cenozoic rocks (Ekdale, 1988). Bromley (1990) speculates that the booming of *Thalassinoides* after the beginning of the Mesozoic may have displaced *Zoophycos* to deeper environments.

Surveys of trace fossils in sediments as old as Cretaceous have been conducted in several DSDP sites, which have found *Zoophycos* as the most distinctive trace fossil in water depths greater than 2,000 m (Ekdale, 1977).

It has been pointed out in the literature that trace fossil assemblages are influenced less by bathymetry than by variations in environmental factors (e.g. temperature, light penetration, wave or current energy, sedimentation rate, sediment grain size, and oxygen and food supply); these may in turn may be related to bathymetric trends (e.g. Frey and Seilacher, 1980; Ekdale, 1985, 1988; Pemberton et al., 1992). According to a growing body of evidence, the *Zoophycos* ichnofacies would indicate quiet-water, offshore settings (probably below storm wave base), rather than deep water environments (Frey and Seilacher, 1980; Ekdale and Lewis, 1991). In these quiet settings the muddy or muddy sand substrate is commonly rich in organic matter, but deficient in oxygen (Frey and Seilacher, 1980; Savrda and Bottjer, 1986; Ekdale and Mason, 1988).

Crosscutting relationships recorded in the trace fossil assemblage of CRP/PG-F3 permit the recognition of an important tiering pattern (Bromley and Ekdale, 1986) in some of the uppermost Santonian, Campanian, and Maastrichtian mudstones (Figs. 3.17b and 3.18b). There are up to four tiers, not all of them always preserved in the same core. From the shallowest to the deepest tier, they are: (1) *Zoophycos* (spreiten

structures typically 2-3 mm thick), (2) *Helminthopsis*, (3) *Thalassinoides*, and (? 4) *Planolites*. The *Helminthopsis* tier apparently overlapped considerably with the *Thalassinoides* tier, because mutual overprinting of these two ichnogenera is common. *Planolites* is a relatively restricted ichnogenus, thus its position in the tiering succession above should be considered tentative. Like *Zoophycos* and *Helminthopsis*, *Thalassinoides* and *Planolites* also have been found in bathyal or abyssal sediments (e.g. Hayward, 1976; Ekdale, 1977; Wetzel and Werner, 1981). However, *Thalassinoides* and *Planolites* tend to occur in better-oxygenated seafloors (Savrda and Bottjer, 1986; Bromley, 1990). Thus, the sequence of emplacement of burrows described above would characterize a trend of gradual increase in bottom-water oxygenation, from the Coniacian/lowermost Santonian to the uppermost Santonian/ Campanian/Maastrichtian. This trend of increasing oxygenation would agree with the low content of total organic carbon (< 1 %) preserved in most of the late Turonian to early Paleocene successions in the Campos basin (Guardado et al., 1990).

The absence of surface traces (resting and crawling traces) in CRP/PG-F3 may have resulted from the action of frequent and erosive turbidity currents (more likely during the Coniacian/Santonian). Deep deposit-feeder structures (*Zoophycos*, *Helminthopsis*) and mid-tier deposit-feeder structures (*Thalassinoides*) probably had better chances for surviving the erosion by turbidity currents. Also the very

restricted occurrence of relatively permanent dwelling burrows of suspension feeders (e.g. *Skolithos* and *Arenicolites*), may have been induced by the high frequency of turbidity currents or, as suggested by D'Alessandro et al. (1986), by the lack of bottom currents transporting a continuous supply of suspended food across the ocean floor.

### 3.3.4. Facies CRP/PG-F4: deformed, interbedded mudstones and thin-bedded sandstones

**Description:**

CRP/PG-F4 comprises contorted, folded, or simply overturned interbeddings of coherent bioturbated mudstones and thin-bedded, fine-grained sandstones (Figs. 3.9 and 3.19). The soft-sediment deformation is the only feature used to differentiate CRP/PG-F4 from the facies CRP/PG-F2 and CRP/PG-F3.

The deformed rocks of CRP/PG-F4 make irregularly-shaped packages, mostly thinner than 1 m (but up to 3 m thick), which are preserved within undeformed successions of mudstones or in between coarse-grained turbidites.

Mudstones largely dominate over the thin-bedded sandstones in the deformed successions (Fig. 3.9). The sandstones may still display the original stratification (Fig. 3.19a), but more commonly the stratification is masked by the intense disruption of the original fabric and the abundant

Fig. 3.19 - **FACIES CRP/PG-F4:** Deformed interbeddings of mudstones and thin-bedded sandstones.


(a) Deformed bioturbated mudstones and parallel-stratified, fine-grained sandstone. Convoluted sand injections (i) and carbonaceous plant fragments (c) occur in the mudstones. Well CRP-11; depth: 2,999.5 m.


(b) Deformed bioturbated mudstones and medium-grained sandstone. The sandstone is strongly cemented by calcite and contain squeezed mud intraclasts (m). Convoluted sand injections (i) occur in the lower mudstone. Well PG-27A; depth: 3,032.7 m.
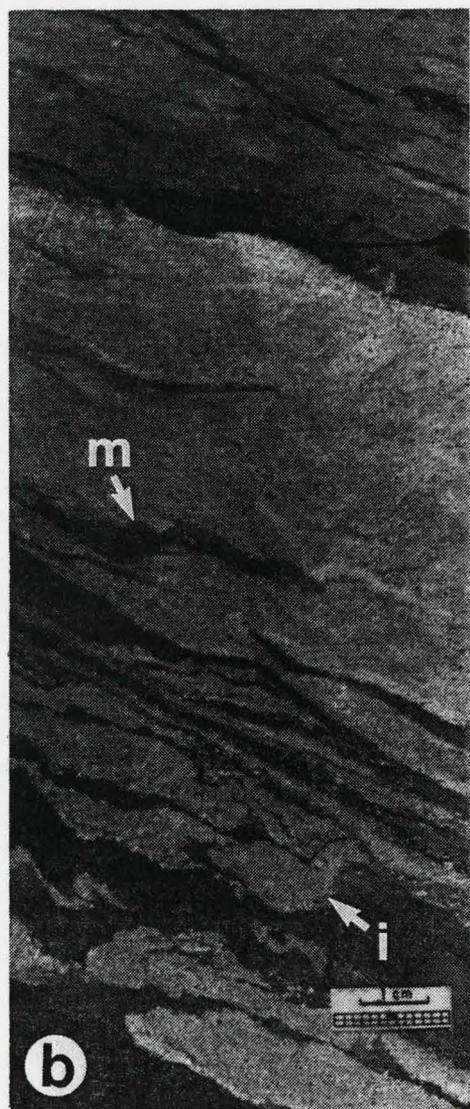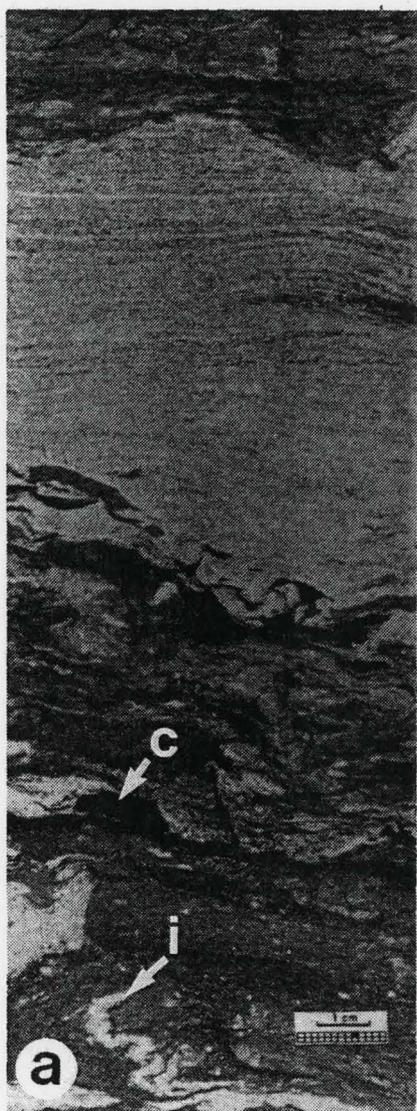
calcite cementation (Fig. 3.19b). Convoluted sand-injection structures, and squeezed, mud and organic matter intraclasts also are characteristic features of CRP/PG-F4 (Figs. 3.9 and 3.19).

**Interpretation:**

The common occurrence of deformed fine-grained facies underlying undeformed, coarse-grained turbidites may suggest the effects of the overloading by these thick, suddenly emplaced deposits. In this case, the unstable, fluid-saturated fine-grained sediments would have suffered deformation *in situ*, at the bottom of the Carapeba/Pargo trough. On the other hand, the deformed strata surrounded by undisturbed mudstones may have originated as slides or slumps, possibly triggered by gravitational instability along the faulted margins of the trough or by cyclic and/or isolated earthquake shakings (e.g. Allen, 1986; Raja Gabaglia, 1991).

## 3.3.5. Facies CRP/PG-F5: disorganized, intraclastic mudstones and sandstones

**Description:**

CRP/PG-F5 includes disorganized, intraclastic mudstones and sandstones, which contain cobble- to granule-sized mud intraclasts (mostly pebbles) and subordinate pebble- to granule-sized clasts of organic matter dispersed in a matrix

with variable content of mud and sand (Figs. 3.15 and 3.20).
The content of mud in the matrix typically exceeds 20 %, and
the gravel-sized intraclasts may comprise up to 50 % of the
rocks. Cementation by calcite is very intense in the rocks
containing a larger proportion of sand in the matrix (Figs.
3.15 and 3.20b).

CRP/PG-F5 typically comprises beds thinner than 1 m (e.g.
Fig. 3.15), but thicker (up to 5 m) deposits have been
recognized. Relatively few beds of disorganized, intraclastic
mudstones and sandstones were cored in the Carapeba and Pargo
fields; e.g. only three thin (<1 m) beds were recognized in a
86 m thick cored section in the well CRP-11. They occur
preferentially interbedded with the bioturbated mudstones of
the facies CRP/PG-F3, showing sharp basal contacts, and
poorly-defined upper contacts due to the common bioturbation
(Fig. 3.15).

**Interpretation:**

The random dispersion of large mud intraclasts in a
poorly-sorted muddy and sandy matrix suggests that this facies
was deposited from debris flows. The strength and buoyancy of
the muddy and sandy matrix would have supported the larger
clasts during a mostly laminar flow, with very little fluid
mixing (Middleton and Hampton, 1973). The matrix usually
presents an elevated pore pressure that diminishes the
frictional resistance to flow (Pierson, 1981). Debris flows

Fig. 3.20 - **FACIES CRP/PG-F5:** Disorganized, intraclastic mudstones and sandstones.

(a) Pebble- to granule-sized mud intraclasts dispersed in a matrix of mud-rich, fine-grained sandstone. Well PG-27A; depth: 3,047.3 m.

(b) Pebble-sized mud intraclasts dispersed in a calcite-cemented matrix of very coarse-grained sand. Well CRP-11; depth: 2,964.8 m.
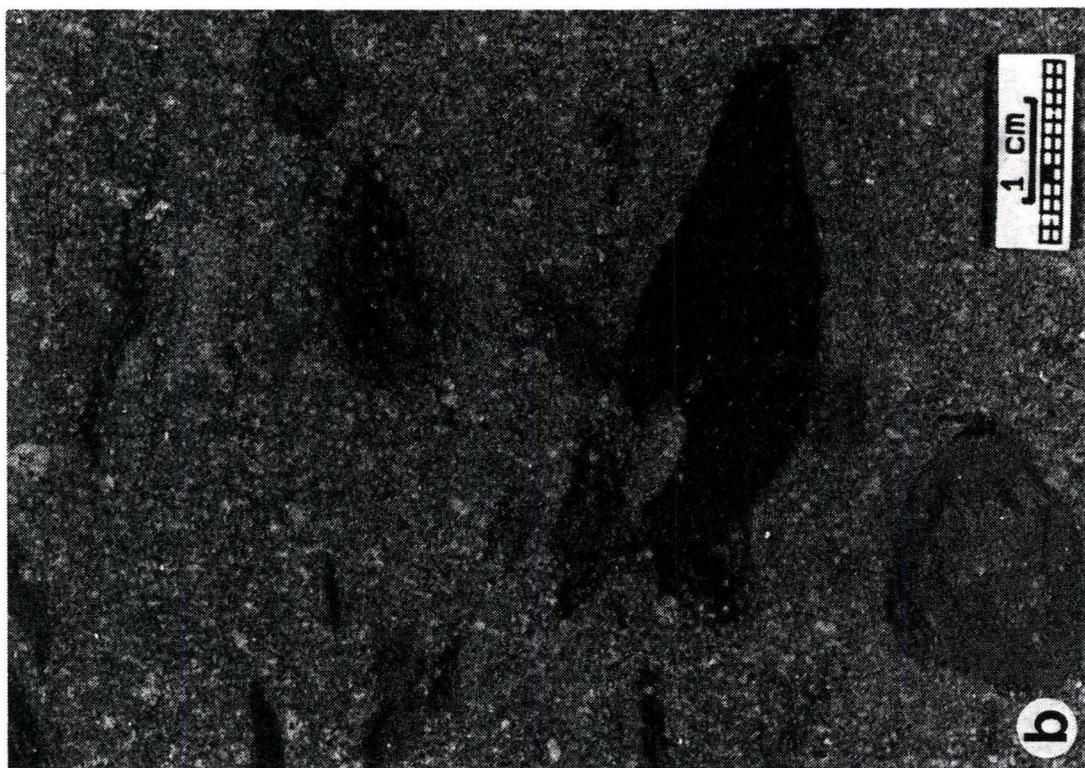
move in response to deformation in a basal zone of high shear stress, and deposition takes place almost instantaneously when the bed shear stress drops to a value lower than the yield strength (Middleton and Hampton, 1973; Lowe, 1982). The resulting deposits are characterized by a chiefly disorganized fabric as in the facies CRP/PG-F5.

### 3.3.6. Well log response

The facies described in the Carapeba/Pargo turbidite system each have typical well log responses, particularly in the gamma-ray, resistivity, and density logs. These responses can be characterized by the distribution of absolute values (Table 3.3) or by log patterns. The recognition of well log responses permitted the mapping of different facies in areas of the Carapeba and Pargo fields lacking core control.

The conglomerates and sandstones of facies CRP/PG-F1 present very uniform values in the gamma-ray log (Table 3.3), defining a typical boxy pattern (Figs. 3.4, 3.5, and 3.6). The mud intraclasts, even in large proportions, do not increase significantly the gamma-ray log response, because of the intense silicification (with removal of most of potassium). The density log, however, is very sensitive to the grain-size and sorting variations presented by the graded beds. It displays upward-decreasing density values that indicate the conspicuous normal grading and upward improvement in sorting

**Table 3.3 - Typical well-log radioactivity, resistivity and density readings for the facies defined in the Carapeba/Pargo turbidite system[a].**

| FACIES | RADIOACTIVITY (API) | RESISTIVITY ($\Omega$.m) | DENSITY (g/cm$^3$) |
|---|---|---|---|
| CRP/PG-F1 | 45 - 55 | 1 - 2 | 2.25 - 2.55 |
| Coarse- to medium-grained sandstones | | | 2.25 - 2.30 |
| Very coarse-grained sandstones | | | 2.30 - 2.35 |
| Conglomerates/ conglomeratic sandstones | | | 2.35 - 2.55 |
| CRP/PG-F2 | 60 - 85 | 4 - 8 | 2.40 - 2.50 |
| CRP/PG-F3 | | | |
| Coniacian/ Santonian | 85 - 100 | 5 - 6 | 2.53 - 2.56 |
| Campanian/early Maastrichtian/ lowermost late Maastrichtian | 100 - 115 | 4 - 5 | 2.53 - 2.56 |
| uppermost late Maastrichtian[b] | 115 - 130 | 4 - 5[c] | 2.55 - 2.58 |
| early Paleocene[b] | 115 - 130 | 3 - 4 | 2.46 - 2.49 |
| CRP/PG-F5 | 60 - 75 | 3 - 4 | 2.40 - 2.45 |

[a] Well-log readings for CRP/PG-F1 and CRP/PG-F2 include only the conglomerate and sandstone values. Their mudstone responses are included in the CRP/PG-F3 distribution. Values for CRP/PG-F4 are the same for CRP/PG-F2 (sandstones) and CRP/PG-F3 (mudstones).
[b] Included in CRP/PG-F3, but without core control.
[c] Most of values constant around 5 $\Omega$.m.

(Figs. 3.5 and 3.6). Table 3.3 presents the typical density values for the facies that comprise the graded beds. These values should be taken as approximate, considering that most of the graded beds comprise a continuous gradation of many of the facies above.

Most of the graded beds are characterized in the density logs by: (1) an abrupt increase in density at the coarser-grained, base of the bed (where it truncates the finer-grained top of an underlying bed); and (2) a following gradational density decrease, characterizing normal grading and upward improvement in sorting (Figs. 3.5 and 3.6). The sandy successions of the Carapeba/Pargo turbidite system seem texturally monotonous on the gamma-ray log response, but they represent the multiple stacking of texturally-variable turbidites. The density logs of the Carapeba and Pargo fields permit not only the mapping of the vertical and lateral textural variations presented by their reservoirs, but also characterize a unique situation where individual graded beds (or individual turbidites) can be correlated in the subsurface for up to 20 km.

Calcite cementation or concentrations of large mud and marl intraclasts tend to increase the rock density (e.g. turbidites K2 and K4 in Fig. 3.5), leading to possible misinterpretation of coarser-grained facies (or the basal portion of a graded bed) in non-cored wells. Situations such as the examples in figure 3.5 occur in about 5 % of cored

graded beds. However, calcite-rich horizons tend to be laterally discontinuous, and rarely can be correlated between two adjacent wells.

The thin-bedded sandstones of facies CRP/PG-F2, and the facies CRP/PG-F5 have higher radioactivity and resistivity than the sandstones of CRP/PG-F1, because of their higher contents of muddy matrix and calcite cement, respectively. Well log patterns are difficult to define for these rocks due to the small bed thickness. The thickest (5 m) debris flow deposit recorded in the Pargo field displays a blocky log pattern.

The well log responses for the mudstones of the Campos Formation (including CRP/PG-F3; Table 3.3) permit the mapping of successions with different ages in wells without paleontology data (e.g. Fig. 3.4). The well logs of the Maastrichtian and early Paleocene mudstones define general trends of upward increasing radioactivity and decreasing resistivity, which illustrates the general muddier-upward character of the marine transgressive megasequence in the Campos basin (Fig. 3.4). Thin (< 1m) horizons richer in clay minerals may comprise high radioactivity well log markers, wich can be correlated for significant portions of the study area. Good examples are provided by the markers S-1 (Santonian), S/C (boundary between Santonian and Campanian), and M-1 and M-3 (Maastrichtian) (Fig. 3.4).

CRP/PG-F4 displays on well-logs the same responses as its

undeformed equivalents (CRP/PG-F2 and CRP/PG-F3) (Table 3.3). Thicker deformed successions tend to show serrate patterns on well-logs.

### 3.3.7. Reservoir properties

CRP/PG-F1 contains all of the oil-producing rocks in the Carapeba and Pargo fields. The sandstones of CRP/PG-F2, CRP/PG-F4 and CRP/PG-F5 do not form reservoir rocks because their higher mud and calcite cement contents do not allow permeabilities to exceed 1 mD. Table 3.4 shows the porosity and permeability distribution according to the different reservoir rocks of CRP/PG-F1.

The porosity and permeability of the Carapeba and Pargo reservoirs are relatively high, despite their great burial depth (2,900 to 3,350 m). The excellent reservoir quality at such depths can be explained by a combination of factors including: (1) late burial or little time of residence at great depths (Bruhn, 1990); (2) an important phase of generation of secondary porosity in the diagenetic evolution of the reservoirs, through the dissolution of a large amount of calcite cement by organic acids derived from late Cretaceous shales (Moraes, 1989); and (3) early oil migration from underlying early Cretaceous source rocks, preserving a significant portion of the diagenetically enhanced porosity (Moraes, 1989).

**Table 3.4 - Porosity and permeability characterization of the Carapeba and Pargo field reservoirs[a].**

| FACIES | TYPICAL DISTRIBUTION RANGE[b] (AVERAGE)[c] | |
| --- | --- | --- |
| | POROSITY (%) | PERMEABILITY (mD) |
| Conglomerates and conglomeratic sandstones | 15 - 20 (17) | 100 - 800 (308) |
| Very coarse-grained sandstones | 18 - 22 (19) | 300 - 1,000 (698) |
| Coarse-grained sandstones | 19 - 23 (20) | 100 - 900 (491) |
| Medium-grained sandstones | 20 - 25 (23) | 100 - 900 (438) |
| Calcite-rich facies[d] | < 10 | < 50 |
| Intraclast-rich facies[e] | 15 - 22 (19) | < 100 (43) |

[a] Based on 747 measurements of porosity and permeability in rock plugs collected from cores at an average distance of 30 to 40 cm. Source: PETROBRÁS.
[b] It includes at least 75 % of measured values for each facies.
[c] Arithmetic mean for porosity, and geometric mean for permeability.
[d] All facies, but with a calcite cement content > 10 %.
[e] All facies, but with a mud intraclast content > 15 %.

Remnants of calcite cement and mechanically compacted mud intraclasts may reduce significantly the porosity and permeability of the Carapeba and Pargo reservoirs. In the zones intensely cemented by calcite (e.g. Fig. 3.8) the porosity and permeability are less than 10 % and 10 mD, respectively. The squeezed, silicified mud intraclasts are

particularly efficient in reducing the permeability of the reservoirs; in rocks with intraclast content higher than 15 % the permeability never exceeds 100 mD. Mud intraclasts also introduce significant amounts of microporosity (pores < 2 $\mu$m) in the reservoirs, which retain non-mobile water and reduce the rock resistivity. There are oil-producing intervals in the Carapeba field with average resistivity of only 2.5 $\Omega$.m (Cândido, 1990a). However, calcite- and intraclast-rich horizons have a relatively restricted occurrence in the Carapeba/Pargo turbidite succession, with the variations in the porosity and permeability of the reservoirs being primarily justified by syndepositional textural parameters.

Better sorting favours higher porosities, as shown by the finer-grained facies (coarse- and medium-grained sandstones; Table 3.4). On the other hand, coarser-grained facies (conglomerates, conglomeratic sandstones, and very coarse-grained sandstones) tend to present larger pore throats, which favour high permeabilities (Table 3.4). The combination of sorting and grain-size in the very coarse-grained sandstones makes them the best reservoirs of the Carapeba and Pargo fields (Table 3.4).

## 3.4. HIGH-RESOLUTION STRATIGRAPHY AND RESERVOIR GEOMETRY

### 3.4.1. Geological cross sections and basis for correlation

The detailed stratigraphic analysis and the geometrical characterization of the Carapeba and Pargo turbidites were largely based on 20 geological sections, which include almost all of the wells drilled in these two fields (Fig. 3.3).

Nine sections were constructed for Pargo field, using the base of the widely distributed sandstone K as the datum (Fig. 3.4). This datum is very convenient because of its proximity to most of the oil-bearing turbidites in the field (sandstones F to N; Fig. 3.4).

The eleven sections for Carapeba field were constructed with a different datum, the radioactive S/C log marker (approximate boundary between the Santonian and Campanian stages; Fig. 3.2). This was because most of the oil accumulations are concentrated in the uppermost sandstones (sandstones M to W; Fig. 3.2) and many of the wells drilled in Carapeba did not reach sandstone K.

Gamma-ray, density and resistivity well logs were used to construct the sections. Gamma-ray logs are particularly efficient in the separation of sandstones from mudstones, and in the definition of trends in sandstone thickness variation. Density logs permit the individualization of turbidites making part of the same, composite sandstone body, and the recognition of lateral and vertical trends of grain size distribution. Resistivity logs are important for the mapping of different mudstone packages.

A total of 23 sandstone bodies, composed of the coarse-

grained, graded beds of facies CRP/PG-F1, were defined and mapped on the basis of purely descriptive features such as the continuity of interbedded mudstones, or the significant changes in grain size distribution within sandy successions. These sandstone bodies comprise the most important elements for detailed correlation within the thick, sand-rich turbidite succession of the Carapeba and Pargo fields. The Coniacian/ Santonian succession comprises 21 sandstone bodies, named A to U (from the oldest to the youngest), and the early Maastrichtian succcession includes the sandstones V and W (Fig. 3.4). Each of the sandstones A to W comprises a single graded bed, or up to 18 amalgamated turbidites. Individual turbidites were numbered; e.g. turbidites K1, K2, K3, and K4 form sandstone K in the well PG-4 (Fig. 3.5).

The sandstones A to W, and most of their component individual turbidites (coarse-grained, graded beds of the facies CRP/PG-F1) were correlated throughout the geological sections located in figure 3.3. The sandstones A to H were not cored, thus their interpretation and mapping is supported only by well logs. Four sections are reproduced in figures 3.21 to 3.24, which illustrate the major textural and thickness variations, and also the detailed stratigraphic relationships recognized within the Carapeba/Pargo turbidite system.

The cross sections presented in figures 3.2 and 3.4 are simplified, i.e. they show the distribution of sandstones A to W, but they do not display the correlation of individual

Fig. 3.21 - Geological cross section longitudinal to the Carapeba/Pargo canyon, typical of the Pargo field. Section shows the easternmost terminations of most of the CRP/PG-S5, CRP/PG-S6, and CRP/PG-S8 sandstones, and emphasizes the great continuity of sandstones and interbedded mudstones of CRP/PG-F4. A relatively thick (5 m) debris flow deposit is recognized in the well PG-27A. Datum is the base of the widely distributed K sandstone.   S-1,   S/C,   M-1 and  M-3  are radioactive (mudstone) log markers. S/C indicates the approximate boundary between Santonian and Campanian. The uppermost turbidite succession (CRP/PG-S8) dates from the early Maastrichtian, but there is no well log response that can be correlated to the boundary between early and late Maastrichtian. Arrows (fu) indicate major fining upward successions as defined by density logs. Well logs used to construct the section: gamma-ray, resistivity, and density. Vertical scale = 2.5 x horizontal scale. Section location is shown in figure 3.3.

NW

PG-27A  RJS-52  PG-12D  PG-10D  PG-21D  PG-11D  PG-25D  PG-19D  PG-8D  SE

MARINE REGRESSIVE MEGASEQUENCE

MARINE TRANSGRESSIVE MEGASEQUENCE

MID EOCENE

EARLY PALEOCENE

LATE MAASTRICHTIAN

LATE MAASTRICHTIAN

EARLY MAASTRICHTIAN

CAMPANIAN

CONIACIAN/SANTONIAN

CRP/PG - S8
CRP/PG - S6

CRP/PG-FS: Debris flow deposits

CRP/PG - S5

CRP/PG - S4

CRP/PG - S3

TURBIDITE SUCCESSIONS: SANDSTONES

Early Maastrichtian

CRP/PG-S8:  W

Coniacian/Santonian

CRP/PG-S6:  Q, R
CRP/PG-S5:  M, N, O, P
CRP/PG-S4:  D, E, F, G, H, I, J, K, L
CRP/PG-S3:  C

CAMPOS FORMATION   CONIACIAN/SANTONIAN

MACAÉ FORMATION   LATE CENOMANIAN/EARLY TURONIAN

Succession bases:
    Conformable contacts
    Regional unconformities
Sandstone boundaries:
Individual turbidites:

0        500        1000 m

Gamma-ray log
Resistivity log
Density log

DATUM

200 m

100

0

BRUHN (1993)

Fig. 3.22 - Geological cross section transverse to the Carapeba/Pargo canyon, typical of the Pargo field. Section shows the northern margin of the canyon, which was eroded into Coniacian/Santonian and late Cenomanian/early Turonian fine-grained rocks. The uppermost, thinner sandstones (L, M, N, and O) may comprise compensation arrangements. Datum is the base of the widely distributed K sandstone. S-1 and M-3 are radioactive (mudstone) log markers. The uppermost turbidite succession (CRP/PG-S8) dates from the early Maastrichtian, but there is no well log response that can be correlated to the boundary between early and late Maastrichtian. Well logs used to construct the section: gamma-ray, resistivity, and density. Vertical scale = 2.5 x horizontal scale. Section location is shown in figure 3.3.

BRUHN (1993)

Fig. 3.23 - Geological cross section longitudinal to the Carapeba/Pargo canyon, typical of the Carapeba field. Section shows the generalized eastward thinning of successions CRP/PG-S4 to CRP/PG-S8. Local erosion surfaces are recognized between successions CRP/PG-S4 and CRP/PG-S5, and CRP/PG-S7 and CRP/PG-S8, respectively. Datum is the radioactive S/C (mudstone) log marker (approximate boundary between Santonian and Campanian). M-1 and M-2 are radioactive (mudstone) log markers. The uppermost turbidite succession (CRP/PG-S8) dates from the early Maastrichtian, but there is no well log response that can be correlated to the boundary between early and late Maastrichtian. Arrows (**fu**) indicate major fining upward successions as defined by density logs. Well logs used to construct the section: gamma-ray, resistivity, and density. Vertical scale = 4 x horizontal scale. Section location is shown in figure 3.3.

WNW — CRP-24 — CRP-25 — CRP-4D — CRP-37D — CRP-41D — CRP-23D — CRP-14 — CRP-35D — CRP-31D — RJS-224 — ESE

118

MARINE REGRESSIVE MEGASEQUENCE
MARINE TRANSGRESSIVE MEGASEQUENCE

MID EOCENE
EARLY PALEOCENE
LATE MAASTRICHTIAN
LATE MAASTRICHTIAN
EARLY MAASTRICHTIAN
CAMPANIAN
CONIACIAN/SANTONIAN

CRP/PG-S7
CRP/PG-S8
CRP/PG-S6
CRP/PG-S5
CRP/PG-S4

Gamma-ray log
Resistivity log
Density log

DATUM

s/c

200 m

100

0

BRUHN (1993)

TURBIDITE SUCCESSIONS: SANDSTONES

Succession bases:
Conformable contacts
Local erosion surfaces
Regional uncomformit es

| Early Maastrichtian | Coniacian/Santonian |
|---|---|
| CRP/PG-S8: W | CRP/PG-S6: Q, R, S, T, U |
| CRP/PG-S7: V | CRP/PG-S5: M, N, O, P |
| | CRP/PG-S4: F, G, H, I, J, K, L |

Sandstone boundaries:
Sandstone boundaries:
individual turbidites:

Fig. 3.24 - Geological cross section transverse to the Carapeba/Pargo canyon, typical of the Carapeba field. Section shows the strong fault control on the sedimentation of CRP/PG-S3 and CRP/PG-S4 along the southern margin of the canyon. Datum is the radioactive S/C (mudstone) log marker (approximate boundary between Santonian and Campanian). M-1, C/T-1, and C/T-2 are radioactive log markers. Well logs used to construct the section: gamma-ray, resistivity, and density. Vertical scale = 4 x horizontal scale. Section location is shown in figure 3.3.

WNW                    RJS - 145A                                        CRP - 42D                RJS - 320A        CRP - 25                    ESE  119
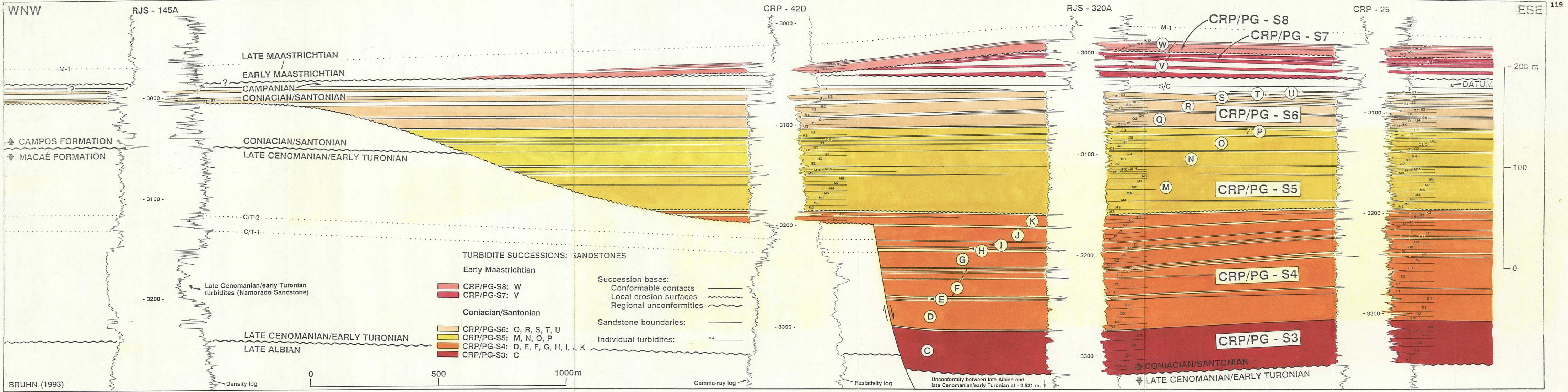
LATE MAASTRICHTIAN                                                                                        CRP/PG - S8
EARLY MAASTRICHTIAN                                                                                       CRP/PG - S7
CAMPANIAN
CONIACIAN/SANTONIAN

CONIACIAN/SANTONIAN
CAMPOS FORMATION                    CONIACIAN/SANTONIAN                                                    CRP/PG - S6
MACAÉ FORMATION                     LATE CENOMANIAN/EARLY TURONIAN

                                                                                                          CRP/PG - S5

C/T-2
C/T-1

                     Late Cenomanian/early Turonian        TURBIDITE SUCCESSIONS: SANDSTONES              CRP/PG - S4
                     turbidites (Namorado Sandstone)
                                                           Early Maastrichtian
                                                                                   Succession bases:
                                                           CRP/PG-S8: W            Conformable contacts
                                                           CRP/PG-S7: V            Local erosion surfaces
                                                                                   Regional unconformities
                                                           Coniacian/Santonian
                     LATE CENOMANIAN/EARLY TURONIAN                                Sandstone boundaries:
                     LATE ALBIAN                           CRP/PG-S6: Q, R, S, T, U                        CRP/PG - S3
                                                           CRP/PG-S5: M, N, O, P   Individual turbidites:    M4
                                                           CRP/PG-S4: D, E, F, G, H, I, J, K
                                                           CRP/PG-S3: C                                    CONIACIAN/SANTONIAN
                                                                                                           LATE CENOMANIAN/EARLY TURONIAN
BRUHN (1993)                    0        500       1000m
                     Density log          Gamma-ray log    Resistivity log    Unconformity between late Albian and
                                                                              late Cenomanian/early Turonian at - 3,521 m.

turbidites that form these sandstones. Figure 3.2 includes a cross section located in the Carapeba field, which is tranverse to the Carapeba/Pargo canyon; this section illustrates the important fault control on the lateral distribution of the Carapeba/Pargo turbidites. Figure 3.4 is oriented longitudinally to the Carapeba/Pargo canyon, and has almost the entire length of the study area. Figure 3.4 provides an integrated view of the stratigraphic relationships recognized in the studied fields.

### 3.4.2. Characterization of facies successions

The Coniacian/Santonian and early Maastrichtian turbidite successions may be subdivided into eight facies successions, chiefly on the basis of striking changes in the vertical trends of grain size distribution (e.g. density logs in Fig. 3.4), and also by different trends in sandstone thickness variation, distinct areas of occurrence, and stratigraphic relationships (including regional unconformities and local erosion surfaces). These eight facies successions are named CRP/PG-S1 to CRP/PG-S8, with the letter **S** indicating succession (Table 3.5).

The Carapeba/Pargo turbidite system is included in the marine transgressive megasequence, which is characterized by onlapping, deepening-upward and muddier-upward (Fig. 3.4) sedimentation throughout the eastern Brazilian marginal basins

**Table 3.5 – Facies successions of the Carapeba/Pargo turbidite system (as characterized only by the CRP/PG-F1 coarse-grained turbidites).**

| SUCCESSION | SANDSTONE BODIES | MAXIMUM THICKNESS (m) | TURBIDITES | |
|---|---|---|---|---|
| | | | NUMBER[a] | AVERAGE THICKNESS (m) |
| EARLY MAASTRICHTIAN | | | | |
| CRP/PG – S8 | W | 10 | 14 | 2.2 |
| CRP/PG – S7 | V | 14 | 7 | 2.3 |
| CONIACIAN/SANTONIAN | | | | |
| CRP/PG – S6 | U | 8 | 4 | 1.9 |
| | T | 4 | 2 | 2.1 |
| | S | 9 | 5 | 2.4 |
| | R | 11 | 5 | 2.5 |
| | Q | 15 | 6 | 2.7 |
| CRP/PG – S5 | P | 16 | 18 – 21 | 2.3 |
| | O | 17 | 6 | 2.9 |
| | N | 20 | 8 – 9 | 3.3 |
| | M | 53 | 19 – 22 | 3.8 |
| CRP/PG – S4 | L | 16 | 20 – 23 | 2.3 |
| | K | 17 | 5 | 3.6 |
| | J | 15 | 5 | 3.7 |
| | I | 5 | 1 | 3.7 |
| | H | 6 | 1 | 3.5 |
| | G | 17 | 3 – 4 | 5.8 |
| | F | 39 | 7 – 8 | 6.4 |
| | E | 12 | 1 | 7.1 |
| | D | 29 | 4 – 5 | 6.6 |
| CRP/PG – S3 | C | 56 | 10 – 11 | 6.2 |
| CRP/PG – S2 | B | 51 | 13 – 15 | 4.4 |
| CRP/PG – S1 | A | 74 | 17 – 18 | 4.4 |
| CARAPEBA/PARGO TURBIDITE SYSTEM | | 286[b] | 181 – 198 | 3.7 |

[a] A range of numbers is indicated for: (1) most of the non-cored or poorly-cored sandstones, and (2) the very discontinuous sandstones, which show common compensation arrangements.
[b] The maximum recorded thickness (well RJS-320A; Fig. 3.24) is smaller than the sum of the maximum thickness for each succession, due to common erosion and compensation arrangements.

(e.g. Chang et al., 1988; Guardado et al., 1990). The successions CRP/PG-S1 to CRP/PG-S8 were stacked in an overall retrogradational pattern, recording the backfilling of the WNW-oriented Carapeba/Pargo canyon (Fig. 3.4).

**Facies succession CRP/PG-S1**

CRP/PG-S1 is composed of sandstone A, which is restricted to the easternmost portion of the Pargo field. It is recorded in only three wells (Fig. 3.25), and its distribution is controlled by a NE-trending fault (Figs. 3.4 and 3.25). CRP/PG-S1 always overlies Coniacian/Santonian mudstones of the Campos Formation, contrasting with the successions CRP/PG-S2 to CRP/PG-S5, which in places overlie the late Cenomanian/ early Turonian marls and mudstones of the Macaé Formation. This suggests that the accommodation space (Jervey, 1988) for the accumulation of CRP/PG-S1 was provided not only by erosion, but also by subsidence along the fault that defines its westernmost limit of occurrence (Fig. 3.4).

CRP/PG-S1 is composed of up to 18 amalgamated turbidites, which display a typical blocky pattern on the gamma-ray logs (Fig. 3.4). These turbidites do not show trends of grain size and bed thickness distribution, and their geometry is poorly defined because of the very limited well control (Fig. 3.25).

**Facies succession CRP/PG-S2**

CRP/PG-S2 comprises sandstone B (Fig. 3.4). It is more

Fig. 3.25 - Net sand map for succession CRP/PG-S1.

SUCCESSION CRP/PG-S1

345 000　　　350 000　　　355 000　　　360 000

N

6
193A
14
224
11
5A
9
52
4
8
7A

7 540 000

0　　　　　3 km
C.I. = 20 m

○ Well control
▲ Cored well

60
40
20
0
?
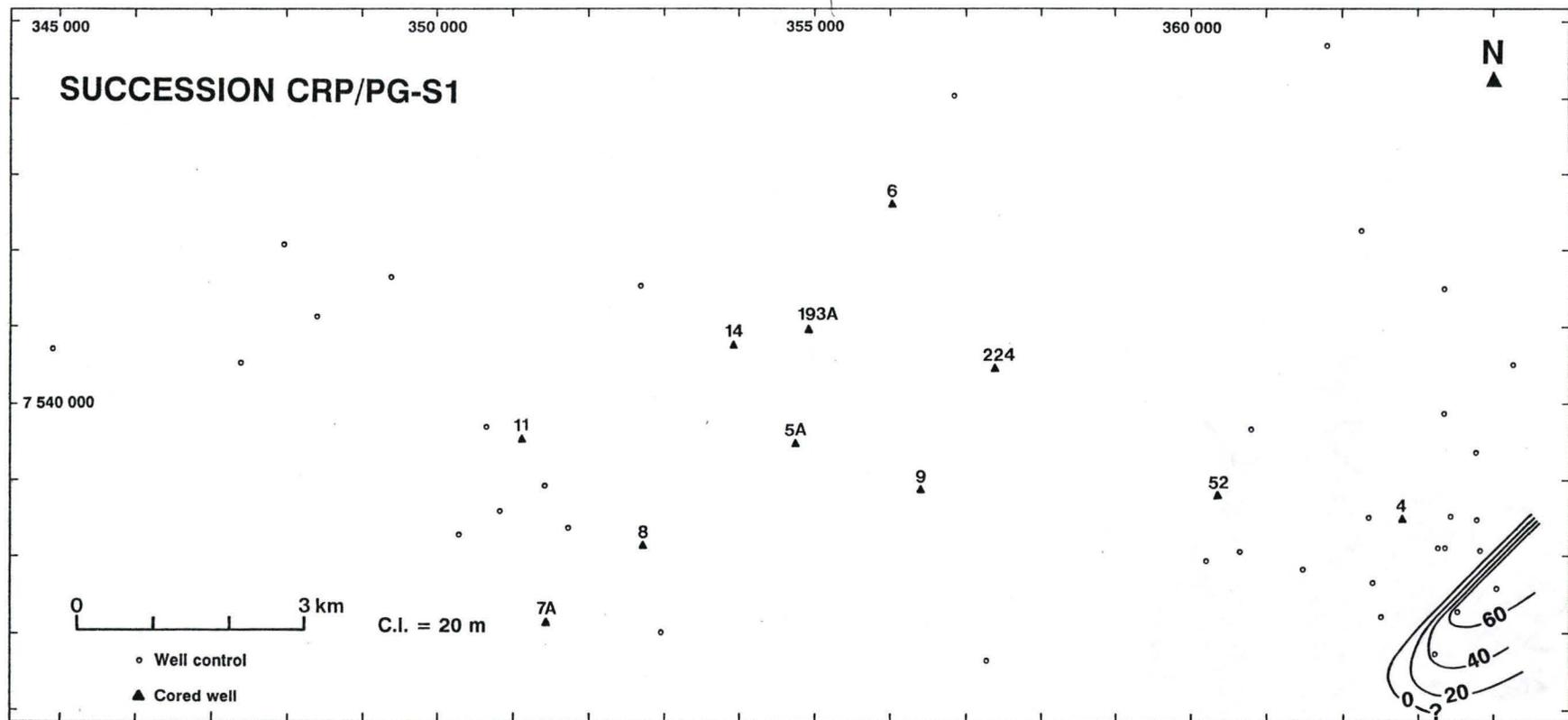
widely distributed than CRP/PG-S1 in the studied area, but it is restricted to the Pargo field (Figs. 3.4 and 3.26). CRP/PG-S2 unconformably overlies late Cenomanian/early Turonian marls of the Macaé Formation in its westernmost area of occurrence, and Coniacian/Santonian mudstones in eastern Pargo field (Fig. 3.4).

CRP/PG-S2 contains up to 15 turbidites, typically forming a fining upward succession (e.g. density log for well PG-8D in Fig. 3.4). These turbidites are confined in a narrow, 1.0 to 1.8 km wide trough (Fig. 3.26).

## Facies succession CRP/PG-S3

CRP/PG-S3 is formed by sandstone C, occurring along the entire area of study (Figs. 3.4 and 3.27). It overlies the regional unconformity between the late Cenomanian/early Turonian and the Coniacian/Santonian in the Carapeba field and in the western Pargo field, and Coniacian/Santonian mudstones in the eastern Pargo field (Figs. 3.4 and 3.21).

CRP/PG-S3 comprises up to 11 amalgamated turbidites, making a typical fining upward succession (e.g. density logs for wells PG-8D and CRP-25 in Fig. 3.4). They were deposited in an elongated, 1.0 to 2.5 km wide trough (Fig. 3.27), with margins that may be defined by faults (Figs. 3.2 and 3.24) or by deep erosion of late Cenomanian/early Turonian marls and Coniacian/Santonian mudstones (Figs. 3.2 and 3.22).

Very few mudstones are interbedded with the turbidites of

Fig. 3.26 - Net sand map for succession CRP/PG-S2.

SUCCESSION CRP/PG-S2

N

6

193A

14    224

11    5A

9    52

8    4

7A

0        3 km

C.I. = 10 m

○ Well control

▲ Cored well

345 000    350 000    355 000    360 000

7 540 000

50  40
30
20
10
0
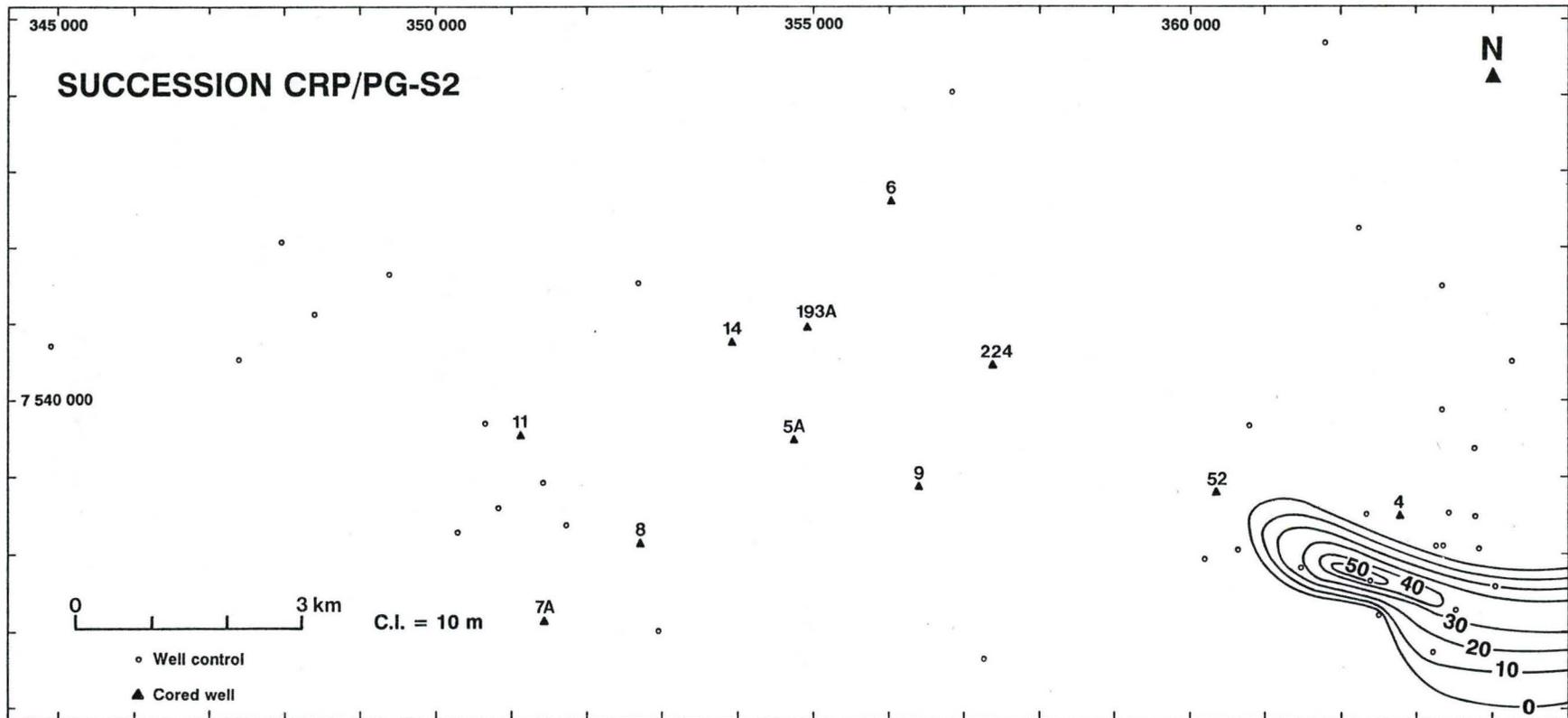
Fig. 3.27 - Net sand map for succession CRP/PG-S3.

SUCCESSION CRP/PG-S3

C.I. = 10 m

o Well control

▲ Cored well
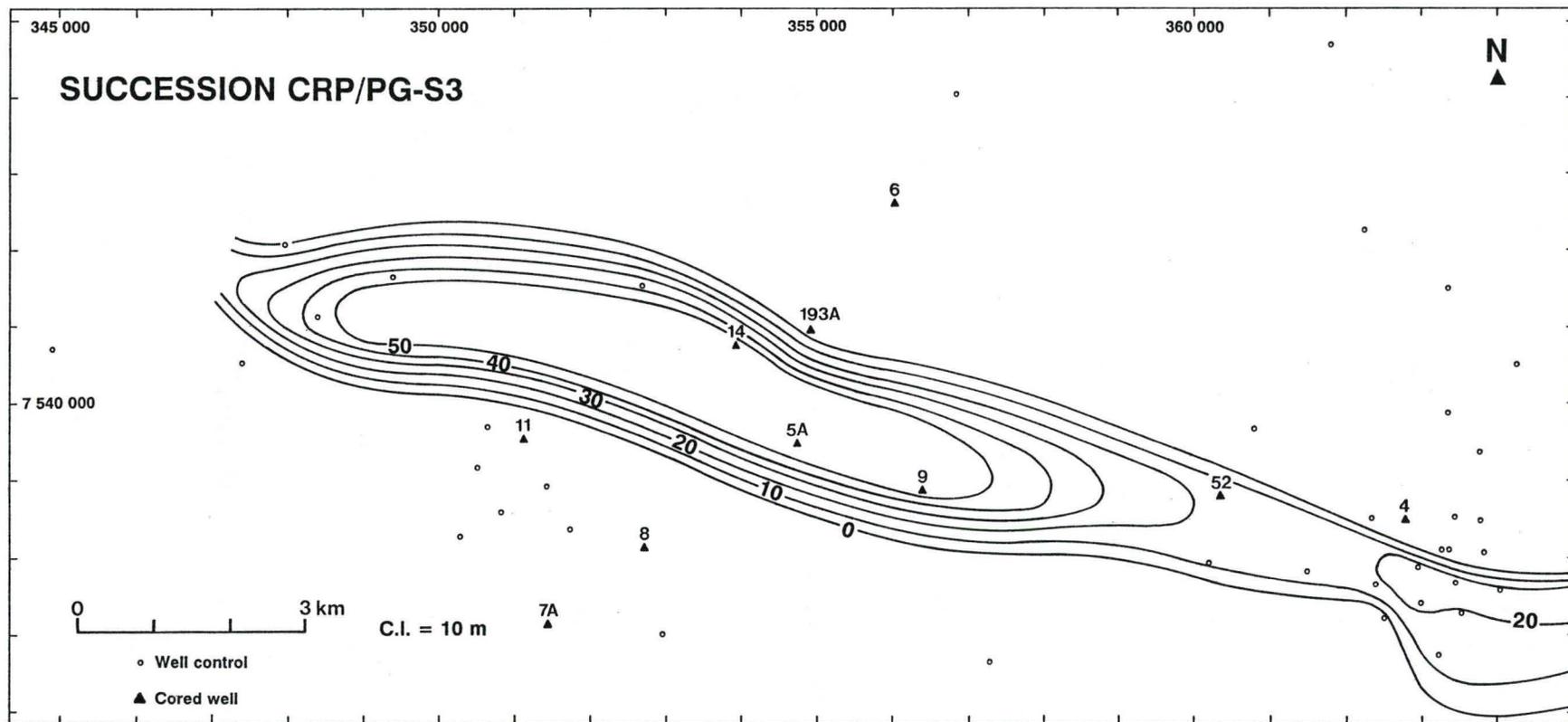
succession CRP/PG-S3, suggesting lack of time for their accumulation, and/or erosion of these finer-grained facies by high-density turbidity currents. Minor erosion at the base of individual turbidites is common, but together the individual turbidites comprise non-channelized sandstone bodies, which can be widely correlated in the studied area (Figs. 3.4, 3.21, and 3.22). The lateral extent of these deposits was controlled by the variable width of the Carapeba/Pargo canyon, which in turn was shaped by the combined effects of subsidence along listric normal faults and erosion by high density turbidity currents.

## Facies succession CRP/PG-S4

CRP/PG-S4 is the thickest (up to 125 m) facies succession (Fig. 3.28), comprising sandstones D to L (Table 3.5, and Figs. 3.2 and 3.4). It overlies CRP/PG-S3 along most of the study area, and is partially eroded by CRP/PG-S5 in the westernmost part of Carapeba field (compare wells CRP-4D and CRP-37D in Fig. 3.23).

The net sand maps for the sandstones D, F, and K (Figs. 3.29, 3.30, and 3.31, respectively) illustrate how the lateral extent of CRP/PG-4 was gradually increasing with time. The lowermost deposits of CRP/PG-4 (sandstone D) occupied an elongated, 1.2 to 3.1 km wide trough (Fig. 3.29). The younger sandstone F shows a wider distribution, extending farther to the west of Carapeba and reaching widths between 1.7 and 5.3

Fig. 3.28 - Net sand map for succession CRP/PG-S4.

SUCCESSION CRP/PG-S4

C.I. = 20 m

○ Well control
▲ Cored well
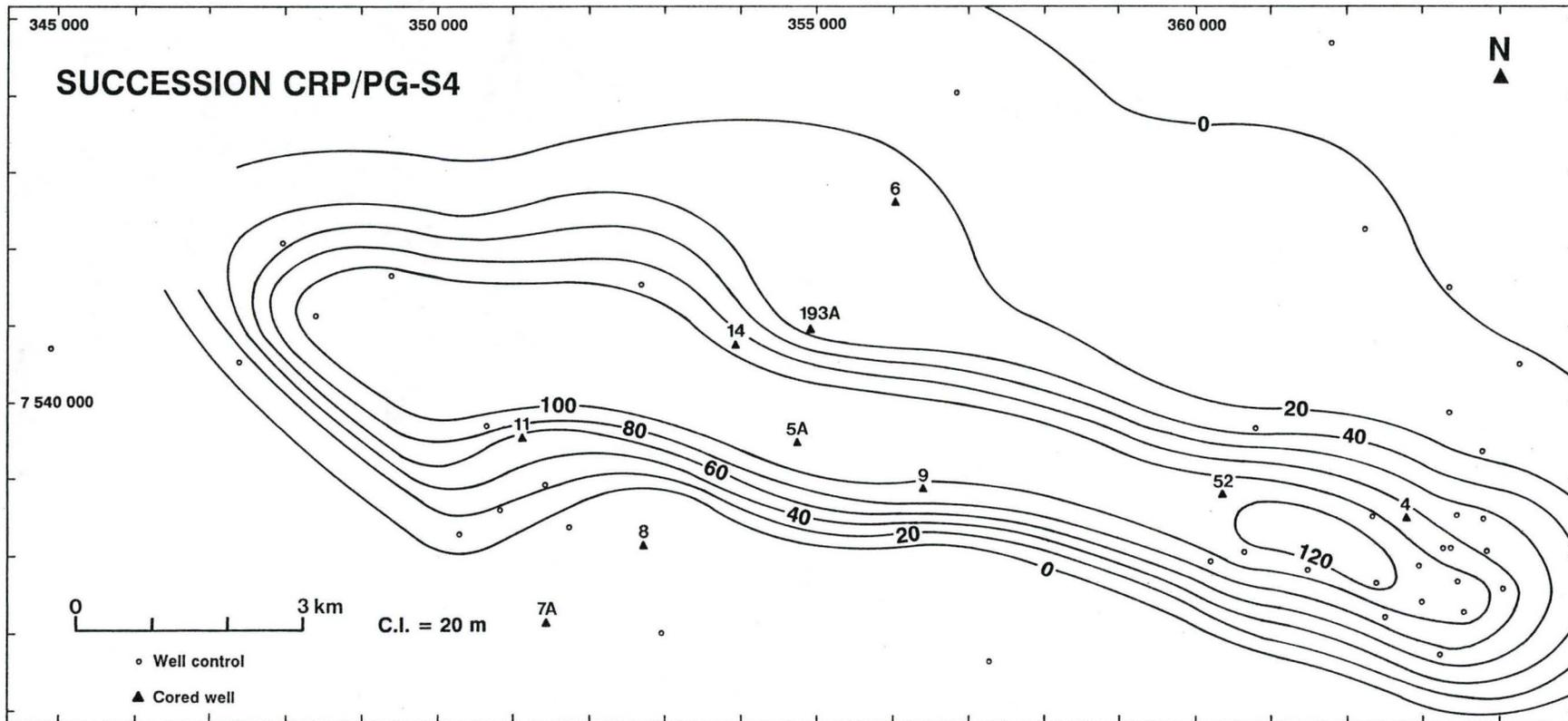
Fig. 3.29 - Net sand map for sandstone D.

SANDSTONE D

N

345 000  350 000  355 000  360 000

6 ▲

193A ▲

14 ▲

7 540 000

20

11 ▲  10

5A ▲

9 ▲

52 ▲

4 ▲

0

20

8 ▲

0  3 km

C.I. = 10 m

7A ▲

○ Well control

▲ Cored well

129
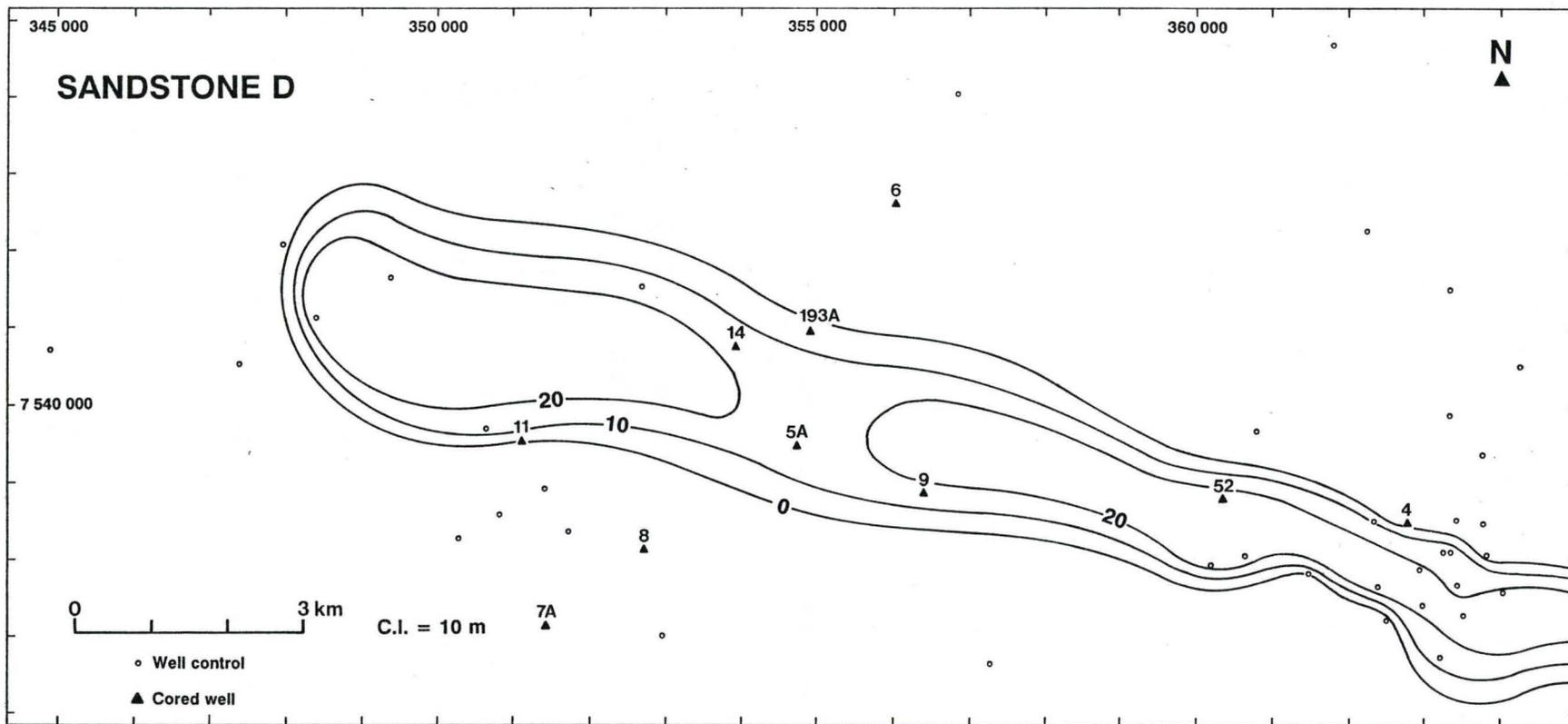
Fig. 3.30 - Net sand map for sandstone F.

SANDSTONE F

N

Well control
Cored well

0          3 km

C.I. = 5 m
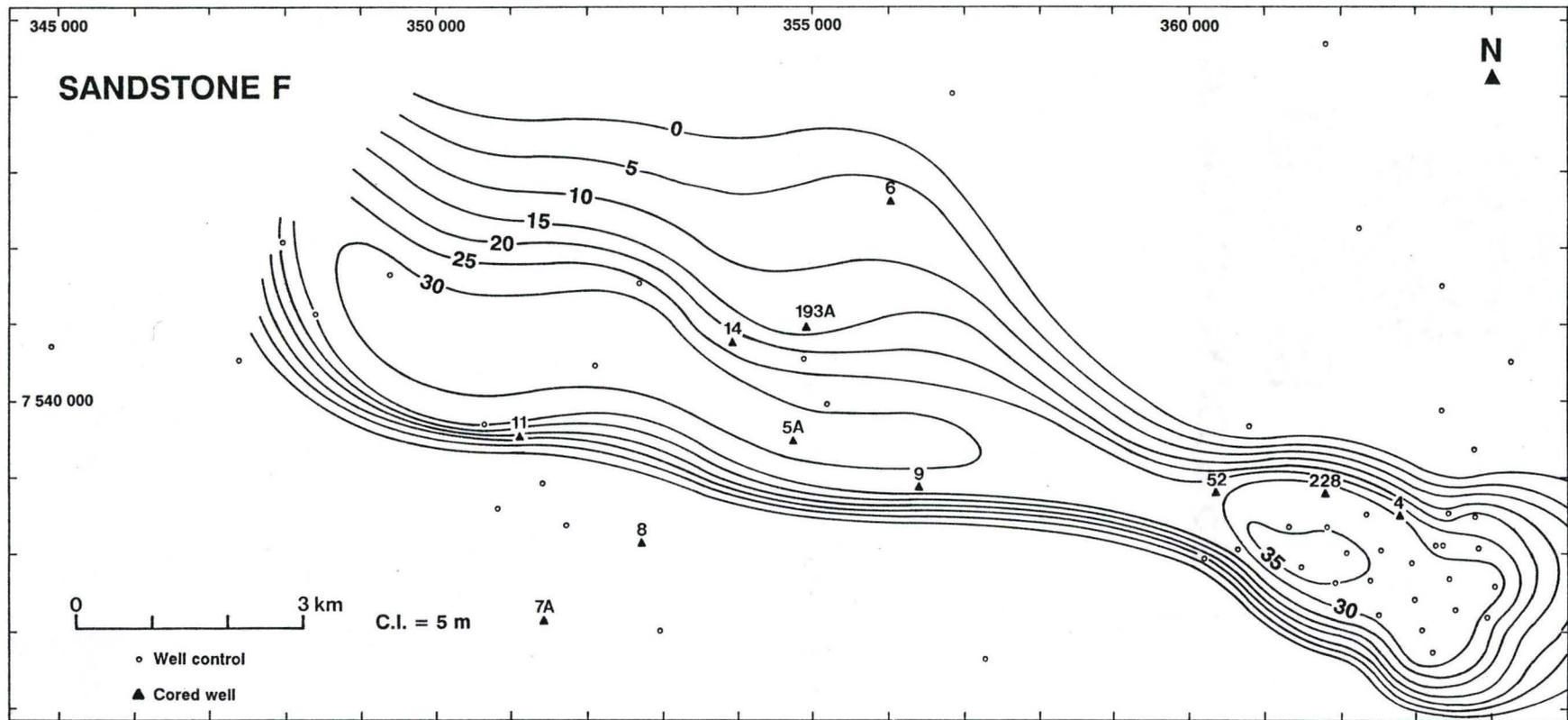
Fig. 3.31 - Net sand map for sandstone K.

SANDSTONE K

N

345 000  350 000  355 000  360 000

7 540 000

0
2
4
6
8
10
12

6

193A

224

14

11  14  12

10

5A

10

9

27A

52  228

4

14

16

12

10

14

8

6

4

2

0

8

7A

0

3 km   C.I. = 2 m

○ Well control

▲ Cored well
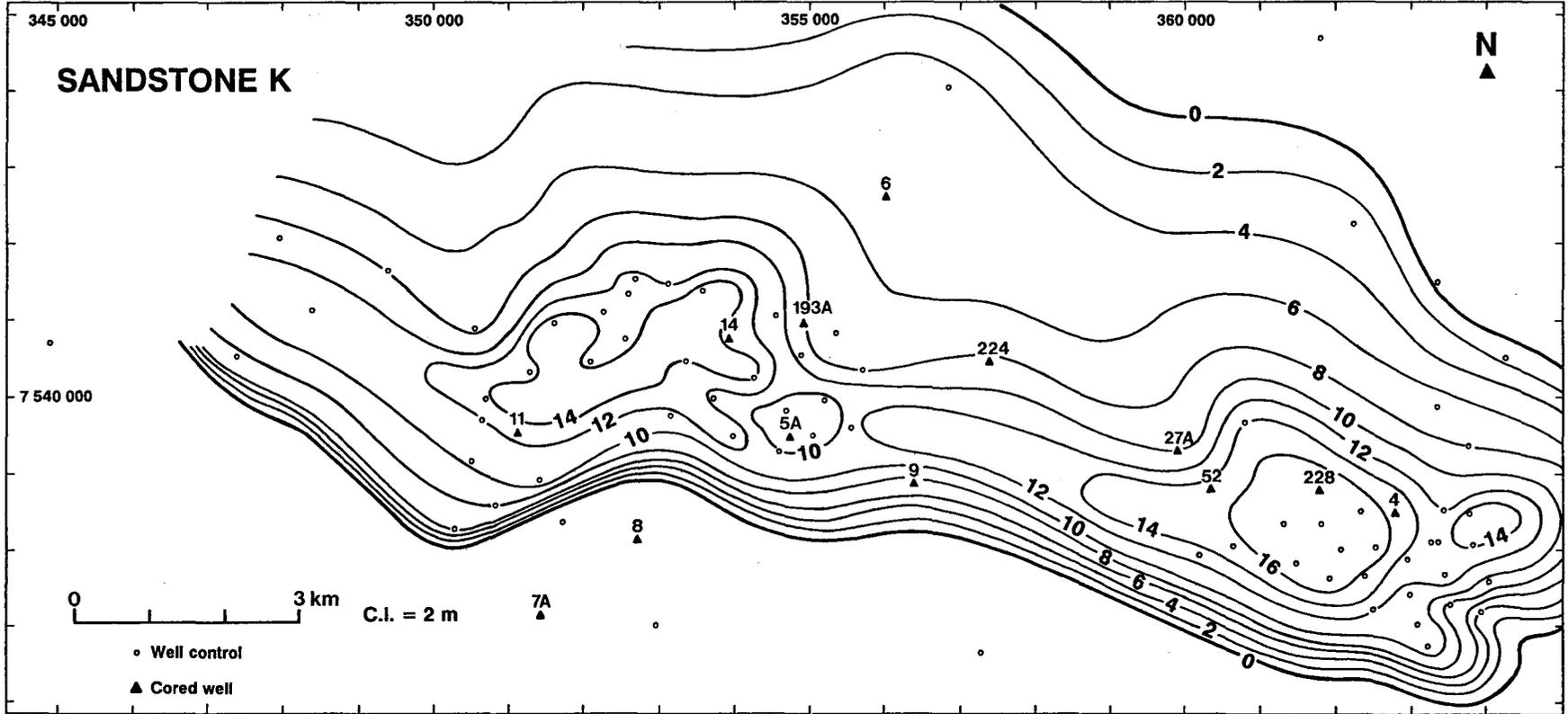
km (Fig. 3.30). Sandstone K, one of the uppermost sandstones of CRP/PG-4 (Fig. 3.2), is the most widespread of the entire succession, with a lateral extent typically exceeding 6 km in the studied area (Figs. 3.2, 3.22, and 3.31). This tendency of increasing lateral extent reflects the decreasing tectonic (faulting) control on the preferential location for turbidite deposition.

The net sand maps for CRP/PG-S4 and its sandstones D, F, and K (Figs. 3.28 to 3.31), also show asymmetrical subsidence along the Carapeba/Pargo canyon during the accumulation of CRP/PG-S4. Higher rates of subsidence and sedimentation are recorded closer to the strongly-faulted southern margins of the canyon, where the isopachs show larger values and closer spacing. Figures 3.2 and 3.24 illustrate some of the very active faults that defined the southern boundaries of the Carapeba/Pargo canyon, whereas figure 3.22 shows the more reduced effects of faulting on the northernmost distribution of the CRP/PG-S4 sandstones in the Pargo field.

The coarse-grained turbidites of CRP/PG-S4 form an overall fining upward trend (e.g. density logs for wells RJS-52 and RJS-222 in Fig. 3.4). They also become finer-grained down canyon, as illustrated by the grain-size distribution in the turbidite E1 (sandstone E; Fig. 3.32). These upward- and eastward-fining trends are defined by a decrease in proportion of gravel and very coarse-grained sand, and an increase in proportion of coarse- to medium-grained sand. However, even

Fig. 3.32 - Isopach map for turbidite E1. Textural lateral variation was mapped on the basis of density log responses (Table 3.3).

TURBIDITE E1

DOMINANT LITHOLOGY:

- Conglomerate/conglomeratic sandstone
- Very coarse-grained sandstone
- Coarse- to medium-grained sandstone

0          3 km

C.I. = 5 m

○ Well control
▲ Cored well
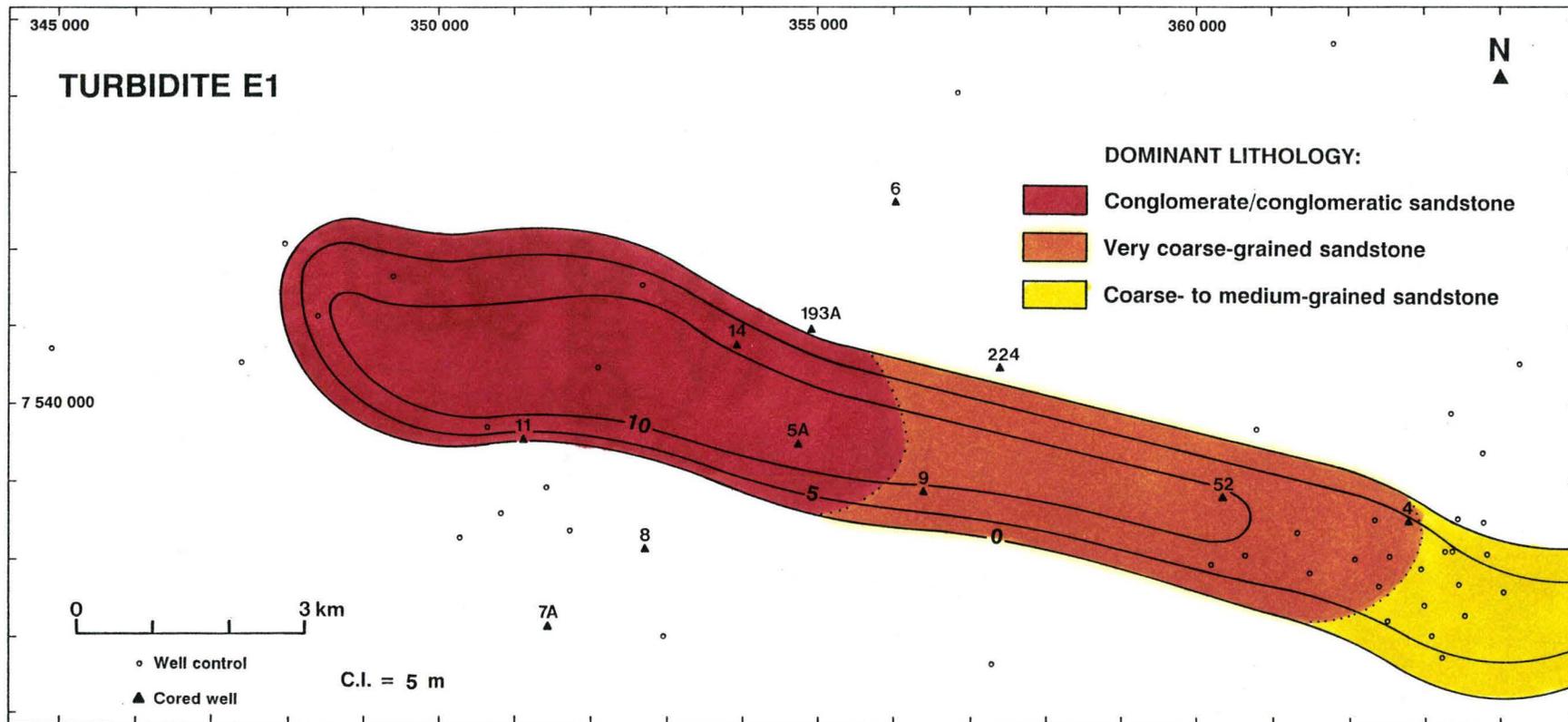
the uppermost sandstones of CRP/PG-S4 are rarely composed of fine-grained sand.

A closer analysis of the general fining-upward trend presented by CRP/PG-S4 reveals a cyclic stacking of at least seven thinner, fining-upward sucessions. They are represented, from the bottom to the top, by the sandstones D, E, F, G to I, J, K and L (e.g. density log for well PG-8D, Fig. 3.4; and cores of well PG-4, Fig. 3.5). Each of these smaller-scale successions comprises one to six amalgamated turbidites. Relatively important mudstone accumulation and erosion took place in between the deposition of some of the smaller-scale successions, particularly closer to the Carapeba/Pargo trough margins. For example, up to 23 m of mudstones and thin-bedded sandstones were preserved between the sandstones F and J in the Pargo field, at the proximity of the trough southern margin (well PG-13D, Fig. 3.22).

The average turbidite thickness calculated for sandstones D to L characterizes the entire CRP/PG-S4 as a thinning-upward succession (Table 3.5). The turbidites (and sandstone bodies) of sandstone L are not only finer-grained and thinner-bedded, but also laterally restricted. They comprise smaller, lobate deposits, which were deposited preferentially in between two previously-deposited lobes, or on the thinner flanks of underlying lobes (Figs. 3.21, 3.22, and 3.23). The term lobe is used **exclusively** to describe the geometry of L sandstone bodies; i.e. as having curved or rounded projections in plan

view, and mounded cross section, with flat or concave upward base, and convex upward top. The geometrical configuration resulting from the tendency of some turbidites to smooth the subtle relief produced by previously-deposited lobate deposits is referred here as a **compensation arrangement.** Compensation arrangements can be recognized by "compensation cycles" (Mutti and Sonnino, 1981) in areas lacking laterally continuous outcrop or well control; they comprise superimposed, small-scale thickenning-upward successions, each containing few (< 10) turbidite beds.

Detailed correlations show that all of the sandstones of CRP/PG-S4 form non-channelized reservoir rocks. Their lateral extent was controlled by fault activity and the resulting variable width of the Carapeba/Pargo trough (sandstones D to I; Figs. 3.2 and 3.24), by the volume of individual turbidity currents (sandstone L; Figs. 3.21 to 3.23), or by both factors (sandstones J and K; Figs. 3.2, 3.22 and 3.24).

**Facies succession CRP/PG-S5**

CRP/PG-S5 is the second thickest (up to 85 m) succession of the Carapeba/Pargo turbidite system (Fig. 3.33), comprising sandstones M to P (Table 3.5 and Fig. 3.4). Its base is defined by a local erosion surface in the westernmost part of Carapeba field, which becomes a correlative, non-erosive surface toward Pargo field (Figs. 3.4 and 3.23). This basal discontinuity is related to local erosion of the entire

Fig. 3.33 - Net sand map for succession CRP/PG-S5.

SUCCESSION CRP/PG-S5

345 000      350 000      355 000      360 000

N

7 540 000

80
70
60
60
50
40
30
20
10
0
0

6
193A
14
224
5A
27A
9
52
228
4
11
8
7A

C.I. = 10 m

0      3 km

○ Well control
▲ Cored well
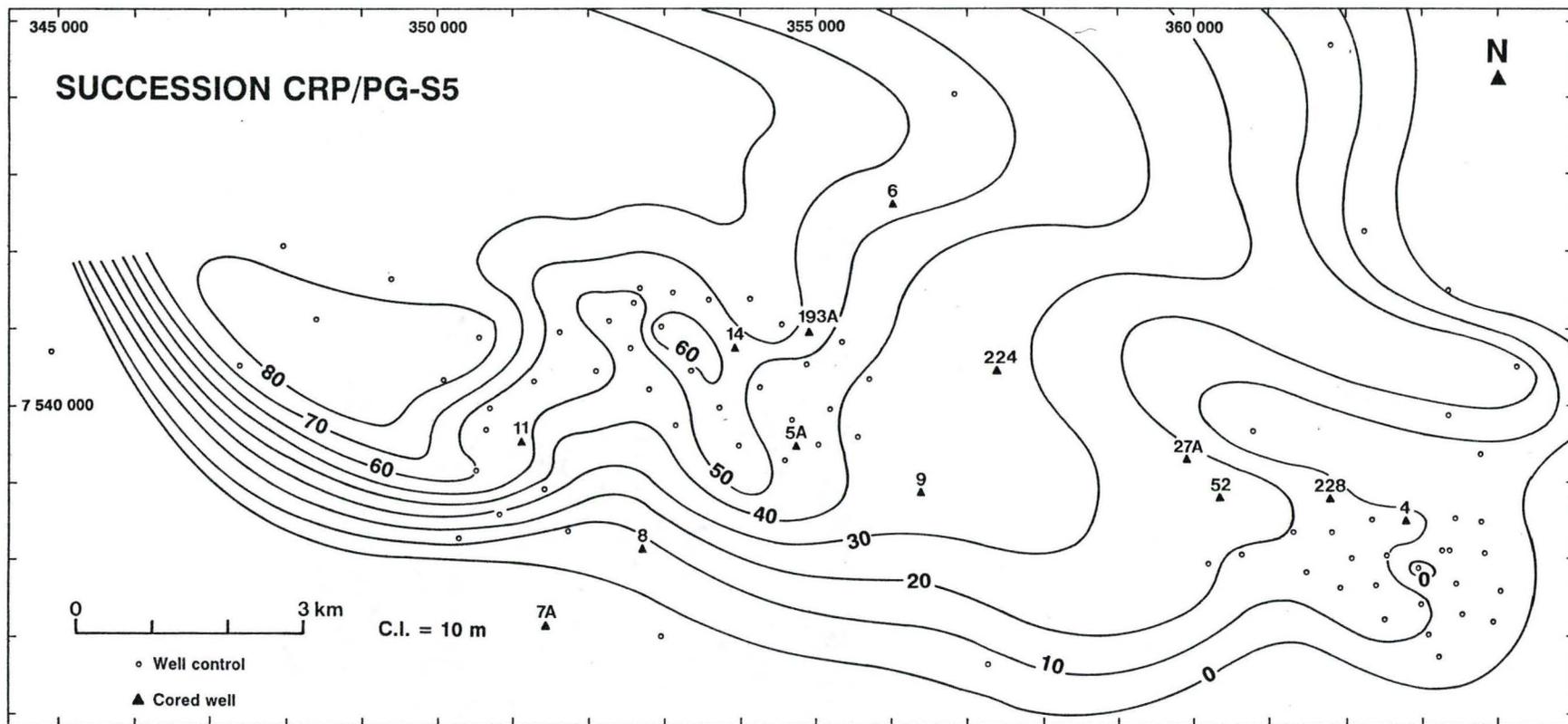
sandstone L and part of sandstone K along the deepest portions of the Carapeba/Pargo canyon (Figs. 3.4 and 3.23).

Some of the faults that controlled the distribution of the underlying CRP/PG-S4 became inactive during sedimentation of CRP/PG-S5 (e.g. Fig. 3.24); this sucession eventually overlies late Cenomanian/early Turonian marls and mudstones, and Coniacian/Santonian mudstones along the southern margin of the Carapeba/Pargo canyon (Fig. 3.24). CRP/PG-S5 does not have the same downstream, eastward extension as CRP/PG-S4, but occupies a much larger trough (up to 12 km; Figs. 3.1 and 3.33).

The coarse-grained turbidites of CRP/PG-S5 comprise a fining-upward and fining-eastward sucession, similar to CRP/PG-S4. These turbidites have a well-defined vertical trend of decreasing grain size, which is recognized in cores (e.g. Fig. 3.6) or indicated by density logs (e.g. well RJS-222 in Fig. 3.4). This trend can be easily differentiated from that defined by CRP/PG-S4 along most of the Carapeba field. However, their separation in the westernmost Carapeba field and in the Pargo field is not as easy because of the stacking of relatively homogeneous coarser-grained deposits westward, and the juxtaposition of only thinner and finer-grained turbidites eastward (compare the wells CRP-25, RJS-222, and RJS-52 in Fig. 3.4). CRP/PG-S5 also can be subdivided into at least two smaller-scale fining-upward successions, which are represented by the sandstones M (19 to 22 turbidites), and N

to P (32 to 36 turbidites) (e.g. density log for the well CRP-14 in Fig. 3.23).

CRP/PG-S5 thins upward, as indicated by the upward decreasing in the average turbidite thickness for the sandstones M to P (Table 3.5), and also becomes thinner down canyon (Figs. 3.4, 3.21, 3.23, and 3.33). The geological sections for the Carapeba field show that sandstones O and P are typically finer-grained, thinner, and laterally more restricted than the sandstones M and N, commonly presenting compensation arrangements (Figs. 3.2 and 3.23). In Pargo field, CRP/PG-S5 is represented almost exclusively by the finer-grained, thinner (terminal) portions of the sandstones M and N, which also may comprise compensation arrangements (Fig. 3.22).

Most of the reservoir rocks of CRP/PG-S5 present a non-channelized geometry; this geometry can be established because of the closely-spaced well control (Figs. 3.21 to 3.24). However, some of the lowermost turbidites of sandstone M (turbidites M1 to M6) may be filling channels eroded into the uppermost part of CRP/PG-S4 (e.g. wells CRP-24, CRP-25 and CRP-4D in Fig. 3.23). The 25-m-isopach curve for the Sandstone M defines three major trends of channelling, and embraces all of the areas where sandstone L (CRP/PG-S4) was partially or totally eroded (Fig. 3.34).

The lateral extent of the CRP/PG-S5 sandstone bodies seems much less controlled by faulting, and more influenced by

Fig. 3.34 - Net sand map for sandstone M.
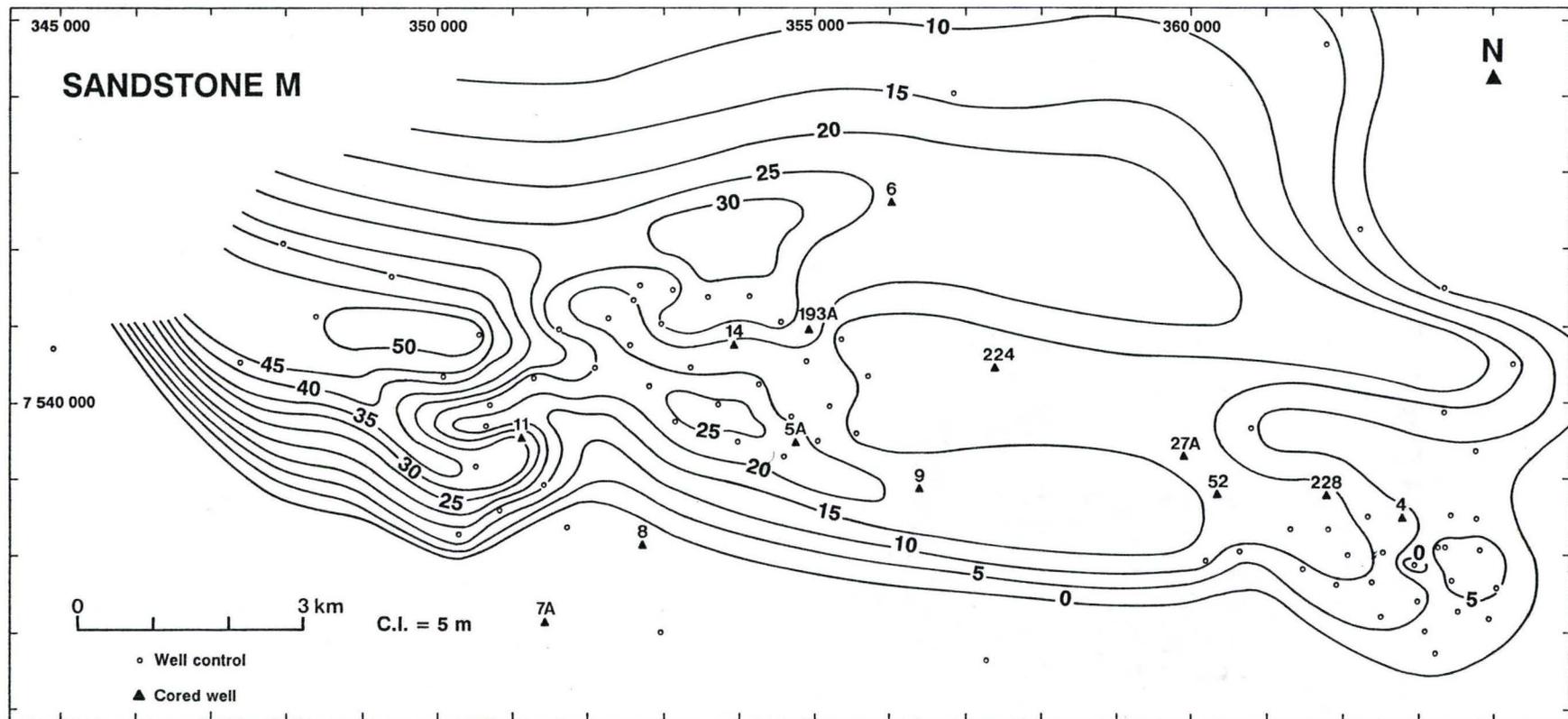
SANDSTONE M

the volume and frequency of turbidity currents than in the underlying successions.

## Facies succession CRP/PG-S6

CRP/PG-S6 contains sandstones Q to U (Table 3.5, and Fig. 3.4). The main criterion for the separation of CRP/PG-S6 from the underlying CRP/PG-S5 succession is its distinct sandstone thickness distribution (Fig. 3.4 and 3.23). The lowermost sandstone bodies of CRP/PG-S6 (sandstones Q and R), besides being thicker than the uppermost sandstone bodies of CRP/PG-S5 (sandstone P), also have a wider areal distribution (Fig. 3.2). However, CRP/PG-S6 shows a much more limited distribution than that of the CRP/PG-S5 succession (compare Figs. 3.33 and 3.35). Except for 2 turbidites that reached the westernmost end of the Pargo field (wells PG-27A and RJS-52; Fig. 3.21), CRP/PG-S6 is restricted to an area up to 7.3 km wide in the Carapeba field (Fig. 3.35).

Net sand maps for sandstones Q, R, and S (Figs. 3.36, 3.37, and 3.38) show a gradual reduction in areal distribution of the turbidites in CRP/PG-S6. CRP/PG-S6 turbidites typically comprise non-channelized sandstone bodies (e.g. Figs. 3.2 and 3.23), with the uppermost sandstones (sandstones S, T and U; e.g. Fig. 3.38) showing a lobate geometry. The lateral distribution of the CRP/PG-S6 turbidites seems primarily defined by the volume of individual turbidity currents, which gradually decreased during the sedimentation of this

Fig. 3.35 - Net sand map for succession CRP/PG-S6.

SUCCESSION CRP/PG-S6

345 000    350 000    355 000    360 000

N

30

7 540 000

0          3 km

○ Well control

▲ Cored well

C.I. = 5 m

6

193A

14

224

11

5A

30

27A

25

9

52

228

20

8

4

15

10

7A

5

0
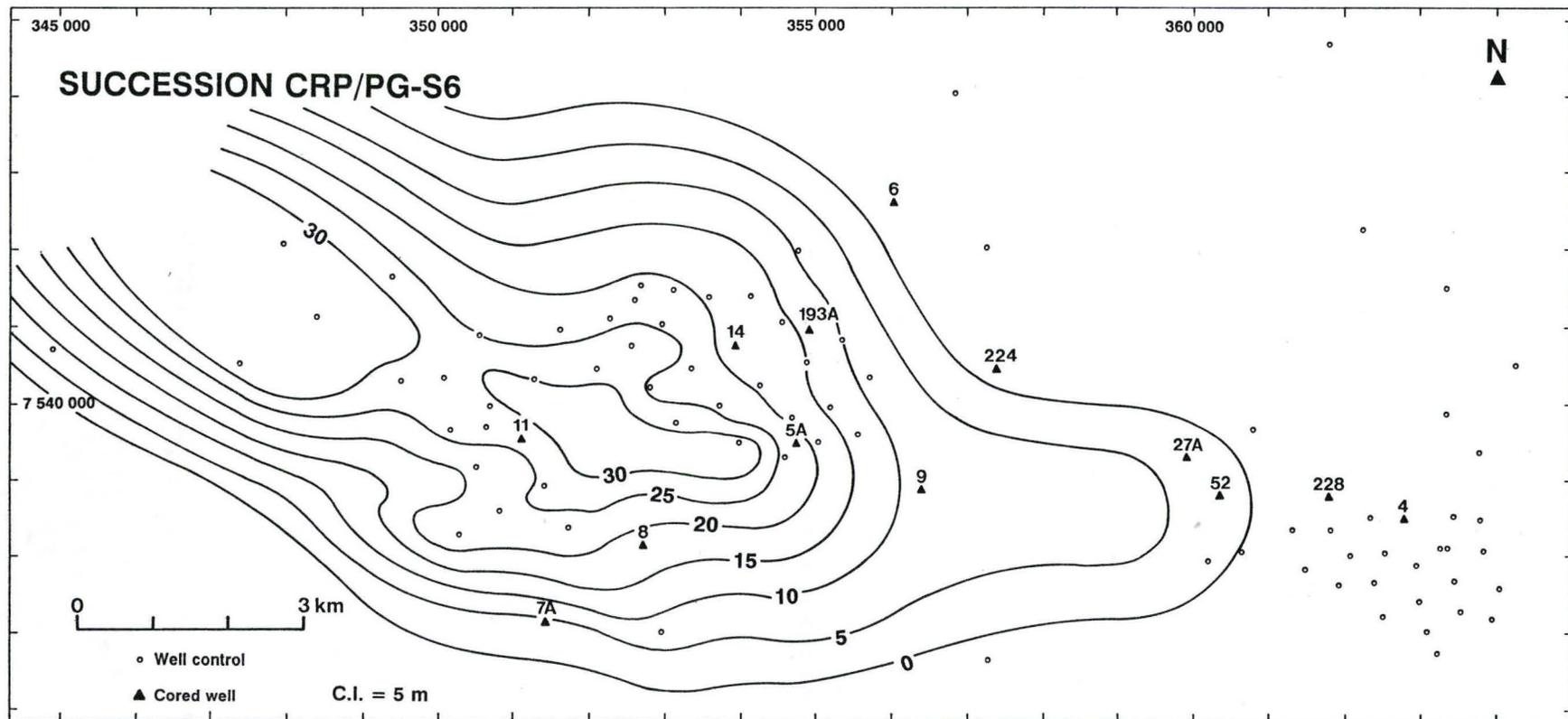
Fig. 3.36 - Net sand map for sandstone Q.

SANDSTONE Q

C.I. = 2 m

○ Well control
▲ Cored well

0        3 km
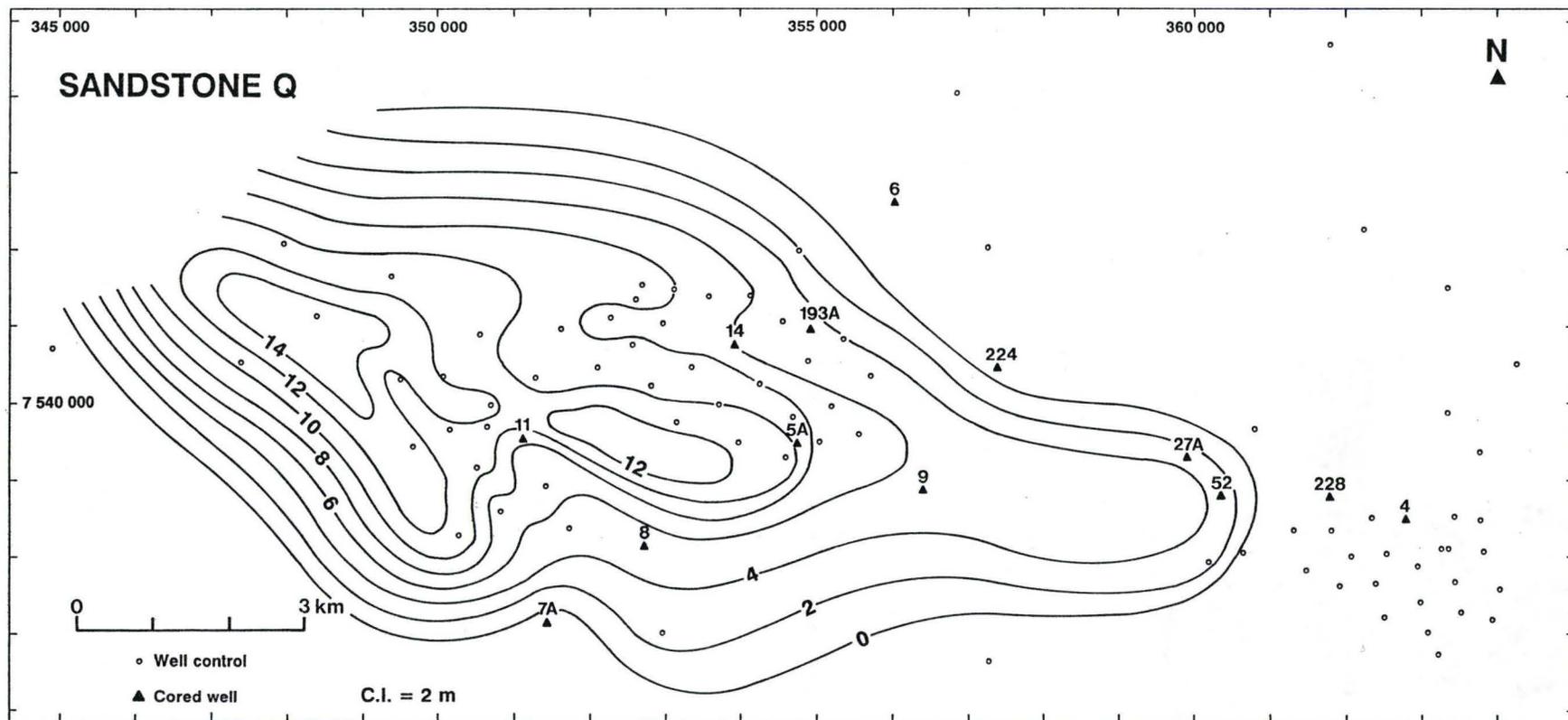
Fig. 3.37 - Net sand map for sandstone R.

SANDSTONE R

345 000    350 000    355 000    360 000

N ▲

6 ▲

193A ▲

14 ▲

224 ▲

10

11 ▲

5A ▲

27A ▲

10

52 ▲

228 ▲

9 ▲

4 ▲

8

8    8

6

7A ▲

4

2

0

7 540 000

0    3 km

○ Well control

▲ Cored well

C.I. = 2 m
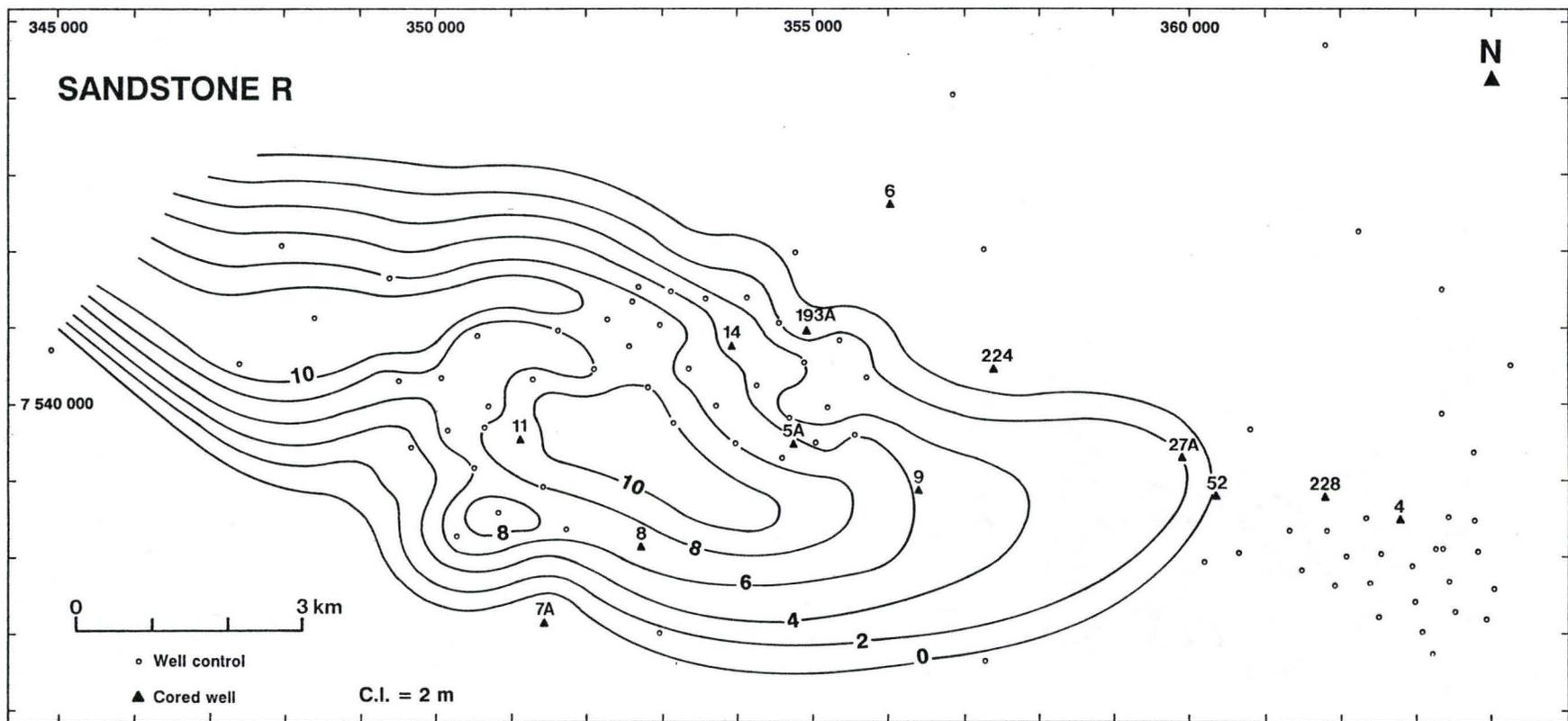
Fig. 3.38 - Net sand map for sandstone S.

SANDSTONE S

6 ▲
6
193A ▲
14 ▲
224 ▲
8
11 ▲
5A ▲
9 ▲
27A ▲
52 ▲
228 ▲
4 ▲
8 ▲
6
4
7A ▲
2
0

345 000        350 000        355 000        360 000

N ▲

7 540 000

0          3 km

∘ Well control
▲ Cored well

C.I. = 2 m
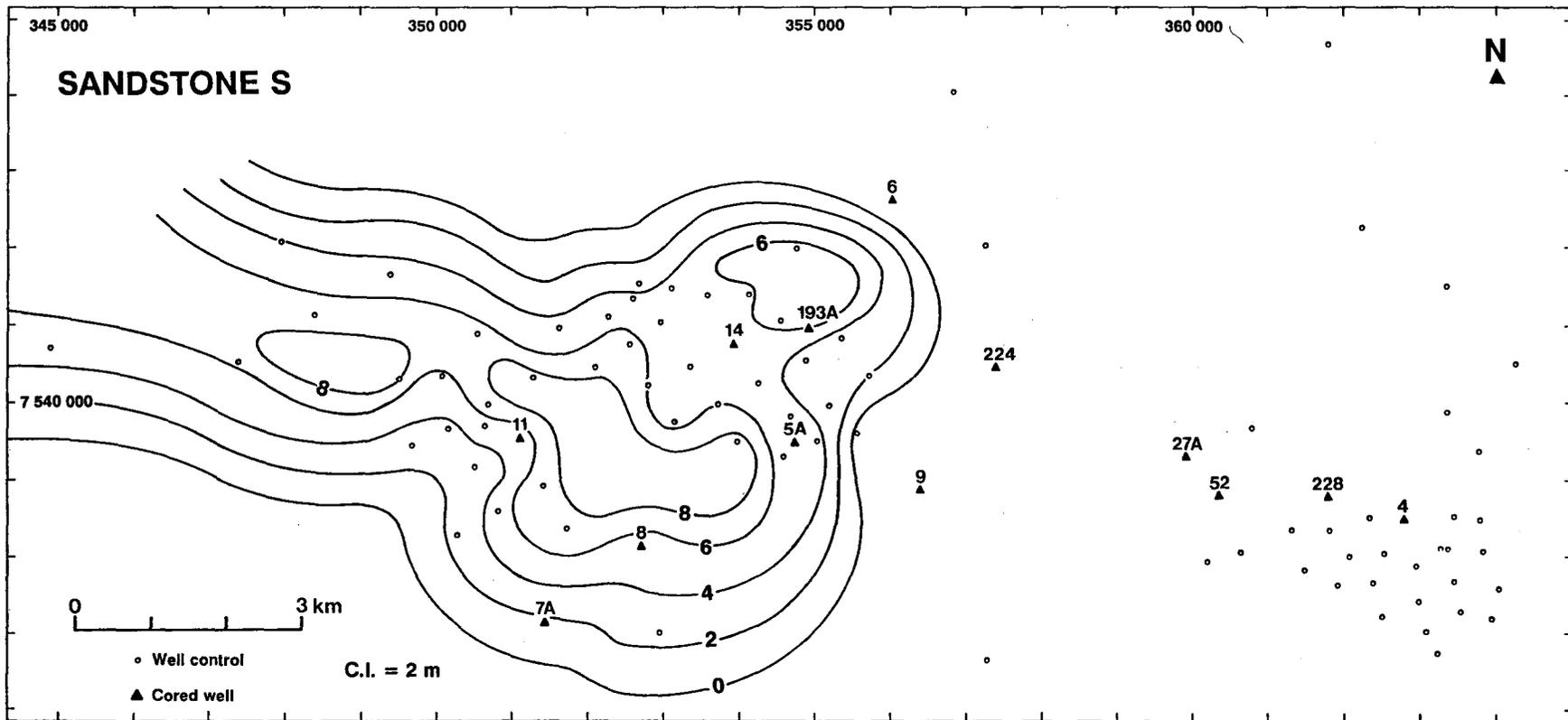
succession. The comparison between figures 3.32 and 3.39 stresses the influence of basin confinement on the geometry of individual turbidites.

CRP/PG-S6, like successions CRP/PG-S4 and CRP/PG-S5, is characterized by an upward and eastward decrease in grain size and bed thickness (Figs. 3.4, 3.23, and 3.39, and Table 3.5). The lateral variation in grain size presented by individual turbidites is illustrated in figure 3.39.

**Facies succession CRP/PG-S7**

CRP/PG-S7 comprises a group of seven turbidites collectively named sandstone V (Fig. 3.4). Some of these turbidites may lie on the regional unconformity between the Campanian and the early Maastrichtian (e.g. turbidite V1 in Fig. 3.24).

The individual turbidites of CRP/PG-S7 comprise non-channelized sandstone bodies, most of them with limited lateral distribution (Figs. 3.2, 3.23, and 3.24). The net sand map for the entire succession (Fig. 3.40) shows greater isopachs in the southwestern part of Carapeba field, which suggest higher subsidence in this area, possibly related to fault reactivation during the early Maastrichtian.

CRP/PG-S7 may comprise fining upward successions in the areas with thicker stacking of turbidites (e.g. density log for well CRP-25 in Fig. 3.23).

Fig. 3.39 - Isopach map for turbidite S2. Textural lateral variation was mapped on the basis of density log responses (Table 3.3).

TURBIDITE S2

DOMINANT LITHOLOGY:

Conglomerate/conglomeratic sandstone

Very coarse-grained sandstones

Coarse- to medium-grained sandstones

C.I. = 1 m

0    3 km

○ Well control

▲ Cored well
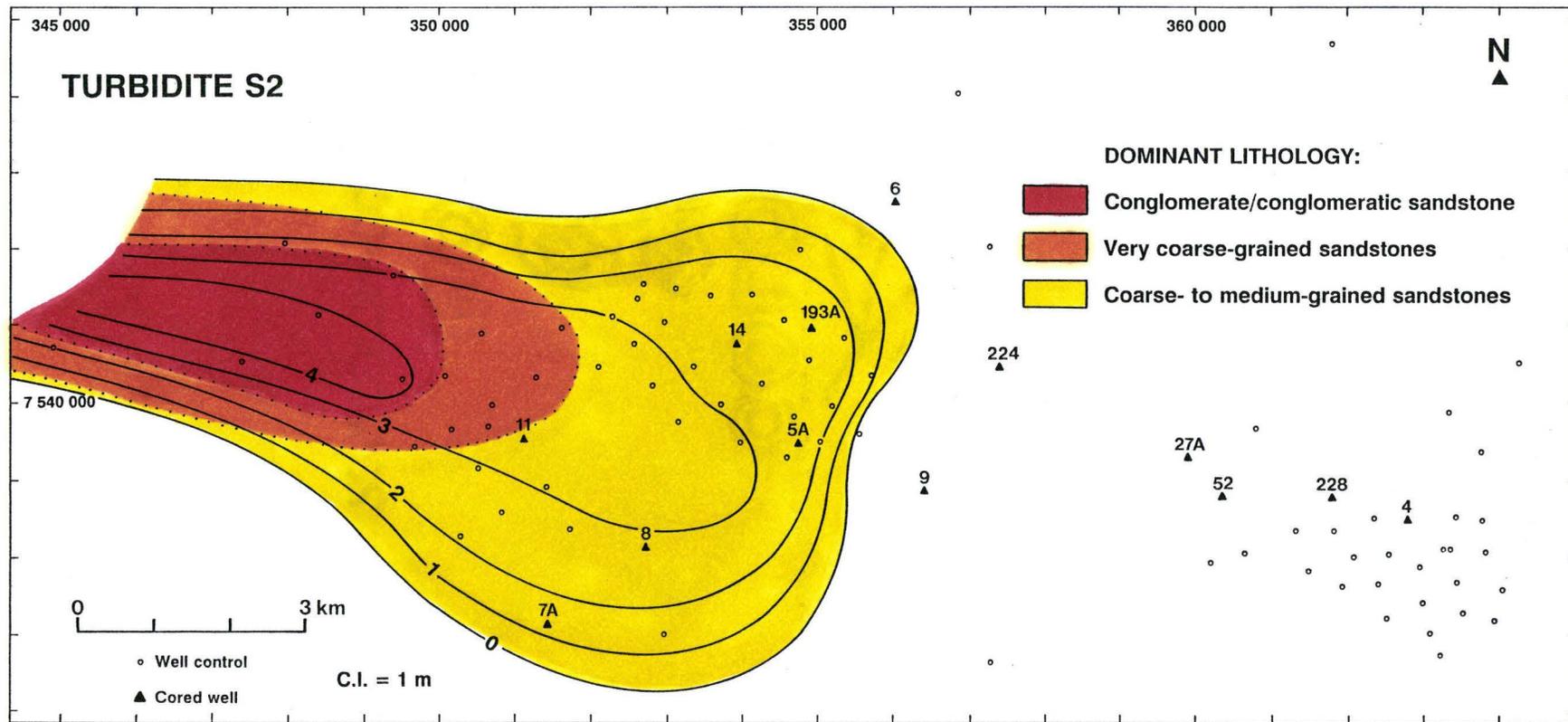
Fig. 3.40 - Net sand map for succession CRP/PG-S7.

SUCCESSION CRP/PG-S7

C.I. = 2 m

○ Well control
▲ Cored well

0          3 km
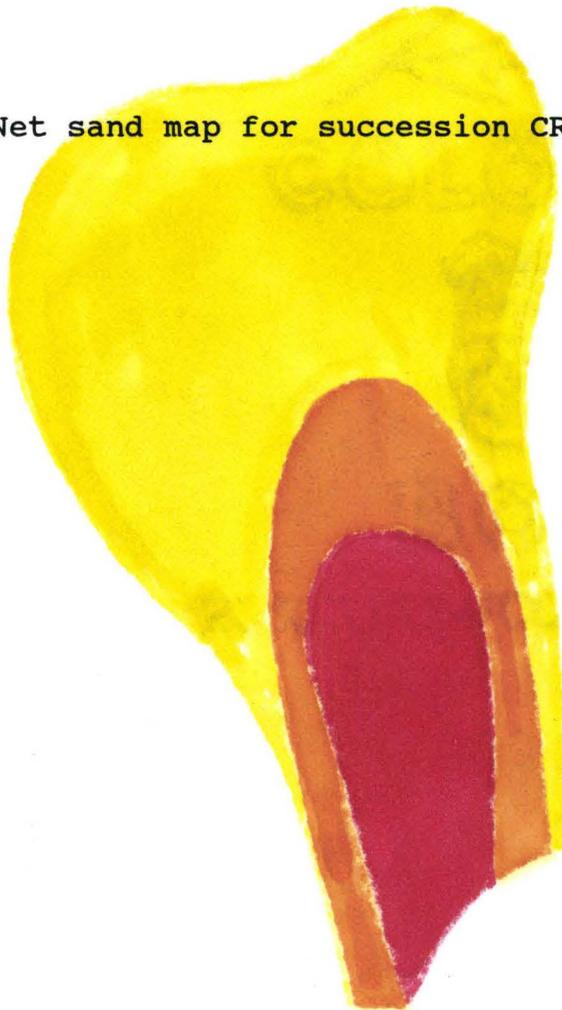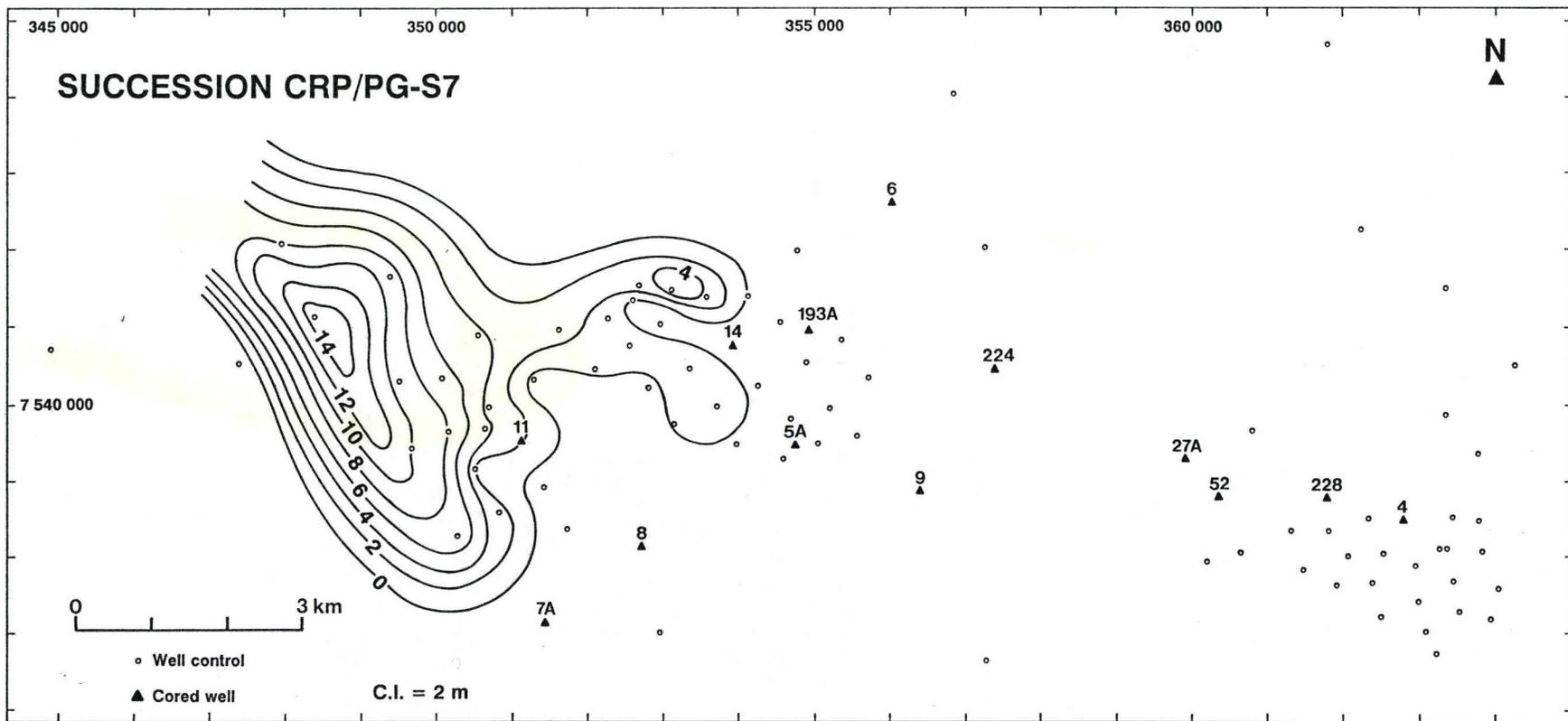
**Facies succession CRP/PG-F8**

CRP/PG-S8 includes 14, non-channelized early Maastrichtian turbidites, collectively named sandstone W (Fig. 3.23). It seems to truncate CRP/PG-S7 in the western Carapeba field, but also overlies the regional unconformity between the Campanian and early Maastrichtian along most of its area of occurrence (Fig. 3.23).

CRP/PG-S8 shows wider distribution than CRP/PG-S7. It is thicker in Carapeba field, but thinner deposits are present in Pargo field (Fig. 3.41). One of the lowermost CRP/PG-S8 turbidites, up to 5 m thick, can be correlated throughout Carapeba field into the western end of Pargo field (turbidite W3; Figs. 3.21 and 3.23). A few thin-bedded turbidites, possibly early Maastrichtian in age, were recognized in the eastern part of Pargo field (turbidites W1, W2, and W6; Figs. 3.21 and 3.22). They were tentatively included in CRP/PG-S8, but their limited distribution makes their correlation with the early Maastrichtian succession of Carapeba field very difficult.

The density logs for the thicker occurrences of CRP/PG-S8 suggest a fining upward trend for this succession (e.g. density log for well CRP-25 in Fig. 3.23), like that recorded for CRP/PG-S7.

## 3.4.3. Recurrence intervals of successions and individual turbidites

Fig. 3.41 - Net sand map for succession CRP/PG-S8.

SUCCESSION CRP/PG-S8

Well control
Cored well

C.l. = 2 m

0        3 km

N

The Coniacian/Santonian successions (CRP/PG-S1 to CRP/PG-S6) are included in the calcareous nannofossil zone *Marthasterites furcatus* (Azevedo et al., 1987b), which has been correlated in the Campos basin to the entire time span of the Coniacian and Santonian stages (5.5 m.y., between 88.5 to 83 Ma; Fig. 3.42). The early Maastrichtian successions (CRP/PG-S7 and CRP/PG-S8) make part of the zone *Tetralithus trifidus* (Azevedo et al., 1987b), which has a time span of 0.8 m.y. (between 73 and 72.2 Ma; Fig. 3.42). Considering the time constraint provided by these two biozones, it can be estimated an average time span of 0.9 m.y. for each of the six Coniacian/Santonian successions, and 0.4 m.y. for each of the two early Maastrichtian successions. The estimate for the Coniacian/Santonian successions should be taken as a maximum value, because an up to 28 m thick succession of Coniacian/Santonian mudstones is preserved below CRP/PG-S1 (Fig. 3.42); the time span and original thickness of these mudstones can not be precised.

The average recurrence intervals for individual turbidites are 31,000 to 34,000 years for the Coniacian/ Santonian successions altogether (160 – 177 turbidites/5.5 m.y.), and 38,000 years for the early Maastrichtian successions (21 turbidites/0.8 m.y.). The shortest recurrence interval estimated for the studied turbidites is about 15,000 years, which is presented by the CRP/PG-S5 turbidites (up to 58 turbidites/0.9 m.y.).

Fig. 3.42 - Comparison between the global sea-level curve of Haq et al. (1988) and the chronostratigraphy, biostratigraphy, and lithostratigraphy of the marine transgressive megasequence in the Carapeba/Pargo area. Only the section between the uppermost part of the Albian and the lowermost part of the Paleocene is represented. Campanian mudstones do not contain the worldwide index fossil (foraminifera) *Globotruncana calcarata* (Caron, 1985); a time span of 2 m.y. was assigned for the missing late Campanian succession, which is equivalent to the time span suggested for the *Globotruncana calcarata* zone by Haq et al. (1988). Biozones recognized in the late Cretaceous successions of the eastern Brazilian marginal basins are traditionally tied to the chronostragraphic column proposed by Harland et al. (1982). The chronostratigraphy presented by Harland et al. (1982) and Haq et al. (1988) show differences of 0.1 to 1.5 m.y. in the time boundaries assigned for the different late Cretaceous stages.

| CHRONO-STRATIGRAPHY[1] | BIOSTRATIGRAPHY[2] | LITHOSTRATIGRAPHY | CHRONO-STRATIGRAPHY[3] | EUSTATIC CURVES[3] |

Dominant lithology:

Sandstone (turbidite)

Mudstone

Marl

Calcilutite
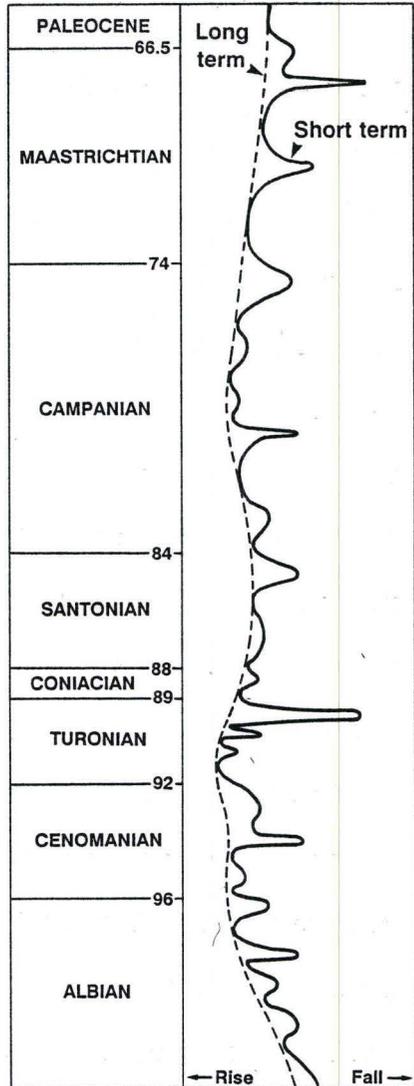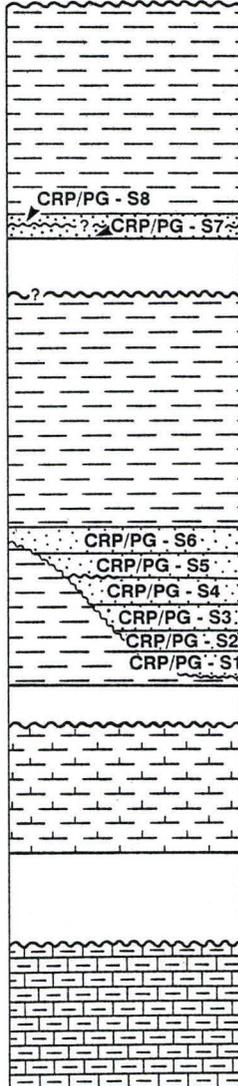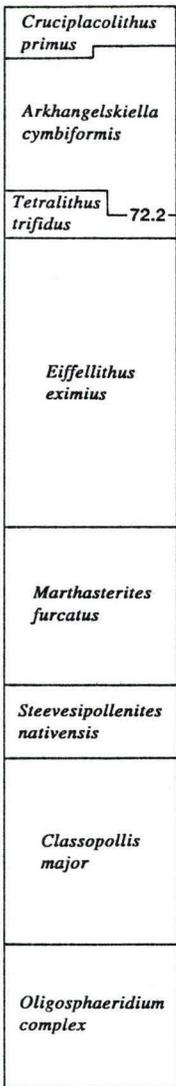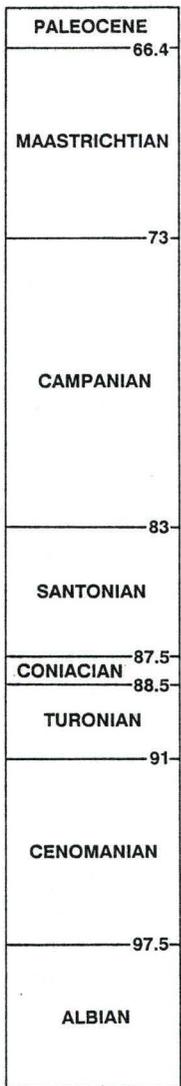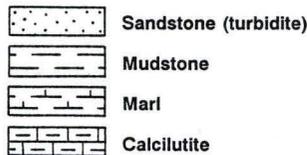
## 3.5. SEDIMENTATION EVOLUTION AND CONTROLS

### 3.5.1. The general picture

The Carapeba/Pargo turbidite system is composed of five major facies: unstratified, graded conglomerates and very coarse- to medium-grained sandstones deposited by high-density turbidity currents (CRP/PG-F1); stratified, mostly fine-grained sandstones deposited by low-density turbidity currents (CRP/PG-F2); bioturbated mudstones (*Zoophycos* ichnofacies), containing a benthic foraminifera fauna typical of mid to lower bathyal (1,000 - 1,500 m) depositional settings (CRP/PG-F3); interbedded mudstones and fine-grained sandstones deformed by slides and slumps, or due to overloading by suddenly emplaced, thick, coarse-grained turbidites (CRP/PG-F4); and disorganized, intraclastic mudstones and sandstones deposited by debris flows (CRP/PG-F5). CRP/PG-F1 is by far the volumetrically most important among all of the sandstone-bearing facies, comprising 95 % of the cores of these rocks. This coarser-grained facies also contains all of the oil-producing rocks in the Carapeba and Pargo fields, with average porosities and permeabilities exceeding 17 % and 300 mD, respectively.

The Carapeba/Pargo turbidite system was built up by 181 to 198 coarse-grained turbidites (Table 3.5), mostly 2 to 4 m thick (range 0.5 - 12 m), which typically form non-channelized

sandstone bodies. The entire turbidite system can be subdivided into six Coniacian/Santonian facies successions (CRP/PG-S1 to CRP/PG-S6) and two early Maastrichtian facies successions (CRP/PG-S7 and CRP/PG-S8), mainly on the basis of the distinct trends of grain size and bed thickness in the unstratified, graded conglomerates and sandstones (Fig. 3.4 and Table 3.6). Some of these successions may also be bounded by regional unconformities or local erosion surfaces (Table 3.6, and Figs. 3.2 and 3.4).

The facies successions have maximum preserved thickness varying from 27 to 140 m (including sandstones and interbedded mudstones), and individually contain 7 to 58 turbidites. Most of the successions (CRP/PG-S2 to CRP/PG-S8) have well-defined, fining-upward and fining-downstream (eastward) trends in grain size distribution (Fig. 3.4). Successions CRP/PG-S4 to CRP/PG-S6 also show well-defined variation trends in sandstone thickness and lateral distribution: younger or more distal sandstones become thinner-bedded and more discontinuous (Fig. 3.4).

The successions have average durations of 0.9 m.y. (CRP/PG-S1 to CRP/PG-S6) and 0.4 m.y. (CRP/PG-S7 and CRP/PG-S8).

The Carapeba/Pargo turbidite system is included in the marine transgressive megasequence, which is characterized by onlapping, deepening-upward sedimentation throughout the eastern Brazilian marginal basins (e.g. Chang et al., 1988;

**Table 3.6 - Area of occurrence and bounding discontinuities of the coarse-grained, turbidite successions of the Carapeba and Pargo fields.**

| SUCCESSIONS | AREA OF OCCURRENCE / BOUNDING DISCONTINUITIES |
|---|---|

EARLY MAASTRICHTIAN

CRP/PG-S8    It occurs throughout the Carapeba field and in the westernmost end of the Pargo field. It is separated from CRP/PG-S7 mostly by the larger area of occurrence of its lowermost sandstone, and also possibly by a local erosion surface. However, CRP/PG-S8 overlies the regional unconformity between the Campanian and the early Maastrichtian along most of its area of occurrence.

CRP/PG-S7    Restricted only to the western Carapeba field. At the base, it is bounded by the regional unconformity between the Campanian and the early Maastrichtian.

CONIACIAN/SANTONIAN

CRP/PG-S6    It occurs throughout the Carapeba field, and in the westernmost part of the Pargo field. CRP/PG-S6 is differentiated from CRP/PG-S5 chiefly on the basis of their distinct trends in bed thickness distribution.

CRP/PG-S5    It occurs in both fields, but is much thinner in the Pargo field. At the base, CRP/PG-S5 is bounded by an erosion surface that cuts out at least 25 m of the upper portion of CRP/PG-S4 in the westernmost Carapeba field, but can not be recognized in the Pargo field. Consequently, the separation between CRP/PG-S5 and CRP/PG-S4 is made chiefy on the basis of their distinct trends in grain size and bed thickness distribution. CRP/PG-S5 may overlie the regional unconformity between late Cenomanian/early Turonian and Coniacian/Santonian in some areas along the southern margin of the Carapeba/Pargo canyon.

CRP/PG-S4    It occurs along the entire studied area. It is separated from CRP/PG-S3 mainly by its distinct trend in grain size and bed thickness distribution. CRP/PG-S4 may overlie the regional unconformity between late Cenomanian/early Turonian and Coniacian/Santonian in some areas along the southern margin of the Carapeba/Pargo canyon.

CRP/PG-S3    It occurs along the entire studied area. It overlies the regional unconformity between the late Cenomanian/early Turonian and Coniacian/Santonian along most of its area of occurrence, but also truncates Coniacian/Santonian mudstones in the eastern Pargo field.

CRP/PG-S2    Restricted to the Pargo field; it overlies late Cenomanian/early Turonian marls and mudstones in the westernmost area of occurrence, and Coniacian/Santonian mudstones in eastern Pargo field. It is bounded at the top by Coniacian/Santonian mudstones or CRP/PG-S3 sandstones.

CRP/PG-S1    Restricted to the easternmost part of Pargo field. It is bounded at the base and top by Coniacian/Santonian mudstones.

Guardado et al., 1990). The successions CRP/PG-S1 to CRP/PG-S8 were stacked in an overall retrogradational pattern, recording the backfilling of the WNW-oriented Carapeba/Pargo canyon (Fig. 3.4).

The interaction of subsidence along listric faults and deep erosion by high density turbidity currents shaped the Carapeba/Pargo canyon, which became gradually larger from the Coniacian/Santonian to the early Maastrichtian (Fig. 3.2). Individual successions show lateral distribution (along strike) ranging from 1 to 12 km. This distribution is largely a function of variable fault activity, but is also controlled by the volume of individual turbidity currents (Fig. 3.2).

Three major questions emerge from the scenario depicted above. They concern: (1) the provenance of the thick (up to 286 m) package of texturally and compositionally immature, coarse-grained turbidites; (2) the development of individual facies successions; and (3) the overall retrogradational stacking of turbidite successions. These three questions will be addressed in the following sections.

### 3.5.2. Source of sediments

The coarse-grained turbidites of Carapeba and Pargo fields are characterized by poorly-sorted, subangular to angular grains, composed largely (40-50 %) of feldspar, and feldspar-rich rock fragments. Their source rock is represented

by upper Proterozoic igneous and high-rank metamorphic rocks, including mostly granites, granulites, and migmatites, which form the coastal mountain range of the Serra do Mar (Fig. 1.7).

The climate along the southeastern Brazilian coastal areas was humid and warm during the late Cretaceous (e.g. Parrish and Curtis, 1982; Lima, 1983). These climatic conditions would eliminate by chemical weathering most of the feldspathic grains made available at the source area, unless the bedrock topography were characterized by steep slopes (e.g. Folk, 1974; Basu, 1985). In a source area characterized by rugged topography, the commonly vigorous (and erosive) streams would decrease the residence time of feldspathic grains in soil profiles, and also cut more deeply through fresh bedrock. Consequently, a large amount of feldspar-rich, coarse-grained and angular sediments would be made available for sedimentation.

Steep slopes in the cratonic area adjacent to the Campos basin could have been produced by continued fault reactivation and relative uplift of Precambrian rocks during the late Cretaceous. This tectonic scenario is suggested by recurrent intrusions of alkaline rocks from Coniacian to Eocene (Ponte and Asmus, 1978; Almeida, 1983), and development of rhombic grabens filled with up to 850 m of late Cretaceous (?) and Tertiary sediments (Melo et al., 1985; Marques, 1990). In the neighbouring Santos basin (Fig. 1.7), the late Cretaceous

tectonic uplift and concomitant high sediment input were able
to surpass the effects of the generalized tendency for sea
level rise, with the development of a thick and coarse-
grained, regressive succession from the late Turonian onwards
(Pereira et al., 1986; Macedo, 1987).

The compositional and textural immaturity of the
Carapeba/Pargo turbidite system also implies that the
sediments derived from rapidly uplifted, faulted highlands
were not submitted to prolonged abrasion (if any) in a
transitional, high-energy depositional setting such as a
beach, shoreface, or wave-dominated delta. The hypothesis of
fan deltas directly feeding a relatively narrow, faulted shelf
is appealing. However, it remains a speculation because of
post-early Paleocene erosion of the shallower-water deposits
equivalent in time to the late Cretaceous turbidites. The
entire late Cretaceous Campos Formation is restricted to
trough-confined, coarse-grained turbidites, and bathyal
mudstones.

### 3.5.3. Development of turbidite successions

**Major controls on turbidite sedimentation**

The accumulation of turbidite successions is controlled
by the complex interaction of three major factors; sea level
fluctuation, tectonic setting and activity, and type and rate
of sediment supply (e.g. Stow et al., 1985; Mutti and Normark,

1987; Pickering et al., 1989). These controls are by no means independent; for instance, significant tectonically-induced uplift made available texturally and compositionally immature sediments to be resedimented in the Carapeba/Pargo area. It is very difficult to isolate the effects of one of these variables, and most attempts are based on assumptions regarding the magnitude and rate of the other two variables (Burton et al., 1987).

Recent literature has highlighted the influence of sea level fluctuations on the development of turbidite systems (e.g. Mutti, 1985; Mutti and Normark, 1987; Posamentier and Vail, 1988; Vail et al., 1991; Walker, 1992). This emphasis is supported by a growing body of evidence that turbidites tend to accumulate preferentially during global or regional sea level falls (e.g. Piper and Normark, 1983; Bouma et al., 1989; Feeley et al., 1990; Nelson, 1990; Nelson and Maldonado, 1990; Weimer, 1990). During sea level falls, the coastal depositional systems tend to prograde over the shelf, moving sediment depocenters closer to the shelf/slope break. The higher rates of sedimentation at this location stimulate slope failures (e.g. slides and slumps; Coleman et al., 1983), and also may increase the amount of sediment to be remobilized by earthquakes (Kastens, 1984; Piper et. al., 1988; Adams, 1989) and storm waves (Dengler et al., 1984; Lee and Edwards, 1986). All of these processes may generate turbidity currents. Canyon initiation and development also is augmented during lowstand

(e.g. Suter and Berryhill, 1985; Carlson and Karl, 1988), mainly by retrogressive slumps (Coleman et al., 1983; Farre et al., 1983; Goodwin and Prior, 1989). In the case of pre-existing canyons, the shift in coastal depocenters would favour the capture by these canyons of sediments in fluvial/deltaic systems and transported by alongshore currents. Increased sediment bypassing of the shelf, resulting in turbidity currents, would enlarge the canyons (Shepard, 1981) and lead to the building of submarine fans on the basin floor (Posamentier et al., 1991).

Tectonics influence turbidite sedimentation mainly by controlling basin size and shape, bottom gradients, type and rate of sediment supply, and local relative sea level changes (e.g. Stow et al., 1985; Mutti and Normark, 1987; Pickering et al., 1989). Tectonics may increase sediment supply by increasing rates of uplift and denudation in the hinterland, by establishing fault-controlled, narrower coastal plains and shelves, and by steepening continental margin gradients. Also important are the earthquake-induced faults, which may almost instantaneously modify relief by tens of meters (or more), and trigger large turbidity currents.

**Global sea level curves**

Sedimentation of the Carapeba/Pargo turbidite system (Coniacian/Santonian to early Maastrichtian) took place during a prominent first-order, eustatic sea level rise during

Mesozoic time (Vail et al., 1977, p.84). Pitman (1978) estimates that sea level was 350 m higher than at present in the Santonian (85 Ma; Fig. 2.4), largely due to the rapid expansion of the mid-oceanic ridge system (increasing in the spreading rate) from 110 to 85 Ma. The overall tendency for sea level rise during the late Cretaceous was punctuated by third-order sea level falls (Haq et al., 1987, 1988; Fig. 3.42), but none of them was able to shift the coastal onlap sufficiently to induce shallow water sedimentation in the Carapeba/Pargo area. From the late Cenomanian to the early Paleocene, sedimentation in the study area always took place in upper bathyal or deeper environments (e.g. Azevedo et al., 1987a; Guardado et al., 1990).

The biostratigraphic units defined for the Coniacian/ Santonian Campos basin do not have sufficient resolution to allow correlations between global sea level curves (e.g. Haq et al., 1987, 1988) and the facies sucessions of the Carapeba/Pargo turbidite system (Fig. 3.42). Also, global sea level curves do not show a comparable number of third-order sea level falls in the Coniacian/Santonian and early Maastrichtian to explain the number of turbidite successions in the study area (Fig. 3.42). However, the effects of two important eustatic sea level falls, respectively in the late Turonian (90-89 Ma) and late Campanian (75-74 Ma) (Fig. 3.42) seem to be recognizable in the eastern Brazilian marginal basins.

The Turonian sea level fall is related to a widespread unconformity, identified in many basins around the world (e.g. North America Western Interior, Weimer, 1984; U.S.A. Atlantic Margin, Poag and Schlee, 1984; Arabian Peninsula, Harris et al., 1984; and offshore western Africa, Seiglie and Baker, 1984). In the Campos basin, the 90 - 89 Ma sea level fall moved the turbidite depocenters seaward, and the canyons in the study area were submitted to erosion by increasingly frequent and powerful turbidity currents. Erosion also took place along most of the westernmost and shallower portions of the Campos basin, induced by processes still poorly understood. This erosion produced a widespread unconformity, which cuts out the sedimentary record of the late Turonian in large areas of the basin. This unconformity is underlain by deep neritic to upper bathyal (100 - 300 m) late Cenomanian/ early Turonian marls and mudstones, and is overlain mainly by mid to lower bathyal (1,000 - 1,500 m) Coniacian/Santonian mudstones. However, along the Carapeba/Pargo trough this unconformity may be truncated by coarse-grained turbidites (successions CRP/PG-S2 to CRP/PG-S6; Figs. 3.2, 3.4, 3.22, and 3.24).

The 75 - 74 Ma sea level fall apparently did not have the same absolute fall magnitude as the 90 - 89 Ma sea level event, but it is also widely recognized (e.g. Fondecave-Wallez et al., 1990; Olsson, 1991). In the Campos basin the Campanian sedimentary record is very thin (a maximum of only 24 m in the

study area; Fig. 3.4). This has been attributed to very low
sedimentation rates following a widespread transgression
(Azevedo et al., 1987a) (Fig. 3.42). However, important
erosion of Campanian and even older sediments is indicated by:
(1) the absence of the worldwide index fossil (foraminifera)
*Globotruncana calcarata* (Caron, 1985) in the Campos basin
(Guardado et al., 1990); and (2) the occurrence of the early
Maastrichtian *Tetralithus trifidus* (calcareous nannofossil)
zone directly overlying the Albian *Nannoconus truitti truitti*
zone in a large area (> 1,300 km$^2$) of the southern Campos
basin (Richter, 1987). This erosion and related unconformity
was probably produced by turbidity currents developed during
the 75 - 74 Ma sea level fall. The early Maastrichtian
successions CRP/PG-S7 and CRP/PG-S8 overlie this unconformity,
as observed for other time-equivalent, canyon-fill (turbidite)
successions in the Espírito Santo and Bahia Sul basins (e.g.
Bruhn and Moraes, 1989).

From the ideas presented above it can be concluded that
global sea level curves do not support or deny the
interpretation that succession development in the study area
was controlled by eustatic sea level fluctuations. The sea
level curves of Haq et al. (1987, 1988) do not show a
comparable number of third-order sea level falls in the
Coniacian/Santonian and early Maastrichtian to be correlated
to the number of (0.4 - 0.9 m.y. duration) Carapeba/Pargo
turbidite successions (Fig. 3.42). However, the unconformities

that define (at least locally) the base of the entire Coniacian/Santonian and early Maastrichtian turbidite successions may be correlated to important sea level falls, respectively at 90 - 89 and 75 - 74 Ma (Fig. 3.42).

**Tectonics**

During the long term sea level rise of the late Cretaceous (Fig. 2.4), the Campos basin also experienced a generalized eastward (seaward) tilting in response to the combined effects of thermal-contraction subsidence and sedimentary loading (Mohriak et al., 1990). Seismic profiles published by Guardado et al. (1990, their figure 5), and Mohriak et al. (1990, their figures 3 and 4) show a gentle flexure of the basement across a coastal hinge line located close to the present limit of occurrence of late Cretaceous rocks (Fig. 3.1). The boundary between the shallow carbonate platform megasequence and the marine transgressive megasequence was tilted down to the east by up to 0.2° (at the position of the study area) from mid Albian to early Paleocene; this represents an average increase of 0.006°/m.y. in the paleogradient of the late Cretaceous Campos basin. Geohistory curves presented by Mohriak et al. (1990, p. 128-129) permit the estimation of regional tectonic subsidence rates of 1.8 - 2.0 cm/1,000 yr. for the time period between 95 and 65 Ma (late Cretaceous).

The generalized tectonic tilting induced downslope creep

of Aptian evaporites by gravitational instability (Figueiredo and Mohriak, 1984). Salt flowage favoured the development of listric faults soling out on evaporite beds, some of them responsible for defining the boundaries of the Carapeba/Pargo canyon and its filling section (e.g. Figs. 1.8, 3.2 and 3.24). Variable subsidence rates along these smaller-scale tectonic features are estimated in three cases described below.

(1) The fault that defines the westernmost occurrence of succession CRP/PG-S1 (Sandstone A; Fig. 3.4) was able to accommodate a 112 m thick package of Coniacian/Santonian mudstones and coarse-grained turbidites. This is a minimum figure, because erosion by high density turbidity currents probably took place along the downthrown block. Considering the average duration of the Coniacian/Santonian successions (0.9 m.y.), the average subsidence rate along this fault would have been at least 12.4 cm/1,000 yr.

(2) Figure 3.24 illustrates fault-controlled turbidite sedimentation along the southern margin of the Carapeba/Pargo canyon. A cumulative throw of 221 m is recorded for the fault located between the wells CRP-42D and RJS-320A, which was created during the combined times for sedimentation of the late Cenomanian/early Turonian marls and mudstones of the Macaé Formation, the entire succession CRP/PG-S3, and most of succession CRP/PG-S4 (sandstones D to J). This displacement can be calculated by comparing the structural position of the unconformity between the late Albian and late Cenomanian/early

Turonian successions on both sides of the fault. The well RJS-320A records a 145 m thick succession (136 m of coarse-grained turbidites; sandstones C to J), which is absent in the well CRP-42D, and also a succession of late Cenomanian/early Turonian marls and mudstones, which is 11 m thicker than its counterpart in the hanging wall (well RJS-145A). From these numbers it can be inferred that the fault-controlled subsidence was able to accommodate not only the 145 m thick turbidite succession, but also at least 11 m of late Cenomanian/early Turonian marls and mudstones. Considering the average duration of the successions CRP/PG-S3 and CRP/PG-S4 (0.9 m.y. each), the average subsidence rate along this fault would have been at least 8.1 cm/1,000 yr. in Coniacian/Santonian times.

(3) Figure 3.2 shows three faults also located in the southern margin of the Carapeba/Pargo trough. Their throws are 28, 60, and 108 m, respectively, from south to north. Well RJS-221 records a 167 m thick (144 m of turbidites) succession (all of the succession CRP/PG-S4 and most of the succession CRP/PG-S5), which is absent in well CRP-3D (Fig. 3.2). In this case, the local tectonic subsidence was not able to accommodate by itself the entire turbidite succession. The remaining necessary space (59 m), was probably created by the erosion of Coniacian/Santonian mudstones by high density turbidity currents. This erosion is indicated by the much thinner record of Coniacian/Santonian mudstones and the

absence of the markers C/S-1 and C/S-2 in well RJS-221. Considering the average duration for the successions CRP/PG-S4 and CRP/PG-S5 (0.9 m.y. each), the average subsidence rate along the fault between wells CRP-11 and RJS-221 (Fig. 3.2) would have been about 6.0 cm/1,000 yr.

In the Carapeba/Pargo area, subsidence rates along local faults seem to have decreased during the sedimentation of the Coniacian/Santonian turbidite successions (from 12.4 to 6.0 cm/1,000 yr.). Fault control on the lateral distribution of the sandstone bodies also diminished (Fig. 3.2, and also compare the net sand maps for the successions CRP/PG-S2 to CRP/PG-S6; Figs. 3.26, 3.27, 3.28, 3.33, and 3.35). Some degree of fault reactivation during the early Maastrichtian could be suggested for the time of deposition of CRP/PG-S7 and CRP/PG-S8, particularly in the southwestern part of Carapeba field (Figs. 3.40 and 3.41). However, the magnitude of this early Maastrichtian, fault-controlled subsidence would be very small compared with the Coniacian/Santonian subsidence. This decreasing trend of local tectonic activity probably reflects diminishing rates in evaporite flowage in those portions of the Campos basin presently under water depths less than 200 m (Fig. 3.1).

Despite the exponentially decreasing rates of thermal contraction subsidence in the basin (Fig. 2.4), important uplift and sediment input persisted in the basin margin and Precambrian source area, which led to the development of the

regressive marine megasequence from the mid Eocene onwards (Chang et al., 1988; Guardado et al, 1990; Fig. 1.8). Macedo (1987) suggests that opposing isostatic forces may have kept the Serra do Mar uplifting during the development of the transgressive and regressive megasequences: an uplifting force due to load release by erosion onshore, and a downwarping force produced by sediment load offshore.

**Development of the Carapeba/Pargo turbidite successions**

Two major hypotheses are presented here to explain the development of successions CRP/PG-S1 to CRP/PG-S8. The first possibility, mostly **autocyclic**, considers the development of successions by switching depocenters of feeding deltas or fan-deltas along the basin margin. The second scenario, essentially **allocyclic**, considers the development of successions by the interaction of (a) tectonics, (b) sediment supply, and (c) sea level fluctuations. Both autocyclic and allocyclic hypotheses are essentially qualitative and tentative due to the limitations of the data base; the study area comprises only a 20 km-long portion of a system at least 150 km-long, and there is a lack of preservation in the Campos basin of the late Cretaceous, shallower-water sedimentary record.

**Autocyclic hypothesis:** According to a mostly autocyclic hypothesis, the establishment of a new succession would take place following the migration of deltas or fan deltas toward

a position where their coarse-grained sediments would be remobilized and then resedimented preferentially in the Carapeba/Pargo canyon. Conversely, the building of a succession would stop with the switching away of the feeding depositional systems. This hypothesis is not totally autocyclic, because in the high relief, rapidly uplifting margin of the late Cretaceous Campos basin the establishment and migration of coastal depositional systems probably had a strong tectonic control.

The well-defined fining- and thinning-upward character exhibited by most of the turbidite successions (e.g. Fig. 3.4) could be related to the gradual withdrawal of delta/fan delta depocenters. During this time, the amount and rate of accumulation of coarser-grained sediments in areas more susceptible to failure would decrease, with turbidity currents becoming less frequent and finer-grained. Eventually this process could lead to the interruption of turbidite sedimentation in the Carapeba/Pargo canyon, which would then be blanketed by mudstones. This interpretation would imply that the deposition of individual successions would have taken place during time intervals shorter than the previously estimated 0.4 to 0.9 m.y. Conversely, coarsening- or thickening-upward successions also should be expected as a result of the gradual return of the feeding depositional systems. Thus, the absence of coarsening- or thickening-upward successions in the Carapeba/Pargo turbidite system would

represent a major problem with respect to a purely autocyclic control on the development of the studied successions.

Fining upward and thinning upward sucessions have been interpreted as the result of lateral migration and/or abandonment of channels (e.g. Mutti and Ghibaudo, 1972; Walker, 1978; Link and Nilsen, 1980; Link and Welton, 1982). However, closely-spaced well control and detailed correlations show that most of the Carapeba/Pargo turbidites comprise non-channelized (tabular or lobate) sandstone bodies. It follows that channel filling or channel migration are unlikely to have been responsible for the fining- and thinning-upward successions recorded in the Carapeba/Pargo turbidite system.

**Allocyclic hypothesis:** During the late Cretaceous, the Campos basin was still an immature passive margin basin, recording important uplift in the adjacent hinterland and along its faulted margin, which was probably characterized by a narrow and steep shelf. In this setting, the effects of sea level fluctuations on moving clastic depocenters landward and seaward across the shelf would be minor, with the source areas remaining relatively close to the shelf/slope break even during highstands. Additionally, the interpretation of succession development purely controlled by third-order, eustatic sea level falls has problems regarding their required 0.4 - 0.9 m.y. reccurrence. Growth and melting of continental ice masses is the only well-known mechanism that can induce

eustatic sea level to change at rates exceeding 1 cm/1,000 yr. (up to 1,000 cm/1,000 yr.), and with a magnitude of tens of meters (up to 150-200 m) (e.g. Pitman, 1978; Pitman and Golovchenko, 1983; Revelle, 1990). However, there is an important gap in the glacial record between the Triassic and early Tertiary (Eyles and Eyles, 1992), and the Cretaceous possibly comprised the warmest interval in Earth history (Barron 1983; Frakes and Francis, 1990). Following glacio-eustasy, variations in the volume of the mid-ocean ridges (acceleration of the sea-floor spreading rate) represent the most important mechanism for eustasy, but it can account for maximum rates of only 0.67 cm/1,000 yr. (Pitman, 1978).

Tectonic activity in the late Cretaceous Campos basin probably exerted an important control on sediment supply (as discussed in section 3.5.2) and sea level fluctuations. In large portions of the Campos basin, deep neritic to upper bathyal (100 - 300 m) late Cenomanian/early Turonian marls and mudstones are unconformably overlain by mid to lower bathyal (1,000 - 1,500 m) Coniacian/Santonian mudstones (Azevedo et al., 1987a). This large increase in depth (at least 700 m) took place in less than 2 m.y. (minimum rate of 35 cm/1,000 yr.), and probably results from the effects of the first-order, (eustatic) late Cretaceous sea level rise, amplified by tectonic subsidence.

The scenario described above suggests the interpretation that **tectonically-controlled sediment supply at the basin**

**margin would have represented the most important control on the development of Carapeba/Pargo turbidite successions.** In this context, the deposition of each succession would have followed a relatively abrupt increase in sediment supply through delta/fan delta systems, which in turn would have responded to phases of fault reactivation and/or increasing upflift in the ancestral Serra do Mar. These pulses of increasing sediment supply would have been able to shift coastal depocenters seaward, and possibly to induce short-term, **relative** sea level falls. However, the change from an overall transgressive setting to a regressive regime took place in the Campos basin only after the early Paleocene (e.g. Chang et al., 1988; Guardado et al., 1990).

An essentially allocyclic explanation for the fining- and thinning-upward successions of the Carapeba/Pargo turbidites is very difficult to define. A possible explanation, albeit purely theoretical, would consider these successions as produced by slope failures (and related turbidity currents) that were gradually less frequent and involved finer-grained material, as a result of decreasing tectonically- and climatically-controlled sediment supply, and related change from relative lowstand to rising sea level conditions (inducing landward shift of coarse-grained depocenters). In this context, the decreasing sediment supply via delta/fan delta systems would have resulted from the progressive erosion of uplifted continental blocks and following slope reduction

in the source area. Consequently, the amount and rate of accumulation of coarser-grained sediments in areas more susceptible to failure would have decreased. This trend experienced successive interruptions by tectonic reactivations (or climatic fluctuations), which effects included the re-establishment of steeper slopes in the source area, the development of delta/fan delta systems capable of carrying larger amounts of coarse-grained sediments at the basin margin, and eventually the development of canyon-fill, turbidite successions.

Variations in sediment supply along the Campos basin margin also could have been influenced by climatic variations, considering the large average duration of the Carapeba/Pargo turbidite successions. A mostly warm and humid paleoclimate is interpreted for the eastern Brazilian coast during the late Cretaceous (e.g. Parrish and Curtis, 1982; Lima, 1983), but it is very probable that climatic fluctuations (e.g. Milankovitch cyclicity; Imbrie and Imbrie, 1980) took place from the Coniacian to the Maastrichtian. In this context, periods of higher seasonal precipitation would induce higher denudation rates in the source area, and related higher rates of sediment supply to the basin margin. For example, in areas with high seasonal precipitation the erosion rates may be twice as much those in semi-arid areas with the same relief (Stow et al., 1985).

The magnitude of the tectonic reactivations or relative

sea level falls required to develop the successions CRP/PG-S1 to CRP/PG-S8 would not have to be very large, considering that the Carapeba/Pargo turbidite system is thick (due to structural confinement), but not volumetrically impressive. The total volume of coarse-grained turbidites along the 150 km long Carapeba/Pargo canyon (Fig. 3.1) is less than 200 km$^3$ (individual turbidites averaging < 1 km$^3$). There are many examples of **individual** turbidites exceeding 100 km$^3$ (e.g. Elmore et al., 1979; Ricci Lucchi and Valmori, 1980; Mutti et al., 1984; Piper et al., 1988), and also turbidite systems developed in equivalent or smaller time span exceeding 500 km$^3$ (e.g. Droz and Bellaiche, 1985; Damuth et al., 1988; Weimer, 1989, 1990; Azambuja, 1990; Martins et al., 1990; Peres, 1993). Additionally, the recurrence intervals for the studied turbidites (15,000 to 38,000 years) are very large, considering that earthquakes of magnitude sufficient to cause large-scale turbidity currents ($M_s$ > 7; Seguret et al., 1984; Piper et al., 1988) may occur in passive continental margins every few hundred years (Basham and Adams, 1983).

## 3.5.4. Retrogradational stacking

As considered for the development of individual successions, **autocyclic** and **allocyclic** controls also could be proposed to explain the overall retrogradational stacking and the well-defined fining- and thinning-upward successions

recorded by the Carapeba/Pargo turbidite system.

**Autocyclic hypothesis:** The gradual switching away of a feeding delta/fan delta system could represent a possible autocyclic control on the fining- and thinning-upward trends presented by the Carapeba/Pargo turbidite successions (as discussed in the previous section). However, this autocyclic control could not account by itself for the overall deepening-upward sedimentation indicated by the benthic foraminifera found in the interbedded mudstones (Azevedo et al., 1987a).

Based on the offset termination of the various turbidite successions (Fig. 3.4), a minimum retrogradation of 20 km can be estimated for the Carapeba/Pargo turbidite system. Thus, the feeding depositional system would have to retrograde at least 20 km (considering a constant basin gradient), in order to induce the general retrogradational stacking presented by the turbidite successions (Fig. 3.4). Such landward shifting would hardly take place by a purely autocyclic mechanism, considering the high relief, fault-controlled margin of the late Cretaceous Campos basin.

**Allocyclic hypothesis:** In this context, the backfilling of the Carapeba/Pargo canyon would represent the effects of the generalized, long-term sea level rise recorded in the Campos basin, which gradually would have moved the coastal depocenters landward. As a result, the amount and rate of accumulation of coarser-grained sediments in sites more susceptible to failure (e.g. shelf/slope break) would

decrease), with turbidity currents becoming less frequent, smaller, and finer-grained. Middleton and Neal (1989) demonstrated experimentally that turbidite thickness and lateral extent (or travel distance of turbidity currents) can be related to the original volume and concentration of the turbidity currents, their speed, and the settling velocity of the grains transported by them. All other things being equal, larger turbidity currents would travel longer distances. It follows that the long-term trend of sea level rise likely would result in deposition from turbidity currents in successively shorter distances from their point of initiation. Thus, the depocenters of coarse-grained turbidites would tend to migrate upcanyon, giving rise to retrogradational successions.

It is important to point out that, regardless of the influence of sea level fluctuations, turbidite sedimentation within a canyon would take place **only** if there is a significant reduction in the gradient of the canyon floor, causing the turbidity currents to decelerate. Therefore, the hypothesis for retrogradational stacking presented above requires that the increase in basin floor gradient by thermal contraction and sediment load be minimal; otherwise, the increasing gradient would result in turbidite accumulation in the same position, or even farther basinward, bypassing the study area. Passive margin basins are characterized by a series of half-grabens stepping-down seaward; however, the

common rotation of blocks along listric faults may reduce (or even reverse) basin floor gradient in many of these fault-bounded basin segments (e.g. Fig. 1.8). Typical seismic profiles of the Campos basin (e.g. Guardado et al., 1990, their figure 5) show throughout the marine transgressive megasequence a steeper profile for the most proximal, 60 km-wide part of the basin. Beyond this point, including the Carapeba/Pargo area, a much more gentle profile (flat or even dipping landward) is presented. Another cause for local decrease in basin floor gradient is related to the creep and withdrawal of underlying evaporite beds. It has been suggested (Figueiredo and Mohriak, 1984; Guardado et al., 1990) that salt flowage favoured the development of the listric faults (including those that bound the Carapeba/Pargo canyon) and also formed depresssions capable of impounding turbidites.

The drop in sea-level recorded in the late Campanian (75 - 74 Ma; Fig. 3.42) along with possible shorter-lived, relative sea level falls, would have allowed only shorter-distance, seaward shifts of the preferential sites for turbidite accumulation. As a result, the Carapeba/Pargo turbidites and associated mudstones formed a muddier- and deepening-upward succession, characterized by a general retrogradational stacking.

As discussed in the previous section, tectonically (and/or climatically)-controlled increase in sediment supply, and possibly related third-order, shorter-lived sea level

falls may have defined preferential times for accumulation of coarse-grained turbidites in the Campos basin. However, the general transgressive setting of the late Cretaceous kept these sediments restrained to canyons. Even thin (< 1 m) turbidite beds are mostly (> 95 %) composed of conglomerates to medium-grained sandstones (Figs. 3.5 and 3.6), suggesting that turbidity currents carrying finer-grained sediments may have bypassed the Carapeba/Pargo canyon. However, their sandy load, if any, would have been deposited in areas with present bathymetry exceeding 1,000 m (Fig. 3.1); these areas are very difficult to drill, and little is known about possible turbidite deposition there.

### 3.5.5. Conclusions

The late Cretaceous Carapeba/Pargo turbidite successions are included in the marine transgressive megasequence, which is characterized by onlapping, deepening- and muddier-upward sedimentation throughout the eastern Brazilian marginal basins.

Eight coarse-grained turbidite successions, with 0.4 - 0.9 m.y. durations, were developed mostly in response to phases of relatively abrupt increase in sediment supply via delta/fan delta systems, which in turn responded to fault reactivation and/or increasing upflift in the ancestral Serra do Mar. These pulses of increasing sediment supply would have

been able to shift coastal depocenters seaward across a narrow and steep shelf, and possibly to induce short-term, **relative** sea-level falls.

Progressive erosion of uplifted continental blocks and resulting slope reduction in the source area may have been responsible for decreasing the amount and rate of accumulation of coarser-grained sediments in areas more susceptible to failure. As a result, slope failures (and related turbidity currents) would have become gradually less frequent and finer-grained, giving rise to well-defined fining- and thinning-upward trends in most of the Carapeba/Pargo turbidite successions.

Variable subsidence along listric faults soling out on creeping evaporite beds represented the major control on the shape of the Carapeba/Pargo canyon and the geometry of its filling turbidite successions.

The overall retrogradational stacking exhibited by the Carapeba/Pargo turbidite successions probably represents the effects of the first-order, eustatic sea level rise in the Campos basin during most of the late Cretaceous, which gradually would have moved the coastal depocenters landward, and would have kept coarse-grained turbidites restrained to canyons.

# 4. LAGOA PARDA FIELD, ESPÍRITO SANTO BASIN

## 4.1. LOCATION AND DATA BASE

Lagoa Parda field is located in the southern Espírito Santo basin (Fig. 1.7), near mouth of the Doce River at the Atlantic Ocean (Fig. 4.1). Its reservoirs are contained within a thick (up to 400 m) succession of early Eocene, coarse-grained turbidites (Fig. 4.2), deposited in the 15 km long, up to 6 km wide Regência canyon (Figs. 4.1 and 4.3). The NE-oriented Regência canyon was filled by up to 1,000 m of mostly early Maastrichtian, late Paleocene, and early Eocene deep water sediments (Figs. 4.3 and 4.4).

Lagoa Parda field was discovered in 1978 by the wildcat LP-2. Subsequent drilling of 12 step-out- and 71 exploitation wells (between 1978 and 1990) permitted the mapping of a 2.7 km$^2$ oil accumulation (Fig. 4.1), containing an original oil-in-place volume of 7.8 x 10$^6$ m$^3$ (49.3 million bbl), and ultimate recoverable reserves of 3.9 x 10$^6$ m$^3$ (24.3 million bbl) (Cosmo et al., 1991). Lagoa Parda is a stratigraphic trap, with the oil distribution being primarily controlled by reservoir pinch-out. Its only oil/water contact is located

Fig. 4.1 - Location of the Lagoa Parda field and boundaries of the Regência canyon (as defined with seismic data by Oliveira et al., 1985). Note that the Regência canyon has about the same width, length, and orientation as the Dundas Valley, where McMaster University is located. However, the Dundas Valley and the Regência canyon were shaped and filled by different processes. The Regência canyon was defined by subsidence along listric faults and erosion by high-density turbidity currents. By contrast, the Dundas Valley is generally interpreted as a preglacial river valley, which was widened and modified by glacial erosion, and partially filled with glacial till and glacial lake sediments (e.g. Straw, 1968; Middleton, 1982).
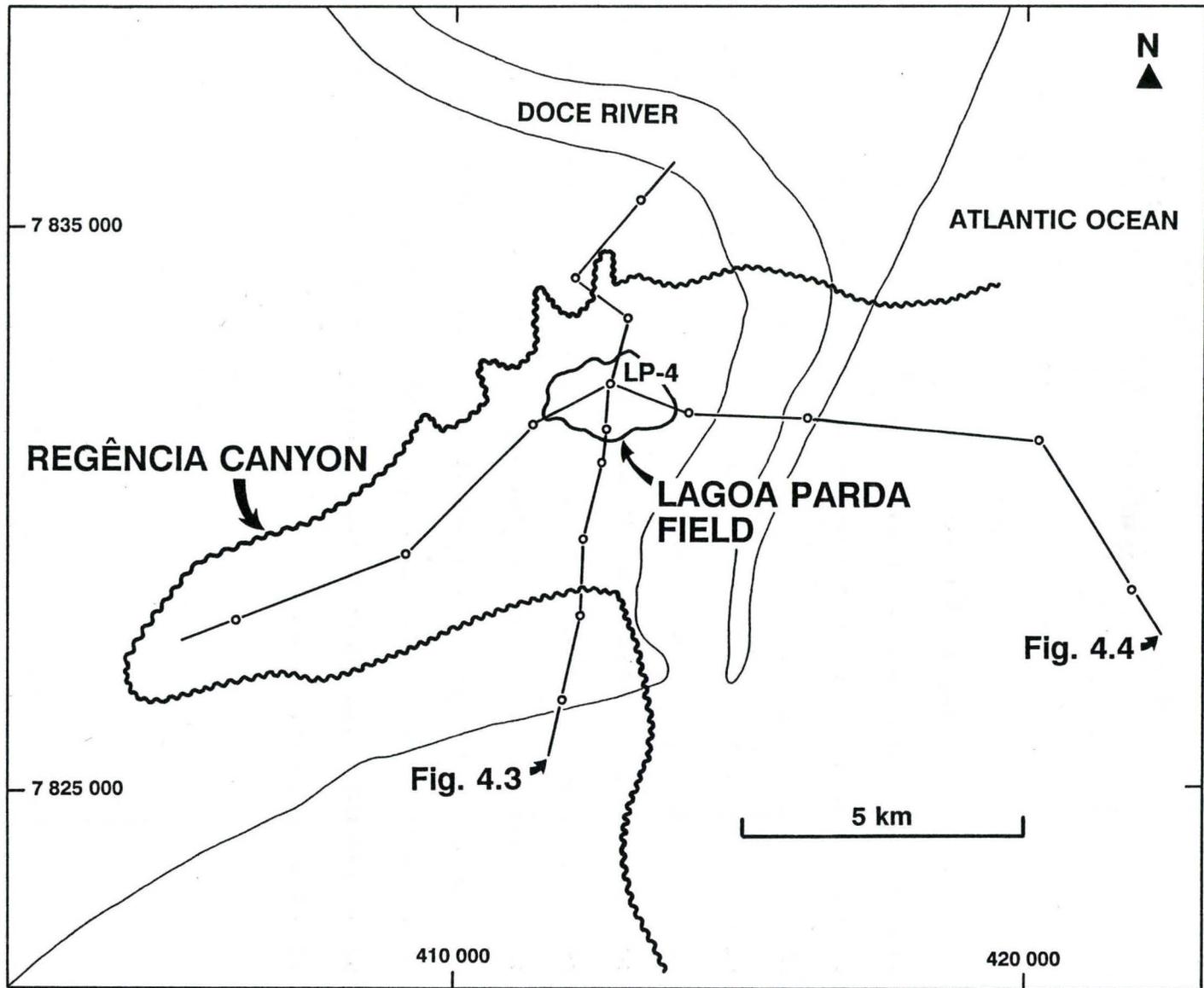
Fig. 4.2 - Typical gamma-ray and resistivity logs for the Lagoa Parda turbidite system. Well LP-4 was drilled in the thalweg of the Regência canyon (Fig. 4.3). There are at lest nine channel-complexes in the early Eocene, *Neochiastozygus chiastus* zone. The three uppermost channel complexes (LP-CC1 to LP-CC3) were studied in detail. LP-CC3 is poorly developed in well LP-4, but it may comprise up to 27 m of sandstones in the southeastern part of Lagoa Parda field. The resistivity curve is shown in amplified scale for the mud-rich successions of the *Neochiastozygus chiastus* (upper part), *Tribrachiatus orthostylus*, and *Discoaster lodoensis* zones. High-resistivity horizons located below the oil/water contact are composed of boulder- to pebble-rich conglomerates. D is a high-resistivity mudstone containing siderite, rhodochrosite and pyrite; it makes a well log marker that can be widely correlated across the Lagoa Parda field, which was used as datum for the cross sections of figures 4.11, 4.23, and 4.24.

**LP - 4**

MARINE REGRESSIVE
MEGASEQUENCE

MARINE TRANSGRESSIVE
MEGASEQUENCE

[Late] early Eocene:
*Discoaster lodoensis* **zone**

[Mid] early Eocene:
*Tribrachiatus orthostylus* **zone**

-1400-

D

**LP - CC3** ➡ 9

**LP - CC2** ➡ 8

Oil
Water

-1600-

**LP - CC1** ➡ 7

6

[Early] early Eocene:
*Neochiastozygus chiastus* **zone**

5

-1800-

4

3

2

-2000-
(m)

1

Early Maastrichtian:
*Broinsonia parca* **zone**
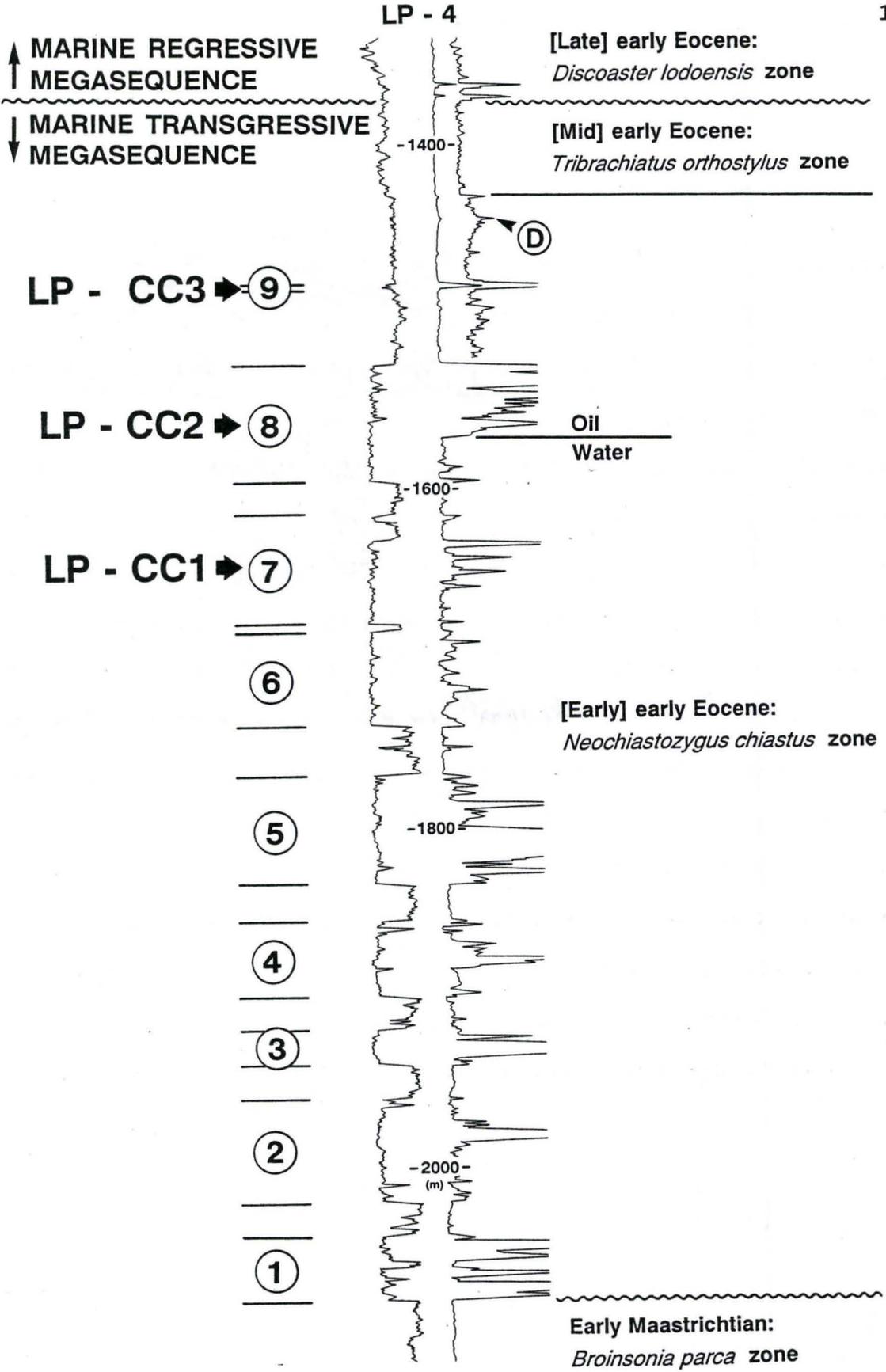
Fig. 4.3 - Geological cross section transverse to the Regência canyon. Dashed lines indicate the studied succession. The canyon margins are controlled mainly by listric faults soling out on anhydrite beds of the transitional evaporitic megasequence. Six major unconformities occur in the marine transgressive- and marine regressive megasequences [late Turonian(?) to mid Eocene]; they are numbered 1 to 6, from the oldest to the youngest. The marine transgressive megasequence is bounded by unconformities 2 (or very locally by 1) and 5. Calcareous nannofossils zones from the early- and mid Eocene successions (Antunes, 1990a): (a) *Neochiastozygus chiastus*, (b) *Tribrachiatus orthostylus*, (c) *Discoaster lodoensis*, (d) *Discoaster kuepperi*, (e) *Chiasmolithus staurion*, and (f) *Chiasmolithus grandis*. Combined thickness of conglomerates and sandstones in the early Eocene, *Neochiastozygus chiastus* zone is indicated (between parenthesis) for each well in the cross section. Lithology symbols are explained in figure 4.4. Vertical scale = 3 x horizontal scale. Section location is shown in figure 4.1.

N ... S

| LPN-1 (0) | LPB-1A (0) | LP-5 (46) | LP-4 (400) | LP-2 (252) | LP-55 (210) | LPS-1 (140) | FRG-2 (0) | FRG-1 (0) |

Datum: - 800 m

Mid Eocene (e/f)

MARINE REGRESSIVE MEGASEQUENCE

⑥

- 1,000

Late Turonian(?)/ Santonian

Early Eocene/ Mid Eocene (c/d)

①   ⑤

Early Paleocene   ④

Campanian ③

①

④

- 1,500

Early Eocene (b)

Early Eocene (a)

⑤

SHALLOW CARBONATE PLATFORM MEGASEQUENCE

Studied succession (Fig. 4.11)

④

MARINE TRANSGRESSIVE MEGASEQUENCE

②

TRANSITIONAL EVAPORITIC MEGASEQUENCE

- 2,000

CONTINENTAL RIFT MEGASEQUENCE

Early Maastrichtian

Precambrian Basement

0   1   2   3 km

- 2,500 (m)

182

Fig. 4.4 - Geological cross section longitudinal to the Regência canyon. Dashed lines indicate the studied succession. The reactivation (up to early Eocene) of a fault transverse to the canyon allowed the exposure of Precambrian rocks along the canyon floor in its western portion. Six major unconformities occur in the marine transgressive- and marine regressive megasequences [late Turonian(?) to mid Eocene]; they are numbered 1 to 6, from the oldest to the youngest. In this cross section, only unconformities 2 to 6 can be observed. The marine transgressive megasequence is bounded by unconformities 2 and 5. Calcareous nannofossils zones from the early- and mid Eocene successions (Antunes, 1990a): (a) *Neochiastozygus chiastus*, (b) *Tribrachiatus orthostylus*, (c) *Discoaster lodoensis*, (d) *Discoaster kuepperi*, (e) *Chiasmolithus staurion*, and (f) *Chiasmolithus grandis*. Combined thickness of conglomerates and sandstones in the early Eocene, *Neochiastozygus chiastus* zone is indicated (between parenthesis) for each well in the cross section. Vertical scale = 6 x horizontal scale. Section location is shown in figure 4.1.

W — LC-1 (25) — LP-62 (20) — LP-22 (141) — LP-4 (400) — LP-17 (336) — RD-5 (77) — ESS-40 (36) — ESS-62 (22) — E

Datum: - 800 m

Mid Eocene (e/f)

Early Eocene/Mid Eocene (c/d)

Early Eocene (b)

Early Maastrichtian

Precambrian Basement

Studied succession

MARINE REGRESSIVE MEGASEQUENCE

Early Eocene (a)

SHALLOW CARBONATE PLATFORM MEGASEQUENCE (?)

Late Paleocene

MARINE TRANSGRESSIVE MEGASEQUENCE

DOMINANT LITHOLOGY

Mudstone (marine)/Sandstone/Conglomerate

Carbonate

Anhydrite/Dolomite

Sandstone/Conglomerate

Sandstone/Mudstone (lacustrine)

High-rank metamorphic rock

CONTINENTAL RIFT MEGASEQUENCE

Early Maastrichtian

TRANSITIONAL EVAPORITIC MEGASEQUENCE

0    2    4    6 km

- 1,000

- 1,500

- 2,000

- 2,500

- 3,000
(m)

183

1,559 m below sea level (Cosmo et al., 1991). The source rocks are late Neocomian, lacustrine mudstones of the rift megasequence, which are eroded at the base of the Regência canyon (Estrella et al., 1984) (Figs. 4.3 and 4.4).

The turbidite system sampled in the Lagoa Parda field was studied along a 2.8-km-long, 2.5-km-wide area, where 70 wells were drilled on an average spacing of 200 - 250 m (Fig. 4.5). The reservoirs were cored in seven wells (LP-3, LP-4, LP-8, LP-10, LP-33, LP-36, and LP-85; Fig. 4.5), permitting the description of a cumulative 324 m thick succession of rocks.

The wells drilled in the Lagoa Parda field present a comprehensive suite of high-quality well logs, including gamma-ray, spontaneous potential, resistivity, density, neutron, caliper, sonic, and dipmeter logs. The facies defined in the seven cored wells were calibrated with well log responses, and hence could be recognized in the non-cored wells.

A detailed calcareous nannofossil biostratigraphy for the filling-section of the Regência canyon was established by Antunes (1990a). It includes 5 Cretaceous zones (late Turonian to Maastrichtian), and 10 Tertiary zones (Paleocene to mid Eocene). Palynomorph zones are available for the well LP-2 (Fig. 4.3) (Dino, 1989, unpublished data). Paleoecological studies based on benthic foraminifera were conducted in four wells from the Espírito Santo basin (including the well FCL-1; Fig. 4.4) by Azevedo (1985).

Fig. 4.5 - Location map of wells and detailed geological cross sections in the Lagoa Parda field. Four of these cross sections are reproduced in figures 4.23 and 4.24. Dashed line indicates the maximum areal extent of the oil accumulation.

LAGOA PARDA FIELD

Fig. 4.23a

Fig. 4.24b

Fig. 4.23b

Fig. 4.24a

N

8

10

33

85

4

3

36

0    500 m

o   Well control

▲   Cored well

413 000

412 000

7 833 000

7 832 000

7 831 000
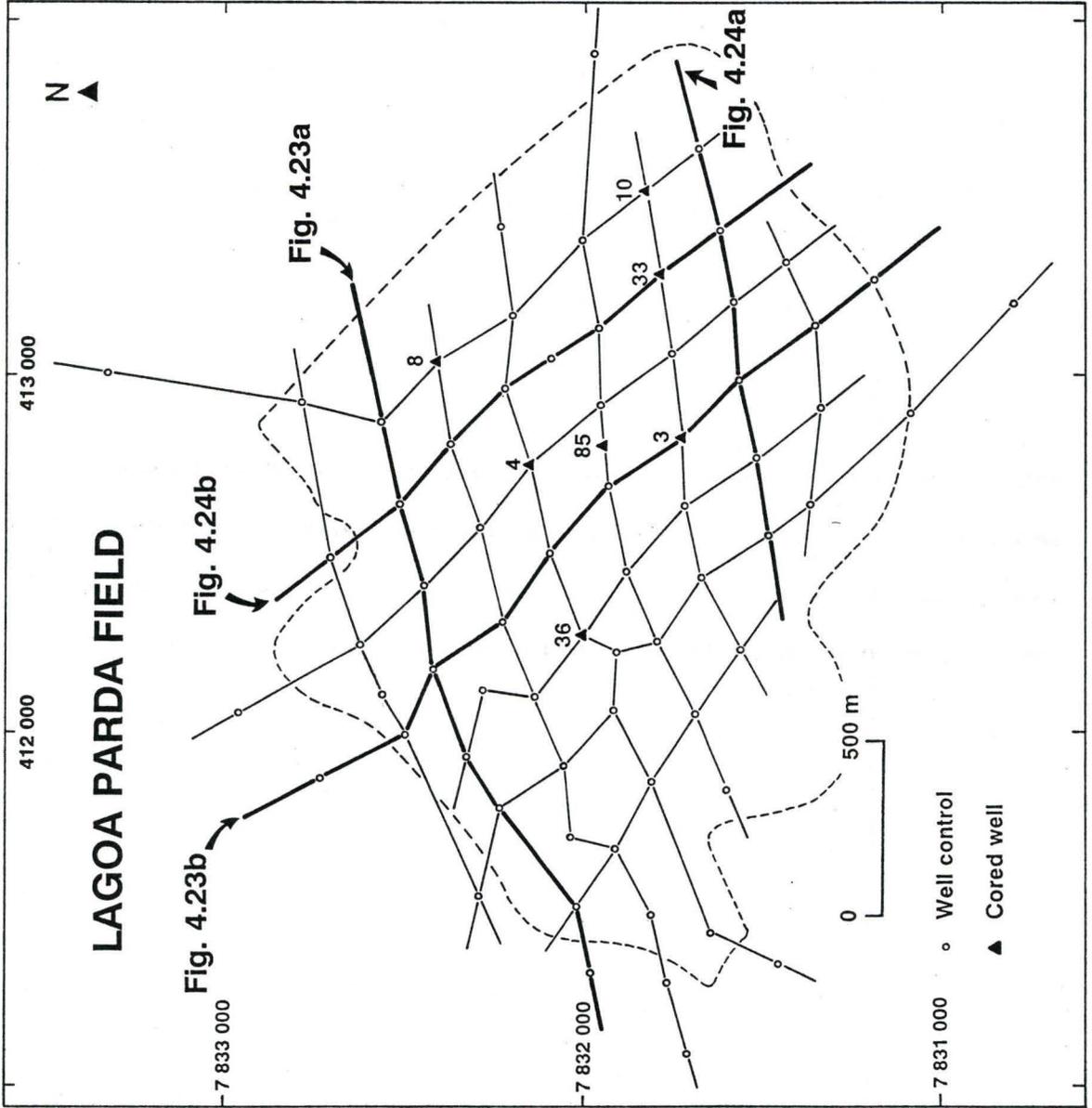
A comprehensive description of the development of the Lagoa Parda field is presented by Cosmo et al. (1991). A few sedimentological and petrographic studies have been made of the Lagoa Parda reservoirs, including those by Bagnoli (1984), and Bruhn and Moraes (1988).

## 4.2. GENERAL GEOLOGICAL SETTING

### 4.2.1. Stratigraphy

The Lagoa Parda reservoirs consist of sandy and conglomeratic turbidites, which form part of the marine transgressive megasequence (also studied in the Carapeba/Pargo area; Fig. 1.8). These canyon-fill turbidites are included in the Urucutuca Formation, which embraces all of the deep water facies (turbidites and interbedded mudstones) recognized in the transgressive and regressive megasequences of the Espírito Santo and Bahia Sul basins (Fig. 1.7).

Lagoa Parda turbidites make part of the filling-section of the Regência canyon, which is one of several large submarine canyons excavated along the western margin of the Espírito Santo and Bahia Sul basins after the mid Albian (Fig. 2.5). The NE-oriented Regência canyon was filled by up to 1,000 m of mostly early Maastrichtian, late Paleocene, and early Eocene deep water sediments (Fig. 4.3). Antunes (1990a,

1990b) recognizes nine major phases of erosion and filling in the late Cretaceous to mid Eocene section of the Regência canyon, mostly based on missing calcareous nannofossil zones. Figures 4.3 and 4.4 illustrate the six most important of these unconformities, which are numbered 1 to 6, from the oldest to the youngest.

Lagoa Parda reservoirs comprise the uppermost portion of an early Eocene succession, which is the thickest (up to 650 m) and coarsest-grained (up to 400 m of conglomerates and sandstones) filling-section of the Regência canyon (Figs. 4.2 and 4.3). These rocks are included in the calcareous nannofossil zone *Neochiastozygus chiastus* (Antunes, 1990a), which has a time span of about 1.3 m.y. (between 57.8 and 56.5 Ma).

Seismic stratigraphic studies (e.g. Oliveira et al., 1985) have recognized that the Lagoa Parda reservoirs make part of a transgressive, onlapping succession, which spans the late Paleocene to the early Eocene (5.1 m.y., between 58.8 and 53.7 Ma; Fig. 4.4). This succession probably records the culmination and maximum coastal onlap of the generalized transgression that took place along the eastern Brazilian margin during the late Cretaceous and early Tertiary. Late early- to mid Eocene (53.7 to about 40 Ma), mud-rich facies may also fill the Regência canyon (Fig. 4.3), but they comprise the basal portion of the offlapping and progradational marine regressive megasequense (Oliveira et

al., 1985).

## 4.2.2. Tectonics and magmatism

The structural framework of the Regência canyon area is characterized by two sets of normal faults, respectively NE- and N-oriented (Oliveira et al., 1985).

Reactivations in the NE-oriented fault system induced the establishment of listric normal faults soling out on the transitional evaporitic megasequence; these basement-detached faults, in turn, controlled the evolution of the Regência canyon boundaries (Fig. 4.3), and also originated smaller tributary troughs along its northern margin (Fig. 4.1).

The N-oriented fault system was successively reactivated up to the early Eocene, when Precambrian high-grade metamorphic rocks were exposed along the canyon floor in its western portion (Fig. 4.4).

The Coniacian to Eocene recurrent magmatic activity recorded in the Campos basin was equally important in the Espírito Santo basin. Basaltic lava flows of this age are found in many offshore and onshore wells. The large Abrolhos volcanic complex (Fig. 2.5), located about 85 km northeast of the Lagoa Parda field, was built essentially by late Cretaceous to Eocene volcanic rocks and sediments derived from a pre-existing narrow continental shelf (Ponte and Asmus, 1978). The magmatic activity centered on the Abrolhos bank is

probably related to the development of a hot spot associated with the Vitória-Trindade seamount chain (Ponte and Asmus, 1978).

### 4.2.3. Paleoenvironment

The fauna described for the Eocene mudstones drilled by the well FCL-1 (Fig. 4.4) is very diversified. A deep neritic to upper bathyal (200 - 500 m) association of benthic foraminifera has been identified (Azevedo, 1985); its most common genera are *Planulina*, *Uvigerina*, *Bulimina*, *Globocassidulina*, *Lenticulina*, *Trifarina*, *Cibicidoides*, *Bathysiphon*, *Haplophragmoides*, and *Quinqueloculina*.

Organic geochemistry studies of Eocene mudstones in well LP-22 (Fig. 4.4) have found low total organic carbon content (1 - 2 % by weight), a large dominance of terrestrially-derived kerogen, and poor preservation of organic matter produced by marine phytoplankton (Estrella et al., 1984). These conditions characterize a highly oxygenated environment, which is also suggested by the large number of genera and individuals of benthic foraminifera (Azevedo, 1985).

The abundance of plant debris in the cores of the Lagoa Parda field suggest a warm and humid climate for the early Eocene Espírito Santo basin. An important continental runoff and a local salinity decrease in the early Eocene Regência canyon is suggested by the small number of individuals in the

calcareous nannofossil assemblage (Antunes, 1990a), and also by the large amount of woody organic matter, and high ratio of spores and hydrophytic pollens to dinoflagellates in the palynomorph assemblage of well LP-2 (Dino, 1989, unpublished data). These local observations agree with global paleoclimatic reconstructions, which suggest a relatively warm and humid (moderately high rainfall rates) climate for the Espírito Santo basin during most of the late Cretaceous and early Tertiary (e.g. Parrish and Curtis, 1982; Parrish et al., 1982).

## 4.3. FACIES CHARACTERIZATION

The description of 324 m of cores recovered from 7 wells (Fig. 4.5) permitted the recognition of five major facies in the early Eocene succession of the Lagoa Parda field. These facies were distinguished chiefly on the basis of texture, physical sedimentary structures, bed thickness, and bioturbation. The facies are given the following names:

(1) **Facies LP-F1: UNSTRATIFIED, BOULDERY TO PEBBLY CONGLOMERATES AND VERY COARSE-GRAINED SANDSTONES;**

(2) **Facies LP-F2: GRADED BEDS OF UNSTRATIFIED COARSE-GRAINED SANDSTONES AND PARALLEL-STRATIFIED FINER-GRAINED SANDSTONES;**

(3) Facies LP-F3: INTERBEDDED BIOTURBATED MUDSTONES AND
THIN-BEDDED SANDSTONES;

(4) Facies LP-F4: INTERBEDDED STRATIFIED SANDSTONES AND
INTRACLASTIC CONGLOMERATES;

(5) Facies LP-F5: MUDSTONES.

The abbreviation **LP** come from the name Lagoa Parda, and has been used by PETROBRÁS to designate all of the wells drilled in this oil field. Figures 4.6 and 4.7 present the facies distribution in two extensively cored wells, which were selected in order to illustrate the most important facies recognized in the Lagoa Parda turbidite system.

**Readers who do not need the descriptive details, sedimentological interpretation, well log response, and reservoir properties of each of the five facies can proceed to section 4.4 (High-resolution stratigraphy and reservoir geometry) or section 4.5 (Sedimentation evolution and controls).**

**4.3.1. Facies LP-F1: unstratified, bouldery to pebbly
conglomerates and very coarse-grained sandstones**

**Description:**

LP-F1 essentially includes unstratified, bouldery to pebbly conglomerates, conglomeratic sandstones, and very coarse- to coarse-grained sandstones (Figs. 4.6 to 4.10),

Fig. 4.6 - Typical facies and respective well log responses of Lagoa Parda turbidite system. Explanation of symbols used in this figure is provided in page 70.

# LP - 33

Gamma-ray log

Resistivity log

Levee succession G

LP - F3     $\theta$ Th, Op, Pl

Th

Th, Op

1520

Channel fill 33

$\theta$ Th, He

$\theta$ Th, Op

$\theta$ Th, Op

$\theta$ Th, He

Channel fill 30

LP - F2     $\theta$ Th, Op, Pl

LP - F1

1540

Channel fill 26

Channel fill 23

1560

Channel fill 22

Oil

Water

Channel fill 14

?

?

?

1580

(m)

50  100 API

p
g
vc
c
m
f
vf
s
c

2    20 Ω.m

Fig. 4.7 - Typical facies and respective well log responses of Lagoa Parda turbidite system. Explanation of symbols used in this figure is provided in page 70.

193



LP - 36

Gamma-ray log

Resistivity log

Levee succession D

LP - F3

Channel fill 26

Channel fill 22

Channel fill 15
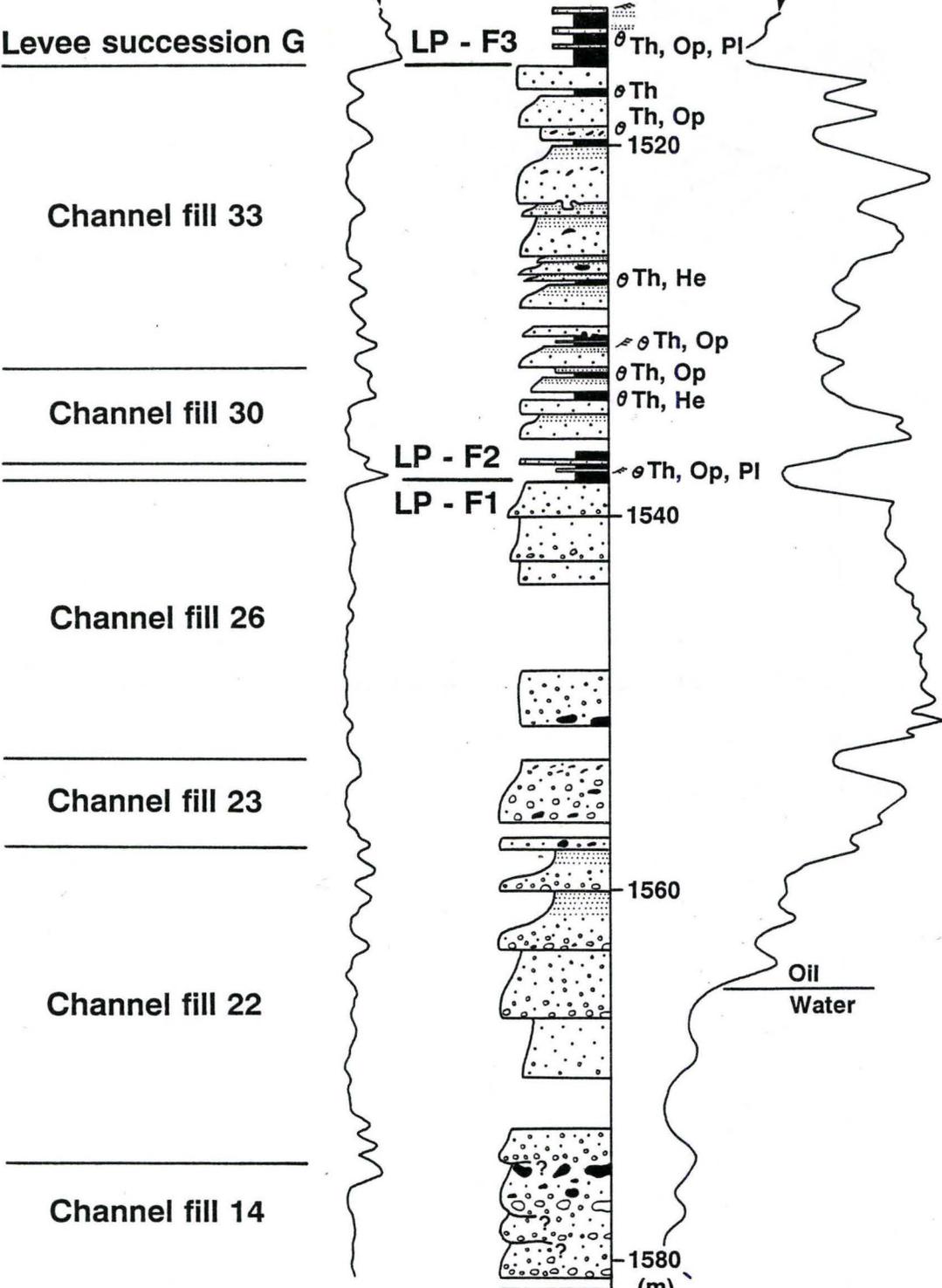
LP - F1
LP - F2

Channel fill 12

Channel fill 11

θ Th, He, Pl
θ Th, He, Pl

θ Th, He, Pl

1540

1560
(m)

θ Th

θ Th

Oil
Water

50 100 API

2          20 Ω.m

p
g
vc
c
m
f
vf
s
c

Fig. 4.8 - **FACIES LP-F1:** Unstratified, bouldery to pebbly conglomerates and very coarse-grained sandstones; **m** = boulder of high-rank metamorphic rock; **i** = boulder-sized intraclast of contorted mudstone. Channel fill 14; well LP-33; depth: 1,574.8 - 1579.6 m.
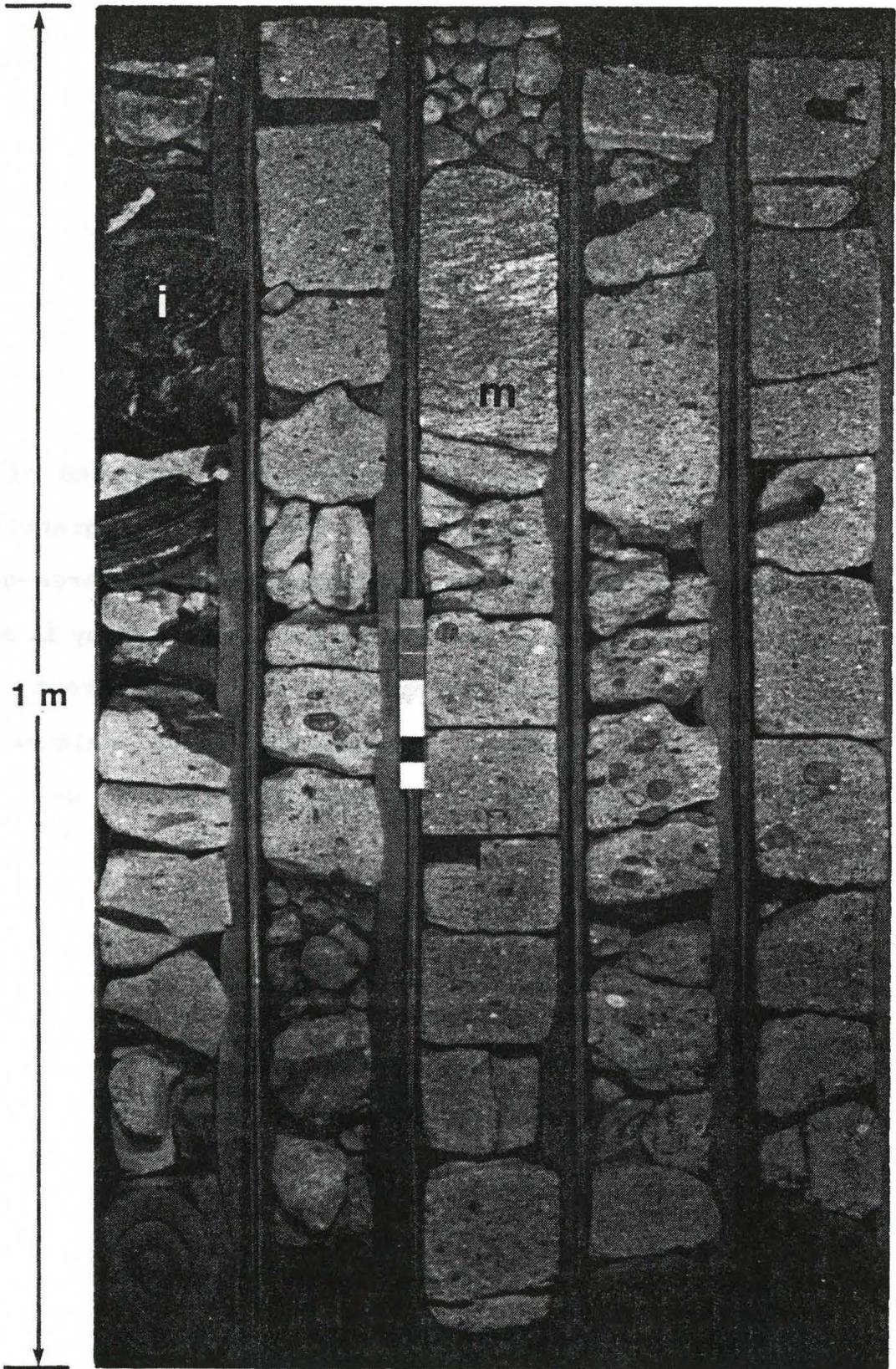
Fig. 4.9 - **FACIES LP-F1**: Two graded beds composed of (from bottom to top): unstratified, boulder- to granule-rich conglomerate, conglomeratic sandstone, and very coarse-grained sandstone. Cobble-sized mud intraclast indicated by i. Most of rocks are friable because of their low cement content, little mechanical and chemical compaction, and related high porosities and permeabilities. Channel fill 15; well LP-36; depth: 1,557.7 - 1,562.5 m.
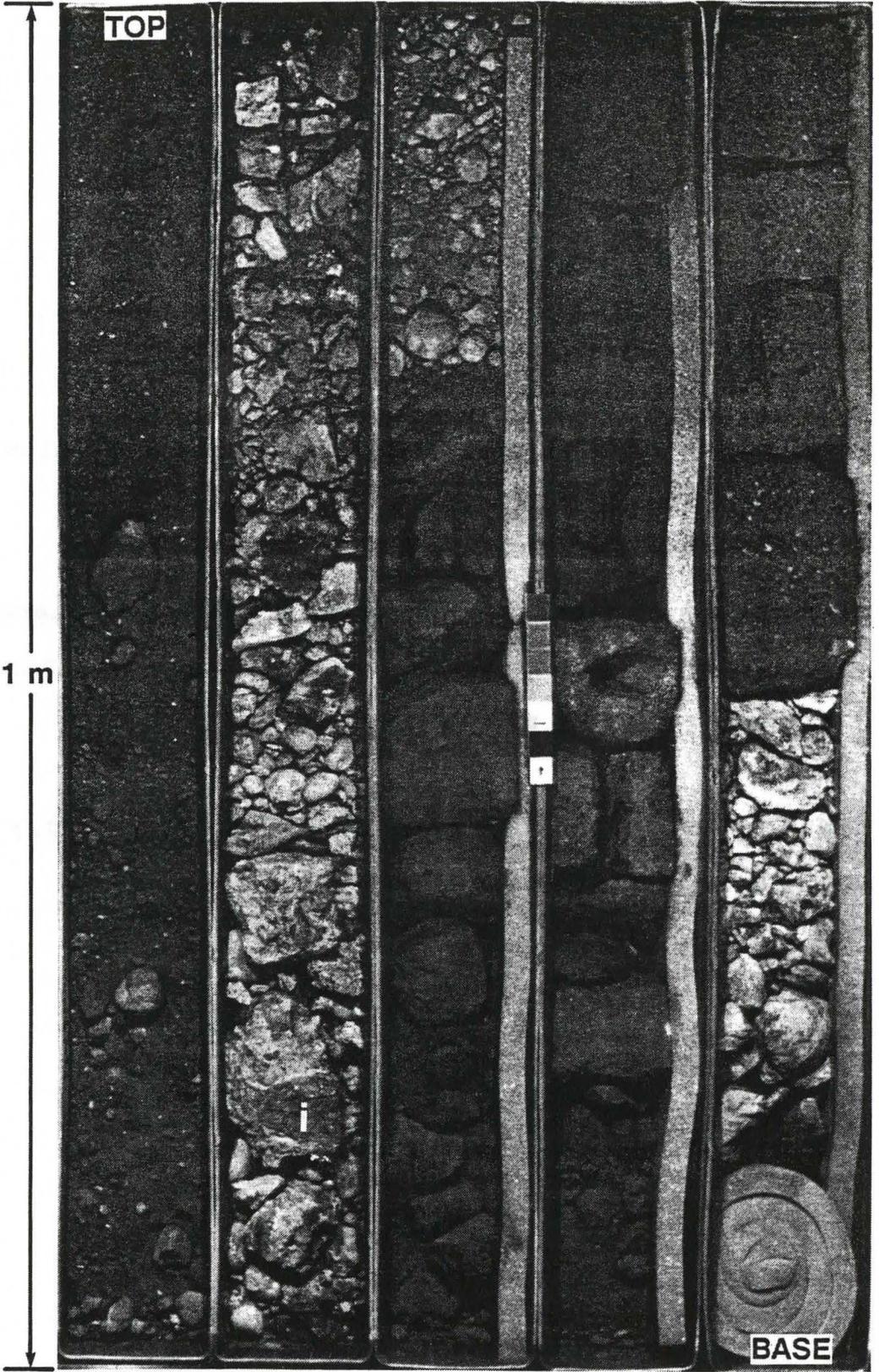
Fig. 4.10 - **FACIES LP-F1:** Unstratified, conglomerates and very coarse-grained sandstones.

(**a**) Pebble (< 2.5 cm)- to granule-rich conglomerate, with matrix of very coarse-grained sand. Channel fill 26; well LP-36; depth: 1,539.4 m.

(**b**) Very coarse-grained sandstone. Channel fill 22; well LP-33; depth: 1,569.0 m.
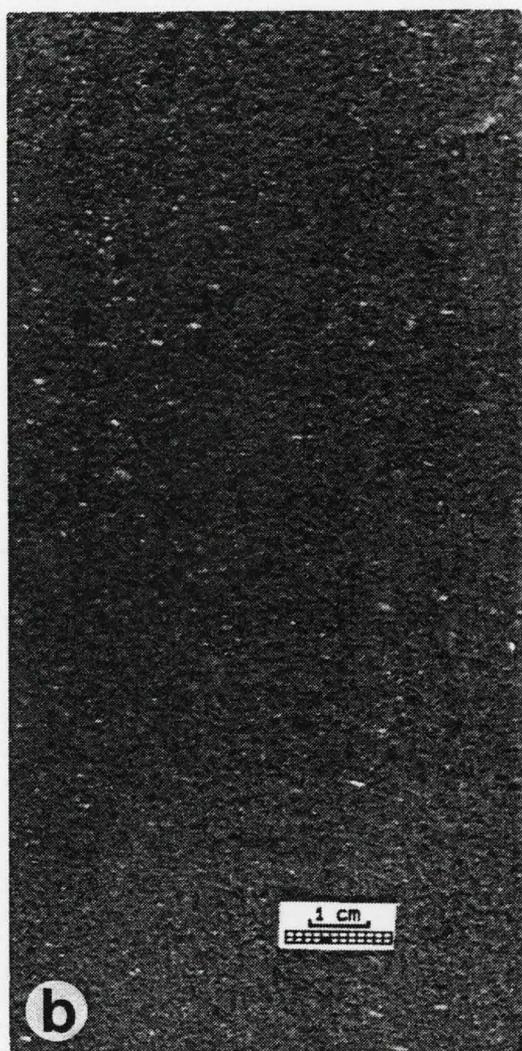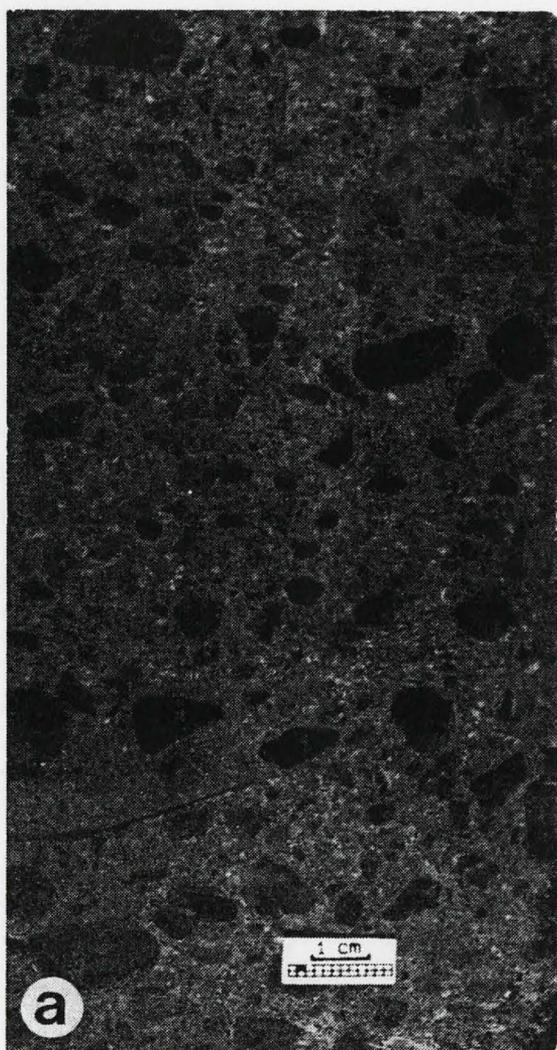
which typically comprise normally graded beds ranging in thickness from 0.6 to 6.4 m (Figs. 4.6, 4.7, and 4.9). A few graded beds of LP-F1 are capped by 0.1 - 1.2 m thick, parallel-stratified, medium- to fine-grained sandstones, which are similar to the stratified sandstones described for the facies LP-F2 (Fig. 4.6). Inverse grading is very subordinate in facies LP-F1; where present, there is a gradation from very coarse-grained sandstone or conglomeratic sandstone to pebbly and bouldery conglomerate, in a basal zone up to 60 cm thick.

The gravel portion of LP-F1 is composed mostly of pebbles to boulders (up to 40 cm diameter) of quartzo-feldpathic high-grade metamorphic rocks (Figs. 4.8, 4.9, and 4.10a), mud intraclasts (Figs. 4.8), and carbonaceous plant fragments. The exogenic, gravel-sized components tend to be concentrated at the base of individual beds, and their upward decrease in size and proportion defines the common coarse-tail grading presented by LP-F1. The gravel-sized intraformational clasts may occur concentrated at the base of the graded beds (Fig. 4.9), but they also may occur widely- and randomly-distributed in some beds (Fig. 4.8).

The uppermost portion of the graded beds is formed mainly by very coarse- to coarse-grained sandstone, characterized by a gravel content smaller than 5 %, and content grading.

The rocks that comprise LP-F1 are also characterized by poor sorting, and low (< 5 %) muddy matrix content. The sandstones and the sandy matrix of conglomerates are composed

of subangular to angular grains, contrasting with the exogenic, boulder- to pebble-sized components of conglomerates, which are sub-rounded to rounded (Figs. 4.8 and 4.10a).

LP-F1 is characterized by the common amalgamation of many graded beds (Figs. 4.6 and 4.7), which results in the development of sandstones packages up to 55 m thick without interbedded mudstones. The contacts between individual graded beds are typically sharp, and in places clearly indicate erosion of the underlying bed. The very coarse-grained beds of LP-F1 typically show sharp contacts with underlying or overlying mudstones and finer-grained sandstones of facies LP-F2, LP-F3, LP-F4, and LP-F5, but also may grade upward and laterally to LP-F2.

Bagnoli (1984) presented a petrographic study of the Lagoa Parda conglomerates and sandstones. He described the framework of typical rocks of the facies LP-F1 as composed mainly of quartz (monocrystalline and polycrystalline grains), feldspar (chiefly microcline, with subordinate plagioclase, orthoclase and perthite), and fragments of quartzo-feldspathic, high-grade metamorphic rocks (e.g. migmatites and granulites). The average framework composition shows 62 % quartz, and 38 % feldspars and rock fragments. LP-F1 rocks are mostly arkoses (McBride, 1963), and suggest a continental block provenance (Dickinson and Suczek, 1979).

Accessory components are represented by boulder- to sand-

sized muddy intraclasts, carbonaceous plant fragments, muscovite, biotite, glauconite, garnet, zircon, tourmaline, and staurolite. Except for the mud intraclasts (up to 20 %), the accessory minerals represent less than 1 % of the rocks.

The diagenetic mineral assemblage includes mostly kaolinite (average 13 %) and calcite (average 10 %) cements, and very subordinate (< 1 %) amounts of quartz, feldspar, pyrite, and dolomite cements (Bagnoli, 1984).

**Interpretation:**

The unstratified, coarse-grained, graded beds of LP-F1 probably were formed mostly by the rapid deposition of suspended load carried by high-concentration (or high-density, > 1.1 $g/cm^3$) turbidity currents (Kuenen and Migliorini, 1950; Middleton, 1967, 1970; Lowe, 1982). However, the common occurrence of boulder- to pebble-sized clasts in LP-F1 suggests also the transport and deposition by flows where larger clasts are supported by the combined effects of fluid turbulence and dispersive pressure resulting from grain collisions (Hein, 1982; Lowe, 1982).

The only organization displayed by LP-F1 is grading, indicating that its deposition took place mostly at high suspended-load fallout rates, which did not allow a sufficient time for the development of bed traction (Walker, 1978; Lowe, 1982). Normal grading is well-defined throughout most of the turbidites of Lagoa Parda field (Figs. 4.6, 4.7, and 4.9).

Coarse-tail grading is the most common type of normal grading, suggesting that at least the coarser fraction of the sediment cloud may have settled as a non-turbulent suspension (Middleton, 1967). The subordinate inversely-graded deposits record the development of traction carpets (Hein, 1982; Lowe, 1982), where concentrated mixtures of coarse sediments are maintained at the base of the turbidity current by grain collisions (dispersive pressure; Bagnold, 1956).

Boulder- to pebble-sized mud intraclasts are found mostly at the base of the graded beds, but they can also be widely- and randomly-distributed in some beds (Fig. 4.8). These large intraclasts were probably derived from the erosion and collapse of channel margins, and were deposited within a very short distance. These large intraclasts could eventually be incorporated into the deposits of the same turbidity current that induced channel wall collapse. Closely-spaced well control and detailed correlations show that LP-F1 always comprises channel fill deposits in the Lagoa Parda field (Fig. 4.11); their geometry is detailed in section 4.4 (High-resolution stratigraphy and reservoir geometry).

## 4.3.2. Facies LP-F2: graded beds of unstratified coarse-grained sandstones and parallel-stratified finer-grained sandstones

**Description:**

Fig. 4.11 - Schematic cross section presenting the stratigraphic relationships among the levee successions and the most important channel fills of the Lagoa Parda turbidite system. Twenty six channel fills are represented by their maximum width and thickness. The section illustrates levee asymmetry and the overall trends of channel fills that become narrower, thinner, and finer-grained upward. Datum is a high-resistivity, mudstone horizon rich in siderite, rhodochrosite, and pyrite, which is subparallel to the contact between the zones *Neochiastozygus chiastus* and *Tribrachiatus orthostylus*. Vertical scale = 5 x horizontal scale.

# LAGOA PARDA CHANNEL COMPLEXES



NW

Tribrachiatus orthostylus zone

DATUM

Neochiastozygus chiastus zone

SE
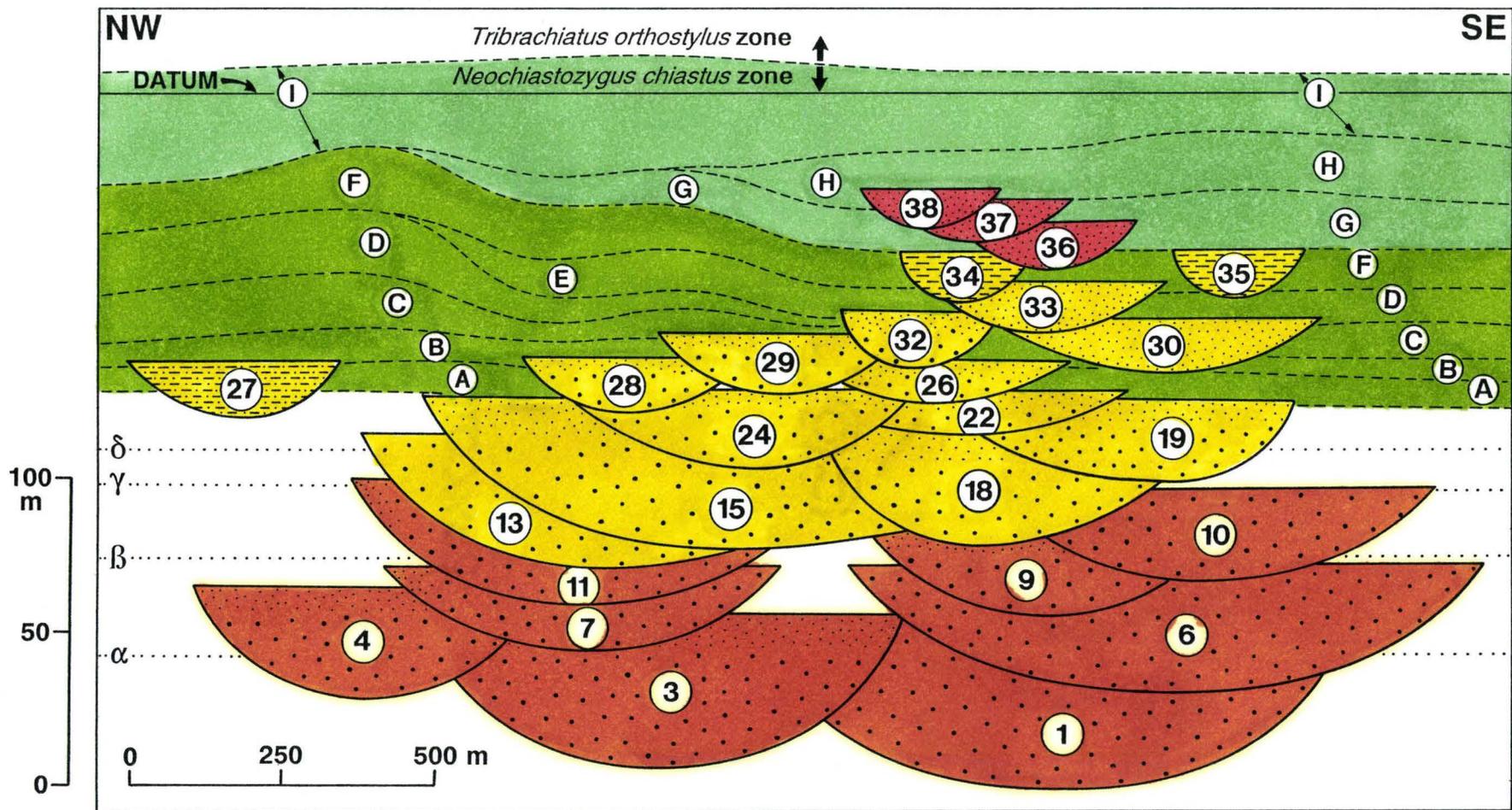
| CHANNEL COMPLEXES: | LP-CC1 | FACIES: | LP-F1 | LP-F3 (Channel fill) | LP-F4 |
| | LP-CC2 | | LP-F2 | LP-F3 (LP-CC2 levees) | LP-F5 |
| | LP-CC3 | | | LP-F3 (LP-CC3 levees) | |

201

LP-F2 comprises normally graded beds starting at the base with unstratified, very coarse- to (mostly) coarse-grained sandstones, which grade upward to parallel-stratified, medium- to fine-grained sandstones (Figs. 4.6, 4.12, and 4.13). The thickness of these graded beds ranges from to 0.3 to 3.8 m. A few graded beds of LP-F2 are capped by thin (< 0.1 m), ripple cross-laminated, fine-grained sandstones (e.g. turbidite b1 in Fig. 4.12).

LP-F2 also includes thin (< 0.3 m) interbedded bioturbated mudstones, which are similar to the mudstones described for facies LP-F3. The stratified sandstones may also show a pervasive bioturbation in their uppermost part. The trace fossil assemblage recognized in LP-F2 includes mainly *Thalassinoides*, *Ophiomorpha*, *Planolites*, *Palaeophycus*, and *Helminthopsis*, and very subordinate *Asterosoma*, *Skolithos*, *Cylindrichnus*, *Chondrites?*, *Zoophycos?*, and *Anconichnus?*. A more detailed characterization of these trace fossils is presented in the description and interpretation of facies LP-F3.

The lack of conglomerates with exogenic clasts, and the abundance of stratified sandstones in facies LP-F2, are the main criteria for its differentiation from LP-F1. However, boulder- to granule-sized mud intraclasts are also common in LP-F2, locally forming unstratified, intraclastic sandstones (Figs. 4.13 and 4.14a) or intraformational conglomerates (Fig. 4.13).

Fig. 4.12 - **FACIES LP-F2:** Graded beds of unstratified, very coarse- to coarse-grained sandstones and parallel stratified, medium- to fine-grained sandstones. Five graded beds are illustrated, which bases are labeled **b1** to **b5**, from bottom to top. The lowermost turbidite (**b1**) also shows ripple cross-laminated, fine-grained sandstones in its upper part, which are overlain by bioturbated mudstones. Turbidite **b3** contains cobble-sized mud intraclasts (**i**). Most of very coarse- to coarse-grained sandstones are friable because of their low cement content, little mechanical and chemical compaction, and related high porosities and permeabilities. Channel fill 33; well LP-33; depth: 1,523.1 - 1,528.6 m.

TOP
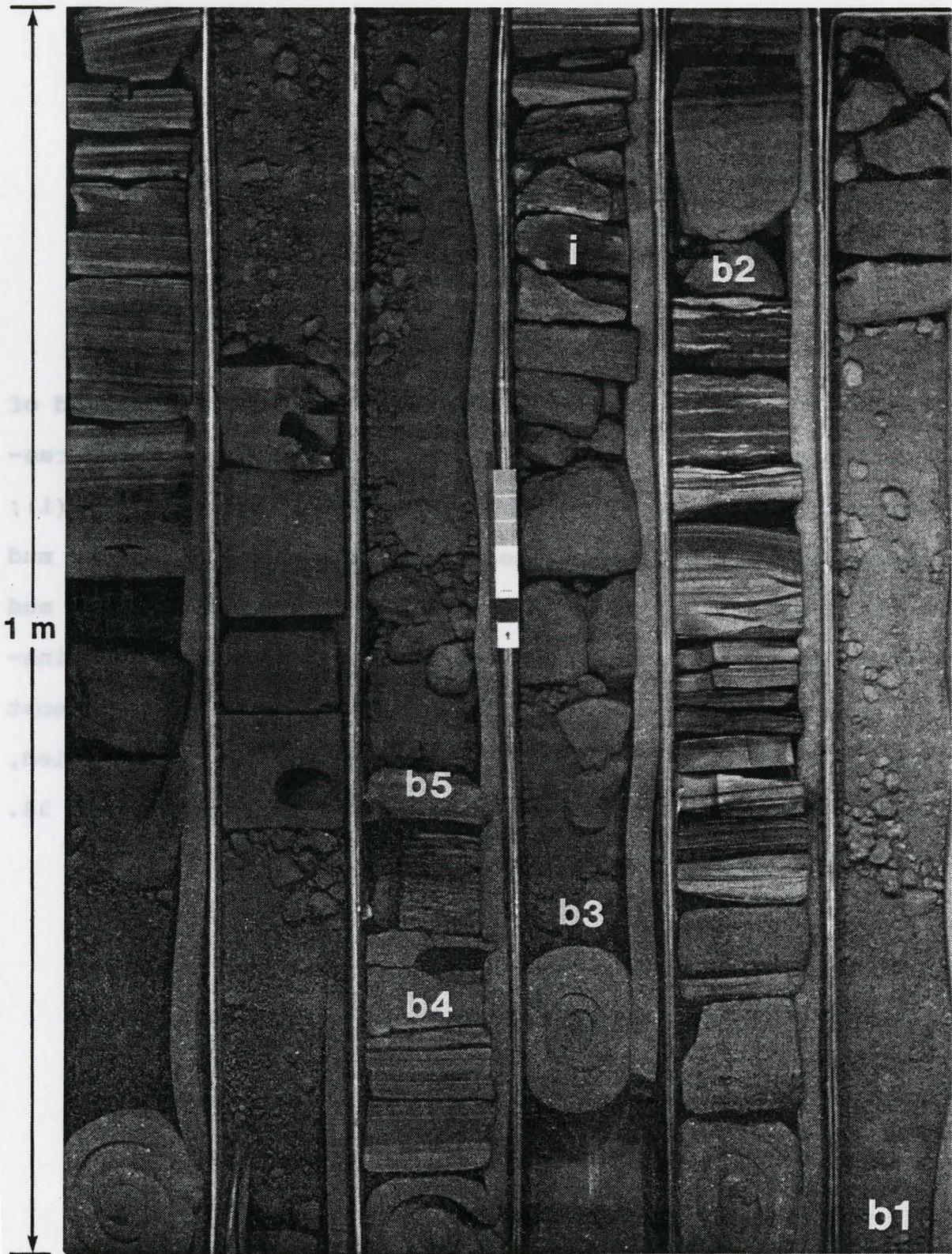
1 m

BASE

Fig. 4.13 - **FACIES LP-F2:** At the base, graded bed composed of (from bottom to top): unstratified, very coarse- to coarse-grained sandstone with cobble-sized mud intraclasts (**i**); intraclastic, medium-grained sandstone (5 - 30 % mud intraclasts) (**is**), and intraclastic conglomerate (> 30 % mud intraclasts) (**ic**); and parallel-stratified, medium- to fine-grained sandstone (**p**). This graded bed comprises the uppermost turbidite of channel fill 37; it is overlain by unstratified, very coarse- to coarse-grained sandstone of channel fill 38. Well LP-3; depth: 1,490.5 - 1,495.2 m.
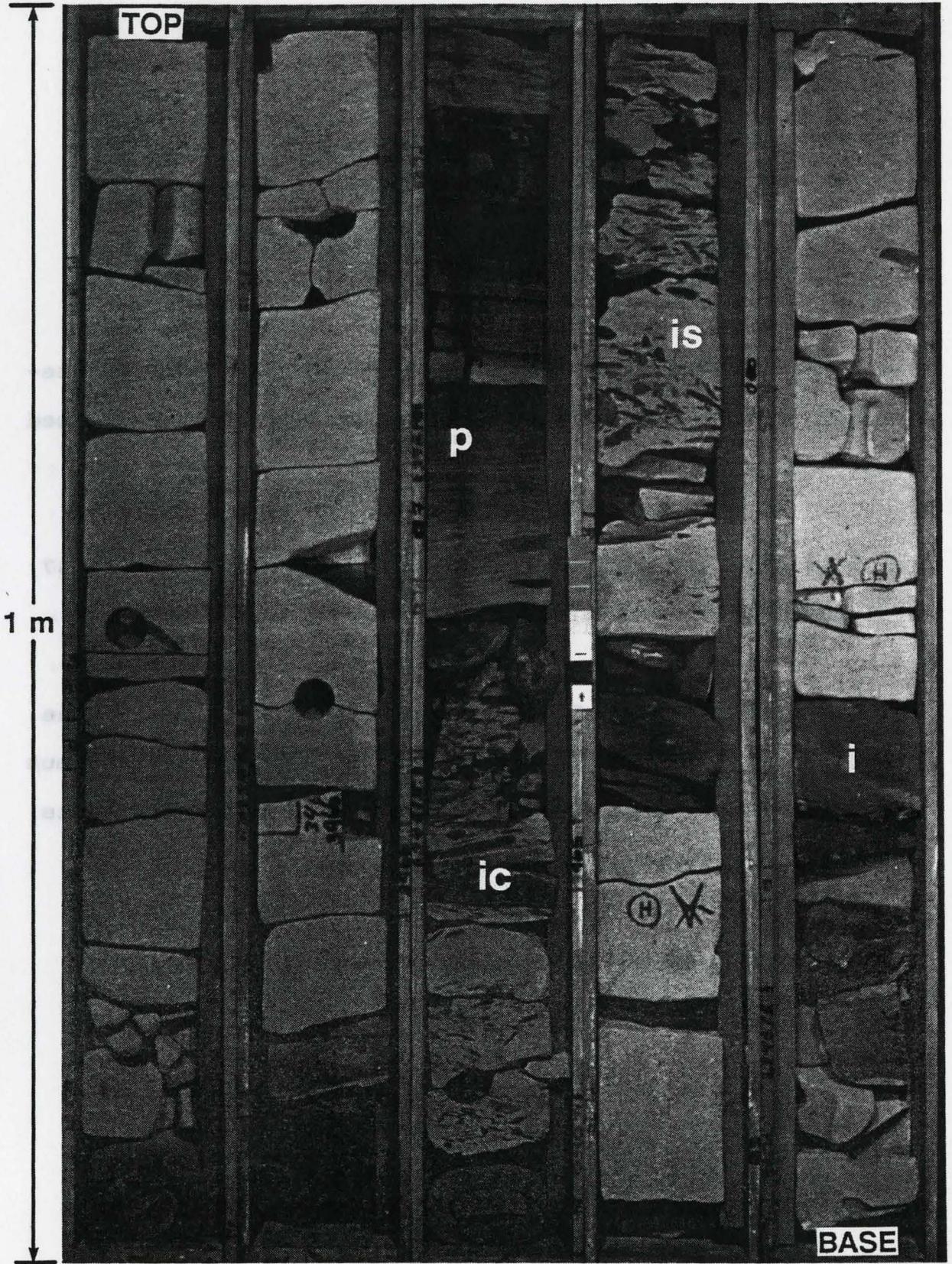
Fig. 4.14 - **FACIES LP-F2:** Graded beds of unstratified, coarse-grained sandstones and parallel-stratified, finer-grained sandstones.

(a) Intraclastic, medium-grained sandstone. Channel fill 37; well LP-3; depth: 1493.5 m.

(b) Parallel-stratified, medium-grained sandstone. Stratification is defined by concentrations of carbonaceous plant fragments, mica flakes, and flattened mud intraclasts. Channel fill 33; well LP-33; depth: 1,523.5 m.
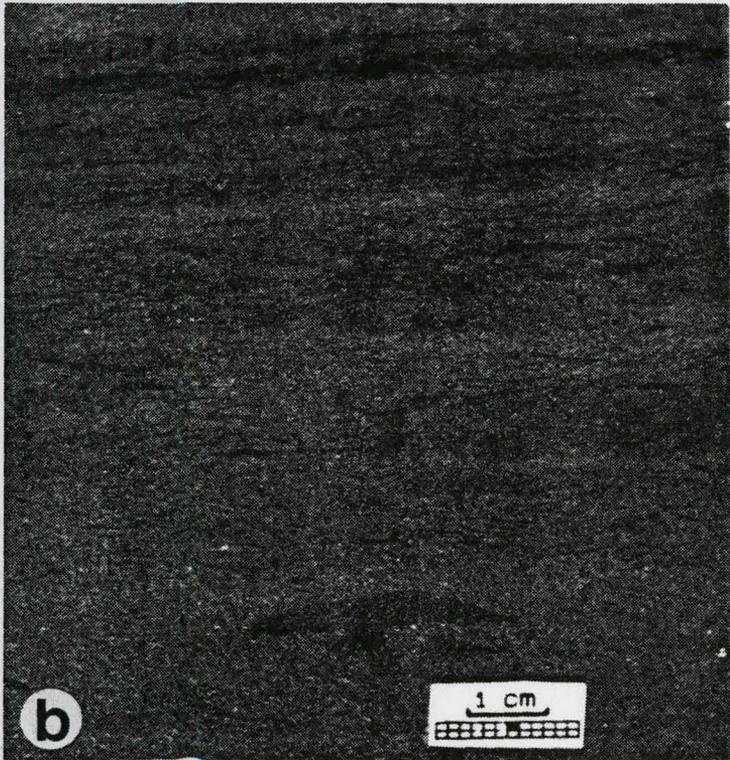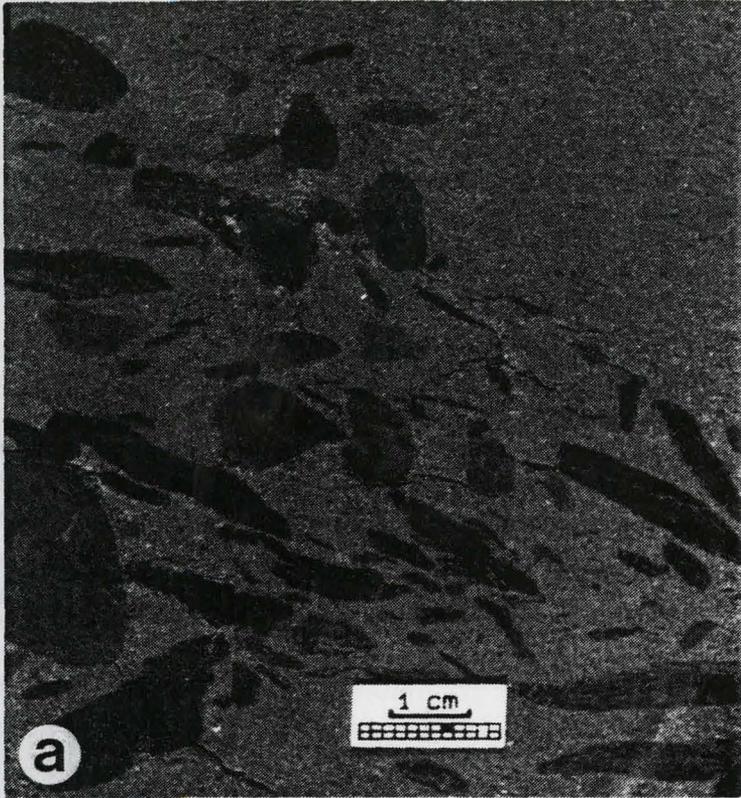
Stratification is well-defined in the upper portion of LP-F2 graded beds due to the important concentration of carbonaceous plant fragments, mica flakes, and flattened mud intraclasts (Fig. 4.14b). In a very few beds the stratification is deformed by water escape structures (pillars).

The rocks that comprise LP-F2 are also characterized by poor to moderate sorting, subangular to angular grains, and low mud matrix content (< 5 %).

The contacts between superimposed graded beds, or between graded beds and underlying mudstones are typically sharp (Fig. 4.6), but they may be deformed by loading, including the development of injection structures and centimeter-sized, ball-and-pillow structures. LP-F2 successions, typically 5 - 25 m thick, may grade upward or laterally to LP-F4, or be sharply underlain or overlain by LP-F1 and LP-F3 successions.

The average framework composition, and diagenetic mineral content of the LP-F2 unstratified sandstones are very similar to those of LP-F1 rocks (Bagnoli, 1984). They are mostly arkoses (64 % quartz, and 36 % feldspars and quartzo-feldspathic rock fragments), cemented mainly by kaolinite (10 %) and calcite (8 %). The parallel-stratified sandstones also have a similar framework composition (62 %, and 38 % feldspar and quartzo-feldspathic rock fragments). However, the stratified sandstones have a much higher average content of carbonaceous plant fragments (24 %), micas (7 %), and mud

intraclasts (4%), and a lower average content of kaolinite (5 %) and calcite (1 %) cements.


## Interpretation:

The unstratified, very coarse- to coarse-grained sandstones of LP-F2 and LP-F1 probably had a similar origin; i.e. both were formed by the rapid deposition of the suspended load transported by high-density turbidity currents (Kuenen and Migliorini, 1950; Middleton, 1967, 1970; Lowe, 1982).

LP-F2 stratified sandstones, however, were probably deposited by low-density turbidity currents (Lowe, 1982), where slower deceleration permitted the transfer of sediment from suspended to bed load, followed by traction sedimentation to form parallel-stratified sandstones, and subordinate ripple cross-laminated sandstones. These low-density turbidity currents may have originated as residual currents following the deceleration of high-density turbidity currents and the deposition of their coarser-grained load (Lowe, 1982). The resulting low-density turbidity currents would be able to deposit their load immediately above coarser-grained turbidites (Figs. 4.6), or to bypass areas of high-density turbidity current sedimentation.

LP-F2 rocks also may contain many boulder- to granule-sized mud intraclasts, which occur concentrated at the base or widely- and randomly-distributed through the graded beds (Fig. 4.13). As observed for LP-F1, these large intraclasts were

probably derived from the erosion and collapse of channel
margins, with their deposition taking place within a short
distance. Closely-spaced well control and detailed
correlations show that both LP-F1 and LP-F2 always comprise
channel fill deposits in the Lagoa Parda field (Fig. 4.11);
their geometry is detailed in section 4.4 (High-resolution
stratigraphy and reservoir geometry).

### 4.3.3. Facies LP-F3: Interbedded bioturbated mudstones and thin-bedded sandstones

**Description:**

LP-F3 includes interbedded mudstones and thin-bedded,
parallel- to ripple cross-laminated, fine- to very fine-
grained sandstones (Figs. 4.15 and 4.16). Both mudstones and
sandstones show a pervasive bioturbation, with the degree of
bioturbation ranging between 30 and 90 % by volume in most
cores of LP-F3 (Figs. 4.15 to 4.20). LP-F3 comprises up to 120
m thick successions, with a sand/mud ratio that ranges between
0.2 and 0.8.

Most of the sandstone beds are 2 to 8 cm thick, but a few
thicker (up to 70 cm) sandy successions also can be recognized
(Fig. 4.15). Individual beds typically contain Bouma's (1962)
divisions, mainly $T_{bc}$ (Fig. 4.17a), $T_b$, and $T_c$. Thicker sandy
successions (> 10 cm) are composed of amalgamated $T_{bc}$ divisions
(Figs. 4.15 and 4.17a). The ripples are commonly climbing

Fig. 4.15 - **FACIES LP-F3:** Interbedded bioturbated mudstones and thin-bedded sandstones. Sandstones are mostly fine- to very fine-grained, and show parallel- and ripple cross-lamination. Bioturbation is pervasive, particularly in the mudstones. Trace fossil assemblage is largely dominated by *Thalassinoides*, followed by *Ophiomorpha* (in the sandstones), *Planolites*, and *Helminthopsis*. The cored interval makes part of a thinning- and fining-upward succession. Levee succession D; well LP-33; depth: 1504.9 - 1510.7 m.
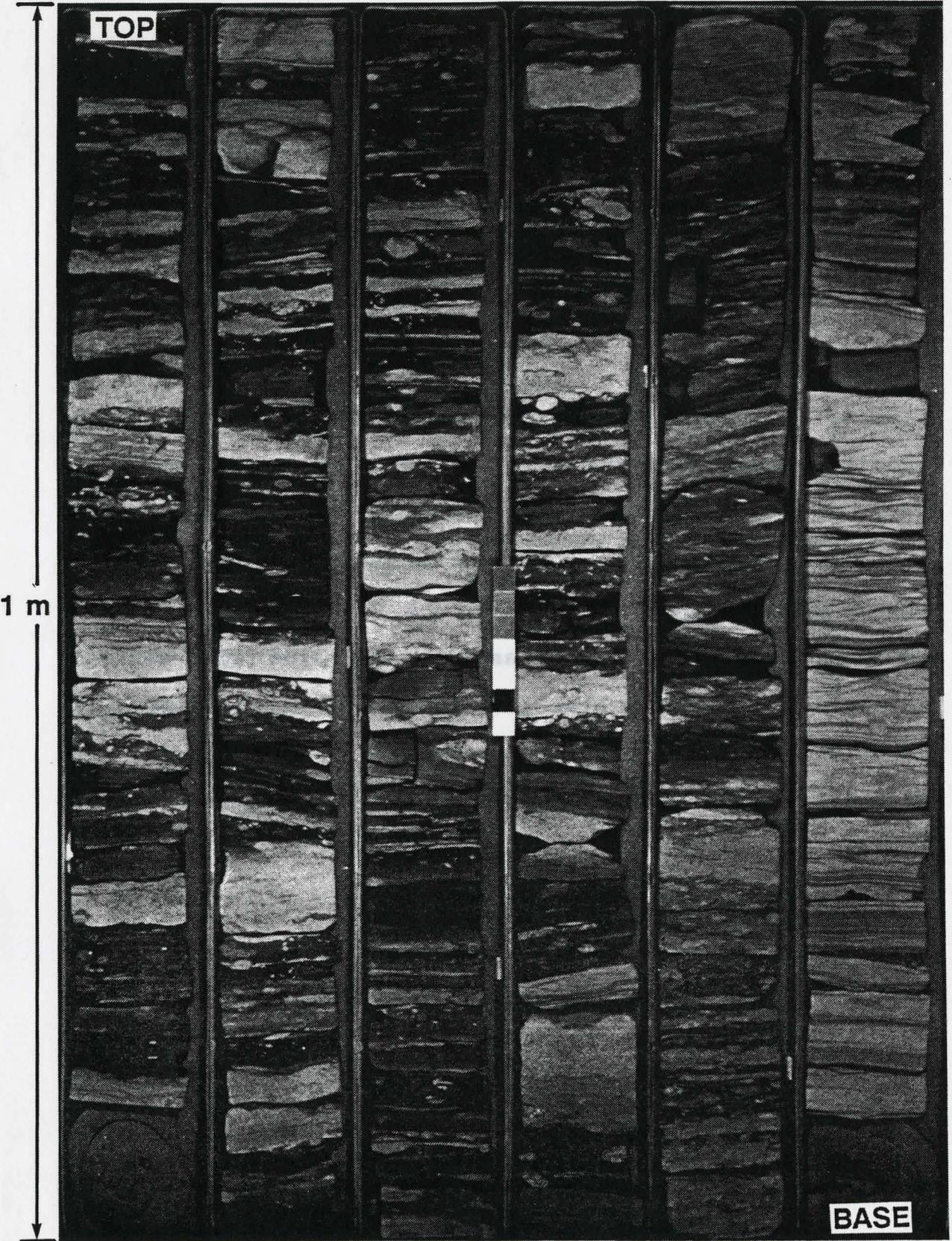
Fig. 4.16 - **FACIES LP-F3:** Interbedded bioturbated mudstones and thin-bedded sandstones. Sandstones are mostly fine- to very fine-grained, and show parallel- and ripple cross-lamination; their beds dip as much as 10°, which correspond to the original depositional slope. A 3.8 m thick, mud-rich succession occurs at the base; it contains disorganized, intraclastic conglomerates (**ic**). Trace fossil assemblage is largely dominated by *Thalassinoides*, *Helminthopsis*, and *Planolites*. Levee succession D; well LP-36; depth: 1,523.7 - 1,531.2 m.

Fig. 6.17 – FACIES 18-23: Thin-bedded turbidites and debris
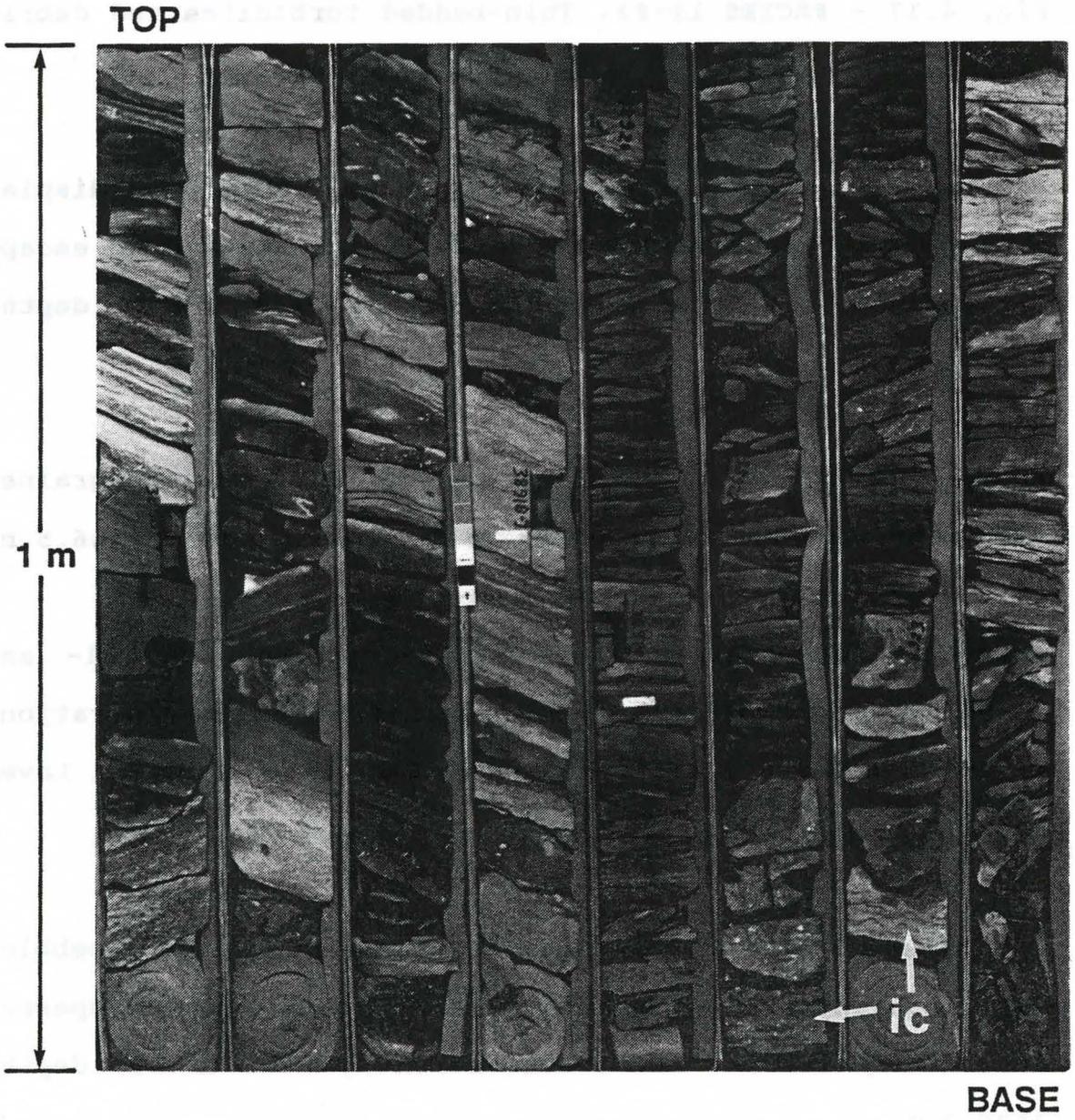
Fig. 4.17 - **FACIES LP-F3**: Thin-bedded turbidites and debris flow deposits.

(a) Two amalgamated $T_{bc}$ turbidites. Rippled divisions display climbing ripples, and the upper turbidite contain an escape (?) trace fossil. Levee succession G; well LP-33; depth: 1510.4 m.

(b) $T_{abc}$ turbidite composed of medium- to very fine-grained sandstone. Levee succession G; well LP-10; depth: 1,546.5 m.

(c) Very fine-grained sandstone displaying parallel- and convolute lamination. Lamination is defined by concentrations of carbonaceous plant fragments and mica flakes. Levee succession G; well LP-10; depth: 1,546.3 m.

(d) Intraformational conglomerate containing contorted pebble-sized mud intraclasts and very coarse-grained sand dispersed in a muddy matrix. Levee succession D; well LP-36; depth: 1530.2 m.

The facing-page caption text is partially visible through the page (mirror image):

Fig. 4.12 — FACIES LP-F3: Bio...

(a) Large Thalassinoides (Th)...

(c) Thalassinoides (Th) as roun...
and also as monische, back-f...
appearing zone; lower occurr...
(Pl); Zoophycos (Zo); and Helm...
G; well LP-33; depth: 1,909.1...
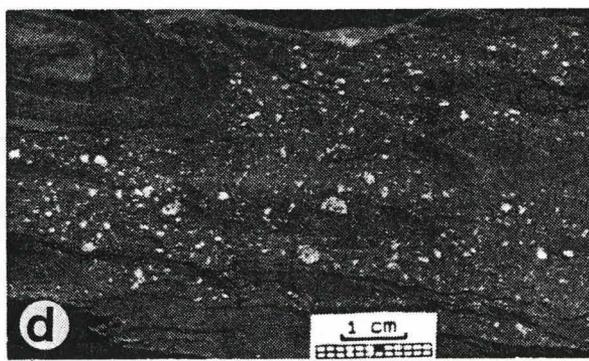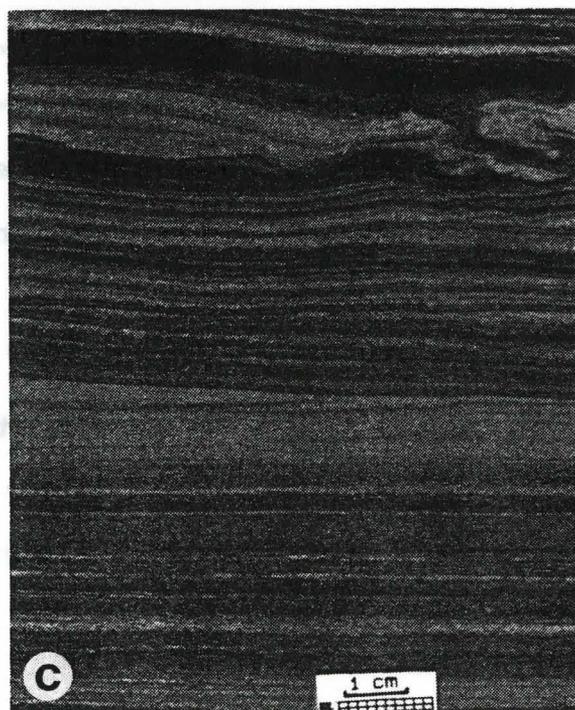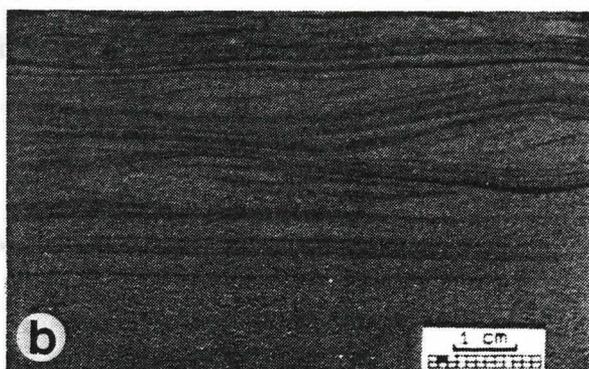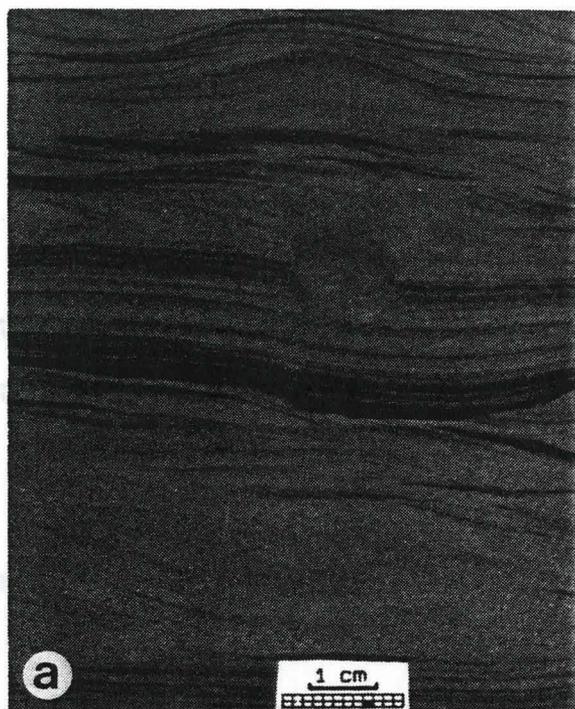
Fig. 4.18 - **FACIES LP-F3:** Bioturbated mudstones.


(a) Large *Thalassinoides* (**Th**); sand-filled *Planolites* (**Pl**); *Palaeophycus* (**Pa**); and *Cylindrichnus* (**Cy**). Levee succession G; well LP-33; depth: 1,505.4 m.


(b) Same sample of (a); plan view at the level of *Planolites* (**Pl**).


(c) *Thalassinoides* (**Th**) as rounded burrows (upper occurrence), and also as meniscate, back-filled forms (oblique, mottled-appearing zone; lower occurrence); sand-filled *Planolites* (**Pl**); *Zoophycos* (**Zo**); and *Helminthopsis* (**He**). Levee succession G; well LP-33; depth: 1,509.1 m.


(d) Same sample of (c); plan view at the level of uppermost *Thalassinoides* (**Th**).
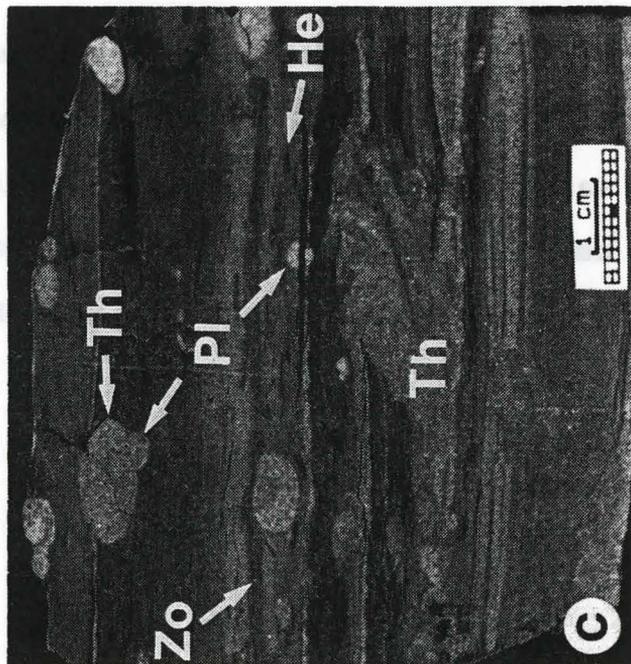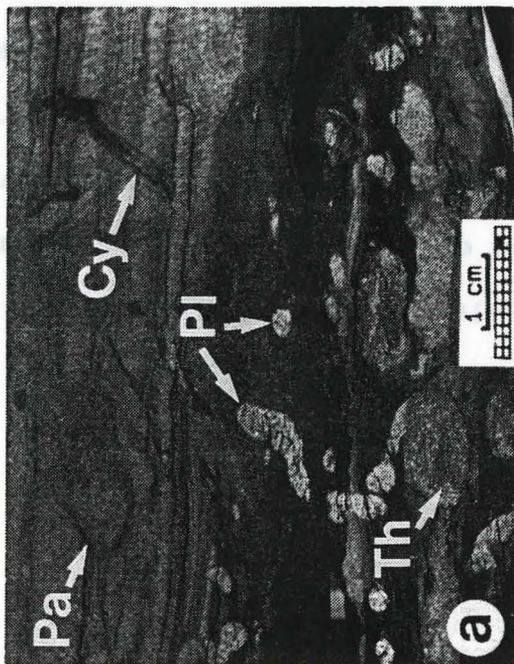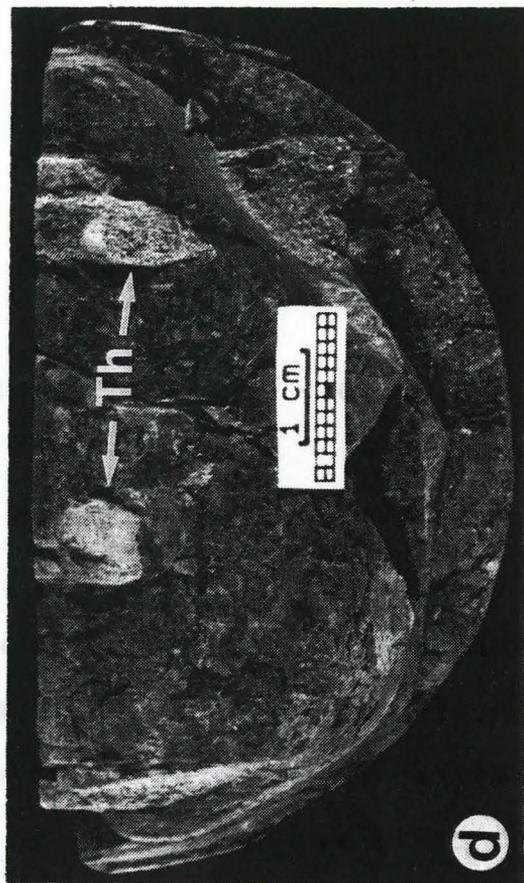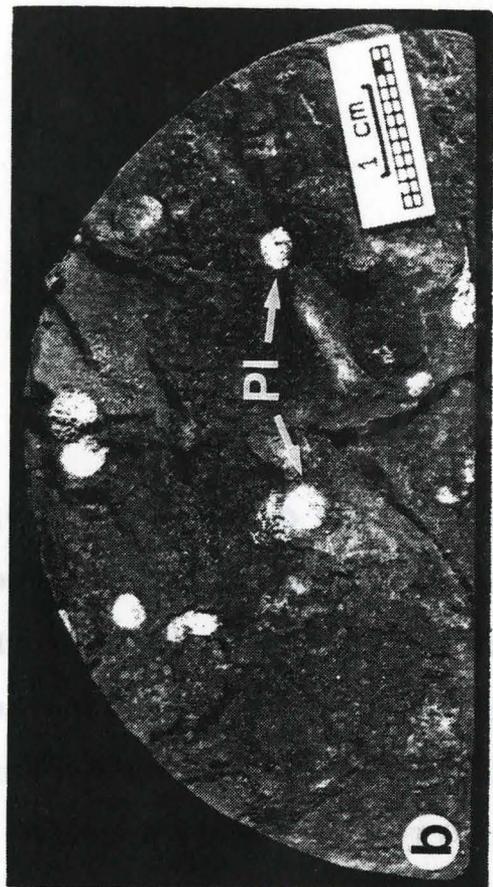
Fig. 4.19 - **FACIES LP-F3:** Bioturbated mudstones.

(a) *Thalassinoides* (**Th**) in the mudstone; and *Ophiomorpha* (**Op**; *Ophiomorpha nodosa* ?) in the sandstone. *Thalassinoides* and *Ophiomorpha* may be part of a contemporaneous, open network burrow system made by the same trace maker, but responding to different substrates. Levee succession I; well LP-10; depth: 1,514.0 m.

(b) Rhodochrosite (**r**) concretion overlain by mudstone containing *Helminthopsis* (**He**) and *Thalassinoides* (**Th**). This sample makes part of a high-resistivity marker-bed, which was used as datum in the cross sections of figures 4.11, 4.23, and 4.24. Levee succession I; well LP-10; depth: 1,483.0 m.
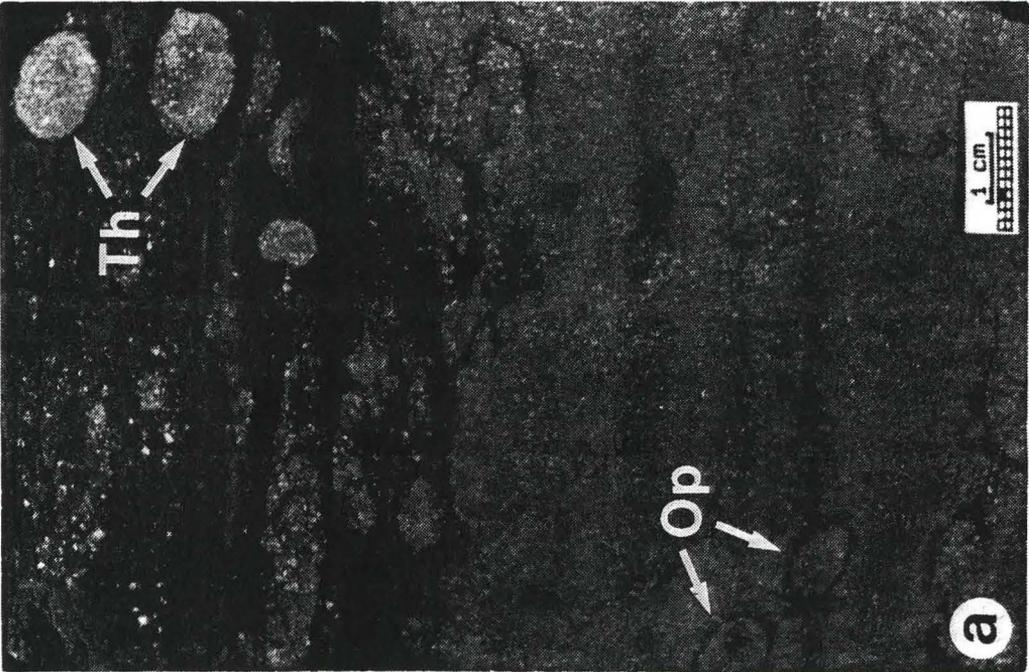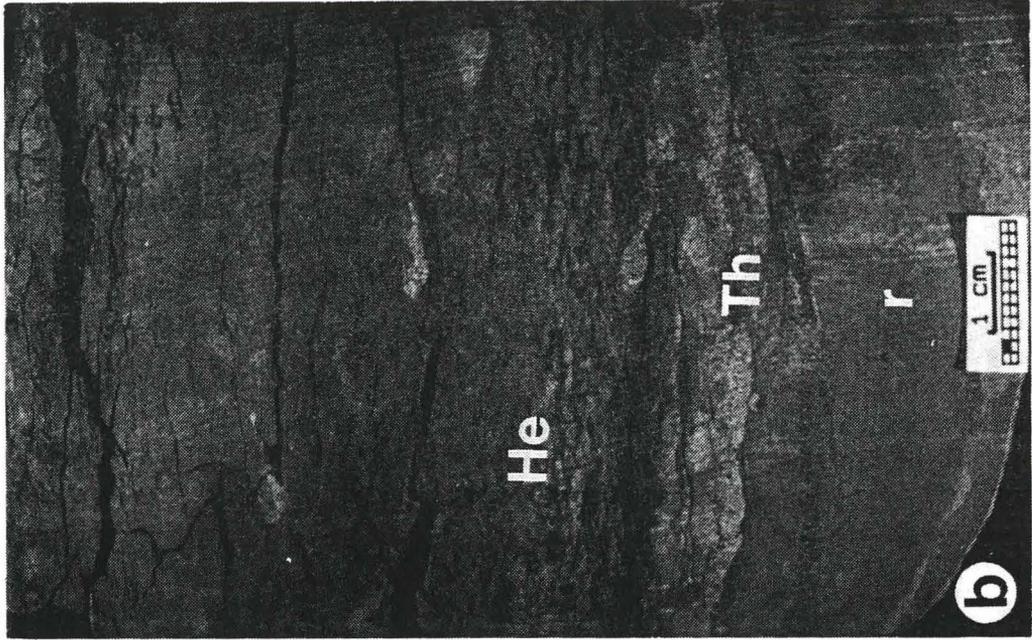
Fig. 4.20 – **FACIES LP-F3**: Bioturbated mudstones.

(a) *Thalassinoides* (**Th**) as rounded, sand-filled burrows (lower occurrence), and also as muddy, irregularly-shaped forms (upper occurrence); small, mud-lined *Palaeophycus* (**Pa**); sand-filled *Planolites* (**Pl**); *Asterosoma* (**As**); and mud-filled *Chondrites* (**Ch**). Levee succession I; well LP-10; depth: 1,500.6 m.

(b) Pervasive bioturbation mostly by *Helminthopsis*. Levee succession I; well LP-10; depth: 1,524.0 m.
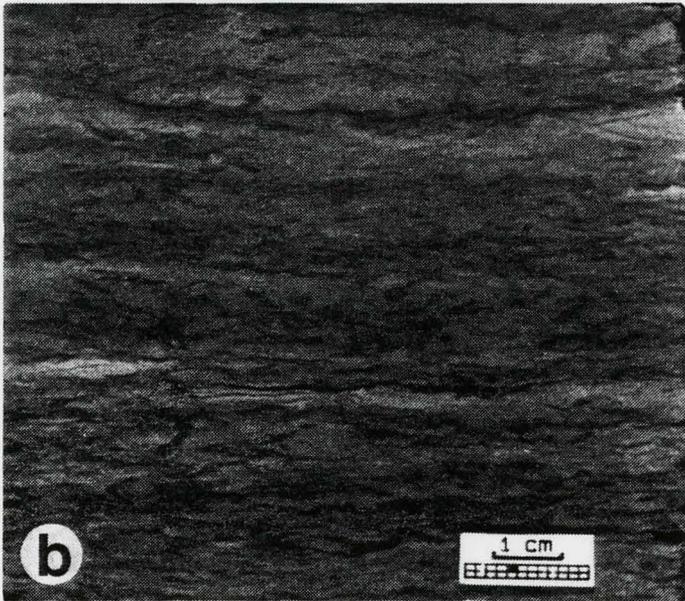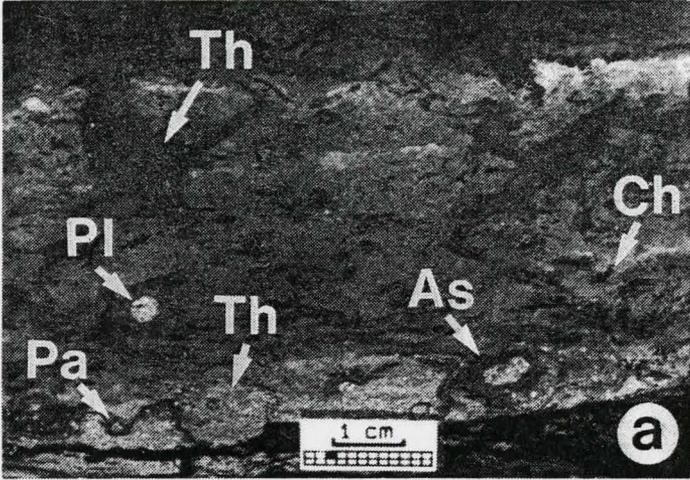
(Fig. 4.17a). Convolute lamination is also a common feature of LP-F3 sandstones (Fig. 4.17c). Coarse- to medium-grained sandstones are present in LP-F3, but are very subordinate (< 10 %). These coarser-grained sediments typically form the 5 - 10 cm thick, basal part of Bouma's $T_{ab}$, $T_{abc}$ (Fig. 4.17b), and $T_{abcde}$ beds.

Some LP-F3 cores show thin-bedded sandstones dipping as much as 10° (Fig. 4.16). The successions containing dipping sandstone beds may overlie sub-horizontal successions of facies LP-F1, LP-F2 or LP-F3. Because there was no fault activity within the Lagoa Parda field, it follows that these thin-bedded turbidites indicate their original depositional slopes. Mudstone-rich, dipping LP-F3 successions may contain thin (< 50 cm) horizons of deformed mudstones, and disorganized, intraformational conglomerates (Fig. 4.16). These conglomerates contain contorted, cobble- to granule-sized mud intraclasts dispersed in a poorly-sorted matrix composed of variable proportions of mud and sand (Fig. 4.17d).

LP-F3 sandstones are mostly arkoses (65 % quartz, and 35 % feldspars), cemented by kaolinite (7 %) and calcite (5 %) (Bagnoli, 1984). The high average content of carbonaceous plant fragments (16 %), micas (6 %), and sand-sized mud intraclasts (4 %) (Bagnoli, 1984) help to define the sandstone stratification (Fig. 4.17).

The trace fossil assemblage is largely dominated by the ichnogenus *Thalassinoides*, which is characterized by 1 - 3 cm

diameter, unlined and unornamented, mostly sand-filled burrows (Figs. 4.18 and 4.19). These burrows comprise a mainly horizontal, but also slightly inclined, poorly-branched network (Figs. 4.18c and 4.18d). *Thalassinoides* traces appear in the Lagoa Parda cores mostly as well-defined sub-circular burrows (Figs. 4.18c and 4.19a), but some oblique, mottled-appearing zones also have been recognized, which probably represent meniscate, back-filled forms (Fig. 4.18c). Mud-filled, irregularly-shaped *Thalassinoides* (Fig. 4.20a) are also present in LP-F3, but they are very subordinate.

*Ophiomorpha* (including *Ophiomorpha nodosa*) is the most important ichnogenus in the thin-bedded sandstones of facies LP-F3. It comprises horizontal, 1 – 2 cm diameter, sand-filled burrows, with pelleted walls forming external knobby linings (Figs. 4.19a). It seems that the *Ophiomorpha* and *Thalassinoides* traces are part of contemporaneous, open network burrow systems made by the same trace maker, but responding to different substrates. Unlined burrows are produced in more stable, muddy substrates, whereas in sandy substrates the burrows are reinforced with fecal pellets (Fig. 4.19a).

*Planolites* and *Helminthopsis* are common ichnogenera in LP-F3, but almost always subordinate to *Thalassinoides* and *Ophiomorpha*. The ichnogenus *Planolites* is characterized by unbranched, 3 – 5 mm diameter, sand-filled tubes (Figs. 4.18 and 4.20a). Tiny, dark fills of the ichnogenus *Helminthopsis*

may be concentrated in some thin (< 10 cm) muddy beds (Fig. 4.20b).

Much less common traces are *Palaeophycus* (Figs. 4.18a and 4.20a), *Asterosoma* (Fig. 4.20a), *Skolithos*, *Cylindrichnus* (Fig. 4.18a), *Chondrites*? (Fig. 4.20a), *Zoophycos*? (Fig. 4.18c), and *Anconichnus*?.

LP-F3 mudstones are mainly dark gray, but the siltier or more bioturbated deposits contain more calcite and are paler in colour. The mineralogical composition of the mudstones, expressed in terms of major components, is presented in tables 4.1 and 4.2. The variations in the contents of clay minerals (all types together), quartz, K-feldspar, and plagioclase are primarily a function of texture and bioturbation. Siltier or more bioturbated mudstones (particularly those bioturbated by *Thalassinoides-* and *Planolites*-makers) tend to be poorer in clay minerals and richer in quartz and feldspars. Coarser-grained mudstones also have a kaolinite content slightly higher than finer-grained mudstones. The calcite content in the LP-F3 mudstones is typically less than 5 %. Thin (< 5 cm), reddish-brown concretion horizons containing siderite, rhodochrosite, and pyrite are common, and eventually they can be correlated for large portions of the Lagoa Parda field. These concretion horizons occur typically in mudstones colonized by *Helminthopsis* (e.g. Fig. 4.19b).

**Interpretation:**

LP-F3 thin-bedded sandstones were probably deposited by low-density turbidity currents (Lowe, 1982), where slow deceleration permitted the transfer of sediment from suspended to bed load, followed by traction sedimentation of the Bouma $T_b$ (parallel-laminated) and $T_c$ (ripple cross-laminated) divisions (Walker, 1965).

**Table 4.1 - Mineralogical composition of the mudstones of the facies LP-F3[a].**

| Major components | Distribution range (%) | Average (%) |
|---|---|---|
| Clay minerals | 20 - 65 | 46 |
| Quartz | 20 - 40 | 27 |
| K-Feldspar | 0 - 10 | 6 |
| Plagioclase | 10 - 25 | 14 |

[a] Based on 9 X-ray diffraction analyses. Source: Anjos et al. (1991).

**Table 4.2 - Clay mineralogy of the mudstones of the facies LP-F3[a].**

| Major components | Distribution range (%) | Average (%) |
|---|---|---|
| Illite/smectite interlayerings[b] | 40 - 50 | 45 |
| Illite | 30 - 45 | 36 |
| Kaolinite | 15 - 30 | 19 |

[a] Based on 9 X-ray diffraction analyses. Source: Anjos et al. (1991).
[b] Disordered interlayerings, with illite content of 45-60 %.

The common occurrence of climbing ripples in LP-F3 suggest high rates of deposition from suspension during rippling (Walker, 1985). Also, the common development of convolute lamination may be related to the rapid accumulation of sediments with low strength, thus more susceptible to convolution by shear from turbidity currents (Walker, 1985).

LP-F3 contains thin (< 50 cm) horizons of contorted mudstones, surrounded by undisturbed mudstones, which may have originated as slumps. LP-F3 also includes thin (< 50 cm) intraformational conglomerates composed of contorted, cobble-to granule-sized mud intraclasts ramdonly dispersed in a poorly-sorted muddy and sandy matrix. These conglomerates probably were deposited from debris flows, where the strength and buoyancy of the matrix would have supported the larger clasts during a mostly laminar flow, with very little fluid mixing (Middleton and Hampton, 1973).

Closely-spaced well control and detailed correlations show that facies LP-F3 may comprise channel fills (e.g. channel fills 34 and 35 in Fig. 4.11), but it mostly builds levees related to LP-F1 and LP-F2 channel fills (Fig. 4.11). LP-F3 geometry is detailed in section 4.4 (High-resolution stratigraphy and reservoir geometry). The interpretation of LP-F3 mainly as levee deposits is also supported by the description in cores of: (1) facies recording original depositional slopes; (2) finer-grained, thin-bedded sandstones rapidly deposited by low-density turbidity currents; and (3)

slump and debris flow deposits. Slumps and debris flows were probably triggered by gravitational instability on the slopes of the levees.

The trace fauna recognized in LP-F3 is relatively diverse and abundant, but is dominated by horizontal to slightly inclined, poorly-branched networks of *Thalassinoides* and *Ophiomorpha*. The ichnogenus *Thalassinoides* may dominate shelf and nearshore sediments, but also can be found in deeper depositional settings (Bromley, 1990). The major paleoenvironmental significance of *Thalassinoides* and *Planolites* (a subordinate, but common ichnogenus in LP-F3) is probably their preferential development on well-oxygenated seafloors (Savrda and Bottjer, 1986; Bromley, 1990). The oxygen-rich environment suggested by the LP-F3 ichnofauna agrees with the low organic carbon content (1 - 2 % by weight), the poor preservation of organic matter produced by marine phytoplankton (Estrella et al., 1984), and the abundant and diversified benthic foraminifera (Azevedo, 1985) found in Lagoa Parda mudstones. However, the common ocurrence of *Helminthopsis* associated with horizons rich in siderite, rhodochrosite, and pyrite suggest at least localized variation in the oxygen content in sea bottom and interstitial waters. *Helminthopsis* has been related to poorly-oxygenated settings (Savrda and Bottjer, 1986; Ekdale and Mason, 1988), and the origin of siderite, rhodochrosite, and pyrite is related to the degradation of organic matter by sulphate-reducing

bacteria in suboxic zones (Coleman, 1985; Curtis, 1987).

*Ophiomorpha* has been described in different types of sediments, including turbidites, and also fluvial, beach/ intertidal sandflat, and shallow subtidal deposits (Ekdale, 1988). The environmental parameter common to all of these occurrences is texture and stability of the substrate; *Ophiomorpha* is developed almost always in unstable, clean sand, deposited in hydrodynamically energetic environments (Ekdale, 1988; Bromley, 1990). Pelleted *Ophiomorpha* and non-pelleted *Thalassinoides* burrow systems seem to be interconnected and genetically related with each other in the Lagoa Parda turbidite system, as also observed in other turbidite successions composed of interbedded sandstones and mudstones (e.g. Kern and Warme, 1974). Both ichnogenera were probably made by the same organism, but responding to different substrates; reinforced *Ophiomorpha* burrows are produced in more unstable, sandy substrates, and smooth-walled *Thalassinoides* colonize stable, muddy substrates (Fig. 4.19a).

## 4.3.4. Facies LP-F4: Interbedded stratified sandstones and intraclastic conglomerates

**Description:**

LP-F4 comprises interbedded parallel- to ripple cross-laminated, fine- to very fine-grained sandstones (50 %), mudstones (40 %), and thin (< 20 cm), intraclastic

conglomerates (10 %) (Fig. 4.21). The absence of unstratified, coarse-grained sandstones, and the greater thickness of the stratified sandstone beds differentiate LP-F4 from LP-F2 and LP-F3, respectively. LP-F4 comprises successions up to 20 m thick, which may represent an upward or lateral gradation from LP-F2, and also may grade upward to LP-F3.

LP-F4 sandstone beds are typically 0.2 to 1.0 m thick. Most of beds are composed of amalgamated $T_{bc}$, $T_b$, and $T_c$ beds (Bouma, 1962). Climbing ripples and soft-sediment deformation (Fig. 4.22a) are common features in the LP-F4 sandstones. Their stratification is well-defined by the high content of carbonaceous plant fragments, mica, and sand-sized mud intraclasts, as observed for the LP-F3 sandstones. The average framework composition, and diagenetic mineralogy of LP-F4 sandstones are very similar to those of the stratified sandstones in LP-F2, and the thin-bedded sandstones of LP-F3 (Bagnoli, 1984).

Extensive bioturbation is recorded in LP-F4, particularly in the mudstones (Fig. 4.21). The trace fossil assemblage is the same as in LP-F3, and consists mainly of the ichnogenera *Thalassinoides*, *Ophiomorpha*, *Planolites*, and *Helminthopsis*, with very subordinate *Palaeophycus*, *Asterosoma*, *Skolithos*, *Cylindrichnus*, *Chondrites?*, *Zoophycos?*, and *Anconichnus?*. A more detailed characterization of these trace fossils is presented in the description and interpretation of the facies LP-F3.

Fig. 4.21 - **FACIES LP-F4:** Interbedded parallel- to ripple cross-laminated, fine- to very fine-grained sandstones, bioturbated mudstones, and intraclastic conglomerates (**ic**). Bioturbation is pervasive, particularly in the mudstones. Trace fossil assemblage is largely dominated by *Thalassinoides*, followed by *Ophiomorpha* (in the sandstones), *Planolites*, and *Helminthopsis*. Channel fill 33; well LP-10; depth: 1,547.0 - 1,553.8 m.

TOP

BASE

ic

1 m
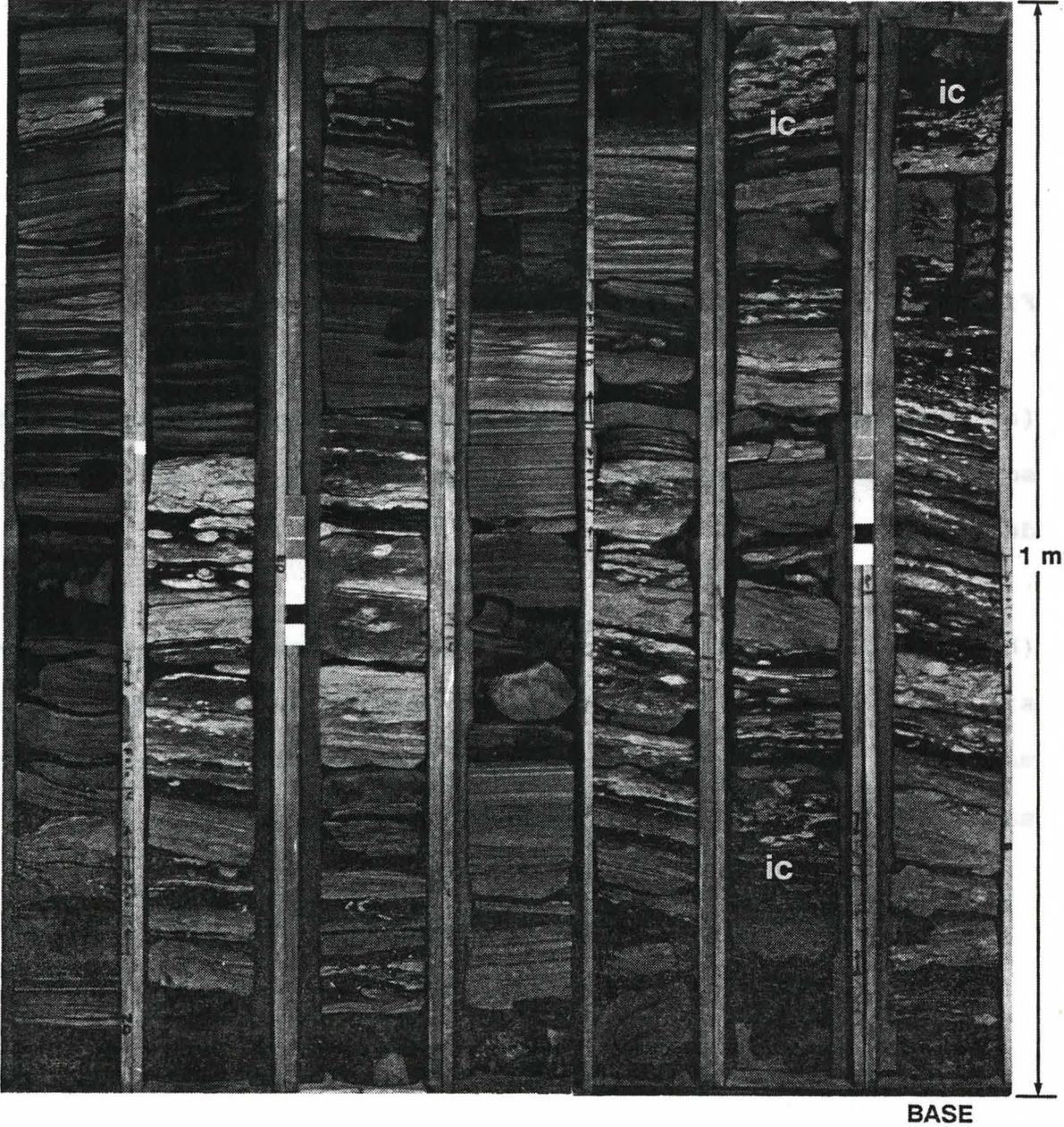
Fig. 4.22 - **FACIES LP-F4:**


(a) Fine-grained sandstone showing contorted lamination, and squeezed mud intraclasts (i). Channel fill 33; well LP-10; depth: 1,547.6 m.


(b) Intraclastic conglomerate containing pebble- to granule-sized mud intraclasts (burrowed by *Thalassinoides*; **Th**), and a matrix of calcite-cemented, very coarse- to coarse-grained sand. Channel fill 33; well LP-10; depth: 1,553.1 m.
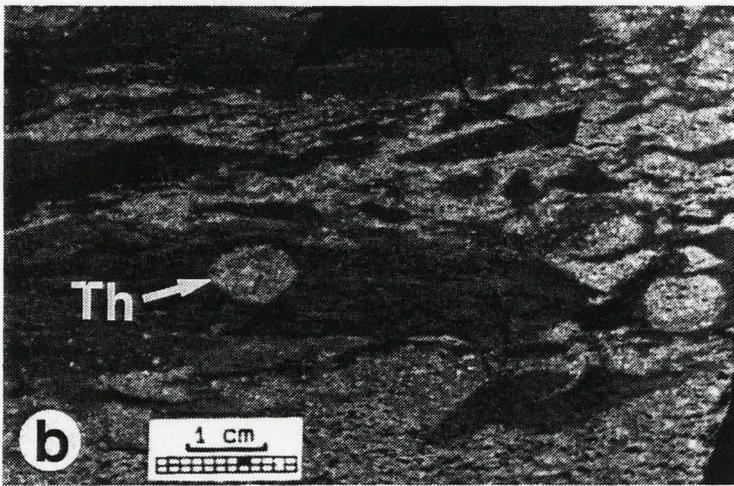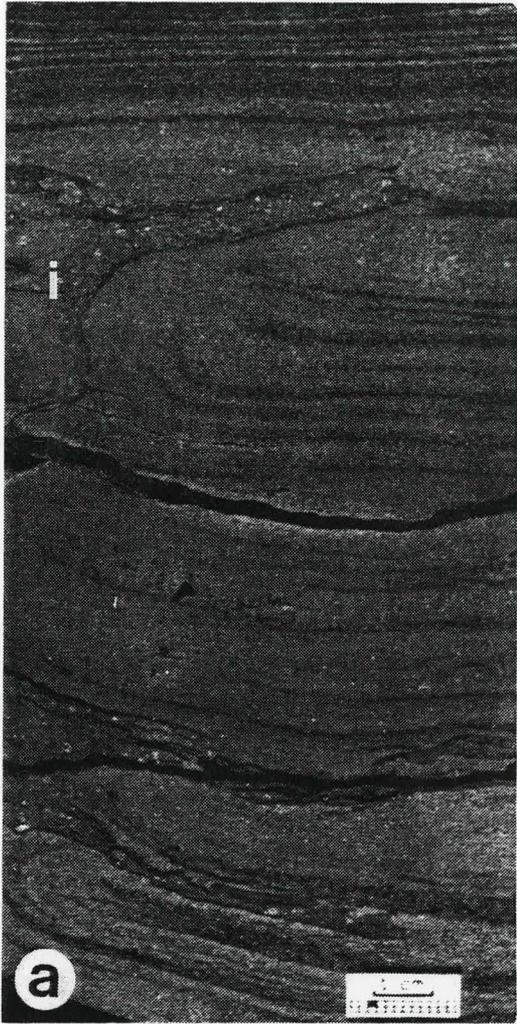
LP-F4 intraclastic conglomerates are composed of mostly angular, cobble- to granule-sized mud intraclasts, and a matrix of very coarse- to coarse-grained sand (Fig. 4.22b). They present sharp lower and upper contacts, both with sandstones and mudstones.

**Interpretation:**

LP-F4 stratified sandstones show the same sedimentary structures as the LP-F3 sandstones, and possibly were produced by similar depositional processes; i.e. low-density turbidity currents (Lowe, 1982). However, LP-F4 stratified sandstones are typically thicker than LP-F3 sandstones (compare Figs. 4.15 and 4.21), and also are restricted to channel fills (e.g. channel fill 27 in Fig. 4.11). Thus, LP-F4 sandstones may represent the passive filling of (at least temporarily) abandoned channels by sediments spilled out from adjacent, active channels; in this context, the thicker stratified sandstones would have been produced by high rates of sedimentation in more confined depositional sites. An alternative hypothesis for the origin of LP-F4 sandstones would consider them as distal equivalents for the facies LP-F2. In both situations, the thin (<20 cm), intraclastic conglomerates of LP-F4 (Fig. 4.22b) would represent lag deposits produced by mainly erosive turbidity currents that episodically bypassed the Lagoa Parda channels and deposited their load farther downstream.

## 4.3.5. Facies LP-F5: mudstones

**Description:**

    LP-F5 comprises a monotonous succession of dark gray mudstones, which may include few thin-bedded (< 10 cm), parallel-stratified to rippled, very fine-grained sandstones, and also thin (< 5 cm), reddish-brown concretion horizons containing siderite, rhodochrosite, and pyrite. Some concretion horizons can be correlated over large parts of the Lagoa Parda field (e.g. markers α, β, γ, and δ; Fig. 4.11). Bioturbation is reduced in LP-F5 in comparison with LP-F3. It comprises mainly *Helminthopsis*, followed by *Thalassinoides* and *Planolites*. A more detailed characterization of these trace fossils is presented in the description and interpretation of the facies LP-F3.

**Interpretation:**

    Facies LP-F5 documents the sedimentary processes operating in the Regência canyon during most of the early Eocene. These mostly fine-grained rocks suggest sedimentation in a relatively quiet environment, with these conditions being episodically disturbed by high- to low-density turbidity currents capable of deeply eroding the canyon substrate and depositing coarser-grained sediments. LP-F5 mudstones contain a benthic foraminifera fauna typical of deep neritic to upper bathyal (200 - 500 m) depositional settings (Azevedo, 1985).

## 4.3.6. Well log response

The facies described in the Lagoa Parda turbidite system each have typical well log responses, particularly in the gamma-ray, spontaneous potential, resistivity, and density logs. These responses can be characterized by the distribution of absolute values (Table 4.3) or by log patterns. The recognition of well log responses permitted the mapping of different facies in areas of the Lagoa Parda field lacking core control.

The conglomerates and sandstones of facies LP-F1 show rather uniform values in the spontaneous potential and gamma-ray logs, defining a typical boxy log pattern (Figs. 4.6 and 4.7). However, larger concentrations of mud intraclasts may induce significant positive deflections in the spontaneous potential logs, or higher radioactivity values in the gamma-ray logs (Figs. 4.6 and 4.7). LP-F1 rocks show resistivities varying mostly between 1 and 2 $\Omega$.m, but conglomerates rich in boulders to pebbles of quartzo-feldspathic metamorphic rocks have resistivities greater than 2 $\Omega$.m, eventually as high as 20 $\Omega$.m. Density logs for LP-F1 indicate textural and compositional variations; coarser-grained and poorer-sorted rocks with a higher content of quartzo-feldspathic rock fragments and mud intraclasts show higher densities (Table 4.3).

**Table 4.3 - Typical well log radioactivity, spontaneous potential, resistivity and density readings for the facies defined in the Lagoa Parda turbidite system.**

| FACIES | RADIOACTIVITY (API) | SPONTANEOUS POTENTIAL[a] (mV) | RESISTIVITY ($\Omega$.m) | DENSITY (g/cm$^3$) |
|---|---|---|---|---|
| LP-F1 | 60 - 100 | -45 - -5 | 1 - 20 | 2.15 - 2.60 |
| ECgl[b] | 60 - 80 | -40 - -5 | 4 - 20 | 2.35 - 2.60 |
| ICgl[b] | 80 - 100 | -40 - -5 | 1 - 2 | 2.35 - 2.60 |
| USds[b] | 60 - 70 | -45 - -30 | 1 - 2 | 2.15 - 2.35 |
| LP-F2 | 60 - 110 | -30 - -5 | 1 - 2 | 2.15 - 2.35 |
| USds[b] | 60 - 70 | -30 - -20 | 1 - 2 | 2.15 - 2.35 |
| SSds[b] | 80 - 110 | -20 - -5 | 1 - 2 | 2.25 - 2.35 |
| LP-F3 | 100 - 130 | -5 - +15 | 2 - 6 | 2.25 - 2.40 |
| LP-F4 | 80 - 120 | -20 - -5 | 2 - 6 | 2.25 - 2.40 |
| LP-F5 | 120 - 130 | +10 - +20 | < 2 | 2.35 - 2.40 |

[a] Absolute readings in spontaneous potential logs are largely a function of the electrical properties of the drilling fluid, which may vary in different wells of the Lagoa Parda field. The values presented refer only to the well LP-33.

[b] ECgl = exogenic (quartzo-feldspathic, metamorphic rock fragments) conglomerates; ICgl = intraformational (mud intraclasts) conglomerates; USds = unstratified sandstones and conglomeratic sandstones; SSds = stratified sandstones with high content of carbonaceous plant fragments, mica flakes, and mud intraclasts.

LP-F2 can be differentiated from LP-F1 mostly by its serrated pattern in radioactivity and spontaneous potential logs (Fig. 4.6). LP-F2 shows higher radioactivities than LP-

F1, particularly the stratified sandstones, due to the higher contents of carbonaceous plant fragments, micas, and mud intraclasts (Fig. 4.6). The lower permeability of the finer-grained, stratified sandstones induces larger values (positive deflections) in the LP-F2 spontaneous potential logs, which also support its separation from LP-F1.

LP-F3 and LP-F4 are characterized by serrated patterns in radioactivity, spontaneous potential, and resistivity logs, due to the common interbedding of thin-bedded sandstones and mudstones. LP-F3 and LP-F4 sandstones induce a few spikes of lower radioactivity or lower spontaneous potential in well logs; these well log signatures are related to sandstones thicker than 50 cm, which are more common in facies LP-F4. LP-F3 and LP-F4 mudstones may contain thin (< 5 cm) concretion horizons of siderite, rhodochrosite, and pyrite, which have resistivity values ranging between 2 and 4 $\Omega$.m.

LP-F5 is differentiated from LP-F3 and LP-F4 by its higher radioactivies and lower resistivities. LP-F5 also displays very uniform radioactivity, spontaneous potential, and resistivity readings, which eventually are disturbed by higher resistivity (> 2 $\Omega$.m) spikes induced by concretion horizons (siderite, rhodochrosite, and pyrite) or few thin-bedded (<10 cm) sandstones.

## 4.3.7. Reservoir properties

LP-F1, LP-F2, and LP-F4 contain the oil-producing rocks in the Lagoa Parda field. Table 4.4 shows the porosity and permeability distribution of the different reservoir rocks. LP-F3 sandstones show porosities and permeabilities similar to those presented by LP-F2 stratified sandstones and LP-F4 sandstones (Table 4.4); however, they do not comprise oil-producing horizons because of their small thickness.

Calcite cement can significantly reduce the porosity and permeability of the Lagoa Parda reservoirs. In horizons intensely cemented by calcite the porosity and permeability are less than 10 % and 3 mD, respectively. However, calcite-rich horizons have a relatively restricted occurrence in the Lagoa Parda turbidite succession, with the variations in the porosity and permeability of the reservoirs being primarily controlled by the content of mud intraclasts, carbonaceous plant fragments, and micas, and by textural parameters.

High contents of mud intraclasts (commonly squeezed, forming compaction matrix), carbonaceous plant fragments, and micas may largely reduce the permeability (especially vertical permeability) of LP-F1 intraformational conglomerates, LP-F2 stratified sandstones, and LP-F3 and LP-F4 thinner-bedded sandstones (Table 4.4). In the case of the intraformational conglomerates, a higher content of mud intraclasts may also significantly reduce their porosity.

**Table 4.4 – Porosity and permeability characterization of the Lagoa Parda field reservoirs[a].**

| FACIES | DISTRIBUTION RANGE (AVERAGE)[b] | |
| --- | --- | --- |
| | POROSITY (%) | PERMEABILITY (mD) |
| LP-F1 | | |
| Exogenic conglomerates | 16 – 24 (21) | 100 – 500 (242) |
| Intraformational conglomerates | 16 – 24 (20) | 1 – 100 (17) |
| Unstratified sandstones[c] | 21 – 30 (25) | 200 – 600 (427) |
| LP-F2 | | |
| Unstratified sandstones[d] | 21 – 30 (25) | 100 – 500 (290) |
| Stratified sandstones | 17 – 28 (23) | 10 – 200 (84) |
| LP-F3 | 16 – 26 (23) | 10 – 200 (72) |
| LP-F4 | 17 – 26 (24) | 10 – 200 (79) |
| Calcite-rich rocks[e] | 6 – 10 (8) | < 3 (0.6) |

[a] Based on 347 measurements of porosity and permeability in rock plugs collected from cores at an average distance of 30 to 40 cm. Source: PETROBRÁS.

[b] Arithmetic mean for porosity, and geometric mean for permeability.

[c] Mostly very coarse-grained sandstones.

[d] Mostly coarse-grained sandstones.

[e] All facies, but with a calcite cement content > 10 %.

Better sorting favours higher porosities, as shown by the unstratified sandstones of facies LP-F1 and LP-F2 (Table 4.4). Coarser-grained facies (exogenic conglomerates and conglomeratic sandstones) tend to have larger pore throats, which favour higher permeabilities (Table 4.4). The combination of sorting and grain-size in the unstratified, mostly very coarse-grained sandstones of facies LP-F1 makes them the best reservoirs of the Lagoa Parda field, followed by the unstratified, mostly coarse-grained sandstones of facies LP-F2 (Table 4.4).

Cores of conglomerates and coarse-grained sandstones are commonly friable (e.g. Figs. 4.9 and 4.12), because of their high porosities and permeabilities, mostly low cement content, and little mechanical and chemical compaction (their burial depth never exceeded 2,000 m; Cosmo et al., 1991).


## 4.4. HIGH-RESOLUTION STRATIGRAPHY AND RESERVOIR GEOMETRY


### 4.4.1. Geological cross sections and basis for correlation

The detailed stratigraphic analysis and the geometrical characterization of the Lagoa Parda turbidites were largely based on 16 geological sections, which include all of the wells drilled in the field (Fig. 4.5). The datum for the sections is a high-resistivity mudstone horizon, containing

concretions of siderite, rhodochrosite, and pyrite (Fig. 4.19b). This datum overlies the studied turbidites, and is subparallel to the contact between two early Eocene calcareous nannofossil zones, respectively *Neochiastozygus chiastus* (older) and *Tribrachiatus orthostylus* (younger) (Figs. 4.11, 4.23, and 4.24). The sections permit detailed correlations within the uppermost 230 m of the *Neochiastozygus chiastus* zone, which is up to 650 m thick (Figs. 4.2, 4.11, 4.23 and 4.24).

Spontaneous potential and resistivity well logs were used to construct the sections. Spontaneous potential logs are particularly efficient in the separation of facies LP-F1 from facies LP-F2, and also in the separation of sandstone-rich facies (LP-F1 and LP-F2) from mudstone-rich facies (LP-F3, LP-F4, and LP-F5). Resistivity logs permit separation of facies LP-F3, LP-F4, and LP-F5, and also the mapping of different successions of rocks composed of facies LP-F3 and LP-F5. In a few wells, poorer-quality spontaneous potential logs were replaced by radioactivity logs. Four sections are reproduced in figures 4.23 and 4.24, which illustrate the detailed stratigraphic relationships and geometry of the Lagoa Parda turbidite reservoirs. In all of these sections the vertical and horizontal scales are the same.

## 4.4.2. Characterization of individual channel fills

Fig. 4.23 - Geological cross sections of the Lagoa Parda turbidite system (channel complexes LP-CC1 to LP-CC3). Datum is a high-resistivity mudstone enriched in siderite, rhodochrosite, and/or pyrite, which is subparallel to the contact between the zones *Neochiastozygus chiastus* and *Tribrachiatus orthostylus*. Thicker lines indicate boundaries of individual channel fills. High resistivity well log markers α, β, γ, and δ are subparallel to the datum. Spontaneous potential and resistivity well logs were used to construct the sections. A resistivity curve in amplified scale is provided for the uppermost, mud-rich successions (levee successions A to I). Arrows indicate trends of resistivity variations. Vertical and horizontal scales are the same. Location of sections is shown in figure 4.5.

(a) Section showing the southwesternmost terminations of LP-CC1 and LP-CC2, and the thick mud-rich succession that separates LP-CC2 from LP-CC1 along most of Lagoa Parda field. Section provides a mostly longitudinal view of levee successions A to I.

(b) Typical cross section of the central part of Lagoa Parda field, which shows the entire width of LP-CC1, and most of the lateral extent of LP-CC2 and LP-CC3. Section also illustrates deep channel incision and the uppermost mostly mud-filled channels of LP-CC2 (34 and 35). Note also the tendency of LP-CC3 levee successions (G to I) to smooth the topography inherited from LP-CC2 levee successions (A to F).

Fig. 4.23a

Fig. 4.23b

CHANNEL COMPLEXES:

LP-CC1: Channel fills ① to ⑫

LP-CC2: Channel fills ⑬ to ㉟
Levee successions Ⓐ to Ⓕ

LP-CC3: Channel fills ㊱ to ㊳
Levee successions Ⓖ to Ⓘ

DOMINANT FACIES:

LP-F1
LP-F2
LP-F4
LP-F5

LP-F3 (Channel fills)
LP-F3 (LP-CC2 levees)
LP-F3 (LP-CC3 levees)

BRUHN (1993)

234

Fig. 4.24 - Geological cross sections of the Lagoa Parda turbidite system (channel complexes LP-CC1 to LP-CC3). Datum is a high-resistivity mudstone enriched in siderite, rhodochrocite, and/or pyrite, which is subparallel to the contact between the zones *Neochiastozygus chiastus* and *Tribrachiatus orthostylus*. Thicker lines indicate boundaries of individual channel fills. High resistivity well log markers α, β, γ, and δ are subparallel to the datum. Spontaneous potential and resistivity well logs were used to construct the sections. A resistivity curve in amplified scale is provided for the uppermost, mud-rich successions (levee successions A to I). Arrows indicate trends of resistivity variations. Vertical and horizontal scales are the same. Location of sections is shown in figure 4.5.

(a) Section showing the maximum lateral extent of LP-CC3; it provides a transverse view of LP-CC3 levee successions (G to I), and a mostly longitudinal view of LP-CC2 levee successions (A to F).

(b) Section illustrates levee asymmetry (higher and thicker levee successions on the left side (looking downstream) of associated channels) in LP-CC2, and also a possibly related average trend of channel avulsion to the right (channel fills 28 to 33). Note also the tendency of LP-CC3 levee successions (G to I) to smooth the topography inherited from LP-CC2 levee successions (A to F). This section also shows deeper incision of lowermost LP-CC2 channels into the uppermost LP-CC1 channel fills; this situation is typical of the northeastern part of Lagoa Parda field.
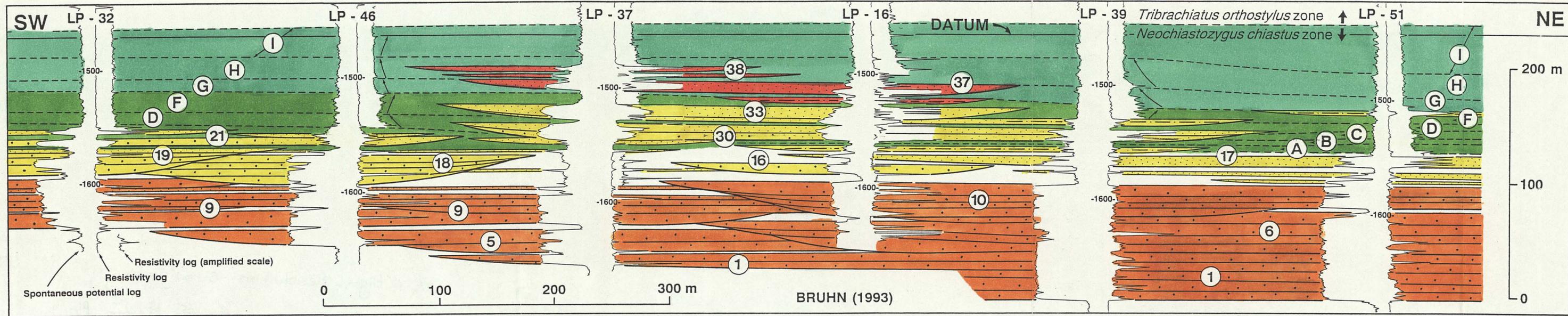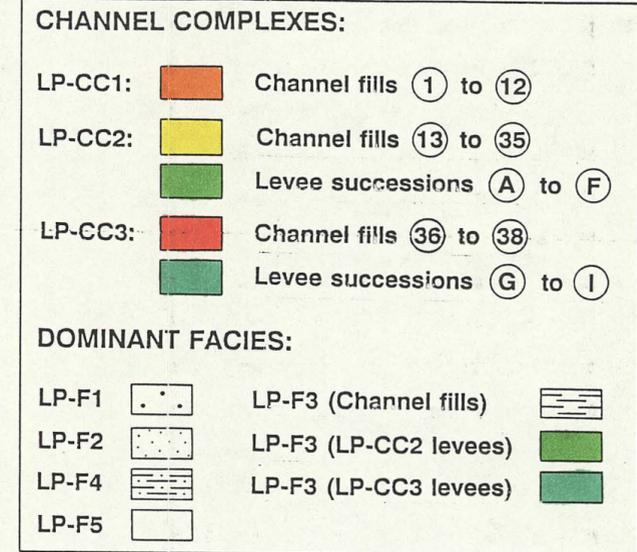
**Fig. 4.24a**

**Fig. 4.24b**
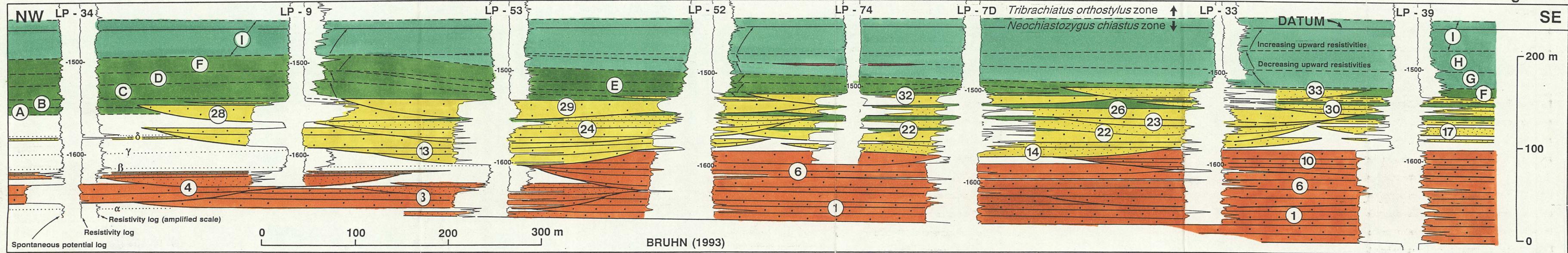
235

Lagoa Parda reservoir rocks (facies LP-F1, LP-F2, and LP-F4) were deposited in channels, which were deeply incised into mudstone-rich successions (LP-F3 and LP-F5) or older channel fills (Figs. 4.23 and 4.24). **At least** 38 major channel fills can be recognized in the study area (numbered 1 to 38, from the oldest to the youngest; Table 4.5).

The separation and mapping of individual channel fills (Figs. 4.25 to 4.35) is easier in cases where coarser-grained turbidites (LP-F1, LP-F2, and LP-F4) are laterally and vertically bounded by mud-rich facies (LP-F3 and LP-F5) along most of their extent. This situation is exemplified by channel fills 9, 18, and 33 in figure 4.23b, and channel fills 30, 33, 37, and 38 in figure 4.24a. However, coarse-grained channel fills may occur partially amalgamated in many places; thus, their separation may be more difficult, eventually involving three-dimensional correlations along the dense grid of cross sections constructed for the study area (Fig. 4.5). The most important criteria for the differentiation and mapping of amalgamated channel fills include: (1) diverse sand body orientations; (2) abrupt facies changes; and (3) different stratigraphic positions of their uppermost sediments. These three criteria, **almost always used in combination**, are described below with examples.

**(1) Diverse sand body orientations:** Channel fills 1 and 3 are characterized by similar well log responses, and seem to be the same in figures 4.23b and 4.24b; however, the net sand

**Table 4.5 - Channel fills of the Lagoa Parda turbidite system.**

| CHANNEL FILL | MAXIMUM THICKNESS (m) | MAXIMUM WIDTH (m) | SAND BODY ORIENTATION (azimuth) | DOMINANT FACIES |
|---|---|---|---|---|
| **CHANNEL COMPLEX LP-CC3** | | | | |
| 38 | 13 | 230 | 128° | LP-F2 |
| 37 | 14 | 270 | 110° | LP-F2 |
| 36 | 15 | 280 | 134° | LP-F2 |
| **CHANNEL COMPLEX LP-CC2** | | | | |
| 35 | 28 | 210 | 093° | LP-F3 |
| 34 | 25 | 220 | 106° | LP-F3 |
| 33 | 16 | 430 | 090° | LP-F2 |
| 32 | 23 | 250 | 098° | LP-F2 |
| 31 | 9 | 240 | 100° | LP-F2 |
| 30 | 17 | 560 | 118° | LP-F2 |
| 29 | 25 | 400 | 095° | LP-F1/F2 |
| 28 | 20 | 350 | 081° | LP-F1/F2 |
| 27 | 26 | 380 | 040° | LP-F4/F2 |
| 26 | 14 | 440 | 133° | LP-F1/F2 |
| 25 | 15 | 260 | ? | LP-F4 |
| 24 | 26 | 600 | 094° | LP-F1/F2 |
| 23 | 16 | 270 | 083° | LP-F2 |
| 22 | 14 | 470 | 098° | LP-F1/F2 |
| 21 | 15 | >300 | ? | LP-F1/F2 |
| 20 | 13 | 290 | 108° | LP-F2 |
| 19 | 27 | 430 | 148° | LP-F1/F2 |
| 18 | 35 | 450 | 132° | LP-F1/F2 |
| 17 | 9 | 240 | 081° | LP-F2 |
| 16 | 9 | 390 | 080° | LP-F1 |
| 15 | 48 | 600 | 108° | LP-F1/F2 |
| 14 | 26 | 430 | 111° | LP-F1 |
| 13 | 42 | 660 | 112° | LP-F1 |
| **CHANNEL COMPLEX LP-CC1** | | | | |
| 12 | 13 | 840 | 066° | LP-F1 |
| 11 | 40 | 780 | 038° | LP-F1/F2 |
| 10 | 31 | >750 | 126° | LP-F1 |
| 9 | 43 | >750 | 156° | LP-F1/F2 |
| 8 | 21 | 350 | 085° | LP-F1 |
| 7 | 35 | 650 | 030° | LP-F1/F2 |
| 6 | 43 | >1,050 | 110° | LP-F1 |
| 5 | 24 | >580 | 90° | LP-F1 |
| 4 | 36 | 570 | 093° | LP-F1/F2 |
| 3 | >50 | 800 | 041° | LP-F1/F2 |
| 2 | >30 | >300 | ? | LP-F1 |
| 1 | 35 | 870 | 119° | LP-F1 |

maps for these rocks indicate two very different sand body orientations, making an angle of 78° between them (compare Figs. 4.25 and 4.26). It is therefore unlikely that the rocks included in channel fills 1 and 3 were deposited in the same channel. The same criterion is applicable for the differentiation of channel fills 13 and 15 (Figs. 4.23a and 4.29), or between channel fills 9 and 10 (Fig. 4.24a, and Table 4.5).

(2) **Abrupt facies changes:** Channel fill 15 comprises a well-defined fining upward succession, characterized by a bell-shaped well-log pattern (Fig. 4.23b). Channel fill 22 (blocky to cylindrical well log pattern) is thought to truncate channel fill 15, with their separation being suggested in figure 4.23b by an abrupt (lateral) facies change between wells LP-11 and LP-47. Additionally, channel fills 15 and 22 can be differentiated by their distinct sand body orientations (respectively 108° and 98°), as suggested by three-dimensional correlations (compare Figs. 4.29 and 4.30). Other examples of how abrupt (lateral) facies changes can support the separation between amalgamated channel fills are provided by channel fills 3 and 5 (Fig. 4.23b), channel fills 22 and 24 (Figs. 4.24b and 4.30), and channel fills 26 and 29 (Fig. 4.24b).

(3) **Different stratigraphic positions of their uppermost sediments:** This criterion helps the separation, for example, of channel fills 22, 23, and 26 (Fig. 4.23b), channel fills 5

and 6 (Fig. 4.24a), channel fills 28, 29, 32, and 33 (Fig. 4.24b), and channel fills 13 and 22 (Fig. 4.24b). The alternation in stratigraphic level (with respect to the datum) shown by the top of mudstone-bounded packages of coarse-grained facies of channel fills 22, 23, and 26 is well-defined between wells LP-3 and LP-26 (Fig. 4.23b); this suggests relatively abrupt channel abandonment and avulsion. Similar relationships can be also recognized between wells LP-52 and LP-74 (channel fills 13 and 22; Fig. 4.24b).

The individual nature of channel fills 5, 6, 9, and 10 (Fig. 4.24a) is supported not only on different stratigraphic levels of their uppermost sediments, but also on striking lateral facies changes and diverse sand body orientations. For example, very high-resistivity conglomerate horizons of channel fills 6 and 10 (well LP-16; Fig. 4.24a) are laterally associated with lower-resistivity very coarse-grained sandstones of channel fills 5 and 9 (well LP-37). These relationships suggest the truncation of the finer-grained, uppermost sediments of channels 5 and 9 by the coarser-grained, lowermost sediments of channels 6 and 10, respectively. Additionally, channel fills 5 and 6 show diverse sand body orientations, as do channel fills 9 and 10 (Table 4.5).

With respect to the application of the third criterion for defining individual channel fills, it is important to emphasize that the effects of differential compaction are

minimum in the studied succession, as suggested, for example, by the flat (and subparallel to the datum) tops of channel fills 9, 10, 17, 30, 33, 37, and 38 (Fig. 4.24a), and high-resistivity markers α, ß, γ, and δ (Fig. 4.23).

Several phases of cutting and filling (or only filling), can be recognized in many individual channels. For example, channels 9 and 15 record at least 6 and 7 major phases of filling, respectively (Fig. 4.23b). The recognition and correlation of different filling phases in non-cored wells was made possible by: (1) mudstone interbeds; (2) basal high-resistivity (exogenic) gravel-rich horizons (e.g. channels 3 and 9 in Fig. 4.23b); (3) basal positive deflections in the spontaneous potential logs, which are due to concentrations of mud intraclasts (e.g. channel 15 in Fig. 4.23); or (4) positive deflections in the spontaneous potential logs produced by parallel-stratified sandstones placed at the top of filling-phases (e.g. channels 37 and 38 in Fig. 4.23b). The well logs used for correlations in the Lagoa Parda field do not show sufficient resolution to allow differentiation of individual turbidites. Density logs, which permitted the mapping of individual turbidites in the Carapeba/Pargo turbidite system, are not available for all of the Lagoa Parda wells, and even when available, they may not cover the entire studied section. As a result, the mapped filling phases of the Lagoa Parda channels may include one or several individual turbidites.

Most of the individual Lagoa Parda channels were mapped only by their coarser-grained fills (facies LP-F1, LP-F2, and LP-F4), which can be differentiated from levee facies (LP-F3) or background facies (LP-F5) by very distinct well log responses. However, the portions of these channels filled with facies LP-F3 can not be differentiated from non-channelized, laterally associated mud-rich facies, except for a few cases (e.g. channels 34 and 35; Fig. 4.23b). In these two examples, the channel fills show decreasing upward resistivities in well logs, contrasting with the increasing upward resistivities shown by laterally associated levee deposits (Fig. 4.23b); the origin of these two channel fills will be discussed in section 4.5.4.

Net sand maps for 21 channel fills composed of facies LP-F1, LP-F2, and LP-F4 are presented in figures 4.25 to 4.32, and 4.35. Many of these channel fills were partially eroded by younger channels (e.g. Figs. 4.25 to 4.29). In some cases the erosion was minor and localized; therefore, it was possible to reconstruct the channel fill geometry by correlations with adjacent logs (e.g. channel fills 22 and 24; Fig. 4.30).

Figure 4.11 presents the stratigraphic relationships among the most important Lagoa Parda channel fills. This **schematic** cross section was built by the projection of 26 channel fills into a single geological section, at a position and orientation similar to that of figure 4.23b. Figure 4.11 overestimates the sand/mud ratio presented by the Lagoa Parda

Fig. 4.25 - Net sand map for channel fill 1. Average paleoflow orientation (indicated by arrow) is interpreted on the basis of sand body orientation, considering turbidity currents flowing down canyon (eastward).
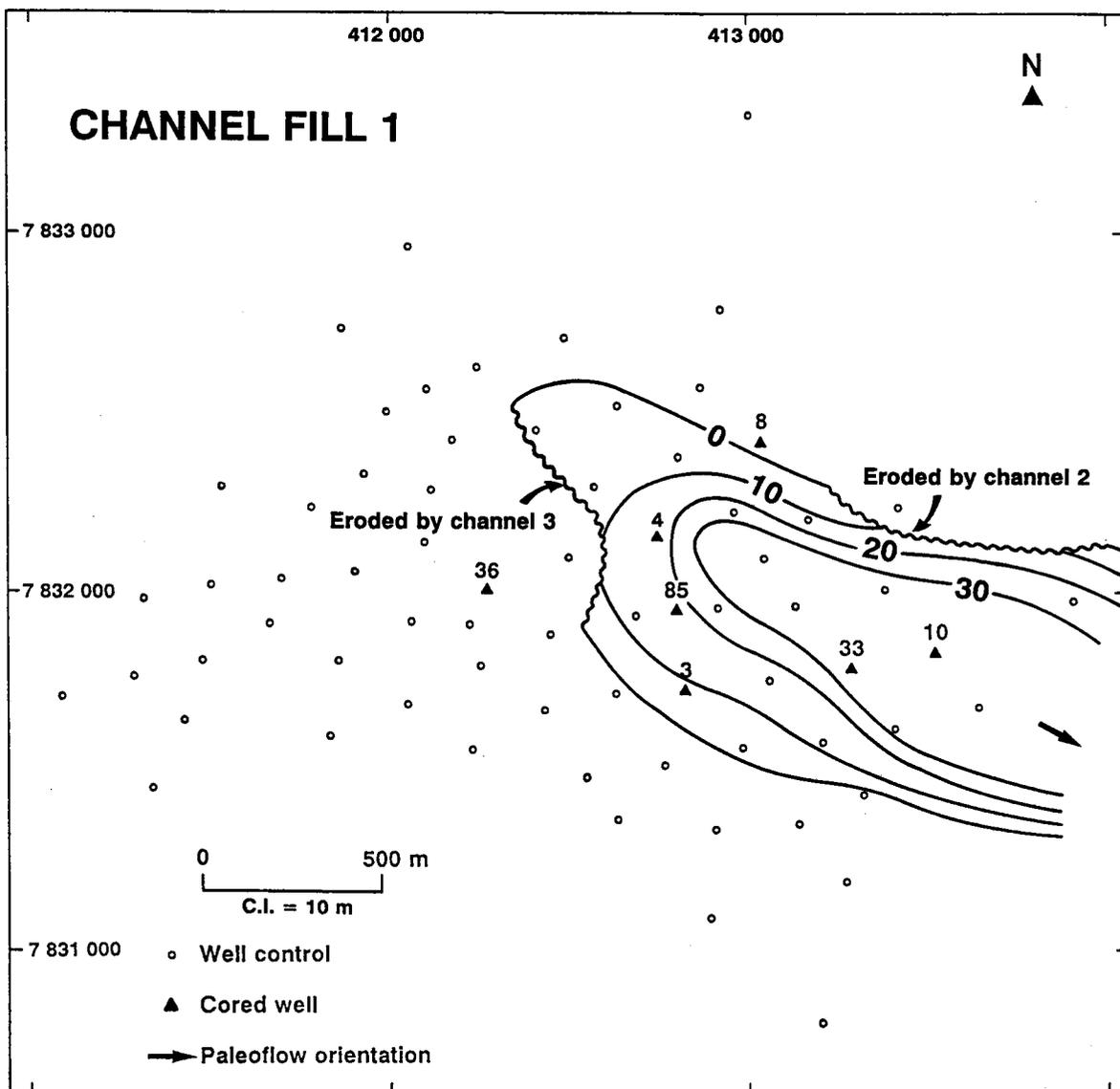
CHANNEL FILL 1

Fig. 4.26 - Net sand map for channel fill 3. Average paleoflow orientation (indicated by arrow) is interpreted on the basis of sand body orientation, considering turbidity currents flowing down canyon (eastward).
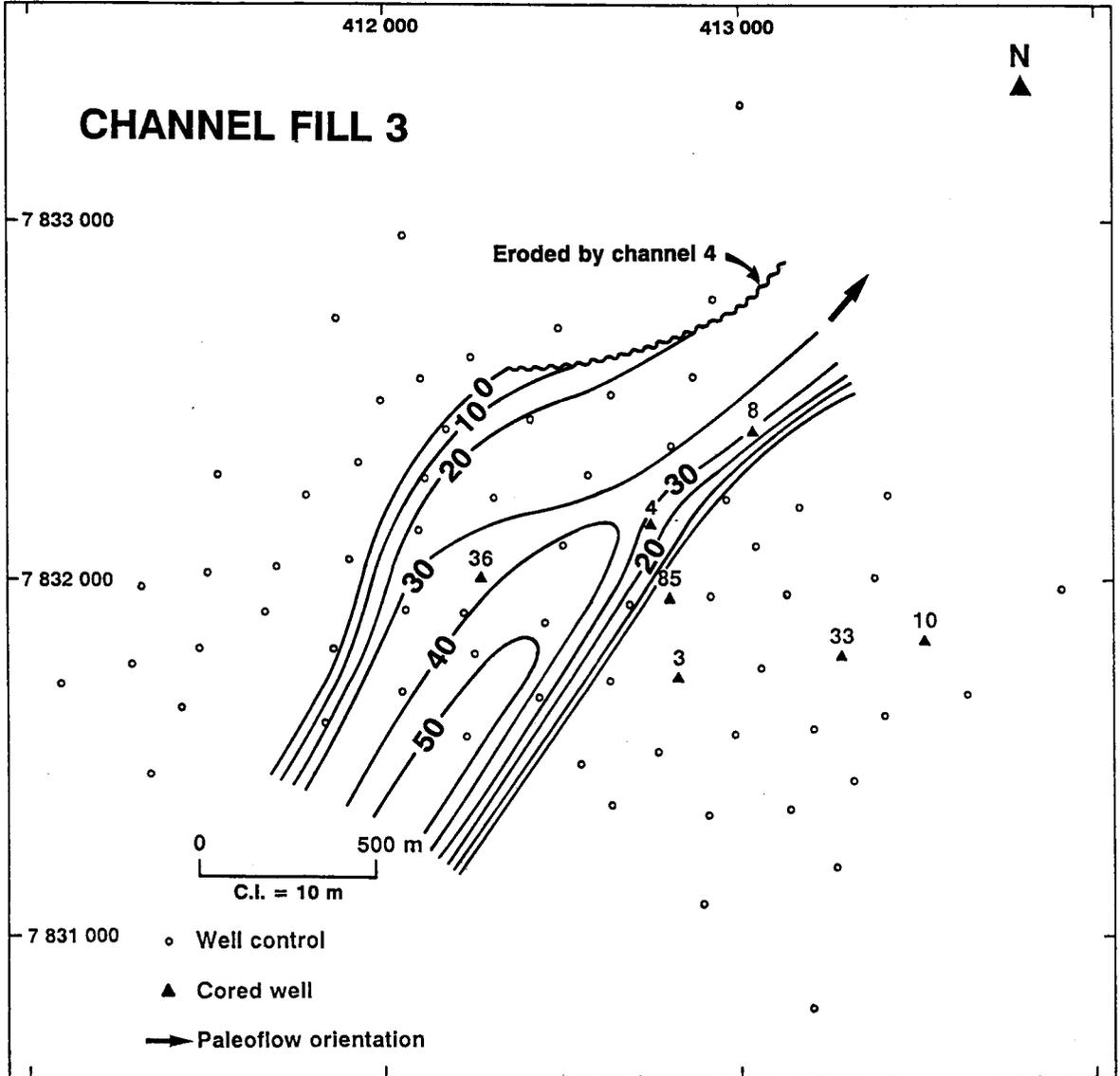
CHANNEL FILL 3

Fig. 4.27 - Net sand maps for channel fills 4, 6, and 7. Average paleoflow orientations (indicated by arrows) are interpreted on the basis of sand body orientations, considering turbidity currents flowing down canyon (eastward).

CHANNEL FILLS 4, 6, AND 7
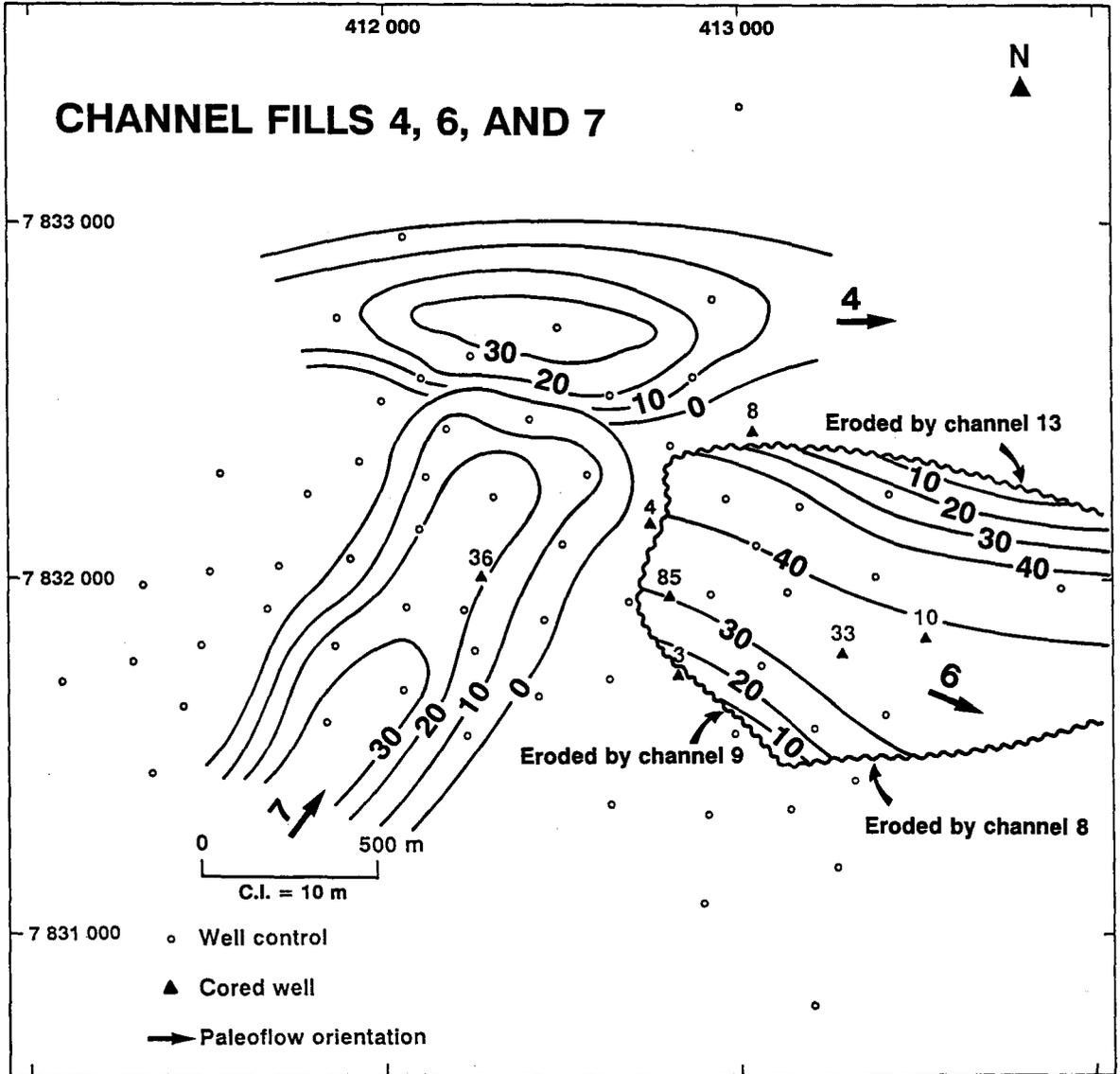
Fig. 4.28 - Net sand maps for channel fills 10 and 11. Average paleoflow orientations (indicated by arrows) are interpreted on the basis of sand body orientations, considering turbidity currents flowing down canyon (eastward).

**CHANNEL FILLS 10 AND 11**

Eroded by channel 13

Eroded by channel 14

C.I. = 10 m

○ Well control

▲ Cored well

→ Paleoflow orientation
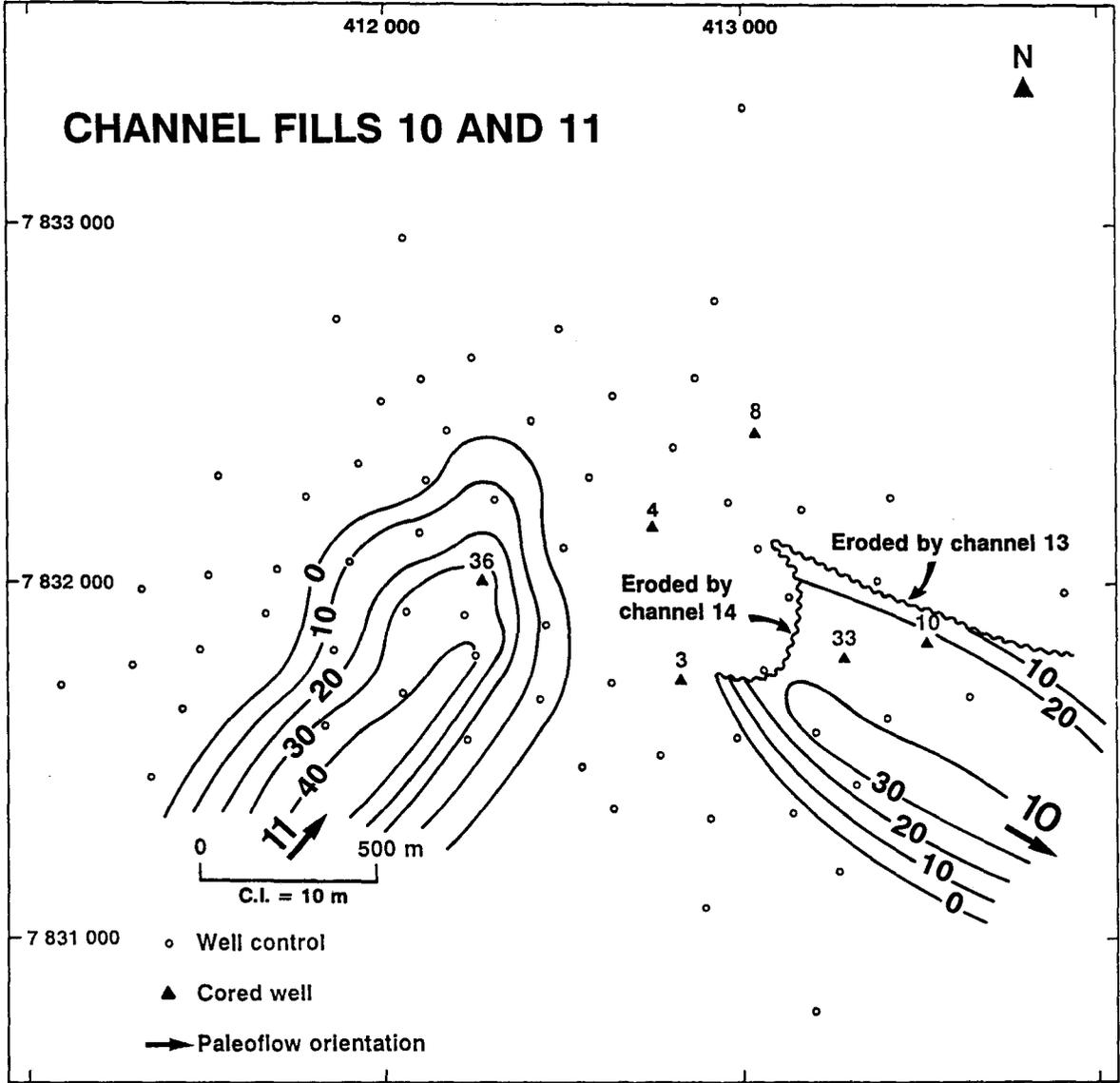
Fig. 4.29 - Net sand maps for channel fills 13, 15, 18, and 19. Average paleoflow orientations (indicated by arrows) are interpreted on the basis of sand body orientations, considering turbidity currents flowing down canyon (eastward).

CHANNEL FILLS 13, 15, 18, AND 19
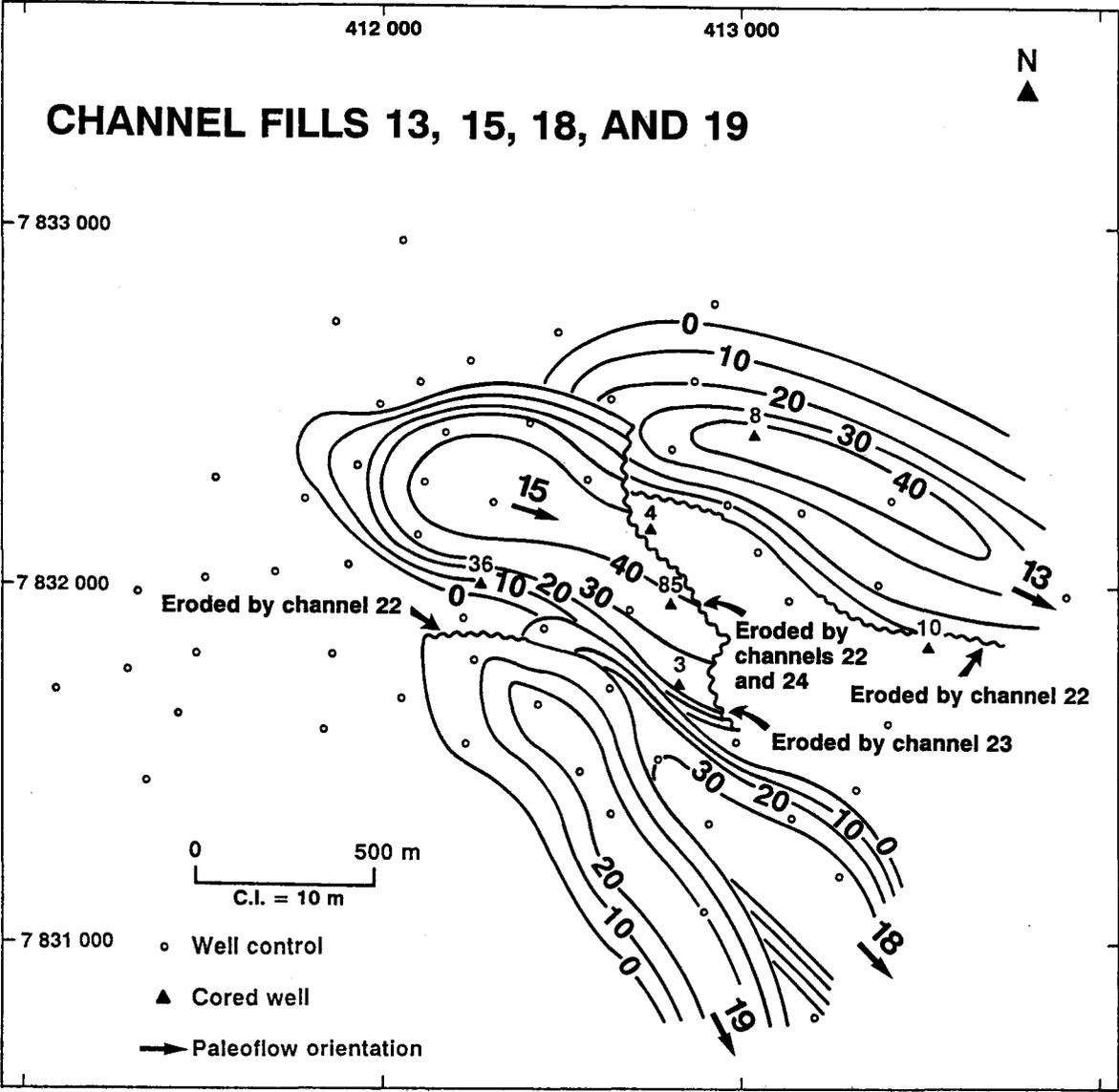
Fig. 4.30 - Net sand maps for channel fills 22 and 24. Average paleoflow orientations (indicated by arrows) are interpreted on the basis of sand body orientations, considering turbidity currents flowing down canyon (eastward).

CHANNEL FILLS 22 AND 24
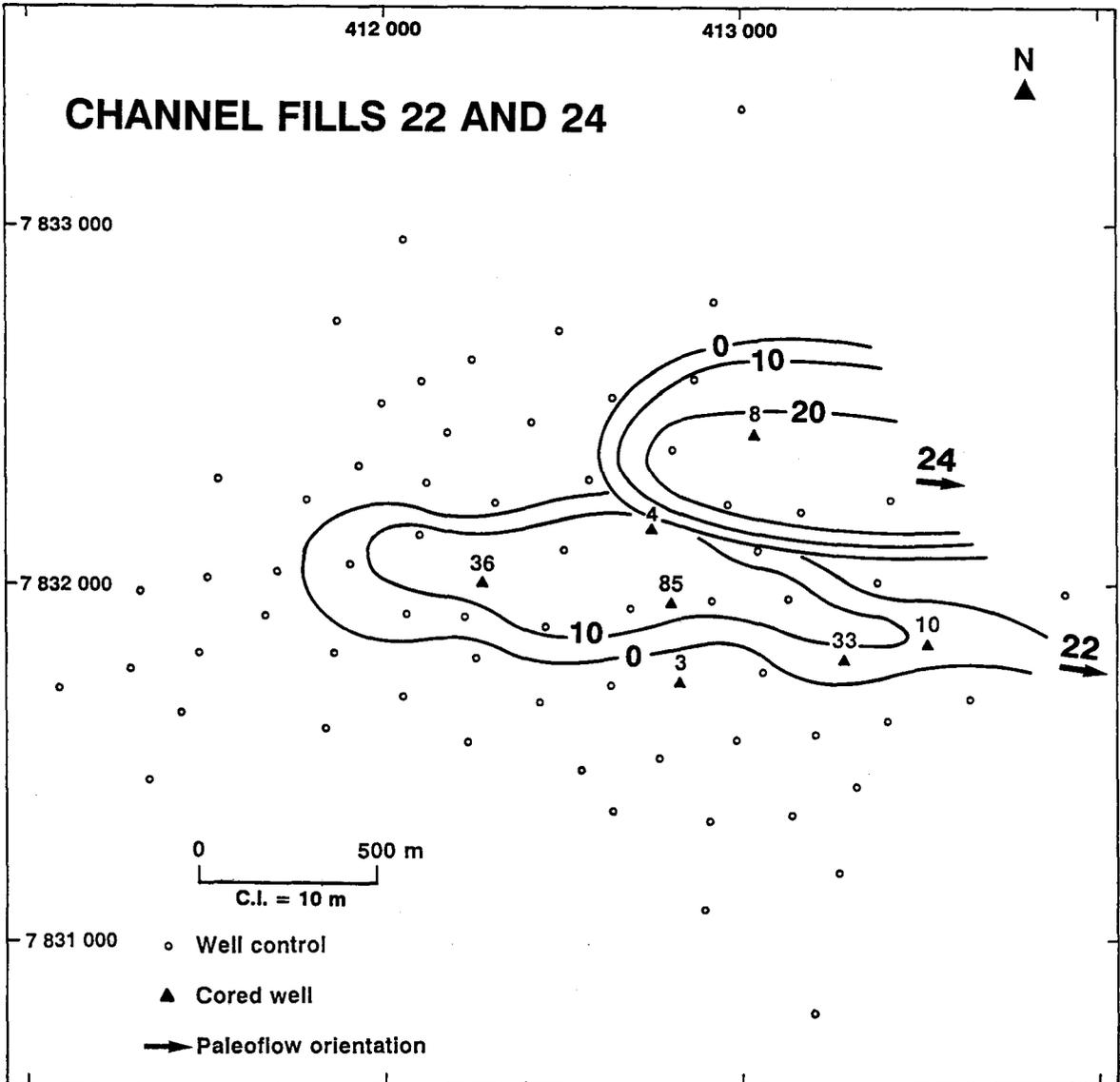
Fig. 4.31 - Net sand maps for channel fills 26 and 27. Average paleoflow orientations (indicated by arrows) are interpreted on the basis of sand body orientations, considering turbidity currents flowing down canyon (eastward).

CHANNEL FILLS 26 AND 27
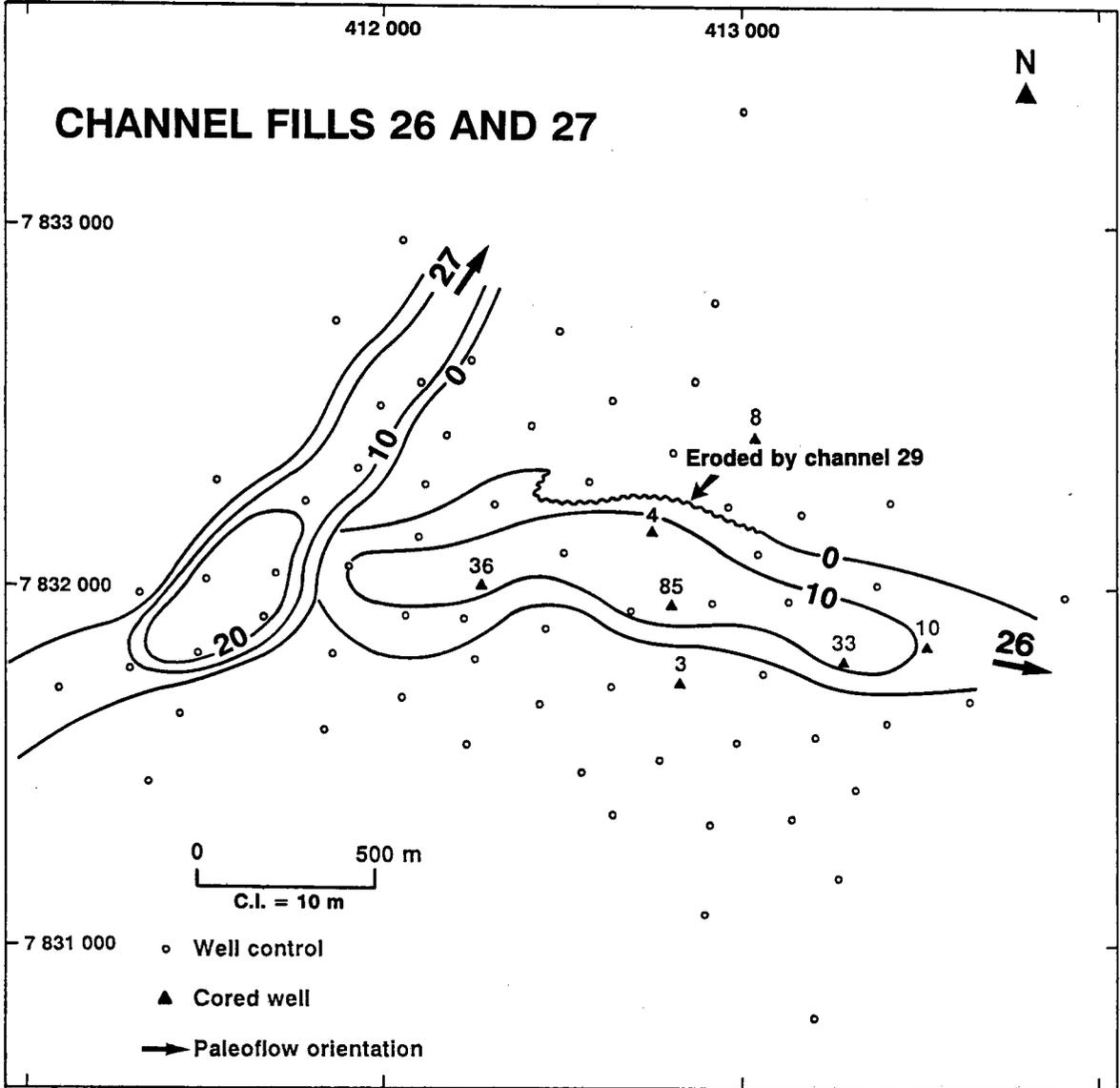
Fig. 4.32 - Net sand maps for channel fills 28, 29, 32, and 33. Average paleoflow orientations (indicated by arrows) are interpreted on the basis of sand body orientations, considering turbidity currents flowing down canyon (eastward).

CHANNEL FILLS 28, 29, 32, AND 33
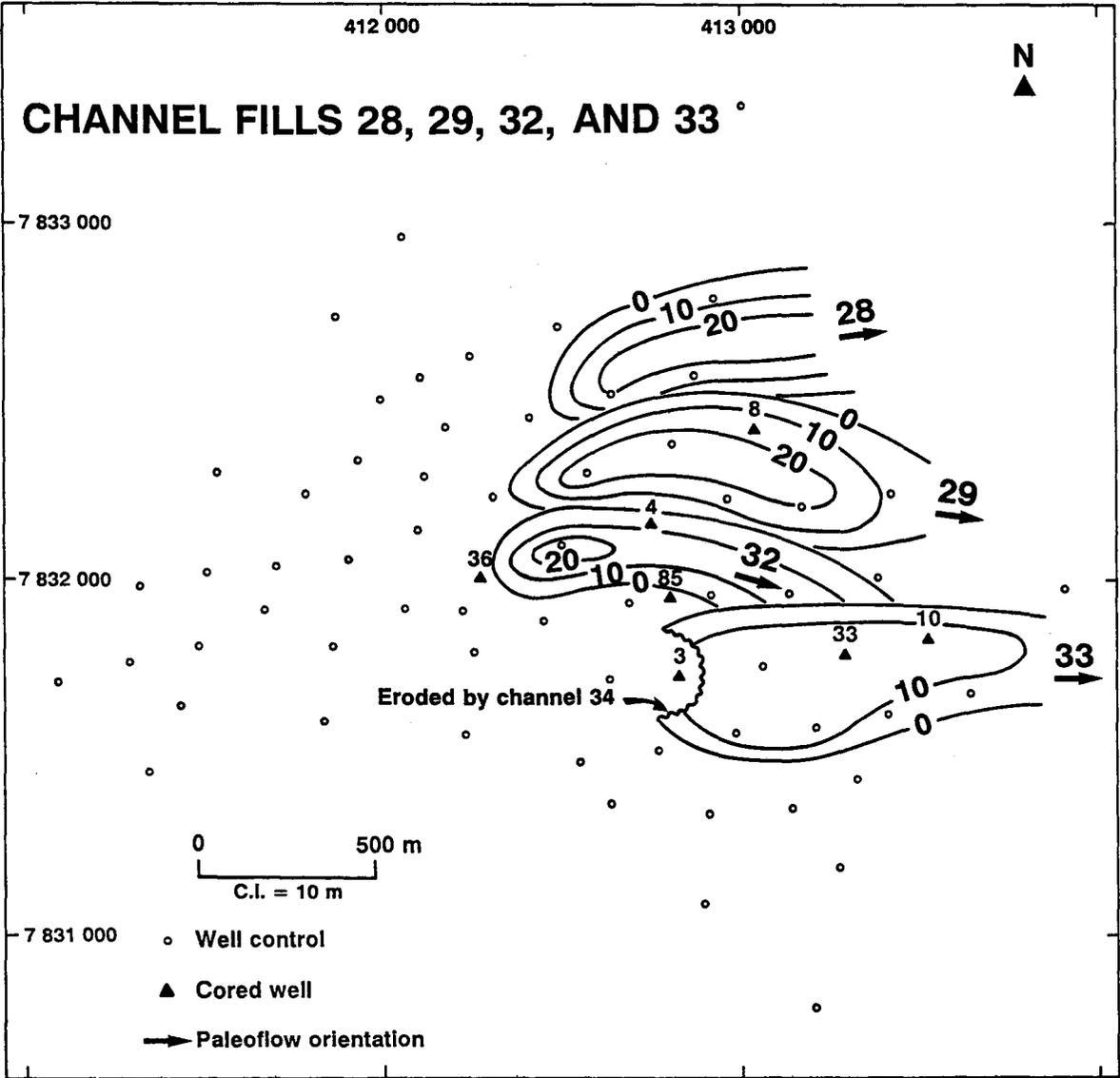
Fig. 4.33 - Isopach maps for channel fills 34 and 35. Average paleoflow orientations (indicated by arrows) are interpreted on the basis of the orientation of channel fills, considering turbidity currents flowing down canyon (eastward).

**CHANNEL FILLS 34 AND 35**
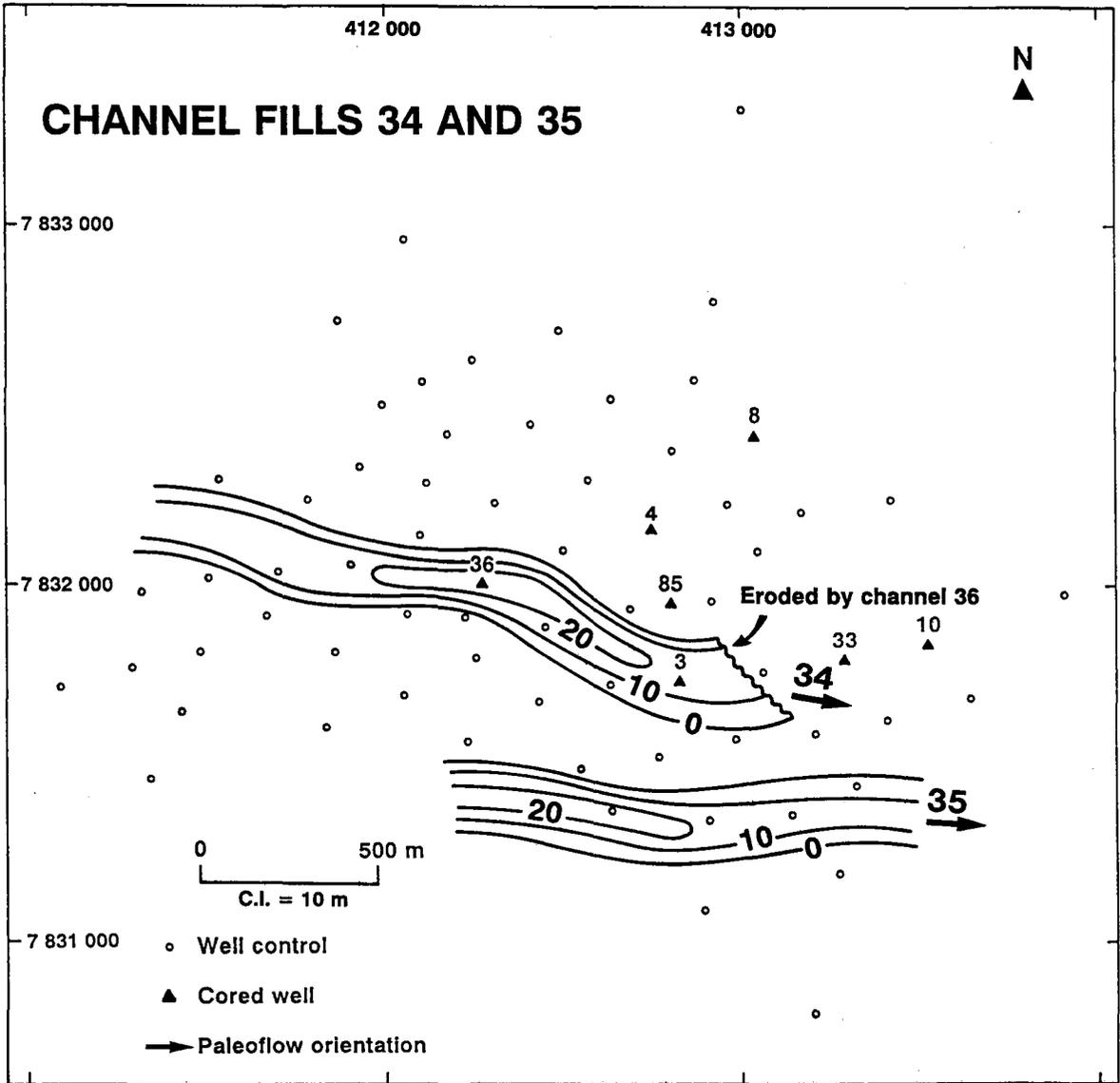
Fig. 4.34 - Isopach map for levee succession D. Note thicker levee deposits on the left side (looking downstream) of the associated channels.

LEVEE SUCCESSION D
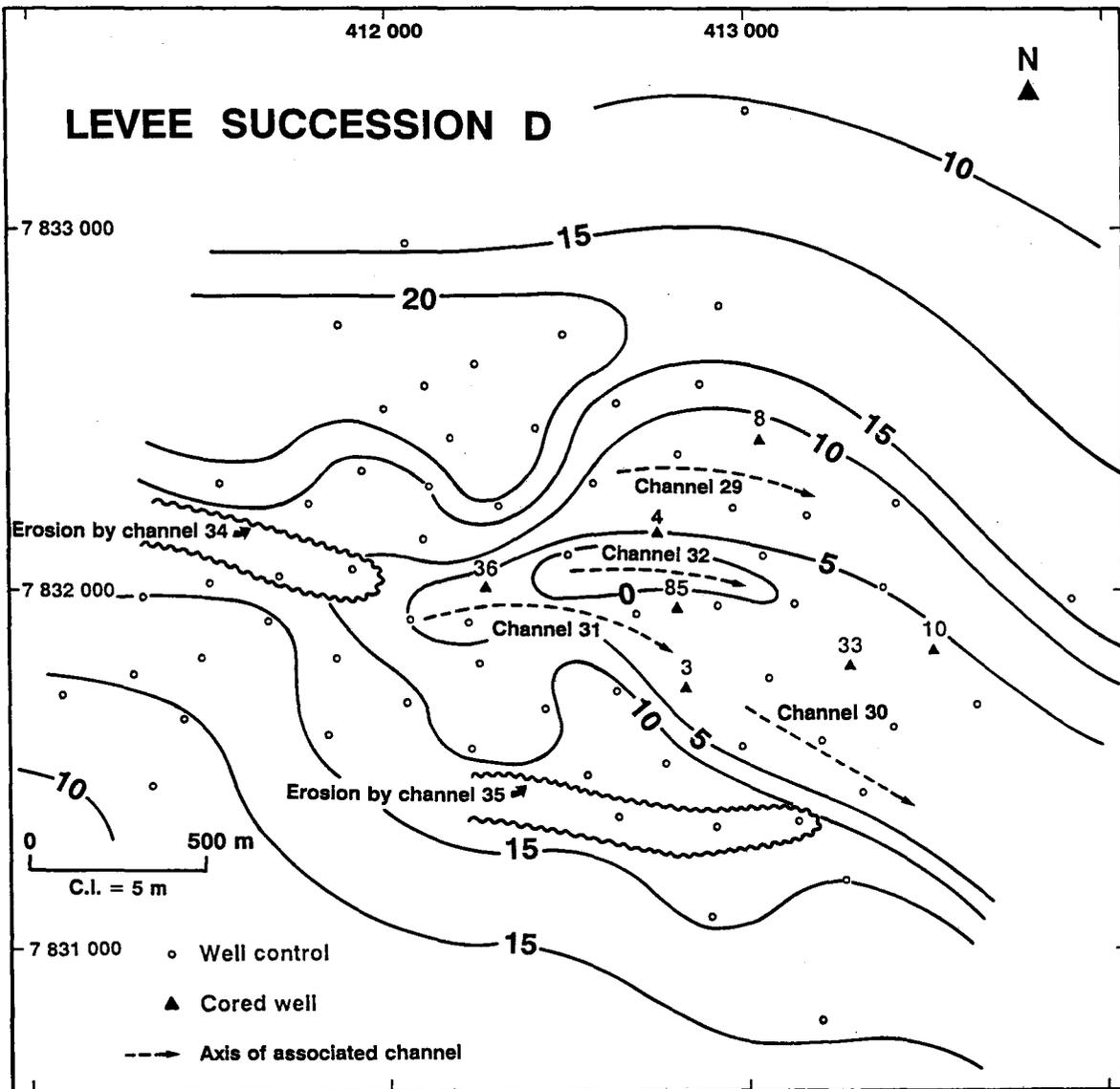
Fig. 4.35 - Net sand maps for channel fills 36, 37, and 38. Average paleoflow orientations (indicated by arrows) are interpreted on the basis of sand body orientations, considering turbidity currents flowing down canyon (eastward).

CHANNEL FILLS 36, 37, AND 38
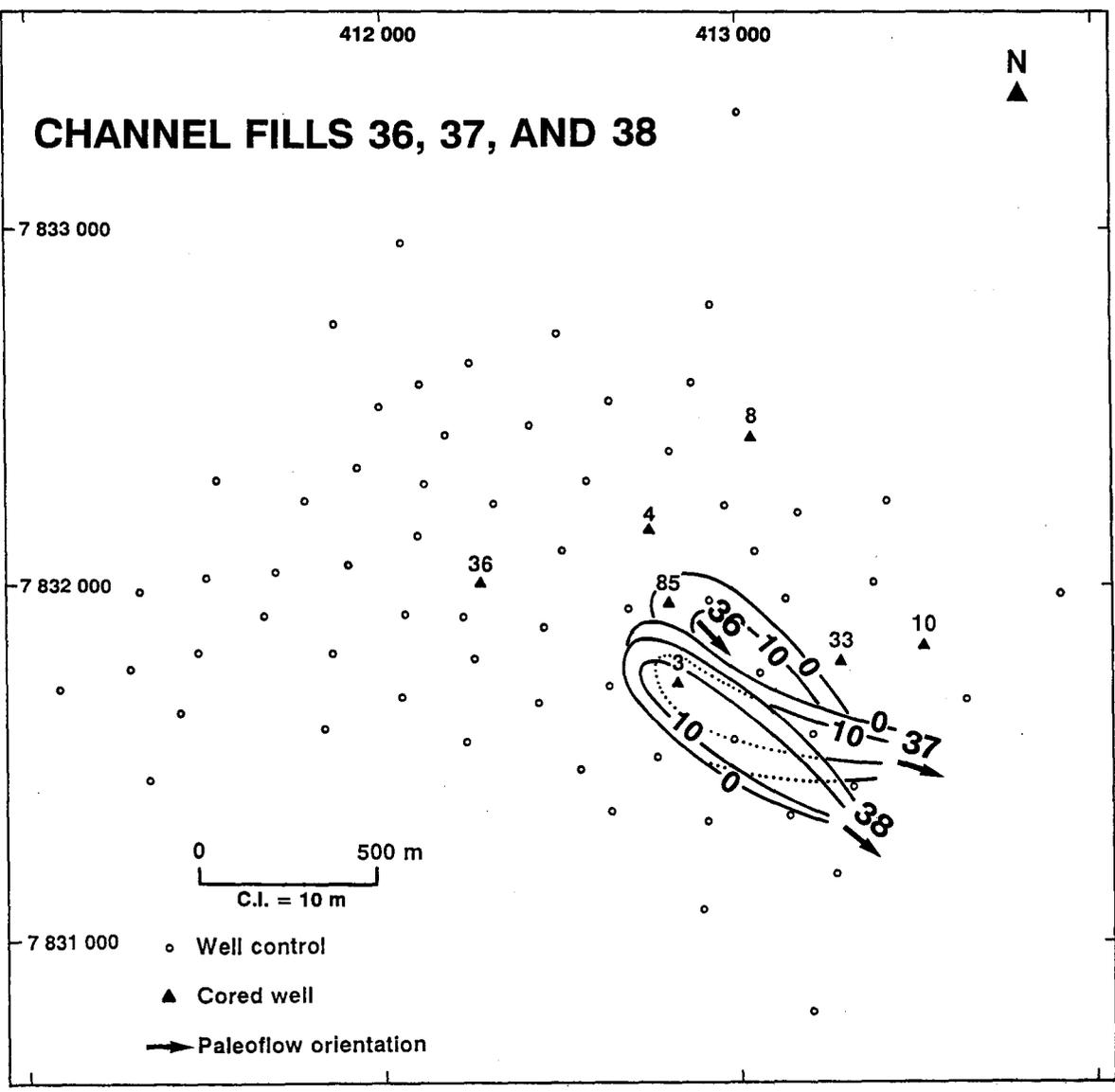
Fig. 4.36 - Isopach map for levee succession H. Note thicker levee deposits on the left side (looking downstream) of the associated channel.

LEVEE SUCCESSION H
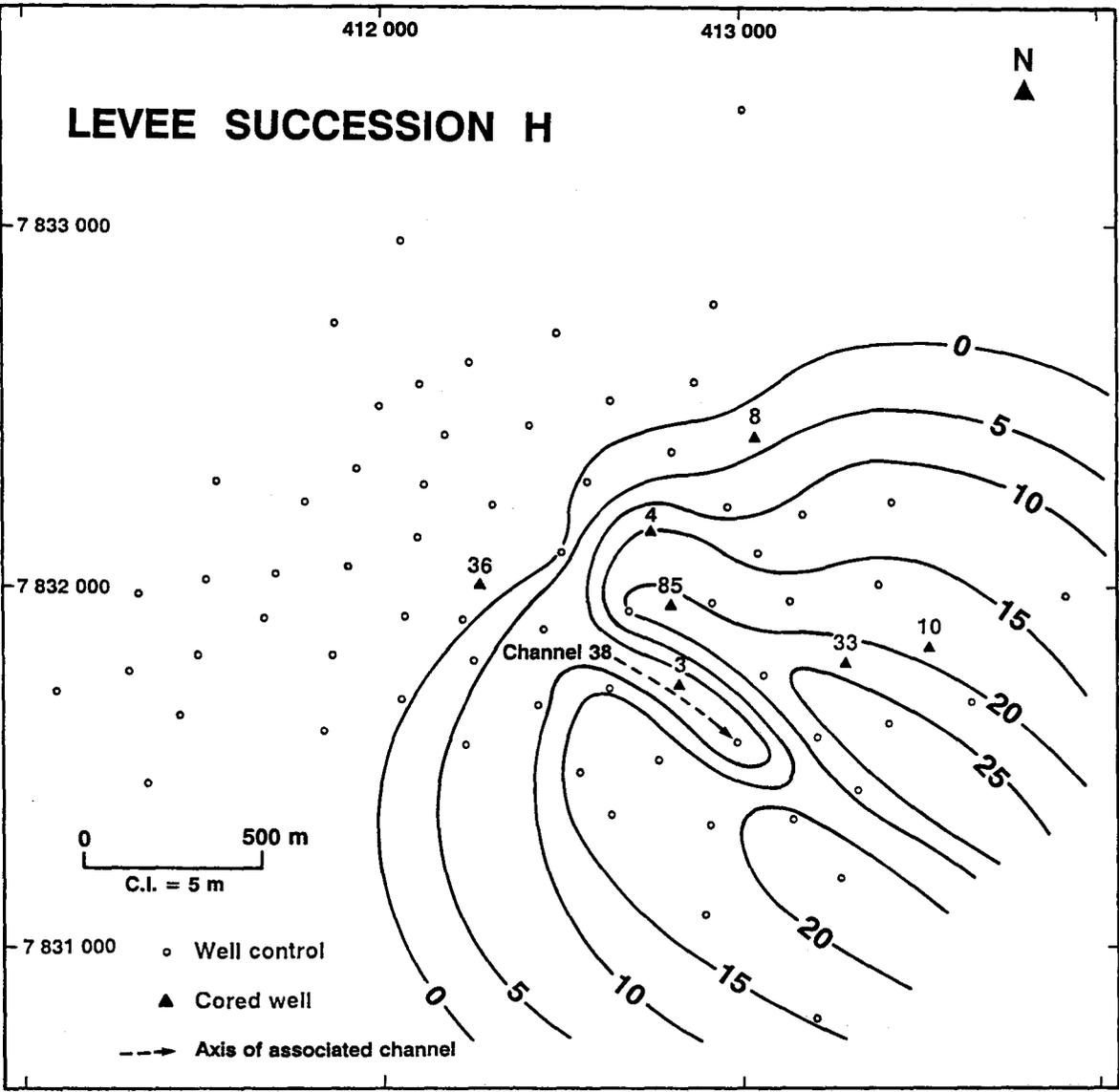
turbidite system because it contains a larger number of channel fills than any other section (compare with Figs. 4.23 and 4.24), and also because the coarser-grained channel fills (facies LP-F1 and LP-F2) are represented by their maximum width and thickness. However, figure 4.11 is important to illustrate the overall trends of channel fills that become narrower, thinner, and finer-grained upward.

### 4.4.3. Characterization of levee successions

Facies LP-F3 typically builds asymmetrical levees, associated with channels 19 to 38 (Table 4.6 and Fig. 4.11). Nine levee successions were differentiated by distinct patterns in resistivity logs. These levee successions are lettered A to I, from the oldest to the youngest (Table 4.6 and Fig. 4.11). Levee successions A, B, C, D, G, and H typically display upward decreasing resistivities, and levee successions E, F, and I show inverse trends (e.g. wells LP-56, LP-20, and LP-40 in Fig. 4.23). Higher resistivities are due to coarser-grained and thicker sandstone beds, or to concentrations of siderite, rhodochrosite, and pyrite in LP-F3 mudstones.

The preservation of some thin (< 0.3 m) beds of bioturbated mudstones and fine-grained sandstones within successions composed mostly of coarser-grained sediments of facies LP-F2 (Fig. 4.6) suggests that overspilling of fine-

**Table 4.6 - Levee successions of the Lagoa Parda turbidite system.**

| LEVEE SUCCESSION | MAXIMUM THICKNESS LEFT SIDE[a] (m) | RIGHT SIDE[a] (m) | MAXIMUM LEVEE SLOPES LEFT SIDE (F.A. - F.C.)[b] | RIGHT SIDE (F.C. - F.A) | ASSOCIATED CHANNELS |
|---|---|---|---|---|---|
| CHANNEL COMPLEX LP-CC3 | | | | | |
| I | 50[c] | | | | |
| H | 26 | 24 | 1.5° - 2° | 2° - 1.5° | 38 |
| G | 15 | 13 | 2° - 4° | 4° - 2° | 36, 37 |
| CHANNEL COMPLEX LP-CC2 | | | | | |
| F | 24 | 19 | 2° - 8° | 4° - 2° | 33 |
| E | 14[d] | | | | 32 |
| D | 22 | 18 | 2° - 10° | 5° - 2° | 30, 31, 32 |
| C | 27 | 15 | 2° - 8° | 5° - 2° | 29, 30 |
| B | 12 | 9 | 1.5° - 5° | 5° - 1.5° | 21 - 28 |
| A | 14 | 11 | 1.5° - 4° | 4° - 1.5° | 19 - 21 |

[a] Looking downstream. Channel paleoflow direction is interpreted on the basis of average sand body orientation, considering that the turbidity currents flowed along the Regência canyon seaward.
[b] F.A. = facing away from channel; F.C. = facing channel.
[c] Levee succession I is probably related to a channel that lies in an unknown location outside the study area; only the maximum thickness recorded in the study area is indicated.
[d] Levee succession E includes part of the levees related to channel 32, and also the passive filling by facies LP-F3 of a NE-oriented, abandoned channel. Its original geometry is poorly preserved; thus, only its maximum preserved thickness is indicated.

grained sediments and levee growth may have taken place during the filling of some channels (e.g. channel 33; Fig. 4.6). On the other hand, there is almost no deposition and/or no preservation of mudstones and fine-grained sandstones within very coarse-grained successions of facies LP-F1 (Figs. 4.6 and 4.7). It follows that two types of stratigraphic relationships may occur between coarser-grained channel fills and laterally associated finer-grained levees: (1) channel fills may erode levee successions, and therefore be younger; or (2) the filling of some channels may have taken place simultaneously to the growth of laterally associated levees.

Levee successions may have been built by finer-grained sediments spilled out from more than one of the mapped channels; for example, levee succession C may have accumulated during the cutting and filling of channels 29 and 30 (Fig. 4.11). On the other hand, fine-grained sediments spilled out from one single channel may have contributed to the formation of more than one of the mapped levee successions; for example, sediments spilled out from channel 30 may have formed part of levee successions C and D (Fig. 4.11). Table 4.6 provides a tentative correlation between levee successions and possibly contemporaneous channels. A more detailed description of the Lagoa Parda levee successions is presented in the next section, and their origin is discussed in section 4.5.4.

Isopach maps for two levee successions are presented in figures 4.34 and 4.36. Smaller isopachs occur in the areas

where contemporaneous, coarser-grained channel fills are located. Eventually, some of the levee successions are partially eroded by younger channels (e.g. levee succession D was locally eroded by channels 34 and 35; Fig. 4.34).

## 4.4.4. Characterization of channel complexes

The 38 channels recognized in the study area can be grouped into three channel complexes, named LP-CC1 to LP-CC3, from the oldest to the youngest (Table 4.5, and Figs. 4.11, 4.23, and 4.24). The nomenclature introduced by Damuth et al. (1983b; 1988) is followed here. An individual channel and its associated levee deposits form a "channel-levee system", and the overlapping, coalescing, or lateral interfingering of channel-levee systems form "channel-levee complexes". However, only the youngest Lagoa Parda channels have levees, so that the abbreviated designation **channel complex** is used here.

The main criteria for the separation of the Lagoa Parda channel complexes include: (1) the presence of thicker interbedded mudstones; (2) different filling facies; and (3) changes in dominant paleoflow orientation. Paleoflow orientations of the Lagoa Parda channels were interpreted from their sand body orientations (Table 4.5), considering that turbidity currents flowed along the Regência canyon seaward (i.e. mostly eastward; Fig. 4.1). Unlike the Carapeba/Pargo turbidite successions (Table 3.6), there are no regional

unconformities or local erosion surfaces bounding the Lagoa Parda channel complexes.

Overall, the turbidite succession composed of channel complexes LP-CC1 to LP-CC3 is characterized by channel fills that become narrower, thinner, and finer-grained upward (Fig. 4.11 and Table 4.5).

The criteria used in the separation between LP-CC1 and LP-CC2, and between LP-CC2 and LP-CC3 are explained in detail below, in the individual characterization of LP-CC2 and LP-CC3, respectively.


**Channel complex LP-CC1**

LP-CC1 comprises the lowermost 12 mapped channel fills, among which are the thickest and widest in the Lagoa Parda field (Table 4.5 and Fig. 4.11). Their average thickness and average width are 33 m and 690 m, respectively.

Channels 1 to 12 were deeply incised, mostly into mudstones and subordinate thin-bedded sandstones of facies LP-F5, without developing laterally associated levees (Figs. 4.11, 4.23, and 4.24). Several high resistivity horizons are widely recognized in the muddy succession eroded by channels 1 to 12 (e.g. markers $\alpha$, $\beta$, $\gamma$, and $\delta$; Figs. 4.11, 4.23, and 4.24). These markers represent flat horizons, parallel to the datum located above the Lagoa Parda turbidite succession.

The most important LP-CC1 channels are 1, 3, 4, 6, 7, 9, 10 and 11 (Fig. 4.11). Channel fills 2, 5, 8, and 12 are

smaller and/or poorly defined in the study area. Channels 1, 4, 6, 9 and 10 have mean sand body orientations ranging between 93° and 156° (paleoflow mostly from NW to SE; Figs. 4.25, 4.27, and 4.28), suggesting that most of the turbidity currents responsible for their erosion and filling originated from the smaller tributary troughs carved at the northern margin of the Regência canyon (Fig. 4.1). Conversely, channels 3, 7, and 11 have mean sand body orientations ranging between 30° and 41° (paleoflow from SW to NE; Figs. 4.26 to 4.28), indicating the activity of turbidity currents along the main thalweg of the Regência canyon. These two major channel orientations, and the stratigraphic relationships exhibited by their channel fills suggest that just one **major** channel was active at any given time in the Lagoa Parda field. The active channel alternated in position mostly between two preferred areas of channel erosion and filling (Fig. 4.11), indicating the intermittent activity of two major source areas. In each of these two groups of channels, the channel fills suggest a relatively constant paleoflow orientation, with the younger channels eroding and possibly occupying part of abandoned, older channels.

LP-CC1 channels were mostly filled with unstratified, boulder- to pebble-rich conglomerates and very coarse-grained sandstones (facies LP-F1; Fig. 4.11). Very high-resistivity horizons composed of conglomerates containing boulders to pebbles of high-rank metamorphic rocks are typical features of

LP-CC1 (e.g. channels 3 and 9 in Fig. 4.23b). LP-F1 grades to LP-F2 at the top and margins of few channel fills (e.g. Fig. 4.11; channel 3 in Fig. 4.23b). The different filling phases of LP-CC1 channels typically record their progressive enlargement (e.g. channels 3 and 9 in Fig. 4.23b); there are only a few examples of filling phases suggesting gradual channel migration. LP-CC1 channel fills end downstream with a relatively abrupt pinch out of coarse grained facies (LP-F1); these may occur interbedded with finer-grained sediments of facies LP-F5. On the other hand, the upstream terminations of LP-CC1 channel fills are located outside the study area.

**Channel complex LP-CC2**

LP-CC2 comprises 23 channel fills (channels 13 to 35, Table 3.5), with an average thickness and average width of 22 m and 390 m, respectively.

LP-CC2 is separated from LP-CC1 by a mud-rich succession up to 48 m thick. This occurs along most of the Lagoa Parda field (e.g. Fig. 4.23a), with the exception of the northeastern part of the study area, where some of the LP-CC1 channel fills (6, 9, and 10) were partially eroded by LP-CC2 channels (numbers 13 and 14; Fig. 4.24b). Channel 11 is not truncated by channels 13 and 15 as indicated in figure 4.11, despite the fact that channels 13 and 15 were able to cut deeper than the stratigraphic position of the top of channel fill 11. These channels were restricted to different areas of

the Lagoa Parda field (compare Figs. 4.28 and 4.29), so that the erosion suggested in figure 4.11 is an artifact produced by projection of many of the channel fills into a single geological section.

LP-CC2 channel fills have relatively constant sand body orientations, with most of them clustering between 80° and 118° (paleoflow from west to east; Figs. 4.29 to 4.33). In contrast to LP-CC1, LP-CC2 was built almost exclusively by channels originating from the smaller tributary troughs located at the northern margin of the Regência canyon (Fig. 4.1). Only channel 27 (Fig. 4.31) suggests paleoflows subparallel to the main canyon thalweg.

LP-CC2 channel fills are typically thinner and narrower than LP-CC1 counterparts (Table 4.5 and Fig. 4.11). They record an overall fining upward succession identified in cores (Fig. 4.6), and suggested by the funnel-shaped spontaneous potential logs, which contrast with the boxy well-log pattern exhibited by LP-CC1 (Figs. 4.23 and 4.24).

Most LP-CC1 channel fills are composed of facies LP-F1, with minor contribution of facies LP-F2 (Table 3.5 and Fig. 4.11). LP-CC2 channels commonly have lower fills of LP-F1, which grade upward to LP-F2 (e.g. Fig. 4.11; channels 15 and 18 in Fig. 4.23b), but they may also be filled exclusively by facies LP-F2 (e.g. Fig. 4.11; channel 30 in Fig. 4.24), LP-F3 (e.g. Fig. 4.11; and channels 34 and 35 in Fig. 4.23b), and LP-F4 (e.g. Fig. 4.11, and channel 27 in Fig. 4.23a).

Very few LP-CC2 channel fills have their downstream terminations drilled and cored in the study area. One example is provided by the channel 33 (Fig. 4.32), where facies LP-F2 (Fig. 4.12) is replaced downstream by facies LP-F4 (Fig. 4.21). The upstream terminations of most of the LP-CC2 channel fills are characterized by a relatively abrupt pinch out of coarse-grained facies (LP-F1 and LP-F2), which are replaced upstream by the facies LP-F3. These finer-grained sediments probably represent the passive filling of abandoned channels by sediments overspilled from adjacent, active channels. The passive filling of most of the abandoned LP-CC2 channels and their associated levees are composed of similar facies and have the same well log response; therefore, channel mapping is restricted in most of the cases to the coarser-grained fills (e.g. Figs. 4.29 to 4.32). Exceptions are provided by channels 34 and 35 (Fig. 4.33), which are filled with facies LP-F3 (Fig. 4.23b). In this case, the channel fills can be separated from the laterally associated levee succession by different trends in resistivity logs; channel fills 34 and 35 display upward decreasing resistivities and the levee succession F shows upward increasing resistivities (compare wells LP-26, LP-3, LP-40, and LP-20 in Fig. 4.23b). The origin of these well log trends and the filling of channels 34 and 35 is discussed in section 4.5.4.

The different filling phases of LP-CC2 channels may record the progressive enlargement of some channels. This

situation is better recognized in its lowermost, larger, and probably deeper channels (e.g. channel 15 in Fig. 4.23b; and channel 13 in Fig. 4.24b).

LP-CC2 also differs from LP-CC1 by the development of asymmetrical levees, which are higher and thicker on the left side (looking downstream) of associated channels (i.e. mostly on their northern side; Table 4.6 and Figs. 4.11, 4.23b, 4.24ba, and 4.34). However, LP-CC2 levees only started to grow during and after the filling of channel 19 (Figs. 4.11 and 4.23b). At the begining, their relief was very subtle (levee successions A and B; Fig. 4.11), but following the development of channel 28, a more prominent levee topography was established in the Lagoa Parda area (levee successions C to F; Figs. 4.11, 4.23b, and 4.24b). There is a well-defined relationship between higher levee topography and narrower, thinner, and finer-grained (facies LP-F2 to LP-F4) channel fills (Fig. 4.11).

Levee slopes may be as steep as 10°, with the slopes facing the channels being typically higher than the back (facing away from the channel) levee slopes (Table 4.6). Cored levee successions may show dipping packages of facies LP-F3, which may include thin (< 1 m) debris flow and slump deposits (Fig. 4.16). Levee asymmetry may also be demonstrated by steeper slopes facing the channel on the left-side levees (Table 4.6).

The mapped levee successions range in thickness from 9 to

27 m (Table 4.6). The lowermost levee successions of LP-CC2 (levee successions A, B, C, and D; Figs. 4.23 and 4.24) typically display upward decreasing resistivities, which are due largely to their fining- and thinning-upward sandstone beds or by their overall muddier-upward character. The uppermost levee successions (E and F; Figs. 4.23 and 4.24) are mostly mud-rich successions, but they show upward increasing resistivities, which are due mainly to an upward increasing concentration of siderite, rhodochrosite, and pyrite in LP-F3 mudstones. The origin of these well log trends and the development of levee successions is discussed in section 4.5.4.

LP-CC2 records successive channel abandonment, probably through relatively rapid avulsions (which sometimes may have involved levee breaching). Most channel avulsions took place randomly (compare Figs. 4.29 to 4.31). However, channel fills 28 to 33 define an **average** southeast trend of avulsion (to the right, looking downcanyon; Figs. 4.11, 4.24b, and 4.32). The development of this trend coincides with the growth of higher, asymmetrical levees (levee successions C to F; Fig. 4.11), suggesting the influence of levee topography on channel avulsion; this subject will be discussed in more detail in section 4.5.4.

**Channel complex LP-CC3**

The uppermost LP-CC3 comprises only three channel fills

(36 to 38), among which are the narrowest and thinnest channel fills in the Lagoa Parda field (Table 4.5). Their average thickness and average width are 14 m and 260 m, respectively.

The lowermost channel of LP-CC3 truncates levee succession F and the essentially mud-filled channel 34 (Fig. 4.11). LP-CC3 channel fills are almost always separated from the LP-CC2 coarse-grained channel fills by a mud-rich succession up to 24 m thick (Figs. 4.23b and 4.24a).

LP-CC3 channel fills have a relatively constant sand body orientation between 128° and 134° (paleoflow from NW to SE; Fig. 4.35). These orientations differ from those of the uppermost channel fills of LP-CC2, but LP-CC3 also was built by channels that originated from the smaller tributary troughs located at the northern margin of the Regência canyon (Fig. 4.1).

The coarser-grained channel fills of LP-CC3 are composed mostly of facies LP-F2. The upstream terminations of LP-CC3 channel fills are characterized by a relatively abrupt pinch out of facies (LP-F2), which are replaced upstream by the facies LP-F3. The downstream terminations of LP-CC3 channels can not be observed in the study area.

LP-CC3 also includes asymmetrical levees, which are slightly higher and thicker on the left side (looking downstream) of associated channels (i.e. mostly on their northeastern side; Table 4.6 and Figs. 4.11 and 4.36). LP-CC3 levees show gentler maximum slopes (≤ 4°) and a less

pronounced asymmetry than LP-CC2 levees (Table 4.6). The two lowermost levee successions of LP-CC3 (G and H) tend to smooth the levee topography inherited from LP-CC2 (Figs. 4.11, 4.23b, and 4.24b).

The mapped levee successions range in thickness from 13 to 50 m (Table 4.6). The lowermost levee successions of LP-CC3 (levee successions G and H; Figs. 4.23 and 4.24) typically display upward decreasing resistivities, which are due largely to their fining- and thinning-upward sandstone beds or to their overall muddier-upward character. The uppermost levee succession (levee succession I; Figs. 4.23 and 4.24) is mostly a mud-rich succession, but it shows upward increasing resistivities, which are due mainly to an upward increasing concentration of siderite, rhodochrosite, and pyrite in LP-F3 mudstones.

The detailed cross sections (e.g. 4.23b and 4.24b) show that only one channel was excavated and filled in the study area at any given time during the growth of LP-CC3. LP-CC3 indicates successive channel abandonment, probably through relatively rapid avulsions. These avulsions took place consistently toward southwest (to the right, looking downstream; Fig. 4.35), or toward the side of the channels with lower levees (Figs. 4.11 and 4.36). This trend of avulsion suggests the influence of levee topography on channel avulsion, as discussed in more detail in section 4.5.4.

## 4.4.5. Reccurrence intervals of channel complexes and individual turbidites

LP-CC1 to LP-CC3 represent the three youngest of at least nine channel complexes (Fig. 4.2) included in the early Eocene calcareous nannofossil zone *Neochiastozygus chiastus* (Antunes, 1990a), which has a time span between 57.8 and 56.5 Ma (1.3 m.y.). It follows that each of the nine channel complexes included in the *Neochiastozygus chiastus* zone has an average duration of about 144,000 years.

The number of turbidites that form the Lagoa Parda channel complexes can only be roughly estimated, using as reference the average thicknesses obtained from cored wells (section 4.3). Channel complex LP-CC2, which is the most extensively cored, is composed of about 180 coarser-grained (facies LP-F1 and LP-F2), channel fill turbidites, and about 1,800 finer-grained (facies LP-F3), levee turbidites. Considering the average duration of each channel complex (144,000 years), it can be estimated average reccurrence intervals of 800 and 80 years, respectively for channel fill and levee turbidites. LP-CC2 is the channel complex that has the largest number of turbidites, thus the estimated figures represent the shortest reccurrence intervals in the study area.

## 4.5. SEDIMENTATION EVOLUTION AND CONTROLS

### 4.5.1. The general picture

The canyon-confined, Lagoa Parda turbidite system is included in the marine transgressive megasequence, which is characterized by onlapping, deepening-upward sedimentation throughout the eastern Brazilian marginal basins (e.g. Chang et al., 1988, 1992). The studied turbidite succession comprises the uppermost 230 m of the up to 650 m thick, early Eocene, calcareous nannofossil zone *Neochiastozygus chiastus* (Fig. 4.2).

The Lagoa Parda turbidite system is composed of five major facies: unstratified, bouldery to pebbly conglomerates and very coarse-grained sandstones, deposited by high-density turbidity currents (LP-F1); graded beds of unstratified coarse-grained sandstones and parallel-stratified finer-grained sandstones, deposited by high- to low-density turbidity currents (LP-F2); interbedded bioturbated mudstones (mostly by *Thalassinoides* and *Ophiomorpha*) and thin-bedded sandstones, deposited by low-density turbidity currents (LP-F3); interbedded stratified sandstones and intraclastic conglomerates, deposited by low- and high-density turbidity currents, respectively (LP-F4); and mudstones containing a benthic foraminiferal fauna typical of deep neritic to upper bathyal (200 - 500 m) depositional settings (LP-F5). LP-F1,

LP-F2, and LP-F4 contain the oil-producing rocks in the Lagoa Parda field; these facies have average porosities and permeabilities ranging between 20 and 25 %, and 72 and 427 mD, respectively.

Lagoa Parda reservoir rocks (facies LP-F1, LP-F2, and LP-F4) were deposited in channels that were deeply incised into mudstone-rich successions (LP-F3 and LP-F5) or older channel fills (Fig. 4.11). Cross-cutting relationships permit the identification of at least 38 major channel fills in the study area (Table 4.5); these channels may show several phases of cutting and filling. Channel fill thicknesses range between 9 and > 50 m, and channel fill widths vary from 210 to > 1,050 m (Table 4.5 and Fig. 4.11). The paleoflow orientations suggested by channel fills cluster into two major groups; 30° to 41° (paleoflow from SW to NE), and 80° to 156° (paleoflow mostly from NW to SE).

Facies LP-F3 typically builds asymmetrical levees, which are slightly higher and thicker on the left side (looking downstream) of their associated channels (e.g. Figs. 4.34 and 4.36). Nine levee successions (up to 50 m thick) are associated with the 20 youngest channels (Table 4.6 and Fig. 4.11); these successions were differentiated by distinct patterns in the resistivity logs. The channel fills suggest successive channel abandonment, probably through relatively rapid avulsions. Some of these avulsions took place consistently to the right (looking dowstream), in an opposite

way to the direction of preferential levee growth.

The 38 channels recognized in the study area can be grouped into three channel complexes (LP-CC1 to LP-CC3; Table 4.5 and Fig. 4.11), which have an average duration of 144,000 years. The main criteria for the separation of channel complexes include thicker interbedded mudstones, different filling facies, and changes in dominant paleoflow orientation. Overall, the turbidite succession composed of channel complexes LP-CC1 to LP-CC3 is characterized by channel fills that become narrower, thinner, and finer-grained upward (Table 4.5 and Fig. 4.11).

Four major questions emerge from the scenario depicted above. They concern: (1) the provenance of the thick (up to 400 m) package of texturally and compositionally immature, coarse-grained turbidites; (2) the development of individual channel complexes; (3) the growth of asymmetrical levees and the establishment of channel avulsions; and (4) the overall trends of decreasing grain-size, thickness, and width of channel fills. These four questions will be adressed in the following sections.

## 4.5.2. Source of sediments

The sandstones and the sandy matrix in the conglomerates of the Lagoa Parda turbidite system are characterized by poorly-sorted, subangular to angular grains, composed largely

(35 - 40 %) of feldspar, and feldspar-rich rock fragments. Their source rocks are upper Proterozoic igneous and high-grade metamorphic rocks, including mostly granites, granulites, and migmatites. These rocks form most of the subparallel, coastal mountain ranges of the Serra do Mar and Serra da Mantiqueira (Fig. 1.7).

The climate along the eastern Brazilian coastal areas was humid and warm during the early Eocene, as suggested by the high content (up to 35 %) of carbonaceous plant fragments in facies LP-F2, LP-F3, and LP-F4, by the small number of individuals in the calcareous nannofossil assemblage (Antunes, 1990a), and by global paleogeographic reconstructions (Parrish and Curtis, 1982; Parrish et al., 1982).

Lagoa Parda turbidites are as compositionally and texturally immature as the Carapeba/Pargo turbidites, and the paleoclimate both in the early Eocene Espírito Santo basin and late Cretaceous Campos basin (section 3.5.2) was humid and warm. Thus, Lagoa Parda turbidites probably also had a source area characterized by rugged topography, where more vigorous and erosive streams would decrease the residence time and chemical weathering of feldspathic grains in soil profiles, and also cut deeper trough fresh bedrock. Consequently, a large amount of feldspar-rich, coarse-grained and angular sediments would be made available for sedimentation.

Steep slopes in the cratonic area adjacent to the Espírito Santo basin or along its margin could have been

produced by continued fault reactivation and relative uplift of Precambrian rocks during the early Eocene. This tectonic scenario is suggested by reactivation of NE- and N-oriented normal faults in the Regência canyon area. These faults affect the Precambrian basement (Oliveira et al., 1985). The N-oriented fault system allowed important tectonic subsidence along the basin margin; its successive reactivation up to the early Eocene exposed Precambrian high-rank metamorphic rocks along the Regência canyon floor in its western portion (Fig. 4.4).

The compositional and textural immaturity of the Lagoa Parda turbidite system also implies that the sediments derived from rapidly uplifted, faulted highlands were not submitted to prolonged abrasion (if any) in a transitional, high-energy depositional setting such as a beach, shoreface, or wave-dominated delta. As suggested for the late Cretaceous Campos basin, the hypothesis of fan deltas directly feeding a relatively narrow, faulted shelf is also appealing for the early Eocene Espírito Santo basin. This hypothesis also remains a speculation in the Espírito Santo basin, because of the lack of preservation of shallower-water deposits equivalent in the time to the early Eocene turbidites.

The early Eocene Regência canyon represents a more proximal depositional setting than the late Cretaceous Carapeba/Pargo trough, as suggested by the turbidite facies and by the fossil assemblages contained in the mudstones. The

early Eocene Regência canyon was filled with mudstones containing deep neritic to upper bathyal (200 - 500 m) foraminifera, whereas the late Cretaceous Carapeba/Pargo trough contains mid to lower bathyal (1,000 - 1,500 m) foraminifera. The Lagoa Parda turbidite system is characterized by deeply incised channels, filled in large proportion by boulder- to pebble-rich conglomerates; on the other hand, the Carapeba/Pargo turbidite system comprises non-channelized deposits, mostly composed of very coarse- to coarse-grained sandstones, and subordinate granule- to pebble (<2 cm)-rich conglomerates. It follows that the more proximal (and deeply incised into the shelf) Regência canyon probably would have been able to capture larger amounts of coarser-grained sediments; these, in turn, could have been introduced by fan deltas, or directly intercepted from littoral-drift systems, as observed in some canyons off California (e.g. Inman et al., 1976; Hess and Normark, 1976).

The exogenic, boulder- to pebble-sized components of Lagoa Parda conglomerates are typically sub-rounded to rounded (Figs. 4.8 and 4.10a), contrasting with their sandy matrix, which is composed of subangular to angular grains. The roundness of these coarser clasts is probably related to the chemical weathering operating at the source area, rather than to physical transformation during sedimentary transport. This situation can be explained with one example from the city of Salvador, northeastern Brazil, where the climate is warm

(annual average temperatures between 24 and 26°C) and humid (annual average precipitation > 2,000 mm). Salvador is located at the fault that defines the eastern margin of the Recôncavo rift-basin (Fig. 1.7), where Precambrian granulites and mostly early Cretaceous sedimentary rocks crop out on the hanging wall and foot wall, respectively. The intense chemical weathering of the relatively homogeneous granulites has developed soil profiles containing scattered, rounded and spherical large clasts. Along the Salvador fault still there is a significant difference in relief, with the Precambrian basement standing tens of meters above the sedimentary basin; thus, during exceptionally rainy seasons, the large granulite clasts may be transported by landslides into the basin. Thus in the study area, it is probable that most of the boulders to pebbles of facies LP-F1 left the source area already rounded, and underwent relatively short transport until their resedimentation in the early Eocene Regência canyon.

## 4.5.3. Development of channel complexes

The accumulation of turbidite successions is controlled by the complex interaction of three factors; sea level fluctuation, tectonic setting and activity, and type and rate of sediment supply (e.g. Stow et al., 1985; Mutti and Normark, 1987; Pickering et al., 1989). Section 3.5.3 (page 157) presents an overview of the literature about how these

parameters control turbidite sedimentation.

## Global sea level curves

The sedimentation of the Lagoa Parda turbidite system (early Eocene, *Neochiastozygus chiastus* zone) took place during the generalized transgression that occurred along most of the eastern Brazilian margin during the late Cretaceous and early Tertiary (e.g. Chang et al., 1988, 1992). The turbidite-bearing *Neochiastozygus chiastus* zone is overlain by the mud-rich *Tribrachiatus orthostylus* zone (also early Eocene in age; Figs. 4.2 and 4.37), which probably records, in the Espírito Santo basin, the culmination and maximum coastal onlap of this long-term, eustatic sea level rise.

The calcareous nannofossil zones defined for the late Paleocene to early Eocene filling sections of the Regência canyon (Antunes, 1990a) have been tied to the chronostratigraphic chart of Berggren et al. (1985), and show time resolution in the range 1.0 to 2.8 m.y. (Fig. 4.37). Global sea-level curves (Haq et al., 1987, 1988) show ten important sea-level falls during the late Paleocene and early Eocene (Fig. 4.37). These, in turn, bound nine third-order sea level cycles with durations between 0.5 to 2.5 m.y., which punctuate an overall transgressive, second-order cycle (TA2; Haq et al., 1988, p.95). Correlations between the late Paleocene to early Eocene biozones (Antunes, 1990a) and the global, third-order sea level cycles (Haq et al., 1987, 1988)

Fig. 4.37 - Comparison between the global sea-level curve of Haq et al. (1988) and the chronostratigraphy, biostratigraphy, and simplified lithostratigraphy of the late Paleocene to mid Eocene successions in the Regência canyon area. Unconformities 4 to 6 are also represented in figures 3.3 and 3.4. Biozones recognized in the Cenozoic successions of the eastern Brazilian marginal basins are traditionally tied to the chronostragraphic column proposed by Berggren et al. (1985). The chronostratigraphy presented by Berggren et al. (1985) and Haq et al. (1988) show differences of 0.6 to 3.8 m.y. in the time boundaries assigned for the different early Tertiary series.

| CHRONO-STRATIGRAPHY[1] | BIOSTRATIGRAPHY[2] | LITHOSTRATIGRAPHY | CHRONO-STRATIGRAPHY[3] | EUSTATIC CURVES[3] |
|---|---|---|---|---|



CHRONO-
STRATIGRAPHY[1]

— 40.0 —

Mid Eocene

— 52.0 —

Early Eocene

— 57.8 —

Late
Paleocene

— 62.0 —

BIOSTRATIGRAPHY[2]

— 40.0 —

*Chiasmolithus
grandis*

— 43.0 —

*Chiasmolithus
staurion*

— 47.0 —

*Chiasmolithus
gigas*

— 50.0 —

*Discoasteroides
kuepperi*

— 52.0 —

*Discoaster
lodoensis*

— 53.7 —

*Tribrachiatus
orthostylus*

— 56.5 —

*Neochiastozygus
chiastus* — 57.8 —

*Fasciculithus
tympaniformis* — 58.8 —

*Heliolithus
kleinpellii*

— 62.0 —

LITHOSTRATIGRAPHY

⑥
⑤
④

CHRONO-
STRATIGRAPHY[3]

— 39.4 —

Mid Eocene

— 49.0 —

Early Eocene

— 54.0 —

Late
Paleocene

— 60.2 —

EUSTATIC
CURVES[3]

Long term    Short term

← Rise    Fall →

[1] Berggren et al. (1985)

[2] Antunes (1990a)

[3] Haq et al. (1988)

DOMINANT LITHOLOGY

| | |
|---|---|
| ‒ ‒ ‒ | Mudstone |
| ∴∴∴ | Sandstone/Conglomerate |

are very difficult, despite their similar time span. The problems involved in these correlations are twofold: (1) different time boundaries have been assigned for the same biozones in the widely-used chronostratigraphic charts published by Berggren et al. (1985), Harland et al. (1990), and Haq et al. (1987, 1988); and (2) the time spacing of third-order sea level falls in the curves of Haq et al. (1987, 1988) is less than the potential error involved in dating these events (Miall, 1991, 1992). These problems will be illustrated with the *Neochiastozygus chiastus* zone, which includes the Lagoa Parda turbidite system.

Antunes (1990a) correlates his *Neochiastozygus chiastus* zone to the Martini's (1971) widely-accepted *Marthasterites contortus* zone (NP10), and Okada and Bukry's (1980) *Tribrachiatus contortus* zone (CP9a). The zones NP10 and CP9a are considered synchronous and comprise the earliest Eocene sedimentary record in the chronostratigraphic charts published by Berggren et al. (1985, p.1412), Harland et al. (1990, p.215), and Haq et al. (1988, p.95). However, these charts assign different time boundaries for NP10 and CP9a, respectively, 57.8 to 56.5 Ma, 56.5 to 55.2 Ma, and 53.7 to 53.0 Ma. Therefore, there is a difference of 4.1 m.y. between the ages assigned by Berggren et al. (1985) and Haq et al. (1988) for the base of zones NP10 and CP9a, i.e. 3.1 to 5.8 times their estimated time span (0.7 to 1.3 m.y.).

The late Paleocene to early Eocene, third-order sea level

falls identified by Haq et al. (1987, 1988) may have been responsible for some of the unconformities recognized in the Regência canyon filling section (Figs. 4.3 and 4.4), including the unconformity placed at the base of the *Neochiastozygus chiastus* zone. However, any attempt to correlate these unconformities and overlying turbidites to the (claimed) eustatic, third-order sea level falls should consider the uncertainties involved. For instance, the curves of Haq et al. (1987, 1988) provide at least three closely-spaced ($\leq$ 0.5 m.y.) sea/level falls in the transition from Paleocene to Eocene that could be correlated to the unconformity at the base of the *Neochiastozygus chiastus* zone (Fig. 4.37).

The major contribution of global sea level curves is to show that the late Paleocene to early Eocene, overall transgressive trend was punctuated by shorter-term sea level falls (Fig. 4.37), which may have induced seaward shifting of coastal depocenters, followed by submarine erosion (by turbidity currents) along the Regência canyon. One important phase of erosion took place in the transition from Paleocene to Eocene, allowing the early Eocene, *Neochiastozygus chiastus* zone to unconformably overlie early Maastrichtian sediments (Fig. 4.3).

**Tectonics and sediment supply**

During the long-term, eustatic sea level rise of the late Cretaceous and early Tertiary, the Espírito Santo basin also

experienced a generalized eastward (seaward) tilting in response to the combined effects of thermal-contraction subsidence and sedimentary loading (Costa, 1988). Subsidence rates in the early Tertiary were higher than in the late Cretaceous (e.g. Chang et al., 1992, their figure 27), largely as a function of sedimentary loading of the lithosphere in response to a higher clastic supply.

The early Eocene, *Neochiastozygus chiastus* zone (57.8 to 56.5 Ma) reaches a maximum thickness of 650 m in the thalweg of the Regência canyon (well LP-4; Figs. 4.2 to 4.4). Therefore, this turbidite-rich succession records average undecompacted sedimentation rates of 65 - 70 cm/1,000 yr., one of the highest sedimentation rates recognized in marine successions throughout the eastern Brazilian marginal basins. Similar or higher sedimentation rates have only been estimated in the last stages of lacustrine, rift sedimentation, i.e. between 122 and 119 Ma (Barremian; e.g. Chang et al., 1992, their figure 15).

The high sedimentation rates recorded by the *Neochiastozygus chiastus* zone suggest a very important sediment supply, derived from a relatively close and rapidly uplifting source area, as also indicated by the very coarse-grained, and compositionally and texturally immature Lagoa Parda turbidites. An important continental runoff, probably induced by the mostly warm and humid early Eocene paleoclimate, is suggested by the high content of carbonaceous

plant fragments (up to 35 %) in Lagoa Parda finer-grained sandstones, the high content of kaolinite (up to 35 %) in the interbedded mudstones, and also by the small number of individuals in the calcareous nannofossil assemblage (Antunes, 1990a).

Despite the high sediment supply, no shallower-water facies were developed and/or preserved in the early Eocene filling section of the Regência canyon. This situation is due mostly to the high rates of tectonic subsidence along the faulted, canyon boundaries (Fig. 4.3), and the generalized trend of sea level rise, which did not allow the progradation of coastal depositional systems. Tectonics was important not only to increase the sediment supply into the Regência canyon, but also to provide accommodation space for sediment accumulation (and preservation). In the Espírito Santo basin, sediment input surpassed the effects of tectonic subsidence and long-term sea level rise only from the latest early Eocene onwards, giving rise to the marine regressive megasequence (Figs. 4.3 and 4.4). For instance, time equivalent sediments to the Lagoa Parda turbidite system are not preserved in Campos basin, where mid Eocene, regressive successions unconformably overlie early Paleocene, transgressive successions (Fig. 3.4).

**Development of the Lagoa Parda channel complexes**

Two major hypotheses are presented here to explain the

development of the channel complexes LP-CC1 to LP-CC3. The first possibility, mostly **autocyclic**, considers the development of channel complexes by switching depocenters of feeding deltas or fan deltas along the basin margin. The second scenario, essentially **allocyclic**, considers the development of channel complexes by the interaction of (a) tectonics, (b) sediment supply, and (c) sea-level fluctuations. Both hypotheses are essentially qualitative and tentative due to the limitations of the data base; the area studied in detail comprises only 7.5 km$^2$, and there is a lack of preservation in the Espírito Santo basin of the early Eocene, shallower-water sedimentary record.

**Autocyclic hypothesis:** According to a mostly autocyclic hypothesis, the establishment of a new channel complex would take place following the migration of deltas or fan deltas toward a position where their coarse-grained sediments would be remobilized and then resedimented preferentially in the Regência canyon. Conversely, the building of a channel complex would stop with the switching away of the feeding depositional systems. However, the establishment and migration of coastal depositional systems would probably not take place by a purely autocyclic mechanism, considering the high relief, fault-controlled margin of the early Eocene Espírito Santo basin.

The trend of decreasing grain size and thickness of channel fills exhibited by LP-CC2 (Fig. 4.11) could be related to the gradual withdrawal of delta/fan delta depocenters.

During this time: (1) the amount and rate of accumulation of coarser-grained sediments in areas more susceptible to failure would decrease, with turbidity currents becoming less frequent and finer-grained; and (2) the littoral-drift systems intercepted by the Regência canyon would get progressively more depleted in coarser-grained sediments. Eventually, this process could lead to the interruption of turbidite sedimentation in the Regência canyon, which would then be blanketed by mudstones. This autocyclic interpretation would imply that the deposition of individual channel complexes would have taken place during time intervals shorter than the previously estimated 144,000 years. On the other hand, successions of coarsening- and thickening-upward channel fills also should be expected as a result of the gradual return of the feeding depositional systems. Thus, the absence of successions of coarsening- and thickening-upward channel fills in the Lagoa Parda turbidite system would represent another major problem with respect to a purely autocyclic control on the development of the studied channel complexes.

**Allocyclic hypothesis:** During the early Eocene, the Espírito Santo basin was still an immature passive margin basin, recording important uplift in the adjacent hinterland and along its faulted margin, which was probably characterized by a narrow and steep shelf. In this setting, the effects of sea level fluctuations on moving clastic depocenters landward and seaward across the shelf would be minor, with the source

areas remaining relatively close to the shelf/slope break even during highstands. Additionally, the interpretation of channel complex development controlled purely by eustatic sea-level falls has problems regarding their required 144,000 year reccurrence. Growth and melting of continental ice masses is the only well-known mechanism that can induce eustatic sea-level to change at this frequency (e.g. Pitman, 1978; Pitman and Golovchenko, 1983; Revelle, 1990). However, the early Eocene has been considered the warmest part of the Tertiary (e.g. Savin, 1977; Shackleton and Boersma, 1981), and most of the paleoclimatic studies based on the fossil record and oxygen stable isotopes suggest that important development of continental ice sheets did not take place before about 40 Ma (transition Eocene/Oligocene; e.g. Crowley, 1983; Miller et al., 1987; Prentice and Matthews, 1988).

The tectonic activity in the early Eocene Espírito Santo basin probably exerted an important control on sediment supply (as discussed in section 4.5.2) and local sea level fluctuations. However, tectonic reactivations are typically spaced at larger time intervals than the average duration (about 144,000 yr.) of the channel complexes included in the *Neochiastozygus chiastus* zone (e.g. Blair and Bilodeau, 1988; Vail et al., 1991). Therefore, the effects of tectonic activity are better recognized in successions composed of more than one channel complex (e.g. LP-CC1 to LP-CC3 combined), which were developed in a larger time span (section 4.4.5).

Variations in the sediment supply along the Espírito
Santo basin margin could have been influenced also by climatic
changes, which may occur during shorter time periods,
particularly due to cyclic, astronomical perturbations in the
Earth's tilt and orbit. These climatic fluctuations, organized
into "Milankovitch cycles", are induced by cyclic changes (1)
in the Earth's axial precession relative to perihelion (modes
at 19,000 and 23,000 yr.), (2) in the Earth's axial obliquity
(modal period of 41,000 yr.), and (3) in the Earth's orbital
eccentricity (several modes, e.g. 98,000, 126,000, 413,000,
and 1,300,000 yr.) (e.g. Imbrie and Imbrie, 1980; Fisher,
1991). The combination of these astronomical changes defines
climatic cycles by influencing the seasonal distribution of
incoming solar radiation on Earth. A mostly warm and humid
paleoclimate is interpreted for the eastern Brazilian coast
during the early Eocene (e.g. Parrish and Curtis, 1982;
Parrish et al., 1982), but it is very probable that climatic
fluctuations took place during the sedimentation of the
*Neochiastozygus chiastus* zone (time span of 1.3 m.y). The
average duration of the Lagoa Parda channel complexes (144,000
yr.) suggests changes in the Earth's orbital eccentricity.
Milankovitch (climatic) cycles probably did not induce
eustatic sea level fluctuations in the early Eocene because of
the lack of important continental ice sheets (e.g. Crowley,
1983; Miller et al., 1987; Prentice and Matthews, 1988).
However, cyclic periods of higher seasonal precipitation would

have induced higher denudation rates in the source area, and hence higher rates of sediment supply at the basin margin. The highest peaks of mechanical denudation rates are reached in temperate humid zones when seasonal or annual rainfall surpass their average levels. In this case, denudation is even higher than that shown by poorly forested semi-arid areas. The highest sediment yield of rivers is found in high relief, tropical regions (e.g. Taiwan, New Guinea, and Hawaii), due to the combination of rapid weathering and abundant running water (Einsele, 1992). For example, in areas with high seasonal precipitation the erosion rates may be twice those in semi-arid areas with the same relief (Stow et al., 1985).

The scenario described above suggests the interpretation that **climatically-controlled sediment supply at the basin margin would have represented the most important control on the development of the Lagoa Parda channel complexes.** In this context, the deposition of each channel complex would have followed an increase in sediment supply through delta/fan delta systems, which in turn would have responded to phases of higher denudation rates in the high relief, ancestral Serra do Mar and Serra da Mantiqueira. These pulses of increasing sediment supply would have been able to shift coastal depocenters seaward, and possibly to induce short-term, **relative** sea level falls. However, the relative sea level falls would have had a reduced magnitude, as suggested by the lack of regional unconformities or local erosion surfaces

bounding the Lagoa Parda channel complexes.

Fluctuations in sediment supply may have controlled the recurrent development of channel complexes in the Regência canyon during part of the early Eocene. However, the ongoing fault-controlled subsidence and the long-term trend of sea level rise did not allow the change from an overall transgressive setting to a regressive regime in the Espírito Santo basin until the latest early Eocene.

## 4.5.4. Growth of asymmetrical levees and channel avulsion

### Levee development

The Lagoa Parda turbidite system records a well-defined relationship between higher levee topography and narrower, thinner, and finer-grained (facies LP-F2 to LP-F4) channel fills (Fig. 4.11). Most of the very coarse-grained channel fills (LP-F1) do not have associated levees (LP-CC1 and lowermost LP-CC2 channel fills; Fig. 4.11); these channels were more deeply excavated, and their phases of filling typically record a progressive enlargement (e.g. channel 15 in Fig. 4.23b; and channel 13 in Fig. 4.24b).

Studies on Navy fan, off California (Piper and Normark, 1983; Bowen et al., 1984), and Laurentian fan, off southern Newfoundland (including the 1929 Grand Banks turbidity current; Stow and Bowen, 1980; Piper et al., 1988), have found that turbidity currents carrying a high proportion of mud are

slower and thicker than those that are predominantly sandy. On the other hand, turbidity currents enriched in coarse-grained sediments tend to be not only faster, but also more erosive, particularly if moving on relatively steep slopes (e.g. Menard, 1964; Shepard and Dill, 1966; Komar, 1973, 1977; Parker, 1982; Fukushima et al., 1985; Siegenthaler and Buehler, 1986; Normark and Piper, 1991).

The set of field evidence, experimental data, and theoretical considerations presented above support the interpretation that LP-CC1 and the lower part of LP-CC2 record the activity of strongly-erosive turbidity currents, enriched in coarser-grained sediments. These flows probably had a relatively reduced thickness; therefore, small amounts of sediments overspilled channel banks to build levees. Levees only started to grow in the Lagoa Parda field area when the turbidity currents became thicker and enriched in finer-grained sediments. At the beginning, levee relief was very subtle (levee successions A and B; Fig. 4.11), but following the development of channel 28 (uppermost part of LP-CC2 and LP-CC3), a more prominent levee topography was established in the Lagoa Parda area (levee successions C to I; Figs. 4.11, 4.23, and 4.24). The finer-grained turbidity currents responsible for levee development had less power to erode the substrate; therefore, the channel fills associated with the highest levees are typically narrower and thinner than the unleveed channel fills (Fig. 4.11).

The lowermost levee successions of LP-CC2 and LP-CC3 (A, B, C, D, G, and H; Figs. 4.23 and 4.24) typically display upward decreasing resistivities, which are induced mostly by their fining- and thinning-upward sandstone beds or by their overall muddier-upward character. The growth of levees seems to be related to the increasing dominance of finer-grained and thicker turbidity currents in the Lagoa Parda channels. Therefore, the levee successions also comprise mostly muddier-upward successions. Eventually, smaller-scale trends of upward decreasing resistivities can be recognized within some of the levee successions; they are probably related to fluctuations in the flow energy, and in the associated grain-size of transported sediments and flow thickness. The definition of thinner, muddier-upward successions also can be considered a result of the building of most of the levee successions by sediments spilling out from more than one channel (Table 4.6).

The uppermost levee successions of LP-CC2 and LP-CC3 (E and F, and I, respectively; Figs. 4.23 and 4.24) are mostly mud-rich, but they show upward increasing resistivities, which are induced mainly by an upward increasing concentration of siderite ($FeCO_3$), rhodochrosite ($MnCO_3$), and pyrite ($FeS_2$) in LP-F3 mudstones (e.g. Fig. 4.19b). The origin of these minerals is related to the degradation of the organic matter contained in the sediments by sulphate-reducing bacteria, which takes place preferentially in sub-oxic environments (e.g. Coleman, 1985; Curtis, 1977). Slower rates of

sedimentation favour more extensive degradation of organic matter and the generation of larger amounts of $CO_2$ and $H_2S$. Higher concentrations of $CO_2$ and $H_2S$ favour the precipitation of siderite/rhodochrosite and pyrite, respectively. This is because the oxygenated (respiration) zone rarely exceeds the uppermost 10 cm of accumulated sediments, and the sulphate reduction zone frequently is thicker than one or two meters (Curtis, 1987). The provenance of the iron and manganese for the precipitation of these early diagenetic minerals is related to the intense early Eocene volcanic activity, particularly in the Abrolhos volcanic complex (85 km northeast of the Lagoa Parda field; Fig. 2.5).

The muddier-upward character and the early diagenetic minerals within the uppermost deposits of LP-CC2 and LP-CC3 suggest that terminal stages of sedimentation in these two channel complexes were characterized by lower rates of sedimentation and progressive channel abandonment. The youngest sediments of LP-CC2 fill channels 34 and 35, which were excavated after the accumulation of levee succession F (Figs. 4.11 and 4.23). As suggested by their fine-grained filling facies (LP-F3) and higher sinuosity (Fig. 4.33), they were probably excavated and actively filled by lower energy, quasi-steady flows of longer duration, although they also may have received sediments overspilled from channels located ouside the study area. On the other hand, the end of the growth of LP-CC3 is marked in the study area by levee

succession I, which is probably related to channel(s) located outside the Lagoa Parda field.

**Levee asymmetry**

The levee successions mapped in the Lagoa Parda turbidite system are typically asymmetrical, i.e. they are higher and thicker on the left side (looking downstream) of associated channels (Table 4.6 and Figs. 4.11, 4.23, 4.24b, 4.34, and 4.36). This asymmetry is probably due to Coriolis force, which produces an apparent deflection of all particles of matter in motion on the Earth's surface (including sediments transported by turbidity currents), perpendicularly to their direction of motion. This deflection is to the right in the Northern Hemisphere, and to the left in the Southern Hemisphere. Therefore, the Coriolis effect would favour the preferential aggradation of left levees of submarine channels located in Southern Hemisphere, as shown by the Lagoa Parda turbidite system. The Coriolis force ($F$) can be expressed as

$$F = 2 \, m \, u \, \Omega \, \sin \phi$$

where $m$ is the mass of the sediment/water mixture in the turbidity current, $u$ is the velocity of the main body of the turbidity current, $\Omega$ is the Earth's angular velocity (= 7.29 x $10^{-5}$ rad/s), and $\phi$ is the latitude; therefore the Coriolis effect would be minimal closer to the Equator, where $\phi$ would approach zero.

Asymmetrical levees associated with recent submarine

channels have been recognized both in the Northern Hemisphere (e.g. Chough and Hesse, 1976, p.530; Cremer et al., 1985, p.118; Nelson and Maldonado, 1988, p.703; O'Connell et al., 1991, p.266) and Southern Hemisphere (e.g. Droz and Mougenot, 1987, p.1358; Carter and Carter, 1988, p.190; Viana et al., 1990, p.322). Paleogeographic reconstructions (e.g. Parrish et al., 1982; Scotese et al., 1988) permit the estimation of a paleolatitude of only 20 to 25°S for the early Eocene Lagoa Parda turbidite system. However, levee successions with well-developed asymmetry have been recognized in present latitudes as low as 19°S (Droz and Mougenot, 1987) or 22°S (Viana et al., 1990). Bowen et al. (1984) express the difference in levee height due to Coriolis effect ($\nabla h_{Coriolis}$) as

$$\nabla h_{Coriolis} = W\ h\ .\ 2\ \Omega\ \sin\ \phi\ /\ u$$

where **W** is the channel width, and **h** is the thickness of the main body of the flow. This equation is valid only for straight partions of channels, where centrifugal effects are null. It follows from the studies of Bowen et al. (1984) that thicker and slower, finer-grained turbidity currents could give rise to levees with more prominent asymmetry than thinner and faster, coarser-grained turbidity currents, even if located at lower latitudes.


**Channel avulsion**

The low sinuosity, Lagoa Parda channel fills record successive channel abandonment, probably through relatively

rapid avulsions, which sometimes may have involved levee breaching. Lagoa Parda channel fills do not have the lateral accretion surfaces or the mega-foreset bedding recognized in some meandering, channel fill turbidite sandstones (e.g. Mutti and Normark, 1991; Bouma and Coleman, 1985; Bouma, 1990). The style of channel avulsion, mostly through relatively "quick jumps", precluded the development of sandier-upward levee successions on one side of the leveed channels; this should be expected toward the direction of gradual, channel lateral migration.

Most of the LP-F1 channel fills suggest random avulsions (Fig. 4.11). However, channel fills 28 to 33 (channel complex LP-CC2, mostly facies LP-F2) define an **average** southeast trend of avulsion (to the right, looking downstream; Figs. 4.11, 4.24b, and 4.32). LP-CC3 channel fills (facies LP-F2) also present a trend of avulsion (toward southwest, or to the right, looking downstream; Fig. 4.35). Both trends of preferential avulsion direction are oriented in an opposite way to the direction of preferential levee growth, on the left side of the channels (Figs. 4.11). Additionally, the establishment of avulsion direction trends coincides with the growth of higher, asymmetrical levees (levee successions C to F in LP-CC2, and levee successions G and H in LP-CC3; Fig. 4.11). Therefore, levee topography represented an important control on channel avulsion in the Lagoa Parda turbidite system. On the other hand, the high degree of cannibalization

shown by Lagoa Parda channel complexes (most of the channel fills are at least partially eroded by younger channel fills) seems to be related to the combined effects of the large sediment supply, the erosive power of high-density turbidity currents moving on relatively steep slopes, and the reduced width (< 6 km) of the early Eocene Regência canyon.

## 4.5.5. Decreasing grain-size, thickness, and width of channel fills

The association of the channel complexes LP-CC1, LP-CC2, and LP-CC3 form a turbidite succession that is characterized by channel fills that become narrower, thinner, and finer-grained upward (Table 4.5 and Fig. 4.11). These trends were developed during a period of more than 400,000 years, a time span larger than that presented by the climatically-induced fluctuations in sediment supply, which may have represented the major controls on the development of **individual** channel complexes.

The faults that define the margins of the Regência canyon (Fig. 4.3) and the fault responsible for exhuming Precambrian basement along its western part (Fig. 4.4) suggest a gradually decreasing tectonic activity during the deposition of the uppermost part of the early Eocene *Neochiastozygus chiastus* zone. This biozone has a very reduced thickness in the westernmost part of the Regência canyon (Fig. 4.4) and beyond

the fault-controlled, northern margin of the canyon (Fig. 4.3). To the south, the turbidite-bearing *Neochiastozygus chiastus* zone is confined to the Regência canyon, and is truncated by late early Eocene sediments of the marine regressive megasequence (Fig. 4.3). The early Eocene structural evolution of the Regência canyon area also records a progressive basin tilting to the south. This tilting induced the transfer of the major site of subsidence and erosion along the canyon to a position southward, as indicated by the thickness distribution of the latest early Eocene sediments (*Discoaster lodoensis* zone; Fig. 4.3).

The decreasing tectonic activity in the Regência canyon area suggests a similar trend in the source area to the west, which would have influenced turbidite sedimentation by reducing the longer-range sediment supply. The progressive erosion of uplifted continental blocks and the decreasing slope in the source area would decrease the amount and rate of accumulation of coarser-grained sediments in areas more susceptible to failure. As a result, slope failures into the Regência canyon would gradually become smaller, less frequent, and finer-grained, giving rise to finer-grained turbidity currents with longer reccurrence interval and decreasing erosional power. Such a decreasing capability in eroding the substrate would favour a gradual reduction in channel cross-sectional area. In a scenario of decreasing fault activity and sediment supply there would also be a lesser incorporation of

coarse-grained sediments into the littoral drift systems eventually intercepted by the Regência canyon.

The tectonically-induced, southward tilting of the basin may explain the increasing importance of turbidity currents that originated from the smaller tributary troughs carved at the northern margin of the Regência canyon (paleoflow orientation mostly from NW to SE; Fig. 4.1). Turbidity currents flowing along the main thalweg of the Regência canyon (from SW to NE; Fig. 4.1) contributed to the building of the lowermost channel complex only.

The long-term, eustatic sea level rise of the late Paleocene/early Eocene (Fig. 4.37) may also have influenced the accumulation of successively narrower, thinner and finer-grained channel fills. This prolonged sea level rise may have moved coastal depocenters landward; therefore, it also may have contributed to the reduction in sediment input (and related turbidity current triggering). The absence of retrogradational stacking in the Lagoa Parda turbidite system is probably due to its structural confinement (Figs. 4.1, 4.3 and 4.4); the study area was always close to the canyon head (2 to 8 km) and its northern margin (< 1 km).

The shorter-term, climatically-induced increments in sediment supply would have been able to reestablish channel complexes in the Lagoa Parda field. However, they were incapable of modifying the overall trends of narrower, thinner, and finer-grained channel fills (Fig. 4.11), which

were induced by the longer-term, decreasing fault activity and rising sea level.

## 4.5.6. Conclusions

The canyon-confined, Lagoa Parda turbidite system is included in the marine transgressive megasequence, which is characterized by onlapping, deepening-upward sedimentation throughout the eastern Brazilian marginal basins. Its internal architecture resulted from the complex interaction of autocyclic and allocyclic factors, operating at different time scales.

Three channel complexes (average duration of 144,000 years) can be mapped in the Lagoa Parda field, on the basis of thicker interbedded mudstones, different filling facies, and changes in dominant turbidity current flow direction. Individual channel complexes were developed mostly in response to climatically-controlled phases of increasing sediment supply, via delta/fan delta and littoral drift systems. These pulses of increasing sediment supply would have been able to shift coastal depocenters seaward across a narrow and steep shelf, thus possibly developing short-term, relative sea level falls. These relative sea level falls would have had a reduced magnitude, as suggested by the lack of regional unconformities or local erosion surfaces bounding the channel complexes.

The three Lagoa Parda channel complexes form a turbidite

succession characterized by channel fills that become narrower, thinner, and finer-grained upward. This succession is associated with progressively finer-grained, less frequent, and less erosive turbidity currents. These trends were induced mostly by a longer-term (> 400,000 years) decrease in sediment supply, which in turn resulted from the combined effects of the overall, eustatic trend of sea level rise, and the decreasing fault activity at the basin margin and source area.

Lagoa Parda channel complexes were built by turbidity currents developed along the main thalweg of the Regência canyon (from SW to NE), or by turbidites that originated from smaller tributary troughs carved at the northern margin of the canyon (mostly from NE to SW). The two uppermost channel complexes were built almost exclusively by southbound turbidity currents, due to the progressive, tectonically-induced southward tilting of the basin.

Individual channel complexes are mostly characterized by coarse-grained channel fills, which may show associated levee deposits. Levee development was favoured by finer-grained, slower, and thicker turbidity currents. Levee successions are typically asymmetrical (higher and thicker on the left side of associated channels), probably as an effect of Coriolis force. The low sinuosity, Lagoa Parda channel fills record successive channel abandonment through relatively rapid avulsions. Avulsions of unleveed channels took place randomly. On the other hand, channels with well-developed levees record

preferential avulsion to the right (looking dowstream), in an opposite way to the direction of preferential levee growth; this suggests that levee topography represented an important autocyclic control on channel avulsion.

Most of the Lagoa Parda channel fills are at least partially truncated by younger channel fills, and the channel complexes are characterized by extensive amalgamation of conglomerate/sandstone bodies. This high degree of cannibalization seems to be related to the combined effects of the large sediment supply, the erosional power of high-density turbidity currents moving on relatively steep slopes, and the reduced width (< 6 km) of the early Eocene Regência canyon.

# 5. SYNTHESIS

The Carapeba/Pargo and Lagoa Parda turbidite systems are composed of thick successions of coarse-grained turbidites that fill fault-controlled canyons. These canyons were deeply incised into the slope and shelf of tectonically active, immature passive margin basins. The Carapeba/Pargo turbidite successions form non-channelized (tabular or lobate) sandstone bodies that normally occupy the entire width of the Carapeba/ Pargo canyon. By contrast, Lagoa Parda coarse-grained turbidites comprise relatively restricted channel fills with variable width, thickness, and orientation, which may be laterally associated with asymmetrical, finer-grained levees. Both of these turbidite systems form part of an overall transgressive succession, developed along the eastern Brazilian margin during the long-term trend of sea level rise of the late Cretaceous and early Tertiary.

Few turbidite systems displaying the characteristics summarized above have been described in the literature. Most of their geometrical and stratigraphic relationships summarized above **can not** be explained by any of the widely-used submarine fan models (e.g. Mutti and Ricci Lucchi, 1972;

Normark, 1978; Walker, 1978; Mutti, 1985) nor by reference to studies of modern submarine fans (e.g. Bouma et al., 1985a; Weimer and Link, 1991; and references therein). Therefore, many of the findings of this thesis may represent important contributions to the establishment of a depositional model for transgressive turbidite systems accumulated in immature passive margin basins.

**The main purpose of this chapter is to present a tentative depositional model for transgressive turbidites from immature passive margin basins, which is elaborated in section 5.5.** The preceeding sections of this chapter include:

(1) a summary of the concepts and problems involved in the comparison between the turbidite systems described in this thesis and widely-used submarine fan models, such as the channel-feeding-lobe models of the 1970's (e.g. Mutti and Ricci Lucchi, 1972; Normark, 1978; Walker, 1978) **(section 5.1)**, and the eustatically-driven model of Mutti (1985) **(section 5.2)**;

(2) a synthesis of the most important ideas derived from studies of modern submarine fans (which are dispersed through many detailed descriptions of individual fans), and a summary of major differences and similarities between modern fans and the studied turbidite systems **(section 5.3)**;

(3) a summary of the most important characteristics of the outcropping turbidite system of the Almada basin (Bruhn and Moraes, 1989), which is the same age as the early

Maastrichtian Carapeba/Pargo turbidite successions, but displays similar facies to those of the early Eocene Lagoa Parda turbidite system **(section 5.4)**. The Almada turbidite system records an important segment of the history of turbidite sedimentation along the eastern Brazilian margin. The integration of the studies of the Almada (Bruhn and Moraes, 1989) and Carapeba/Pargo and Lagoa Parda (this study) turbidites permits a more complete description of the changing styles of turbidite sedimentation developed during the long-term trend of sea level rise of the Coniacian to early Eocene **(also attempted in section 5.5)**.

The last two sections of this chapter show how the turbidite systems studied in this thesis fit into the widely-used Exxon's sequence-stratigraphic scheme (e.g. Posamentier and Vail, 1988; Van Wagoner et al., 1990; Vail et al., 1991) **(section 5.6)**, and how the major contributions of this thesis can be applied to oil exploration and production from similar turbidite systems **(section 5.7)**.

## 5.1. SUBMARINE FAN MODELS OF THE 1970'S

Some very influential depositional models for submarine fans were published in the 70's. These models were based on descriptions of outcrops (Mutti and Ricci Lucchi, 1972, 1974, 1975; Mutti and Ghibaudo, 1972; Mutti, 1977, 1979), on the

acoustic and seismic characterization of recent fans (Normark, 1970, 1978), as also on the integration of both sources of information (Walker and Mutti, 1973; Walker, 1978). Despite their differences, all of these **channel-feeding-lobe submarine fan models (C-F-L models)** typically have three major morphologic divisions (Fig. 1.1). The upper fan portion comprises one single, large channel or fan valley, characterized by prominent levees, where lenticular conglomerates and massive sandstones tend to accumulate (Fig. 1.1). The middle fan is typified by depositional lobes (named "suprafan lobes" by Normark, 1978). In the upper parts of the depositional lobes the turbidity currents flow through many channels, which are narrower and shallower than the single leveed-channel of the upper fan; they also have poorly developed levees. Massive and stratified sandstones tend to be deposited within the smaller channels of the middle fan, whereas thick-bedded turbidites with Bouma divisions accumulate preferentially on the unchannelized outer portions of the middle fan (Fig. 1.1). The lower fan is a topographically smooth, low-gradient area, characterized by the accumulation of hemipelagic muds and thin-bedded turbidites.

By analogy with deltaic deposits, Mutti and Ghibaudo (1972) introduced the idea that thickening- and coarsening-upward successions can be produced during progradation of depositional lobes, and thinning- and fining-upward

successions may represent gradual channel filling and abandonment. These ideas were incorporated into the outcrop-based models (e.g. Walker and Mutti, 1973; Mutti and Ricci Lucchi, 1974; 1975; Walker, 1978), and became very influential. As a result, the recognition of turbidite environments (particularly channels and lobes) has been influenced by the presence of thickening (or thinning) upward and coarsening (or fining) upward successions, rather than by the external geometry of these deposits (e.g. Ghibaudo, 1980; Link and Nilsen, 1980; Link and Welton, 1982). The problems involving the use of these criteria are twofold: (1) trends in bed thickness and grain size variation may be subtle, thus requiring the application of statistical tests for their recognition (e.g. Waldron, 1987; Pickering et al., 1989); and (2) thinning (and fining) upward successions can be produced in more than one way; e.g. channel lateral migration and abandonment; gradual lobe shifting, with lobe margin replacing lobe center depositional environment; and levee building by gradually finer-grained turbidity currents.

C-F-L models are purely autocyclic (sedimentological). They do not consider the influence of allocyclic factors (e.g. tectonics, sediment supply, and sea level fluctuations) on facies development and geometrical variations exhibited by the turbidite systems. They also ignore canyon-fill turbidites, and give little attention to channel-levee complexes.

In the following sections will be presented the major

problems involved in the comparison between C-F-L models and the turbidite systems described in this thesis; these are related to depositional setting, geometry of deposits, dominant facies, and facies successions.

## 5.1.1. Depositional setting

C-F-L models emphasize turbidite sedimentation at the end of a submarine canyon or feeder channel, in base-of-slope to deep basinal settings (e.g. Fig. 1.1). During the 70's, submarine canyons were considered mostly as conduits for turbidity currents, rather than favorable sites for coarse-grained turbidite accumulation; most of the ancient canyon fills described up to that time are largely mud-filled (e.g. Hoyt, 1959; Dickas and Payne, 1967; Cohen, 1976). Only a few descriptions of canyon fill, coarse-grained turbidites can be found in the literature of the 70's (e.g. Stanley, 1967; Stanley et al., 1978). Both Carapeba/ Pargo and Lagoa Parda turbidite systems occur within canyons deeply incised into the slope and shelf.

## 5.1.2. Geometry of deposits

C-F-L models suggest a typical radial profile for the submarine fans, with the geometrical variabilities in the turbidite systems being mostly produced by fan progradation or

switching in position of suprafan lobes (e.g. Fig. 1.1).

Turbidite systems entirely composed of a complex stacking of levee deposits and coarse-grained channel fills, like that of the Lagoa Parda field (e.g. Fig. 4.11), are not part of the C-F-L models. On the other hand, the Carapeba/Pargo sandstones may show lobate geometry (e.g. Figs. 3.37 to 3.39), but they also had their lateral extent controlled by fault activity and the resulting variable width of the Carapeba/ Pargo trough (e.g. Fig. 3.2). However, C-F-L models consider depositional topography and boundaries of sandstone bodies as purely controlled by sedimentological factors (e.g. lobe switching in position and compensation arrangements); they do not emphasize tectonic control on the geometry of deposits.

### 5.1.3. Dominant facies

C-F-L models depict the fans as composed mostly of lobes, which in turn comprise mainly classical turbidites (described by Bouma divisions; Bouma, 1962). The Carapeba/Pargo and Lagoa Parda turbidite systems are largely composed of thick, unstratified conglomerates and coarse-grained sandstones. In these systems, monotonous alternations of parallel-bedded mudstones and sandstones displaying Bouma divisions are very subordinate.

### 5.1.4. Facies successions

Carapeba/Pargo and Lagoa Parda turbidites typically form fining- and thinning-upward successions, which probably were not controlled by autocyclic factors, such as channel lateral migration and abandonment. These successions were mostly controlled by decreasing sediment supply, which in turn would have resulted from the combined effects of an overall, eustatic trend of sea level rise, and decreasing tectonic activity at the basin margin and source area (Carapeba/Pargo, section 3.5.3) or decreasing climatically-controlled denudation rates in the source area (Lagoa Parda, section 4.5.3).

## 5.2. MUTTI'S (1985) MODEL

Mutti (1985) introduced the important idea of allocyclic control on the development of different turbidite types found in the ancient record. He recognized the development of three main types of turbidite depositional systems mostly as a function of different sizes of slope failure, which in turn he related to sea level fluctuations (Fig. 1.5).

Larger slope failures and related larger gravity flows were thought to have developed during lower stands of sea level, giving rise to type I systems (Fig. 1.5b). Type I turbidites are characterized by thick-bedded, non-channelized, and widely-distributed sandstone bodies, which may grade

downcurrent into thinner-bedded and finer-grained fringe deposits. Type I systems do not show time-equivalent channel deposits in an upstream direction, except for coarse-grained lag deposits filling shallow erosional depressions (Fig. 1.5a).

Rising sea level and decreasing slope failures were believed to give rise to turbidite systems of types II and III, successively (Fig. 1.5b). Type II systems include coeval, physically-attached lobes and channel fills; these lobes are typically smaller than type I lobes, but also may grade downstream into thinner-bedded and finer-grained fringe deposits (Fig. 1.5a). Type III systems comprise mud-rich successions showing small (up 100 m wide, and 10 m thick) channel fills of medium- to fine-grained sandstones, which are enclosed by and grade downstream into muddy facies (levee, overbank, and basinal facies) (Fig. 1.5a).

The three types of turbidite systems may develop independently of one another, or successively, in response to sea level fluctuations. Besides introducing the concept of sea level control on turbidite sedimentation, another breakthrough in Mutti's (1985) model is the suggestion that: (1) turbidites of type I and II may occupy individually all of what used to be considered mid and lower fan by the classical models; and, (2) type III turbidites show similar facies to upper fan channel-levee complexes, but they tend to be younger than turbidites type I or II.

As with the C-F-L models, Mutti's (1985) model also has important limitations if it were to be used as a norm to understand the Carapeba/Pargo and Lagoa Parda turbidite systems. The major limitations of Mutti's (1985) model are: (1) Lagoa Parda turbidites consist mainly of coarse-grained channel-levee complexes, which do not fit into any of the three system types; (2) autocyclic controls on turbidite sedimentation are largely ignored; and (3) allocyclic controls on turbidite sedimentation are restricted to sea level fluctuations. Tectonically- and/or climatically-controlled variations in sediment supply probably exerted important influence on the development (and reccurrence) of Carapeba/Pargo successions and Lagoa Parda channel complexes, particularly because these systems accumulated in tectonically-(very) active, immature passive margin basins, during times of ice-free continents.

## 5.3. STUDIES OF MODERN SUBMARINE FANS

During the 80's, significant improvements in the acoustic and seismic characterization of recent fans have changed ideas about the internal composition of submarine fans, and their growth patterns. The best-studied recent fans are the Amazon (Damuth et al., 1983a, 1983b, 1988; Appi et al., 1988; Manley and Flood, 1988; Flood et al., 1991), Indus (McHargue and

Webb, 1986; Kolla and Coumes, 1987; McHargue, 1991), Mississippi (Bouma et al., 1985b, 1989; Stelting et al, 1985b; Weimer and Buffler, 1988; Weimer, 1989, 1990, 1991; Twichell et al., 1991), and Rhone (Droz and Bellaiche, 1985; O'Connell et al., 1991). Valuable information also has been gathered from Navy (Normark et al., 1979; Piper and Normark, 1983), Laurentian (Normark et al., 1983; Masson et al., 1985; Piper et al., 1988), Magdalena (Kolla et al., 1984), and Ebro (Nelson and Maldonado, 1988, 1990) fans. These studies have shown that the upper and middle portions of the recent submarine fans consist mostly (80 - 90 %) of mud-rich, channel-levee systems. The terminology "channel-levee system" was introduced by Damuth et al. (1983b, p.470) to designate "a depositional-erosional channel perched atop a wide natural levee ... that builds upward and laterally through time by overbank spilling" (Fig. 1.2). Equivalent terms provided by the literature are "lenticular acoustic unit" (Droz and Bellaiche, 1985), and "fanlobe" (Bouma et al., 1985b). The channel-levee systems frequently overlap, coalesce, or interfinger laterally, forming large tongue-like or elongate bodies named "channel-levee complexes" (Figs. 1.3 and 1.4). These observations from the modern fans contrast with the emphasis on sand-rich, lobe deposits given by the C-F-L models.

## 5.3.1. Seismic facies

Despite the fact that seismic studies of modern fans represent a major breakthrough in the understanding of the submarine fans, very little is known about the facies that form the fans and their stratigraphic relationships, largely because of few cores and little dating. However, the facies of modern fans have been interpreted on the basis of their seismic responses, which are characterized essentially by amplitude (low, fair, moderate, high), internal reflection configuration (parallel, subparallel, hummocky, mounded, chaotic, divergent), continuity of reflectors (continuous, discontinuous), external geometry of seismically-related successions (lens, wedge, sheet, mound), and even by the absence of reflectors (acoustically transparent). Several "seismic facies" schemes have been proposed (e.g. Kolla et al., 1984; Droz and Bellaiche, 1985; McHargue and Webb, 1986; Kolla and Coumes, 1987; Weimer, 1990). In general, the several seismic facies schemes are similar; some of the differences in intensity of amplitude and degree of continuity of the reflectors are induced by discrepancies among methods of acquisition and processing of the seismic data. A synthesis of these schemes is attempted below, in order to seismically characterize the five major components of the modern submarine fans; i.e. channel fills, levees, non-channelized turbidites, mass transport complexes, and slumps/debris flows related to levee failure.

(1) **Channel fills**: these comprise irregular to lenticular

packages of high-amplitude, discontinuous reflectors (e.g. Figs. 1.2 and 5.1). These reflections typically occur beneath the present channel axes (Figs. 1.2 and 5.1), and are interpreted as having been returned from interbedded coarse- and fine-grained sediments. A thick (> 100 m), fining-upward succession of gravel, sand, and mud was cored in a mid fan channel from the Mississippi fan (DSDP Leg 96, site 621; Stelting et al., 1985a; Stow et al., 1985b).

(2) **Levees**: these consist of wedge-shaped, concave-upward reflection packages, including low- to fair-amplitude, continuous to discontinuous, and diverging (toward channel) reflectors (e.g. Figs. 1.2 and 5.1). Cores of levee deposits from the mid Mississippi fan contain silt-laminated muds, structureless muds and clays, and very subordinate thin-bedded sandstones (DSDP Leg 96, sites 617 and 620; Stelting et al., 1985a; Stow et al., 1985b).

(3) **Non-channelized turbidites**: these consist of widespread, sheet-like packages of moderate- to low-amplitude, continuous, subparallel reflectors (e.g. Figs. 1.2 and 5.1). In the lower Mississippi fan, non-channelized deposits are dominated (38 - 48 %) by 10 cm- to at least 12 m-thick beds of fine sand to coarse silt (DSDP Leg 96, sites 614 and 615; O'Connell et al., 1985; Stow et al., 1985b)

(4) **Mass transport complexes**: these consist of mounded packages lacking internal reflections, or comprise low-amplitude, discontinuous reflectors with chaotic, mounded, or

Fig. 5.1 - Representative seismic-reflection profiles of the uppermost portion of the Amazon fan (Flood et al., 1991): (a) upper fan; (b) middle fan; and (c) lower fan. Typical seismic facies of channel fills (cf), levees (lev), non-channelized turbidites (nct), and mass transport complexes (mtc) are indicated.

TWO-WAY TRAVEL TIME (SECONDS)

2.5 —

UPPER FAN

lev

cf

c

3.5 —

4.5 —

MIDDLE FAN

cf

lev

nct

b

mtc

5.5 —

LOWER FAN

5.5 —

nct

a

6.5 —

10 KM
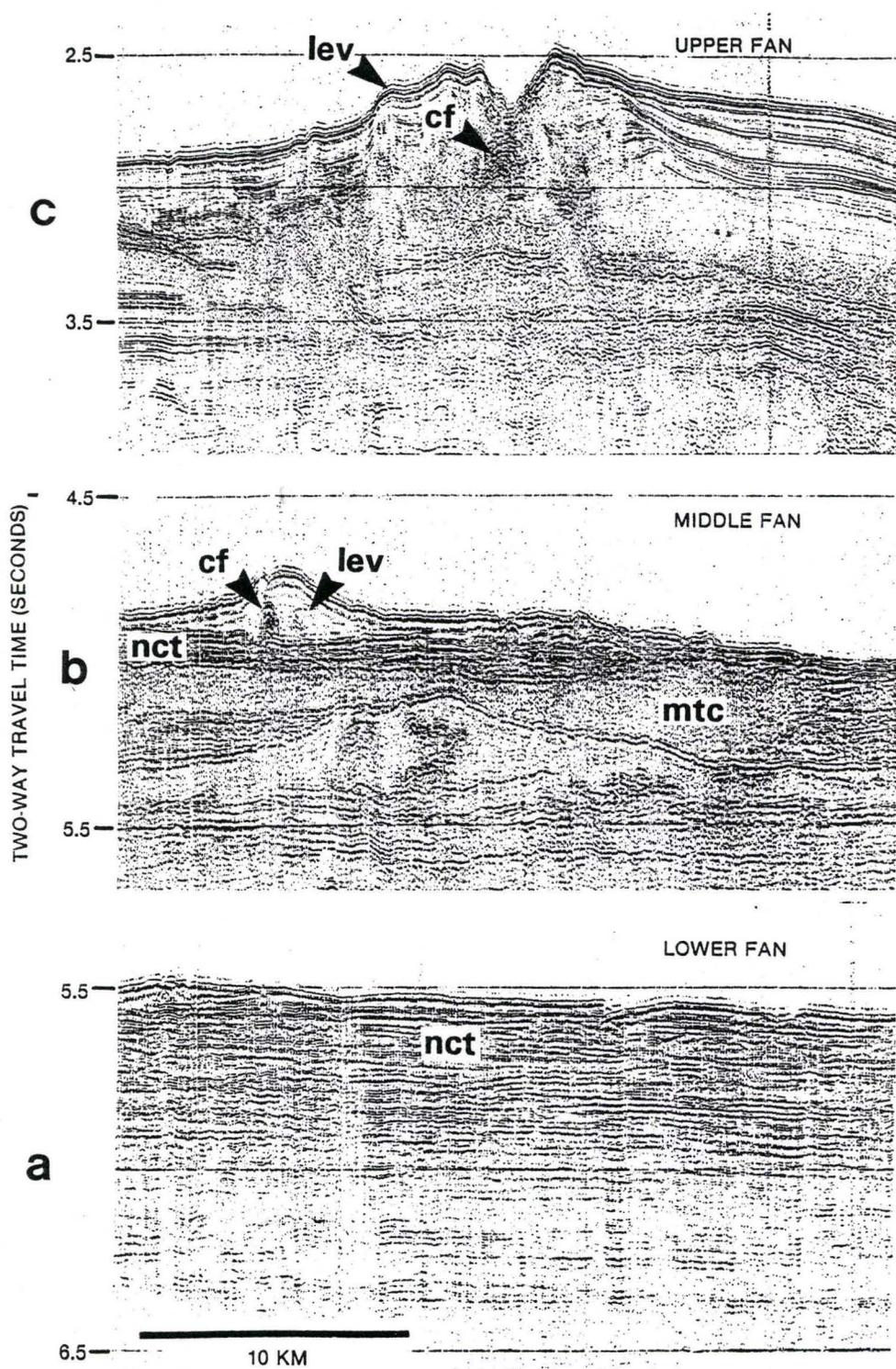
hummocky configuration (Figs. 1.2 and 5.1). Damuth et al. (1988) and Weimer (1989, 1990) interpreted mass transport complexes as associations of disorganized slides, slumps, and debris flow deposits. Three main geometrical types of mass transport complexes were found in the Mississippi fan (Weimer, 1989, 1990): (1) elongated (channel-like) and concave upward; (2) mounded in shape and convex upward; and (3) fan-shaped.

(5) **Slumps/debris flows related to levee failure:** these consist of localized, poorly-organized wedges of low- to fair-amplitude, discontinuous reflectors, which show chaotic, mounded, or hummocky configuration. Inclined or contorted layers of silt-laminated muds were cored in a levee from the middle Mississippi fan, which are probably related to slumping (DSDP Leg 96, site 617; Coleman et al., 1985; Stelting et al., 1985a). Failure of levee sediments is very likely in modern fans, particularly because of the relatively steep slopes (up to 9°; Damuth et al., 1988) that may occur on the backside of levee crests. Important slumps may also have originated from the continental slope, covering large areas of submarine fans, as suggested for the Rhone (Droz and Bellaiche, 1985) and Mississippi (Weimer, 1989, 1990) fans.

## 5.3.2. Facies successions

The analysis of the several modern submarine fans listed above permits the distillation of an overall lateral and

vertical (stratigraphic) organization of channel, levees, non-channelized turbidites, mass transport complexes, and slumps and debris flows related to levee failure.

Recent submarine fans include an upper fan portion characterized by gradients typically over 10 m/km, few channels (generally one at any given time) with well-developed levees. Probably the best seismic studies on the transition feeding canyon/upper fan of a modern fan were conducted in the Indus fan (McHargue and Webb, 1976; McHargue, 1991). McHargue and Webb (1976) recognized three zones in this transition: (1) a degradational zone comprising an erosional, unleveed canyon complex filled with prodeltaic mud; (2) a transitional zone located in the upper fan (but near the canyon mouth), which contains erosional, unleveed channels that are suceeded upward by leveed channels; and (3) an aggradational zone, typified by amalgamated, leveed channels.

The upper fan is followed downfan by the middle fan, where the gradients range from 10 to 3 m/km. In the middle fan the turbidity currents are distributed through sinuous distributary channels with gradually decreasing depths and widths (Table 5.1); also the channel fills (Table 5.1) and levees (Table 5.2) become thinner downfan. Lateral shingling of channels may represent an important characteristic of the middle fan (e.g. Rhone fan, Droz and Bellaiche, 1985; Amazon fan, Damuth et al., 1988, Manley and Flood, 1988). Channel sinuosity and channel bifurcation typically increase from

**Table 5.1 - Typical dimensions of channels and channel fills in modern submarine fans[a].**

| FAN PORTION | CHANNEL WIDTH (km) | CHANNEL DEPTH (m) | CHANNEL FILL WIDTH (km) | CHANNEL FILL THICKNESS[b] (m) |
|---|---|---|---|---|
| Upper fan | 1 - 10 | 50 - 300 | 1 - 12 | 100 - 800 |
| Middle fan | 0.5 - 3 | 20 - 80 | 0.5 - 6 | 20 - 400 |
| Lower fan | < 0.5 | < 20 | ----[c] | ----[c] |

[a] Based mostly on seismic profiles from the Amazon (Damuth et al., 1988; Manley and Flood, 1988; Flood et al., 1991), Indus (McHargue and Webb, 1986; Kolla and Coumes, 1987), Mississippi (Bouma et al., 1985; Stelting et al., 1985b; Weimer, 1989, 1990, 1991), and Rhone (Droz and Bellaiche, 1985) fans.

[b] Agraded (composite) thickness of seismic packages composed mostly of high-amplitude, discontinuous reflectors.

[c] The smaller size of lower fan channel fills makes difficult the estimation of their width and thickness.

**Table 5.2 - Typical dimensions of levees and channel-levee systems in modern submarine fans[a].**

| FAN PORTION | LEVEE WIDTH (km) | LEVEE THICKNESS (m) | CHANNEL-LEVEE WIDTH (km) | CHANNEL-LEVEE THICKNESS[b] (m) |
|---|---|---|---|---|
| Upper fan | 8 - 50 | 100 - 600 | 20 - 100 | 100 - 1,000 |
| Middle fan | 4 - 150 | 20 - 300 | 10 - 300 | 50 - 400 |
| Lower fan | | Poorly-developed levees | | |

[a] Based mostly on seismic profiles from the Amazon (Damuth et al., 1988; Manley and Flood, 1988; Flood et al., 1991), Indus (McHargue and Webb, 1986; Kolla and Coumes, 1987), Mississippi (Bouma et al., 1985; Stelting et al., 1985; Weimer, 1989, 1990, 1991), and Rhone (Droz and Bellaiche, 1985) fans. The term "channel-levee system" refers to an individual channel and its associated levees.

[b] Maximum thickness measured from the base of the lowermost channel fill to the top of the highest associated levee. Channel fills may truncate underlying channel-levee systems.

upper- to middle fan (Flood and Damuth, 1987; Weimer, 1991). Conversely, channel vertical aggradation and channel lateral migration (within the channel valley) tend to be greater in upfan areas (Weimer, 1991). Weimer (1991) found channel lateral migration of up to 12 km in the upper Mississippi fan; seismic profiles from the upper Indus fan (McHargue, 1991) suggest channel lateral migration of 8 to 12 km (e.g. Fig. 5.2).

The upper and middle portions of modern submarine fans are composed mostly (80 - 90 %) of channel-levee complexes, which in turn may comprise several channel-levee systems. For example, the uppermost channel-levee complex of the Amazon fan contains at least seven channel-levee systems (Fig. 1.4). However, mass transport complexes also can be very important; they may comprise thick (up to 250 m), and extensive (up to 40,000 km$^2$) deposits. Mass transport complexes may fill depressions between underlying channel-levee systems and smooth the fan surface (e.g. Amazon fan; Damuth et al., 1988; Manley and Flood, 1988; Figs. 1.2 and 5.1); alternatively, they may erode deeply (up to 200 m) into underlying channel levee systems (e.g. Mississippi fan; Weimer, 1989, 1990), and mimic the geometry of the overlying channels (elongated and concave upward).

The lower fan is characterized by gradients less than 3 m/km, and few (or no) channels. These channels are less sinuous and smaller (Table 5.1), and their levees are poorly

Fig. 5.2 - Interpreted evolution (a - c) of a channel from the upper Indus fan (McHargue, 1991). Dotted pattern indicates channel fills.

(a) Erosional channel associated with small levees.

(b) Early lateral migration of channel allowed continued growth and southeastward migration of the northwestern levee as the southeastern levee was eroded.

(c) Eventually, southeastward migration continued but in association with aggradation. At the time of abandonment, the channel complex was 10 km wide and 550 m thick, with levees 275 m thick. Total lateral migration of channel was about 7 km.

(d) Uninterpreted seismic profile on which this interpretation is based.

NW                    SE Sec.

d

5 Km
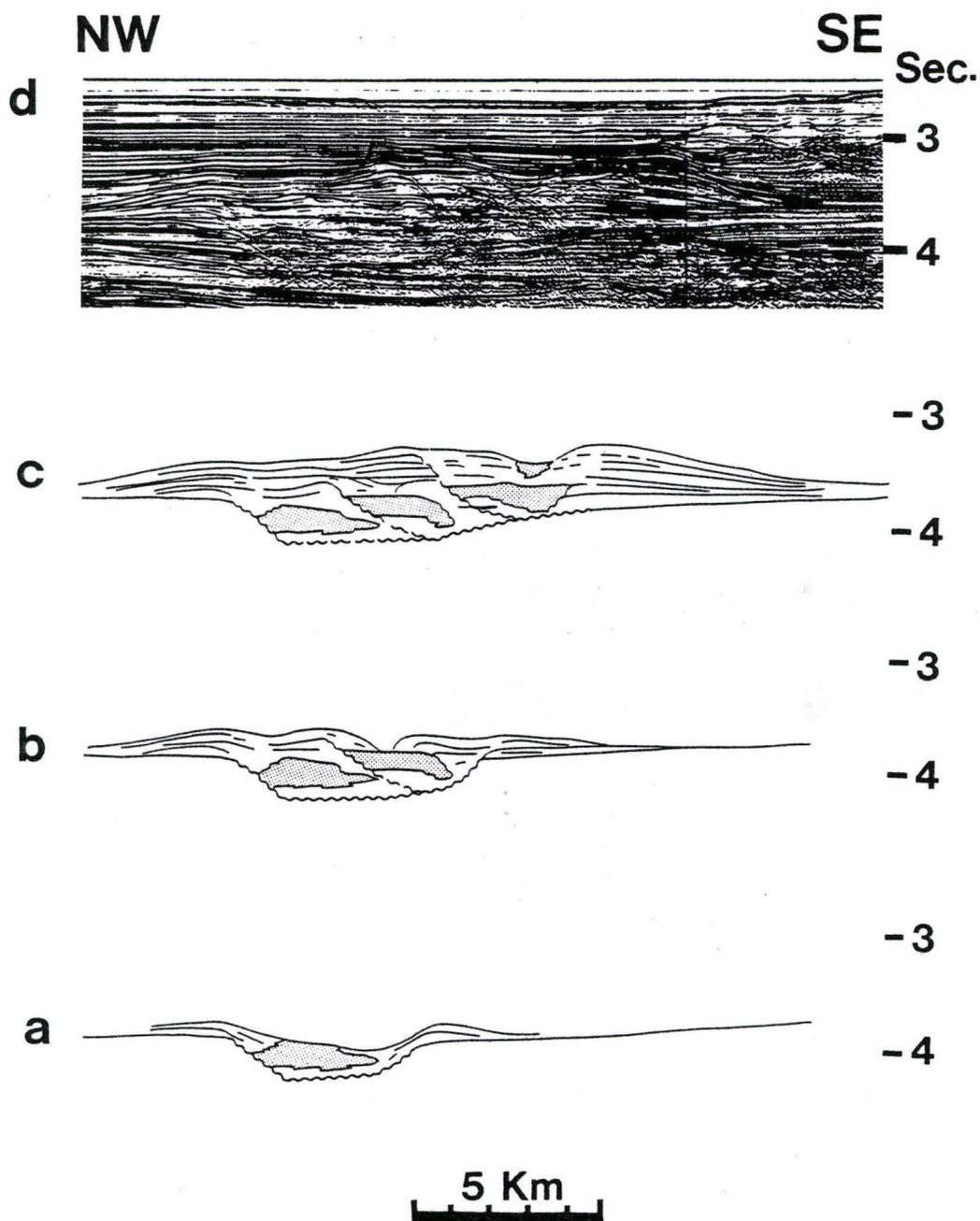
developed. Channel-levee systems and mass transport complexes pinch out as the lower fan is reached, and only widespread, non-channelized (sandy ?) turbidites tend to be found dowfan (Fig. 5.1). This change may take place over relatively short distance (only 10 km in the Amazon fan; Flood et al., 1991). In the middle to lower fan transition the mass transport complexes may show a fan-shaped distribution, increasing in width downfan (Mississippi fan; Weimer, 1990).

Data from the best studied modern fans (references above) support the distillation of at least two preliminary fan models (Walker, 1992; Fig. 5.3). The first model, largely based on the Mississippi fan, suggests that fan sedimentation may start with mass transport complexes, which fill depressions and/or scour older deposits, and are overlain by channel-levee systems (Fig. 5.3a). In the second model, more typical for the Rhone fan, deposition begins with basin-floor non-channelized turbidites, which are also overlain by channel-levee systems (Fig. 5.3b). In both models the lower fan comprises essentially sand-rich, non-channelized (sheet-like or lobate) turbidites.

Future studies will probably find variations on the two models of figure 5.3. In the middle Amazon fan, for example, thick (up to 200 m), disorganized deposits are overlain, successively, by sheet-like deposits and channel-levee systems (Manley and Flood, 1988; Flood et al., 1991; Figs. 1.2 and 5.1). However, these deposits have poorly-constrained ages,

Fig. 5.3 - Preliminary submarine fan models based mostly on studies of modern fans (Walker, 1992).

(a) Model in which fan deposition starts with a mass transport complex (basin floor fan in the terminology of figure 1.6), overlain by channel-levee systems.

(b) Model in which fan deposition starts with sheet-like basin floor turbidites, overlain by channel-levee systems. Note vertical stacking on upper fan (as in the Rhone fan) and lateral shingling on the middle fan. A more detailed explanation for this figure is presented in the text.

**a**

UPPER FAN

MASS TRANSPORT COMPLEX

HEMIPELAGIC DRAPE

CHANNEL-LEVEE SYSTEM

MIDDLE FAN

LEVEE-OVERBANK SLUMP

DEBRIS FLOWS AND TURBIDITES

basin floor fan

lowstand wedge

transgressive/highstand

LOWER FAN

UNCHANNELLIZED LOWER FAN

**b**

UPPER FAN

VERTICAL STACKING

MIDDLE FAN

LEVEE COMPLEX

LATERAL SHINGLING

CHANNEL-LEVEE SYSTEM

SEISMIC SEQUENCE

basin floor fan

lowstand wedge

transgressive/highstand (HEMIPELAGIC BLANKET)

LOWER FAN

UNCHANNELLIZED LOWER FAN (basin floor fan)

and can not be definitely assigned either to fan initiation (mass transport complexes) or to fan termination stages (continental slope and/or levee failures). Flood et al. (1991) suggested that large debris flows may be triggered by diapiric activity, hydrate instability, or sediment overloading at any time during fan growth. In the Rhone fan (Droz and Bellaiche, 1985), slides and slumps occur concurrently with development of channel-levee systems, and eventually are responsible for channel migration and avulsion. Description of cores from the Amazon fan has shown that lower fan deposits are sandier and older than channel-levee systems from the upper- and middle fans (Appi et al., 1988; Flood et al., 1991). However, the lower Rhone and Mississippi fans record relatively discontinuous (< 30 km wide, < 60 km long) depositional lobes that seem time-equivalent to the channel-levee systems located upfan (O'Connell et al., 1991; Twichell et al., 1991; Nelson et al., 1992).

### 5.3.3. Fan evolution

The initiation of fan growth has been related to lowering of relative sea level (e.g. Manley and Flood, 1988; Bouma et al., 1989; Weimer, 1990), when progradation of coastal depocenters toward the shelf/slope break stimulates slope failure, retrogressive slumping, and canyon initiation. Retrogressive slumping may enlarge the canyons (Coleman et al.

1983; Goodwin and Prior, 1989), and the remobilized sediments may give rise to mass transport complexes (Fig. 5.3a). The presence of older canyons preserved from previous sea level cycles would favour direct funnelling of sand down the canyons, and the accumulation of widespread, non-channelized turbidites on the basin floor.

Some studies on modern fans have suggested that continued lowering of relative sea level and/or lowstand conditions would stimulate the direct transport of fluvial and deltaic sediments via submarine canyons to build channel-levee systems onto either mass transport complexes (Fig. 5.3a) or non-channelized turbidites (Fig. 5.3b) (Kolla and Coumes, 1987; Manley and Flood, 1988; Bouma et al., 1989; Weimer, 1990). This idea contrasts with Mitchum's (1985) and Mutti's (1985) models, which suggest that channel-levee complexes tend to develop during relative sea level rise.

The passage from unconfined, sand-rich flows to confined, mud rich flows is still poorly understood. Walker (1992) suggested a theoretical possibility: "... levees [may] initially form on the walls of the incised canyon. As more and more flows use the canyon, with fines spilling up onto and over the levees, the levees lengthen onto the fan surface, and grow in height and width as more and more fine-grained material spills overbank. The suspended fines will lead to levee growth, and the sand will bypass the leveed part of the fan *en route* to the sandy lower fan" (Walker, 1992, p.254-

255).

Recent studies on the lower Rhone and Mississippi fans
(O'Connell et al., 1991; Twichell et al., 1991; Nelson et al.,
1992) have found relatively discontinuous (< 30 km wide, < 60
km long) depositional lobes that seem time-equivalent to the
channel-levee systems located upfan. The depositional lobes
recognized in the lower Mississippi fan are located at the end
of small, shallow (< 5 m) channels; they are believed to have
been deposited 13,000 to 15,000 years ago, in the transition
from lowstand to rising sea level conditions (Twichell et al.,
1991). The sand-rich lobe found in the Rhone fan (O'Connell et
al., 1991) is much younger; core samples from this lobe have
$C^{14}$ ages between 130 ± 50 and 5,250 ± 100 years (Mear, 1984),
suggesting deposition during the Holocene sea level rise.

Most of the studies on modern fans have suggested,
however, that relative rise in sea level would largely
decrease or end active sedimentation on the fan (e.g. Bouma et
al., 1989; Flood et al., 1991). During continuous sea level
rise or highstand the fan surface would be blanketed mostly by
thin, muddy hemipelagic sediments, which eventually would
comprise extensive condensed sections (e.g. Weimer, 1989,
1990). Slumps and debris flows of variable sizes, originating
both from levee- and continental slope failures, could occur
at any time during a sea level cycle. However, the largest
slumps and debris flows recorded so far have been interpreted
as the latest sediments on the fan surface (e.g. up to 200 m

thick, covering up to 46,000 km$^2$ on the Amazon fan; Damuth and Embley, 1981; Damuth et al., 1988).

### 5.3.4. Comparison between modern fans and the studied turbidites

Six major problems are involved in the comparison between modern fans and the studied turbidites:

(1) They have very different scales; for instance, some modern channel-levee systems may be 50 times wider than the Regência canyon, and lower fan sheet-like turbidites may exceed the entire Campos basin in area.

(2) The best studied modern fans occur in **mature** passive basins, where the effects of sea level fluctuations on turbidite sedimentation tend to greatly surpass the influence of tectonics.

(3) As a consequence of their tectonic setting, most modern fans do not show a strong fault control on the geometry of their deposits.

(4) Most modern fans contain mud-rich successions, with subordinate coarse-grained turbidites; this may also be a consequence of their tectonic setting.

(5) The largest modern submarine fans accumulated during the long-term trend of sea level fall of the late Tertiary and Quaternary, whereas the sedimentation of the Carapeba/Pargo and Lagoa Parda turbidite systems took place during the long-

term trend of sea level rise of the late Cretaceous and early Tertiary.

(6) Very little is known about recent sedimentation in submarine canyons, particularly during the Pleistocene lowstand.

However, some important similarities exist between the modern channel-levee systems and the Lagoa Parda turbidite system:

(1) The evolution of channel-levee systems from the upper Indus fan (McHargue and Webb, 1986; McHargue, 1991) shows degradational (erosional) channels with poorly-developed (or no) levees, which are succeeded upward by aggradational, leveed channels. Additionally, both the lateral extent and thickness of seismic packages of high-amplitude, discontinuous reflectors (coarse-grained channel fills) decrease upward. These trends agree remarkably well with observations from the Lagoa Parda turbidite system (Fig. 4.11).

(2) Modern fans (e.g. Mississippi and Indus fan) may show consistent trends of channel lateral migration and avulsion (e.g. Fig. 5.2), and asymmetrical levees, which may represent effects of Coriolis force. Similar features occur in the two uppermost Lagoa Parda channel complexes (LP-CC2 and LP-CC3; Figs. 4.11 and 4.24b).

(3) Many of the Mississippi fan channel-levee systems contain thinning- and fining-upward levee successions as suggested by upward decreasing amplitude in seismic profiles

(Weimer, 1990, 1991). Similar trends occur in the Lagoa Parda levee successions, where they are recognized in cores, or defined by upward decreasing resistivities in well logs (e.g. Figs. 4.15 and 4.24).

(4) Slump-prone, steep slopes are found close to levee crests both in modern fans (up to 9° in the Amazon fan; Damuth et al., 1988) and in the Lagoa Parda turbidite system (up to 10°; Figs. 4.16 and 4.23b).

Although some of the smaller-scale features of modern fans can also be recognized in the Lagoa Parda turbidite systems, most of the geometrical and stratigraphic relationships of the studied turbidites **can not** be explained by reference to studies of modern fans.

## 5.4. OUTCROPPING ANALOGUE IN THE ALMADA BASIN

The Almada basin (also known as a sub-basin of the Bahia Sul basin; Fig. 1.7) is located on the continental margin of Bahia state, northeastern Brazil. Its onshore portion covers only 200 $km^2$, which are occupied by outcrops of the continental pre-rift (late Jurassic), continental rift (Neocomian), and marine transgressive (Maastrichtian) megasequences. Conglomeratic and sandy turbidites, and bioturbated, planktonic-rich foraminiferal mudstones of Maastrichtian age (Urucutuca Formation) are better exposed in

the southern part of the basin (Fig. 5.4). These rocks represent an exhumed portion of the filling-section of the 10 km wide, at least 30 km long Almada canyon, which can be well-mapped seismically in the offshore portion of the Almada basin (Fig. 5.4). Almada basin turbidites are very important because they comprise the only outcropping example of the marine transgressive megasequence turbidites so far recognized along the eastern Brazilian margin.

A diversified fauna of planktonic foraminifera was described from shallow wells drilled in the onshore portion of the basin (Carvalho, 1965). These fossils suggest a Maastrichtian age for the mudstones of the Urucutuca Formation. Carvalho's (1965) paper does not specify the location of his samples; therefore, his paleontological data can not be precisely correlated with the outcropping coarse-grained turbidites. However, new biostratigraphic data (calcareous nannofossils) is available for the offshore well BAS-83 (Fig. 5.4). This well records 43 m of conglomerates and coarse-grained sandstones, which are included in the early Maastrichtian *Broinsonia parca* and *Quadrum trifidum* zones (Antunes, 1990a).

Bruhn and Moraes (1989) described in detail the facies and geometry of the outcropping Almada basin turbidites, which comprise mostly coarse-grained channel fills, and finer-grained levee deposits. The differential weathering of coarse-grained, channelized turbidites (forming sinuous and elongated

Fig. 5.4 - Geological map of the onshore portion of the Almada basin and seismic map in milliseconds of the pre-Urucutuca Formation unconformity, which defines the Almada canyon (contour interval = 100 milliseconds). Turbidite thickness for each exploratory well indicated in parentheses (after Bruhn and Moraes, 1989).

## Legend

| | |
|---|---|
| Marsh area | Quaternary: fluvial and beach sands |
| **Ku** Late Cretaceous: Urucutuca Formation | **JKb** Late Jurassic/Early Cretaceous: Bahia Supergroup |
| Precambrian: igneous and metamorphic basement | Occurrence area of channelized turbidites |

ATLANTIC OCEAN

ALMADA CANYON

City of Ilhéus

Rio Almada

480.000

500.000

8.380.000

8.370.000

FZT-1 (0)

NB-2 (84)

NB-1 (142)

BAS-36 (138)

SSA-1 (352)

BAS-3 (0)

BAS-14 (13)

BAS-71 (0)

BAS - 82 (55)

BAS - 83 (43)

ridges) and of surrounding mudstone-rich successions (low plains almost at sea level; Fig. 5.5) permitted the use of aerial photographs for plan-view study of the channelized conglomerate/sandstone bodies (Fig. 5.6). As seen in the slightly sinuous elongated ridges, the Almada basin channel fills are 30 - 380 m wide (average 165 m), and 250 - 1,650 m long (average 640 m). The entire channel complex occupies a 1.5 km wide, elongated zone, which has the same orientation as one of the main thalwegs of the Almada canyon (Fig. 5.4).

Bruhn and Moraes (1989) recognized two main facies associations in the outcrops of the early Maastrichtian Urucutuca Formation: (1) a channel fill, coarse-grained association, and (2) an interchannel (including levees), fine-grained association. The channel fill facies association includes unstratified, pebbly (petromict) conglomerates (Figs. 5.7 and 5.8a), intraformational conglomerates containing boulder- to granule-sized mud intraclasts (Figs. 5.7 and 5.8b), and unstratified (subordinately stratified), very coarse- to fine-grained sandstones, which commonly form 1 - 10 m thick fining-upward successions (Fig. 5.7). Large mud or petromict clasts are concentrated preferentially in the channel thalwegs, whereas unstratified deposits become stratified in the uppermost portions and margins of channel fills. The interchannel facies association displays mudstones with different degree of bioturbation, thin-bedded (up to 15 cm) "CCC" turbidites (Walker, 1985) (Fig. 5.9), pebbly

Fig. 5.5 - (a) Photograph taken from the southern margin of the Almada basin. In the foreground is one of the ridges supported by coarse-grained turbidites of the Urucutuca Formation (**Ku**), which stands out from surrounding mudstones of the same formation. Other letters indicate the Atlantic Ocean (**AO**), and outcrops of the late Jurassic, pre-rift megasequence (**Js**), and Precambrian, high-rank metamorphic rocks (**P∈**), on the northern boundaries of the basin.

(b) Transverse view of two coarse-grained channel fills. Paleocurrents oriented toward the reader. A section measured in the outcrop (**A-A'**) is shown in figure 5.7. Outcrop location is indicated by number 4 in figure 5.6.
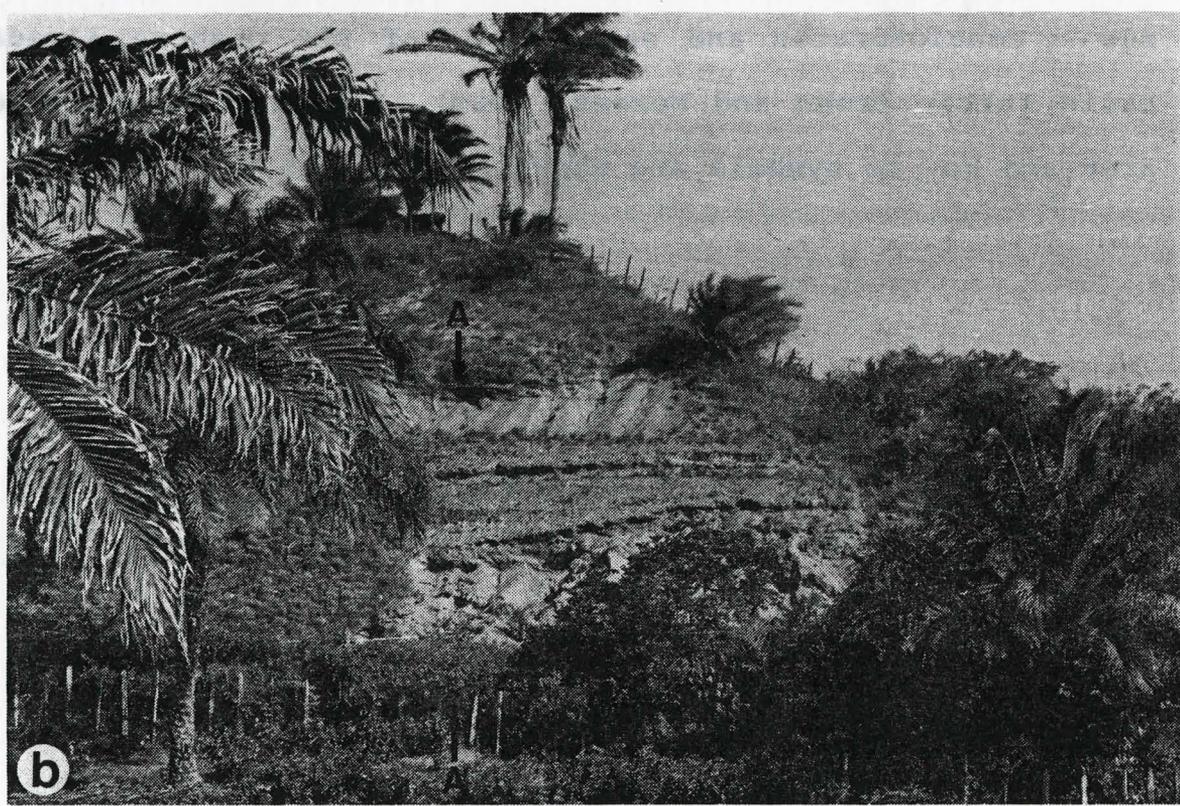
Fig. 5.6 – Detailed map of the channelized turbidites (**cgl &
sds** = conglomerates and sandstones) of the onshore Almada
basin (after Bruhn and Moraes, 1989). Location of detailed
area and key to symbols are shown in figure 5.4.

URUCUTUCA

488.000

Almada River

8.380.000

SAMBAITUBA

2

3

4

5

6

Q

1000m

500

0

cgl & sds

JKb

Ku

ATLANTIC OCEAN

8.376.000

City of
Ilhéus    14km

492.000
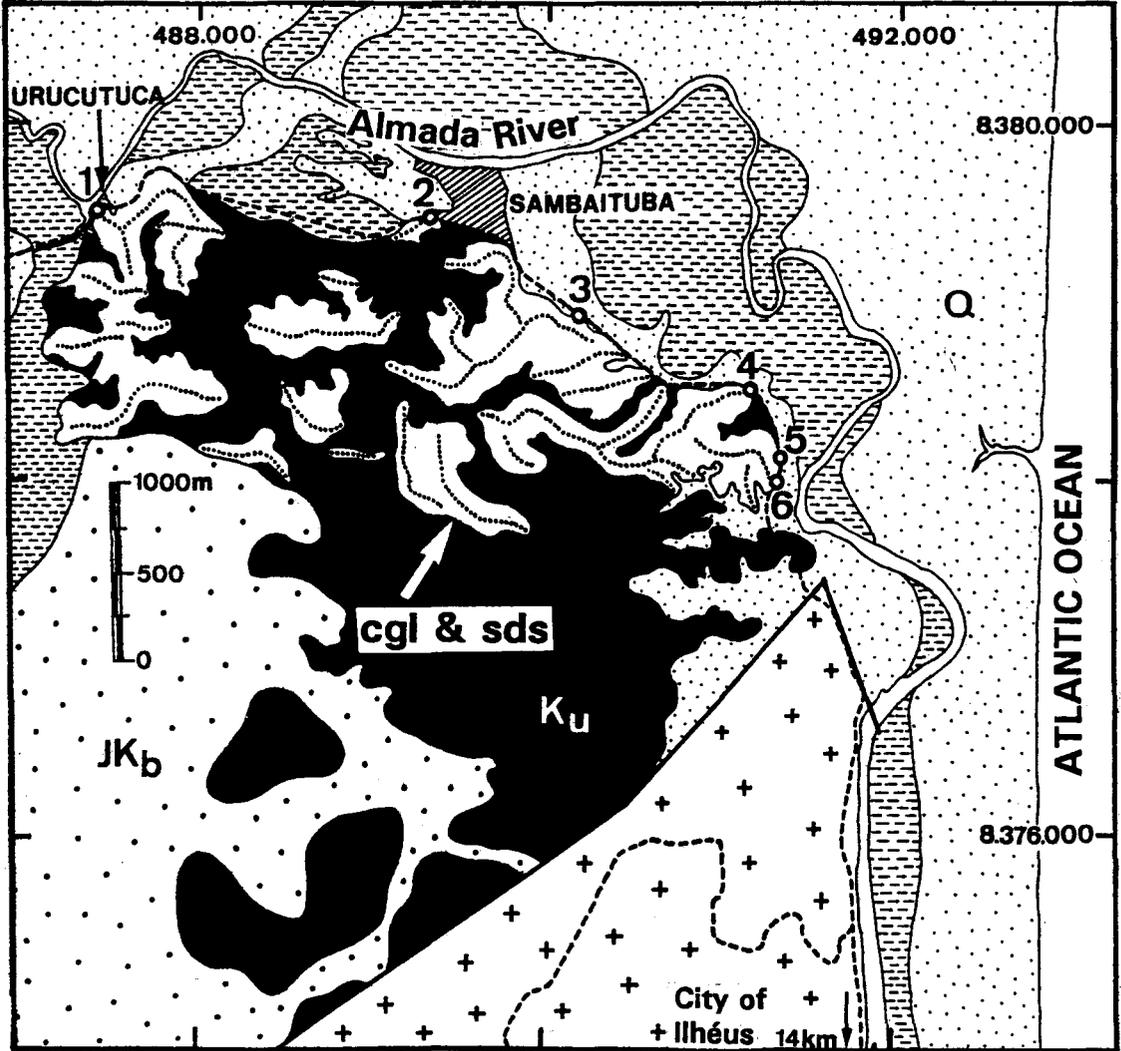
Fig. 5.7 - Typical facies succession of the coarse-grained turbidites of Almada basin. Explanation of symbols used in this figure is provided on page 70. Outcrop location is indicated by number 4 in figure 5.6.
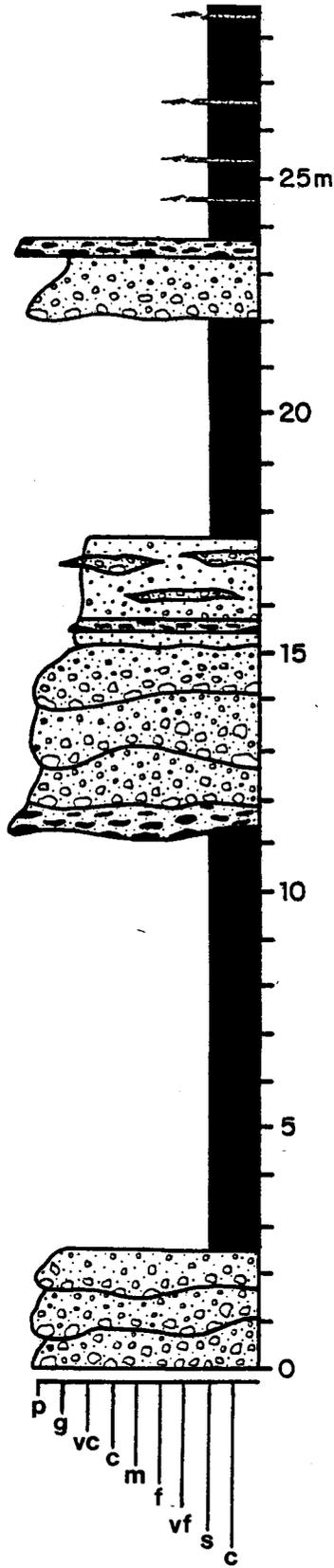
Fig. 5.8 - Common sedimentary facies of the Almada turbidite system.

(a) Unstratified, pebbly (petromict) conglomerate. Outcrop 2 in figure 5.6.

(b) Unstratified conglomerate, containing boulder- to pebble-sized mud intraclasts. Outcrop 1 in figure 5.6.

(c) Disorganized, pebbly mudstone. Outcrop 3 in figure 5.6.

(d) Slumped succession of mudstones and subordinate fine-grained sandstones. Outcrop 3 in figure 5.6.
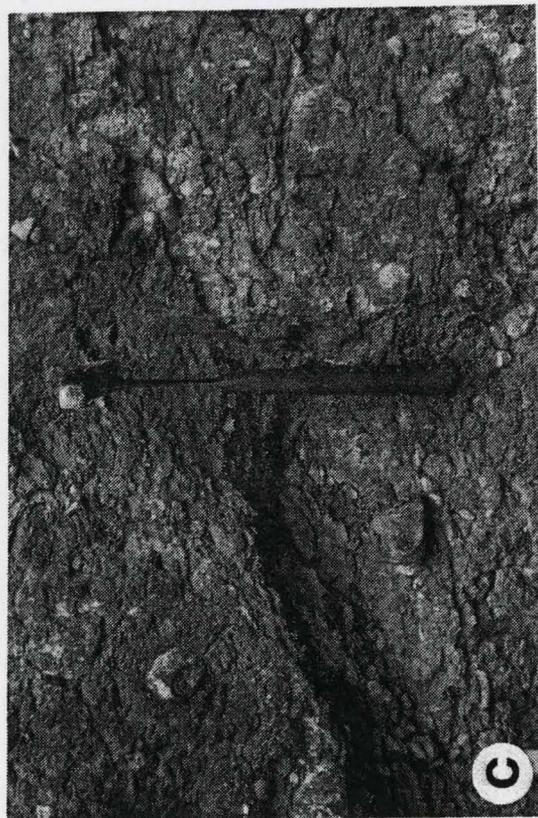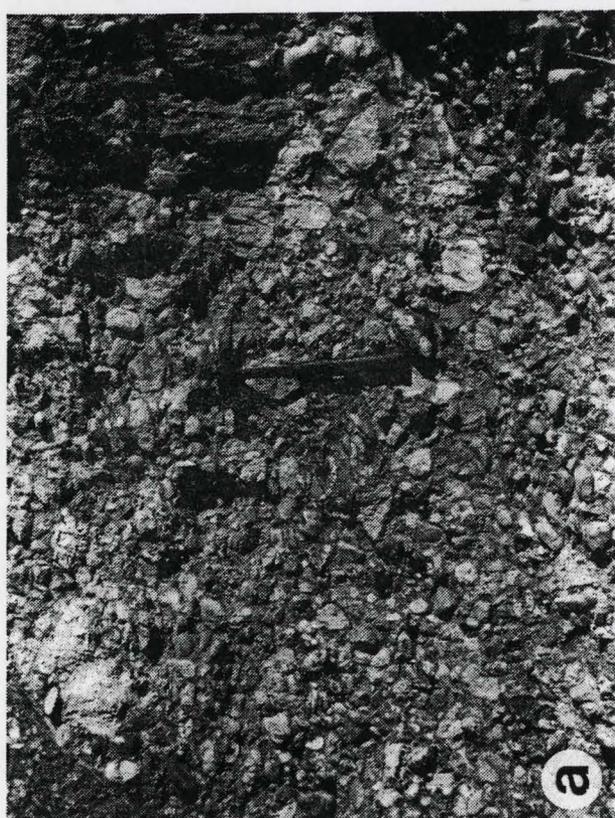
Fig. 5.9 - Coarse-grained channel fills truncating a 10 m thick levee succession composed of interbedded bioturbated mudstones and thin-bedded, sandy turbidites. Outcrop 6 in figure 5.6.

mudstones (Fig. 5.8c), and slump deposits (Fig. 5.8d). Interbedded bioturbated mudstones and thin-bedded turbidites are interpreted as levee deposits; they occur truncated by (Fig. 5.9) or laterally associated with channel fills. Although the Almada basin turbidites are time equivalent to the early Maastrichtian turbidite successions of the Carapeba and Pargo fields, their facies and sand body geometry are very similar to those of the early Eocene Lagoa Parda turbidite system.

## 5.5. INSIGHTS TOWARD A DEPOSITIONAL MODEL FOR TRANSGRESSIVE TURBIDITES FROM IMMATURE PASSIVE MARGIN BASINS

The comparison of the Carapeba/Pargo and Lagoa Parda turbidite systems with C-F-L models, Mutti's (1985) model, and models derived from studies of modern submarine fans has shown that **none** of these models can explain most of the geometrical characteristics and stratigraphic relationships shown by the systems studied in this thesis. Additionally, despite the fact that Carapeba/Pargo and Lagoa Parda turbidites have similar features, they also have important differences. This section contains a discussion of the similarities and differences between the two studied cases, in order to provide insights toward a depositional model for transgressive turbidites from immature passive margin basins.

## 5.5.1. Similarities between the studied turbidites

The most important similarities between the two study cases are:

(1) Carapeba/Pargo and Lagoa Parda turbidite systems are part of an overall transgressive succession that is characterized by onlapping, deepening-upward sedimentation throughout the eastern Brazilian marginal basins.

(2) Both systems accumulated in canyons, whose boundaries and depths were largely controlled by faults with variable orientation and activity (e.g. Figs. 3.2 and 4.3).

(3) Both systems typically comprise fining- and thinning-upward turbidite successions at variable scales. In the Carapeba/Pargo turbidite system these general trends in grain size and bed thickness can be recognized within individual successions (Fig. 3.4), or in groups of successions (e.g. the Coniacian/Santonian CRP/PG-S3 to CRP/PG-S6 successions; Fig. 3.4). In the Lagoa Parda turbidite system the fining- and thinning-upward successions can be recognized within individual channel complexes (e.g. LP-CC2 in Fig. 4.23b), or in the larger-scale succession formed by channel complexes LP-CC1 to LP-CC3 (Fig. 4.11).

(4) Both Carapeba/Pargo and Lagoa Parda turbidites are characterized by coarse-, poorly-sorted, and subangular to angular grains, which are composed largely (35 - 50 %) of feldspar, and feldspar-rich rock fragments. Their source rocks

were Precambrian, feldspar-rich, igneous and high-grade metamorphic rocks, and their source areas (and associated basin margins) were characterized by high-relief, intense tectonic activity (faulting and uplifting), and a mostly humid and warm climate. A similar source area to that of the Carapeba/Pargo and Lagoa Parda turbidites can be found today in the area of Rio de Janeiro. The beauty of this city is largely due to its rugged topography, which comprises steep mountains supported by Precambrian, igneous and high-grade metamorphic rocks, which stand up to 1,025 m above sea level. The climate is also warm and humid, and large portions of these mountains are covered by tropical rain forest.

## 5.5.2. Contrasts between the studied turbidites

The major differences between the Carapeba/Pargo and Lagoa Parda turbidite systems are related to: (1) facies and sand body geometry; (2) relative physiographic position in the basin (i.e. more proximal or more distal, deeper or shallower); and (3) reccurrence intervals of successions or channel complexes, and individual turbidites.

### Facies and sand body geometry

Carapeba/Pargo turbidites consist mainly (> 95 %) of graded beds up to 12 m thick, composed of small pebble (< 2 cm)- to granule-rich conglomerates and very coarse- to medium-

grained sandstones. Minor erosion may have taken place at the base of individual turbidites, but together they form non-channelized (tabular or lobate) sandstone bodies. These sandstone bodies occupy, in most cases, the entire width of the Carapeba/Pargo canyon. The canyon was shaped by the combined effects of subsidence along listric faults and erosion by high density turbidity currents.

The Lagoa Parda turbidite system comprises mostly an association of: (1) graded beds up to 6 m thick, composed of unstratified, bouldery to pebbly conglomerates and very coarse to coarse-grained sandstones, and parallel-stratified, medium- to fine-grained sandstones; and (2) interbeddings of bioturbated mudstones and thin-bedded (< 70 cm), parallel- to ripple cross-laminated, fine- to very fine-grained sandstones. The coarser-grained facies fill deep channels cut by high density turbidity currents, and the finer-grained facies build asymmetrical levees associated with these channels. Lagoa Parda channel complexes are characterized by a high degree of cannibalization, i.e. most of the channel fills eroded at least part of older channel fills and levee successions. As a result of the common amalgamation of up to 23 channel fills and the partial preservation of levee deposits between channel fills, Lagoa Parda channel complexes show a complicated, multi-storied sand body geometry (Fig. 4.11).

Boulder- to large pebble (> 2 cm)-sized exogenic sediments are common in the Lagoa Parda field, but they are

absent in the Carapeba/Pargo area; however, the latter system has no levee deposits and a much smaller proportion of finer-grained sandstones. Most of the fine-grained sand seems to have been flushed downcanyon toward more distal portions of the Campos basin.

The turbidite systems studied in this thesis exhibit not only very different sand body geometries, but they also contain sand bodies with dimensions at distinctly different scales. Carapeba/Pargo sandstone bodies can be one order of magnitude wider and longer than those at Lagoa Parda (Table 5.3). Additionally, Carapeba/Pargo turbidite successions show a retrogradational stacking (Fig. 3.4), whereas Lagoa Parda channel complexes are vertically stacked by up-lap sedimentation (compare Figs. 4.23b and 4.24a, which are transversely- and longitudinally-oriented to the Regência canyon thalweg).

## Physiographic position

The fossil assemblages found in the interbedded mudstones suggest that Lagoa Parda turbidites were deposited in a shallower setting than those at Carapeba/Pargo. The early Eocene Regência canyon was filled with mudstones containing deep neritic to upper bathyal (200 - 500 m) foraminifera (Azevedo, 1985), whereas the late Cretaceous Carapeba/Pargo trough contains mid to lower bathyal (1,000 - 1,500 m) foraminifera (Azevedo et al., 1987a).

**Table 5.3 - Typical geometry and dimensions of sand bodies in the Carapeba/Pargo and Lagoa Parda turbidite systems.**

| TURBIDITE SYSTEM | SAND BODY GEOMETRY | THICKNESS (m) | WIDTH (km) | LENGTH (km) |
|---|---|---|---|---|
| Carapeba/Pargo | | | | |
| Successions | Tabular or lobate | 27 - 140 | 1 - 12 | > 20 |
| Lagoa Parda | | | | |
| Channel fills | Channel fill | 9 - > 50 | 0.2 - 1 | > 1 |
| Channel complexes | Complex, multi-storied | 20 - 100 | 0.3 - 1.2 | > 2 |

Lagoa Parda field is close to the head of Regência canyon (2 - 8 km; Figs. 4.1 and 4.4) and to its northern margin (< 1 km; Figs. 4.1 and 4.3). The head of the canyon that contains Carapeba/Pargo turbidites is not preserved; however, these two fields are located about 90 to 110 km (measured along the canyon axis) from the landward limit of occurrence of late Cretaceous turbidites (Fig. 3.1). It follows that the Lagoa Parda turbidite system accumulated in a more proximal setting than the Carapeba/Pargo turbidite system. This situation is probably one of the main reasons why coarser-grained sediments are preserved in the Lagoa Parda field. Very proximal settings like the Regência canyon probably would be able to capture larger amounts of very coarse sediments; these, in turn, could

have been introduced by fan deltas, or directly intercepted from littoral-drift systems (as observed in some canyons off California; Inman et al., 1976; Hess and Normark, 1976).

**Reccurrence intervals**

Carapeba/Pargo turbidite successions have average durations of 900,000 years (each of the six Coniacian/ Santonian successions) and 400,000 years (each of the two early Maastrichtian successions). Lagoa Parda channel complexes have average duration of only 144,000 years (all of the nine channel complexes included in the early Eocene *Neochiastozygus chiastus* zone span 1.3 m.y.).

The average reccurrence intervals for individual turbidites in the Carapeba/Pargo turbidite system range from 15,000 to 38,000 years. Much shorter reccurrence intervals can be estimated for the Lagoa Parda turbidites, i.e. only 800 and 80 years, respectively for channel fill and levee turbidites.

## 5.5.3. Building a model based on the Carapeba/Pargo and Lagoa Parda turbidite systems

**Texture and composition of sediments**

Despite their textural differences, Carapeba/Pargo and Lagoa Parda turbidites are typically coarse-grained, and texturally- and composionally immature. These characteristics seem to be a function of the high tectonic activity (faulting

and uplifting) in the source area and basin margins, which probably had high relief and steep slopes, and showed deltas/fan deltas directly feeding narrow, faulted shelves.

## Development of turbidite successions

During times of ice-free continents (e.g. late Cretaceous to early Tertiary), short (< 1 m.y.)-time reccurrence in the development of turbidite successions can not be explained purely by **eustatic** sea level fluctuations. In immature passive margin basins, turbidite successions could develop in response to phases of increase in sediment supply via delta/fan delta systems; these, in turn, would respond to fault reactivation and increasing uplift in the source area and basin margins (e.g. Carapeba/Pargo), or to climatic fluctuations (shorter reccurrence intervals; e.g. Lagoa Parda). Such pulses of increasing sediment supply could be able to shift coastal depocenters seaward across narrow and steep shelves, and possibly induce short-term falls of relative sea level. The larger the magnitude of these sea level falls, the greater would be the probability for development of regional unconformities or local erosion surfaces bounding turbidite successions.

## Facies successions

Both Carapeba/Pargo and Lagoa Parda turbidite systems show well-defined fining- and thinning-upward successions.

These successions could have been controlled mostly by decreasing sediment supply, which in turn would have resulted from the combined effects of an overall, eustatic sea level rise, and decreasing tectonic activity at the basin margin and source area (Carapeba/Pargo) or decreasing climatically-controlled denudation rates in the source area (Lagoa Parda). Decreasing tectonic activity would induce progressive erosion of uplifted continental blocks, with resulting slope reduction in the source area. This would be followed by a decrease in the amount and rate of accumulation of coarser-grained sediments in areas more susceptible to failure. As a result, slope failures (and related turbidity currents) would become gradually less frequent and finer-grained, giving rise to fining- and thinning-upward successions. The overall trend of sea level rise, in turn, would not allow progradation of coastal depositional systems, and the possible development of thickening- and coarsening-upward turbidite successions or shallower-water sedimentation. These patterns of sedimentation took place by the combined effects of decreasing tectonic subsidence and long-term sea level fall, as recorded for the (late) early Eocene/mid Eocene to recent, marine regressive megasequence of Campos and Espírito Santo basins (Chang et al., 1988, 1992; Guardado et al., 1990).

**Confinement to canyons and retrogradational stacking**

A generalized, long-term sea level rise would tend to

gradually move coastal depocenters landward; as a result, the amount and rate of accumulation of coarser-grained sediments in areas more susceptible to failure (e.g. shelf/slope break) probably would decrease, with turbidity currents becoming less frequent, smaller, and finer-grained. Middleton and Neal (1989) demonstrated experimentally that turbidite thickness and lateral extent (or travel distance of turbidity currents) can be related to the original volume and concentration of the turbidity currents, their speed, and the settling velocity of the grains transported by them. All other things being equal, larger turbidity currents would travel longer distances. It follows that the long-term trend of sea level rise would likely result in deposition from turbidity currents in successively shorter distances from their point of initiation. Thus, the depocenters of coarse-grained turbidites would tend to migrate upcanyon, giving rise to retrogradational successions. For example, the offset terminations of the various Carapeba/Pargo turbidite successions suggest a minimum retrogradation of 20 km (Fig. 3.4). However, the very proximal Lagoa Parda turbidite system lacks retrogradational stacking, probably due its structural confinenment and lack of available space for retrogradation (during most of the early Eocene the head of the Regência canyon was defined by a N-oriented, very active fault, which was only 2 km distant from Lagoa Parda field; Fig. 4.4).

It is important to point out that, regardless of the

influence of sea level fluctuations, turbidite sedimentation within a canyon would take place **only** if there is a significant reduction in the gradient of the canyon floor, causing the turbidity currents to decelerate. Therefore, the hypothesis for retrogradational stacking presented above requires that the increase in basin floor gradient by thermal contraction and sediment load be minimal; otherwise, the increasing gradient would result in turbidite accumulation in the same position, or even farther basinward, bypassing the study area. Passive margin basins are characterized by a series of half-grabens stepping-down seaward; however, the common rotation of blocks along listric faults may reduce (or even reverse) basin floor gradient in many of these fault-bounded basin segments (e.g. Fig. 5.10). Typical seismic profiles of the Campos basin (e.g. Guardado et al., 1990, their figure 5) show throughout the marine transgressive megasequence a steeper profile for the most proximal, 60 km-wide part of the basin. Beyond this point, including the Carapeba/Pargo area, a much more gentle profile (flat or even dipping landward) is presented. Another cause for local decrease in basin floor gradient is related to the creep and withdrawal of underlying evaporite beds. It has been suggested (Figueiredo and Mohriak, 1984; Guardado et al., 1990) that salt flowage favoured the development of the listric faults (including those that bound the Carapeba/Pargo canyon) and also formed depresssions capable of impounding turbidites.

Fig. 5.10 - Distribution in time and space of the most important styles of turbidite sedimentation developed in the eastern Brazilian margin, during the long-term trend of sea level rise from the Coniacian to the early Eocene. Canyon fill turbidite successions were developed during relative sea-level falls that punctuated an overall transgressive setting. These relative sea level falls were probably induced by phases of increased sediment supply, which, in turn, would have responded to tectonic reactivations in the source area and basin margin, or to climatically-controlled denudation rates in the source area. Some of the unconformities that bound turbidite successions are tentatively correlated (with ages indicated) to eustatic sea level falls recognized by Haq et al. (1988). Dashed lines indicate a typical structural profile into which late Cretaceous and early Tertiary canyons were incised. In general, turbidite styles changed from non-channelized (tabular/lobate) turbidites that accumulated in more distal settings (with gentler canyon floor gradient), to unleveed and leveed, channelized turbidites that incised into more proximal and possibly steeper settings. More distal turbidite successions typically display retrogradational stacking, which may be absent in more proximal turbidite successions due their proximity to the faulted basin margins and related lack of available space for retrogradation. A more detailed explanation for this figure is presented in the text.

W

**Early Eocene/Mid Eocene**

~49.5 - 49 Ma~

Early Eocene

Ⓘ

Ⓗ

~55 - 54 Ma~

Late Paleocene

~58.5 - 57.5 Ma~

Ⓖ

? ?

Maastrichtian/
Early Paleocene

Ⓕ

~75 - 74 Ma~

Ⓔ

Coniacian/
Campanian

Ⓓ

Ⓒ

Ⓑ

LAGOA
PARDA

~90 - 89 Ma~

Ⓐ

ALMADA

CARAPEBA/PARGO

Not to scale

E

Leveed, channelized turbidites

Unleveed, channelized turbidites

Non-channelized turbidites

MARINE REGRESSIVE
MEGASEQUENCE

MARINE TRANSGRESSIVE
MEGASEQUENCE

Canyon-confined
turbidites
|
Basin floor
turbidites

BRUHN (1993)
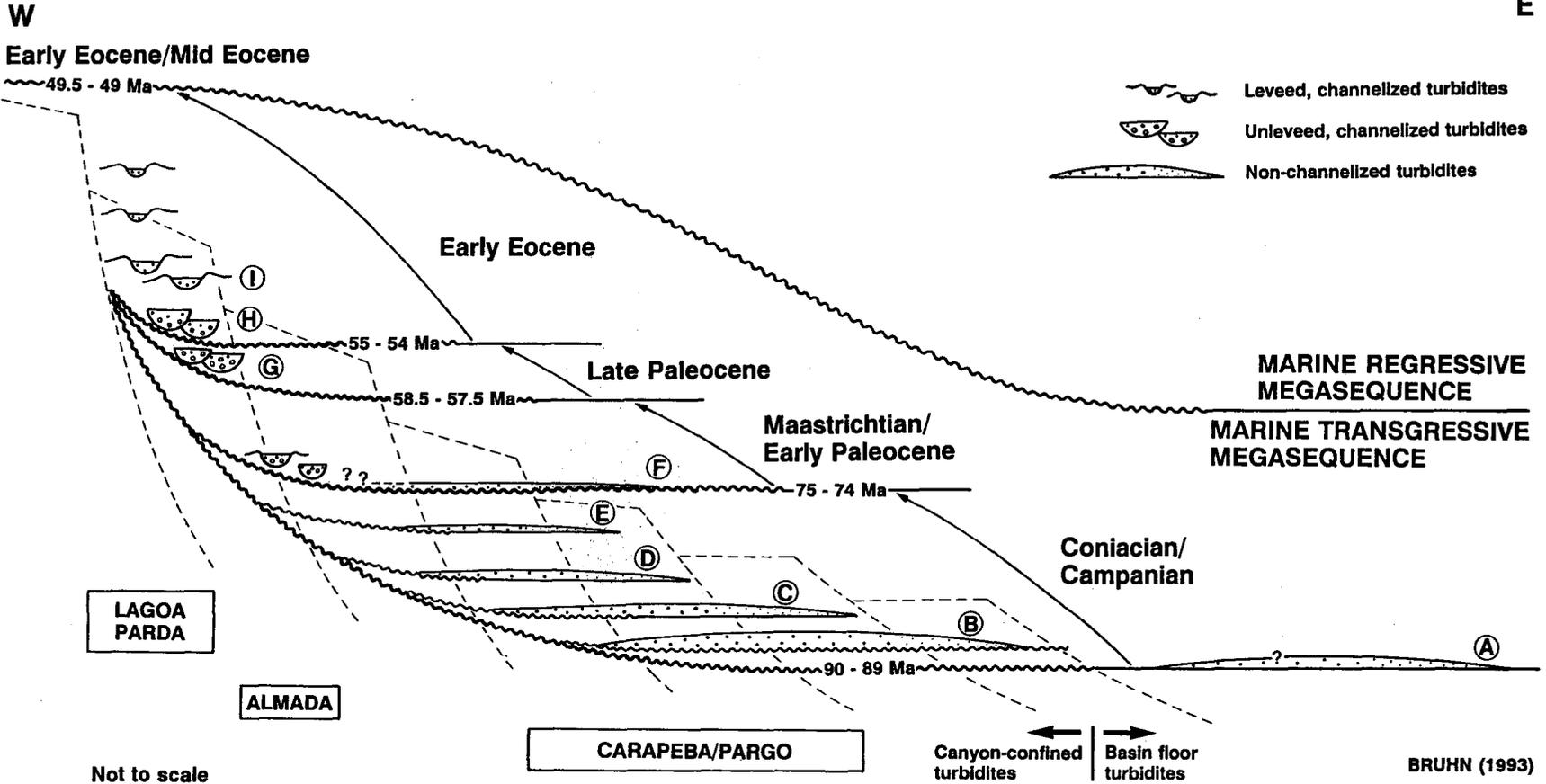
Most modern canyons or submarine channels developed in passive margin basins (e.g. East Coast of North America and Gulf of Mexico) are characterized by mostly muddy axial fills (e.g. Shepard and Dill, 1966; Stubblefield et al., 1982), accumulated during the Holocene highstand. Gravel and sand believed to be relict Pleistocene deposits have also been found in some of these large erosional features (e.g. Farre et al., 1983; Piper et al., 1988). Despite the extensive research on modern submarine canyons of North America (e.g. Shepard and Dill, 1966; Inman et al., 1976; Twichell and Roberts, 1982; Farre et al., 1983; Graham and Bachman, 1983) and Europe (e.g. Kenyon et al., 1978; Malinverno et al., 1988; Nelson and Maldonado, 1988), very little is known about their filling successions, because of the lack of deep coring and extensive dating. The Mississipi canyon is one of the best studied modern canyons along the passive margins of the United States (e.g. Coleman et al., 1983; Goodwin and Prior, 1989). It was cut at least 30,000 years ago, during the late Wisconsin glaciation; it shows a 700 m thick, mostly mud-rich filling section, which is composed of distal prodeltaic sediments, and debris flow and mud flow deposits (Goodwin and Prior, 1989). Most of these sediments (515 m) were deposited between 19,000 and 7,500 years ago. Only 20 m of hemipelagic to pelagic clays have been deposited in the canyon axis in the last 7,500 years, following the Holocene sea level rise. Goodwin and Prior (1989) recognized a progradational, offlap stacking in

the mud-rich filling of the Mississipi canyon, which contrasts with the coarse-grained, retrogradational turbidite successions found in the late Cretaceous/early Tertiary eastern Brazilian margin.

McHargue and Webb (1986) presented probably the only example of retrogradational stacking in the transition canyon/ upper fan channel of a modern fan. They suggested (in their figure 12) that packages containing high-amplitude, discontinuous reflectors (sandy channel fills ?) may onlap packages of low-amplitude, discontinuous reflectors (muddy lateral accretion on canyon walls ?). However, they interpreted this stratigraphic relationship as a result of the great sediment supply in this setting: "initially, flow velocity was sufficient to erode a deep valley beyond the canyon mouth. Eventually, however, the system aggraded, burying the erosional valley, constructing levees, and infilling the canyon mouth" (McHargue and Webb, 1986, p.175).

Several canyons have been incised into the Cenozoic deltaic progradational successions of the Texas Gulf Coast, but they are typically cut into and filled with muddy sediments (e.g. Winker, 1982; Galloway et al., 1991). These canyons may comprise a lower, onlapping fill developed by retrogressive slumping, and an upper offlapping fill recording final canyon filling by coastal progradation toward the shelf edge (Galloway et al., 1991). Contrasting with the successions described in this thesis, the prograding continental margins

of the Texas Gulf Coast are characterized by a long-term history of sediment oversupply (Galloway et al., 1991), which was probably favoured by the Cenozoic, long-term trend of sea level fall (Haq et al., 1988, p.95).

Good examples of channelized, coarse-grained turbidites in fining-upward successions have been found in ancient canyons; e.g. the Eocene Torrey canyon (north of San Diego, California; May et al., 1983), and the Upper Cretaceous Rosario Formation (Baja California, Mexico; Morris and Busby-Spera, 1988). In both examples the fining-upward successions were interpreted to have developed during a lowstand and subsequent rise in sea level, which resulted in a gradual decrease in supply of coarse-grained sediments. In these studies, however, retrogradational stacking of coarse-grained turbidites was not recognized.

The Annot Sandstone (Eocene, French Maritime Alps) may show thick (> 200 m) successions of interbedded mudstones and coarse-grained turbidites (Cremer, 1983). These sandstones typically comprise tabular sandstone bodies that fill deeply incised canyons (e.g. Cremer, 1983, his figures 49, 50, and 56). Some of these tabular sandstone bodies seem to be composed of amalgamated channel fills that internally display lateral accretion surfaces (Bouma and Coleman, 1985; Bouma, 1990). However, a large part of these tabular sandstones lack internal channeling, and, therefore, represent good analogues to the Carapeba/Pargo reservoirs.

## Styles of turbidite sedimentation

The Carapeba/Pargo, Lagoa Parda, and Almada turbidite systems record important segments of the evolution of turbidite sedimentation along the eastern Brazilian margin, from the Coniacian/Santonian (*Marthasterites furcatus* zone; Fig. 3.42) to the early Eocene (*Neochiastozygus chiastus* zone; Fig. 4.37). During this long time interval (about 32 m.y.), the overall sedimentation style in the Campos and Espírito Santo basins was controlled by a generalized, eustatic trend of sea level rise. Almost all of the turbidite systems recognized within this succession fill deeply-incised, fault controlled canyons or shallower, broad troughs established in deep neritic to lower bathyal (200 - 2,000 m) settings.

A tentative model for the distribution in space and time of the most important styles of turbidite sedimentation developed in the eastern Brazilian marginal basins, during the long-term trend of sea level rise from the Coniacian to early Eocene, is presented in figure 5.10. This model is based essentially on the Carapeba/Pargo and Lagoa Parda turbidite systems, with subordinate input from the Almada turbidite system described by Bruhn and Moraes (1989). Limitations of this model are related to the relatively small areas covered in detail by this study. Very little is known about the early Eocene turbidites located outside the onshore Regência canyon. The two wells drilled immediately offshore record a decreasing thickness for the entire early Eocene succession (including

coarse-grained turbidites) (Fig. 4.4); however, the early Eocene canyon could extend farther offshore, with a SE-oriented thalweg located southward from these two offshore wells (Fig. 4.1). In the Campos basin, Coniacian to Maastrichtian turbidites pinch out eastward from Pargo field, over a distance of at least 40 km - beyond this point there is no well control (at about the 1,000 m isobath; Fig. 3.1). Conversely, thick, coarse-grained sandstones interbedded with mudstones containing a mid to lower bathyal foraminiferal fauna can be found upstream from the Carapeba field (Fig. 3.1); however, these rocks are poorly cored and the well control is widely spaced. In the Almada canyon, turbidites were studied only in the outcropping part of the basin; only three wells were drilled in the offshore portion of the canyon (Fig. 5.5), but no cores were recovered.

Five distinct styles of turbidite sedimentation can be identified and are discussed in detail below.


**Style A: <u>unconfined, basin floor turbidites (?)</u> (Coniacian/Santonian; e.g. turbidite succession A in Fig. 5.10).** Turbidite deposition was preceeded by canyon cutting. Although the canyons described from the studied basins had their boundaries and depths largely controlled by faulting, erosion by high-density turbidity currents also was important during their evolution (as shown for the Carapeba/Pargo area; p. 165 - 166). In the Campos basin there is a widespread

unconformity between the late Cenomanian/early Turonian and Coniacian/Santonian successions, which is probably related to an important eustatic sea level fall in the late Turonian (90 - 89 Ma; Fig. 3.42). This sea level fall favoured erosion by high-density turbidity currents along canyons, and probably moved the turbidite depocenters to unconfined settings seaward (**turbidite succession A in Fig. 5.10**). Erosion also took place along most of the western and shallower portions of the Campos basin, where the sedimentary record of the late Turonian is largely missing. However, the occurrence of Coniacian/ Santonian turbidites beyond the present bathymetry of 1,000 m remains a speculation (Fig. 3.1).

**Style B-E: <u>canyon-confined, non-channelized turbidites displaying retrogradational stacking</u>** (Coniacian/Santonian; e.g. turbidite successions B to E in Fig. 5.10): With the return to rising sea level conditions, and following an overall trend of sea level rise, turbidite depocenters would gradually have moved back into canyons carved into the slope and shelf, as long as the canyon floors showed a sufficient gradient decrease to decelerate turbidity currents (Fig. 5.10). In this context, tectonically- or climatically- controlled increase in sediment supply would have induced the development of turbidite successions (and possibly also short- term, relative sea level falls) that punctuated the overall transgressive setting. Some erosion and canyon modification

occurred immediately before or even during the accumulation of a new turbidite succession (e.g. CRP/PG-S4 in Fig. 3.22; and CRP/PG-S4 to CRP/PG-S6 in Fig. 3.24).

Canyon filling would have started during times of larger sediment input, when larger turbidity currents would have deposited thicker, tabular or lobate sand bodies in more distal, low-gradient areas (**e.g. turbidite succession B in Fig. 5.10**); these deposits eventually occupied the entire width of the canyon (e.g. CRP/PG-S3 in Fig. 3.2). During the long-term trend of sea level rise, a series of tabular/lobate turbidite successions back-filled the canyons, in a retrogradational stacking (Fig. 3.4; **turbidite successions B to E in Fig. 5.10**). Depending on the magnitude of the short-term, relative sea level falls, the turbidite successions would be underlain by local erosion surfaces with variable areal extent (e.g. CRP/PG-S5 in Fig. 3.23; **turbidite successions B to E in Fig. 5.10**). These erosion surfaces, in turn, would have been carved by turbidity currents that deposited their load in the Carapeba/Pargo area or farther downcanyon, even in places that have not been drilled yet. An example of the first situation is probably given by succession CRP/PG-S5 (Figs. 3.4 and 3.23). Its base is defined by a local erosion surface in the westernmost part of Carapeba field, which becomes a correlative, non-erosive surface toward Pargo field. Therefore, one could speculate that the turbidity currents that scoured the substrate in Carapeba field may have

deposited their load farther downcanyon in Pargo field.

**Style F: <u>canyon-confined, channelized turbidites (leveed or unleveed) that are replaced (?) downcanyon by non-channelized turbidites</u> (Maastrichtian to early Paleocene; e.g. turbidite succession F in Fig. 5.10):** Eustatic sea level fall occurred at 75-74 Ma (late Campanian) (Haq et al, 1988; Fig. 3.42) and may have been responsible for a relatively short seaward shift of the preferential sites for turbidite sedimentation in the early Maastrichtian (Fig. 3.4, and **turbidite succession F in Fig. 5.10**). The Campanian sedimentary record is very thin in the Campos basin (only 24 m in the Carapeba/Pargo area). This has been attributed to very low sedimentation rates following a widespread transgression (Azevedo et al., 19878a). However, important erosion of Campanian and even older sediments can be indicated by: (1) the absence of the worldwide, late Campanian index fossil (foraminifera) *Globotruncana calcarata* (Caron, 1985) in the Campos basin (Guardado et al., 1990); and (2)  the occurrence of the early Maastrichtian *Tetralithus trifidus* (calcareous nannofossil) zone directly overlying the Albian *Nannoconus truitti truitti* zone in a large area (> 1,300 km$^2$) of the southern Campos basin (Richter, 1987).

However, following the long-term trend of sea level rise believed to be responsible for the retrogradational stacking of style B-E, turbidite depocenters probably would have been

moved landward again, this time even closer to the high-relief, faulted basin margins (Fig. 5.10). These proximal and structurally-confined settings would be characterized by higher sediment input (via deltas/fan deltas or interception of littoral-drift systems) and higher canyon-floor gradients (as for example, the structurally-controlled submarine canyons off California; Shepard and Dill, 1966; Inman et al. 1976; Hess and Normark, 1976). As a result, more erosive turbidity currents would cut channels. The most powerful of these currents probably would be able to form non-channelized sandstone bodies farther downcanyon (**turbidite succession F in Fig. 5.10**), in areas with lower gradient (eventually occupying sites farther downbasin in comparison with older successions; compare CRP/PG-S6 and CRP/PG-S8 in Fig. 3.4, and **turbidite sucessions E and F in Fig. 5.10**). The remaining currents would have filled leveed or unleveed channels (Almada turbidite system, Figs. 5.4 to 5.6; and **turbidite succession F in Fig. 5.10**) in a process still poorly understood. The coarse-grained, late Cretaceous/early Tertiary turbidite channel fills found along the eastern Brazilian margin typically show a small lateral extent, both in transverse and longitudinal direction (e.g. Bruhn and Moraes, 1988, 1989; Cosmo and Palhares, 1988; Alves et al., 1990; Duarte et al., 1990). The longitudinal extent of these channel fills may have been further reduced due to erosion by younger channels, but in many cases their geometry seems to be originally restricted.

One could speculate that coarse-grained turbidites may have been imprisoned within localized depressions or areas with local decrease in gradient within these deeply-incised channels. Leveed channels (some channels of style F, and style I) aggraded onto the canyon floor; therefore, it could also be speculated that the gradient along the thalweg of these smaller, perched channels could be gentler than the adjacent canyon floor gradient, thus favouring local turbidite accumulation.

The more distal, non-channelized turbidites of style F typically comprise thinner deposits than the underlying successions (e.g. compare CRP/PG-S7 and CRP/PG-S8 with CRP/PG-S6 in Fig. 3.4; and **turbidite successions B to F in Fig. 5.10**). It important to point out that, although time-equivalent channelized and non-channelized turbidites have been found in the Almada and Campos basins, respectively, the lateral transition between these two types of deposits has not been documented so far in the marine transgressive megasequence of the eastern Brazilian margin.

**Style G-H: <u>canyon-confined, unleveed, channelized turbidites</u> (late Paleocene to early Eocene; e.g. turbidite successions G and H in Fig. 5.10):** This style is characterized by deeply incised, unleveed channels, which are mostly filled with boulder- to pebble-rich conglomerates and very coarse- to coarse-grained sandstones. Style G-H can be found in the late

Paleocene and early Eocene successions of the Regência canyon (e.g. LP-CC1 and lowermost LP-CC2 channels; Fig. 4.11). These two successions are bounded at the base by unconformities (Fig. 4.4) that become correlative conformities basinward (Gomes et al., 1988). These unconformities are well-defined in the Regência canyon, where late Paleocene or early Eocene turbidite-bearing successions may directly overlie early Maastrichtian counterparts (Figs. 4.3 and 4.4). Exploratory drilling in areas outside the large submarine canyons of Espírito Santo and Bahia Sul basins (Fig. 2.5) has so far not found turbidites equivalent in time to the late Paleocene and early Eocene channel fills. Late Paleocene and early Eocene rocks are largely absent in the Campos basin (Guardado et al., 1990), where mid Eocene sandstones and mudstones of the marine regressive megasequence may unconformably overlie early Paleocene mudstones of the marine transgressive megasequence (e.g. Fig. 3.4).

Style G-H can be differentiated from style F by the absence of time-equivalent non-channelized turbidites, by the absence of levee topography associated with the channel fills, and by the wider channel fills (the average widths of LP-CC1 and Almada basin channels fills are 690 and 165 m, respectively). The unleveed channels of style G-H can be interpreted as having been cut by faster, coarser-grained, and thinner turbidity currents than those responsible for eroding the Almada basin channels. The turbidity currents that cut the

late Paleocene/early Eocene channels were developed in more proximal and possibly steeper settings than the turbidity currents responsible for cutting the early Maastrichtian channels. However, the broader and (possibly) deeper incision of the early Tertiary channels could also be interpreted as an effect of the stronger structural confinement and smaller width of the younger canyons. For example, in the 6 km wide, early Tertiary Regência canyon (Fig. 4.3), a larger number of turbidity currents would have scoured the same site than in the 10 km wide, early Maastrichtian Almada canyon (Fig. 5.4).

**Style I: <u>canyon-confined, leveed, channelized turbidites</u> (early Eocene; e.g. turbidite succession I in Fig. 5.10):** This style is characterized by leveed channels filled mostly with sandstones and very subordinate conglomerates. The uppermost channel fills of LP-CC2 and LP-CC3 are good examples (Fig. 4.11). These channels are interpreted as having been cut and filled by slower, finer-grained, and thicker turbidity currents than those responsible for the development of style G-H channels. The passage from style G-H to style I was probably due to a generalized decrease in sediment supply, which in turn would have resulted from the combined effects of the overall, eustatic trend of sea level rise trend, and the decreasing fault activity at the basin margin and source area of the early Eocene Espírito Santo basin. The channel complexes of styles G-H and I do not show retrogradational

stacking. This is probably due to their structural confinement. Despite the overall sea level rise, little space was available for retrogradation due to deposition close to the high-relief, faulted basin margins (Fig. 4.4; and **turbidite successions G to I in Fig. 5.10**). A similar scenario is found in the modern Lake Tanganyika (east Africa), where high and steep escarpments along the lake margin allow only a minimal lateral facies migration during lake-level fluctuations (Cohen, 1990).

Turbidite sedimentation in very proximal, confined settings (styles G-H and I) can be influenced by higher-frequency variations in sediment supply related to climatic fluctuations. Climatically-controlled increase in sediment supply may have developed pulses of turbidite sedimentation along the canyons (e.g. the nine channel complexes of the early Eocene *Neochiastozygus chiastus* zone; Fig. 4.2); however, the associated relative sea level falls probably had a short duration and small magnitude, as suggested by the lack of erosion surfaces bounding the several channel complexes. The very proximal site of deposition of styles G-H and I could represent one of the causes for the shorter reccurrence interval of individual turbidite beds in the Lagoa Parda field than in the Carapeba and Pargo fields. Larger amounts of coarse-grained sediments could have been intercepted directly from littoral drift systems by the more proximal Regência canyon, as observed in some canyons off California (e.g.

Shepard and Dill, 1966; Inman et al., 1976; Hess and Normark, 1976). Shepard and Dill (1966) described the movement of up to 15 cm-diameter cobbles along Californian canyons.

Sedimentation of the chronostratigraphic packages represented in figure 5.10 ended with turbidite-poor successions, which accumulated during relatively long time spans. These muddy successions indicate times of exceptional sediment starvation along the eastern Brazilian margin. The starvation probably resulted from the combined effects of the long-term trend of sea level rise, and periods of tectonic quiescence in the source areas and basin margins. The duration, maximum thickness, and compacted accumulation rates for the three terminal, turbidite-poor successions identified in this study are as follow: (1) Campanian (*Eiffelithus eximius* zone, 10 m.y.); 24 m in the Carapeba field (0.02 cm/1,000 yr.); (2) late Maastrichtian to early Paleocene (*Arkhangelskiella cymbiformis*, *Cruciplacolithus primus*, and possibly also *Lanternithus duocavus* zones; 7.2 to 10.2 m.y.); 118 m in the Carapeba field (0.11 - 0.16 cm/1,000 yr.); and (3) early Eocene (*Tribrachiatus orthostylus* zone; 2.8 m.y.); 157 m in the Regência canyon (0.56 cm/1,000 yr.). Higher accumulation rates can be estimated for younger turbidite-poor successions. This trend can be explained in two ways: (1) a greater thickness of underlying sediments was eroded along the unconformities that bound the top of older muddy successions; and (2) a larger sediment input was available for the

development of younger and more proximal muddy successions.

The time span considered in the discussion above (from the Coniacian/Santonian *Marthasterites furcatus* zone to the early Eocene *Tribrachiatus orthostylus* zone) is about 34.8 m.y. For at least 23 m.y., or 66 % of that time (Campanian, late Maastrichtian, early Paleocene, and part of early Eocene), no important turbidite sedimentation occurred in the Campos and Espírito Santo basins. It follows that the uppermost portion of the marine trangressive megasequence records sediment starvation, and the accumulation of mostly muddy sediments at very low rates.


## 5.6. EXXON'S SEQUENCE STRATIGRAPHY


"**Sequence stratigraphy** is the study of genetically related facies within a framework of chronostratigraphically significant surfaces" (Van Wagoner et al., 1990, p.1). The sequence is the fundamental stratal unit for sequence-stratigraphic analysis. The **sequence** is defined as "a relatively conformable succession of genetically related strata bounded at its top and base by unconformities or their correlative conformities" (Mitchum, 1977, p.210). The stratigraphic analysis using sequences or unconformity-bounded strata was first developed by Sloss in 1948 (Sloss, 1988). However, the sequence stratigraphic analysis that is widely

applied today was largely improved and promoted by geologists from the Exxon Production Research Company in Houston (e.g. Payton, 1977, and references therein; Vail, 1987; Van Wagoner et al., 1988, 1990; Posamentier and Vail, 1988; Posamentier et al., 1988). Exxon's sequence stratigraphy actually started as seismic stratigraphy ("the study of stratigraphy and depositional facies as interpreted from seismic data"; Mitchum, 1977, p.210), and only more recently it incorporated data from cores, well logs, and outcrops into the stratigraphic analysis (e.g. Van Wagoner et al., 1990).

Depositional sequences are interpreted to be formed during one cycle of eustatic change, and their bounding unconformities are inferred to be related to eustatic-fall inflection points (e.g. Posamentier and Vail, 1988). When the rate of sea level fall exceeds the rate of subsidence, and the shoreline is significantly moved toward the shelf break, widespread erosion takes place, including the cutting of canyons into the slope and shelf. In this case, turbidites accumulate on the slope and in the basin, making part of the lowstand systems tract, which is the lowermost set of contemporaneous and interrelated depositional systems recognized in the sequence (e.g. Posamentier and Vail, 1988; Van Wagoner et al., 1988, 1990) (Fig. 1.6).

Turbidites can be recognized mostly in three different, non-coeval stratigraphic positions within the lowstand systems tract (e.g. Posamentier and Vail, 1988; Posamentier et al.,

1991; Vail et al., 1991): basin floor fan, slope fan, and shingled turbidites on the lowstand wedge. Basin floor fans (**bff** in Fig. 1.6) are composed of sand-rich lobes or sheets accumulated on the sequence basal boundary during relative sea level lowering. Slope fans (lower part of the lowstand wedge; **sf** in Fig. 1.6) include mostly sand-poor, channel-levee complexes, developed on the basin floor fan or on the slope, in response to decreasing rates of sea level fall. Lowstand wedges are largely made of prograding shorelines and deltas; however, besides the slope fans, they also may present localized shingled turbidites, which may be attached to or detached from the clinoform toes of the entire lowstand prograding complex. The lowstand wedge accumulates mostly during the later part of a rapid sea level fall and following lowstand, downlapping the slope fan and basin floor fan. The subsequent successions that comprise a depositional sequence (transgressive- and highstand systems tract; Fig. 1.6) typically lack important turbidite sedimentation (e.g. Posamentier and Vail, 1988; Posamentier et al., 1991; Vail et al., 1991). The transgressive systems tract is composed of a retrogradational succession formed during a time of progressive rise in sea level and decreasing sediment input. The highstand systems tract is represented by an increasingly progradational succession, deposited during highstand.

Principles of Exxon's sequence stratigraphy have been successfully applied in the study of some of the turbidite

successions from the marine regressive megasequence in Brazil (e.g. Beltrami et al., 1989; Guimarães et al., 1989; Carminatti and Scarton, 1991). However, there are many problems in their application to the analysis of turbidite successions from the marine transgressive megasequence, including the turbidites studied in this thesis; these problems will be discussed below.

Thick, coarse-grained (turbidite) sandstone successions displaying blocky well log pattern are typically assigned to lowstand fans (e.g. Vail et at., 1991). These facies comprise most of the Carapeba/Pargo turbidite system; however, in the study area these facies fill structurally-controlled canyons incised into the late Cretaceous slope of Campos basin. On the other hand, slope fans have been considered by Exxon's sequence stratigraphy as largely composed of mud-rich channel-levee complexes (e.g. Posamentier and Vail, 1988; Posamentier et al., 1991). In a more recent paper, Vail et al. (1991, their figure 15) introduced the concept of "proximal slope fans", which are thought to be formed by canyon fill, coarse-grained turbidites, and slump and debris flow deposits. However, Vail et al. (1991) do not explain in their text both the geometry and the spacial and temporal relationships of coarse-grained, proximal slope fans with finer-grained, channel-levee complexes. It follows that one could correlate the Carapeba/Pargo turbidite successions to the proximal slope fans of Vail et al. (1991). However, two aspects must be

considered when correlating each of the Carapeba/Pargo successions to individual sequences:

(1) Some of Carapeba/Pargo turbidite successions are bounded at the base (**in the study area**) by regional unconformities or local erosion surfaces, but there are also others that are bounded by conformable contacts; additionally, the upcanyon extent of these surfaces is largely unknown.

(2) The development of individual successions seem to have been induced by tectonically-controlled increase in sediment supply. The increasing sediment supply may also have induced relative sea level falls and related submarine erosion; however, this influence may have been restricted to the Campos basin, or even only to the Carapeba/Pargo canyon.

Few turbidite systems similar to the canyon fill, coarse-grained channel-levee complexes of the Lagoa Parda field have been described in the literature (e.g. Morris and Busby-Spera, 1988; Bruhn and Moraes, 1989). This type of turbidites are not included in Exxon's sequence-stratigraphic schemes.

## 5.7. CONTRIBUTIONS TO OIL EXPLORATION AND PRODUCTION

Very influential schemes like Exxon's sequence stratigraphy have emphasized the importance of lowstand basin floor fans as major petroleum exploration targets (e.g. Posamentier et al., 1991). These turbidite systems do form the

largest petroleum reservoirs in Brazil (e.g. Carminatti and Scarton, 1991; Peres, 1993). However, this study shows that canyon fill, coarse-grained turbidites may comprise thick successions of potentially high-quality reservoirs. This thesis also suggests that thick successions of coarse-grained turbidite reservoirs can accumulate in passive margin basins even during long-term trends of sea level rise, as long as intense tectonic activity takes place at the basin margin and adjacent hinterland. Coniacian to Maastrichtian, trough-confined turbidites contain an original oil-in-place volume of $243 \times 10^6$ m$^3$ (1.528 billion bbl) in the Campos basin only (Figueiredo and Martins, 1990). In the Gabon basin, time-equivalent turbidites contain about 69 % of the Gabonese oil reserves (Teisserenc and Villemin, 1990).

This thesis provides detailed models of the internal architecture and reservoir geometry of two very distinct types of turbidite reservoirs (Table 5.3). Carapeba/Pargo reservoirs are typically widespread, non-channelized (tabular or lobate) sandstone bodies that occupy in most cases the entire width of a fault-controlled canyon. However, the uppermost sandstones of some of the Carapeba/Pargo turbidite successions are laterally restricted and may display complicated compensation arrangements (Figs. 3.21 to 3.23).

Lagoa Parda reservoirs are relatively restricted channel fills that show variable width, thickness, and sand body orientation (Table 4.5). As a result of the common

amalgamation of many channel fills and the partial preservation of levee deposits between channel fills, Lagoa Parda channel complexes show a complicated, multi-storied sand body geometry (Figs. 4.23 and 4.24). This study shows that a detailed picture of this type of reservoir can be obtained **only** from those oil fields presenting a large number of closely-spaced wells, like Lagoa Parda (Fig. 4.5). Another important contribution of this study is the indication that channel fill reservoirs can also show a relatively restricted longitudinal extent. Submarine channels may extend continuously for thousands of kilometers (e.g. Chough and Hesse, 1976; Carter, 1988), but they may not be entirely filled with sandy turbidites, as they can also be eroded by younger channels.

## 6. CONCLUSIONS


(1) The Carapeba/Pargo and Lagoa Parda turbidite systems fill canyons that were shaped by the combined effects of subsidence along listric faults and erosion by high density turbidity currents. They make part of a late Albian to early Tertiary transgressive succession, which is characterized by onlapping, deepening-upward sedimentation throughout the eastern Brazilian marginal basins.


(2) The Coniaciacian/Santonian to early Maastrichtian Carapeba/Pargo turbidite system was built up by 181 to 198 coarse-grained turbidites (0.5 - 12 m thick). It can be subdivided into eight facies successions mainly on the basis of distinct trends of grain size and bed thickness. Some of these successions may also be bounded by regional unconformities or local erosion surfaces. The successions have average duration in the range 0.4 to 0.9 m.y.


(3) Carapeba/Pargo turbidite successions are 27 to 140 m thick, and contain 7 to 58 turbidites. Seven successions have well-defined fining-upward and fining-downstream (eastward)

trends in grain size distribution, and three successions also show well-defined variation trends in sandstone thickness and lateral distribution: younger or more distal sandstones become thinner-bedded and more discontinuous.

(4) Carapeba/Pargo turbidite successions form 1 to 12 km wide, non-channelized (tabular or lobate) sandstone bodies. In most cases they occupy the entire width of the canyon. They were stacked in an overall retrogradational pattern for at least 20 km, recording the backfilling of the Carapeba/Pargo canyon.

(5) The early Eocene Lagoa Parda turbidite system contains unstratified, coarse-grained beds up to 6 m thick, and interbeddings of bioturbated mudstones and thin-bedded (< 70 cm), stratified, fine-grained sandstones.

(6) The Lagoa Parda coarser-grained facies fill at least 38 deeply-incised channels; the channel fills are 9 to > 50 m thick, 210 to > 1,050 m wide, and > 1 km long.

(7) The Lagoa Parda finer-grained facies typically build asymmetrical levees, which are higher and thicker on the left side (looking downstream) of their associated channels. Levee asymmetry is probably an effect of Coriolis force. Nine levee successions (up to 50 m thick) are associated with the 20

youngest channels.

(8) The channel fills suggest successive channel abandonment, probably through relatively rapid avulsions. Avulsions of unleveed channels took place randomly, whereas leveed channels show preferential avulsion to the right (looking downstream; this is opposite to the direction of preferential levee growth). Levee topography was, therefore, an important control on channel avulsion.

(9) The Lagoa Parda channel fills can be grouped into three channel complexes, on the basis of thicker interbedded mudstones, different filling facies, and changes in dominant paleoflow orientation. These channel complexes seem not to be bounded by regional unconformities or local erosion surfaces. They have an average duration of 144,000 years.

(10) The overall Lagoa Parda turbidite succession is characterized by channel fills that become narrower, thinner, and finer-grained upward. Lagoa Parda channel complexes do not display retrogradational stacking, as was defined in the Carapeba/Pargo turbidite system.

(11) Comparison of the Carapeba/Pargo and Lagoa Parda turbidite systems with the channel-feeding-lobe models of the 1970's and 1980's, and with models derived from studies of

modern submarine fans, has shown that **none** of these models can explain the geometrical characteristics and stratigraphic relationships displayed by the systems studied in this thesis.

(12) Carapeba/Pargo and Lagoa Parda turbidites are largely composed of coarse-grained, texturally- and composionally-immature turbidites, which typically form canyon-confined, fining- and thinning-upward successions. However, their sand body geometry and dimensions are very distinct.

(13) The textural and compositional immaturity of Carapeba/Pargo and Lagoa Parda turbidites seem to be a function of the tectonic activity (faulting and uplifting) in the source area and basin margins, which probably had high relief and steep slopes, and showed deltas/fan deltas directly feeding narrow, faulted shelves.

(14) The development of fining- and thinning-upward successions in the Carapeba/Pargo and Lagoa Parda turbidite systems was probably controlled by decreasing sediment supply, which, in turn, would have resulted from the combined effects of the long term trend of sea level rise of the late Cretaceous and early Tertiary, and phases of decreasing tectonic activity at the basin margin and source area (Carapeba/Pargo turbidite successions) or decreasing

climatically-controlled denudation rates in the source area (Lagoa Parda channel complexes).

(15) The first-order, eustatic sea level rise in the eastern Brazilian margin during the late Cretaceous and early Tertiary gradually would have moved the coastal and turbidite depocenters landward, and would have kept coarse-grained turbidites restrained to canyons.

(16) Canyon fill turbidite successions were developed in the eastern Brazilian margin during relative sea level falls that punctuated the overall transgressive setting of the late Cretaceous and early Tertiary section. Only a few of these turbidite successions can be correlated with global, eustatic sea level curves. The relative sea level falls were probably induced by phases of increased sediment supply, which, in turn, would have responded to tectonic reactivation in the source area and basin margin, and/or to climatically-controlled denudation rates in the source area.

(17) Different styles of turbidite sedimentation can be recognized in the Coniacian/Santonian to early Eocene, transgressive succession of the eastern Brazilian marginal basins. In general, turbidite styles changed from non-channelized (tabular/lobate) turbidites accumulated in more distal settings (with a gentler canyon floor gradient)

(Coniacian/Santonian to early Maastrichtian Carapeba and Pargo turbidites), to unleveed and leveed, channelized turbidites incised into more proximal and possibly steeper settings (early Eocene Lagoa Parda turbidites). More distal turbidite successions typically display retrogradational stacking, which may be absent in more proximal turbidite successions due their proximity to the faulted basin margins and related lack of available space for retrogradation.

(18) Influential schemes such as Exxon's sequence stratigraphy have emphasized the importance of lowstand basin floor fans as major petroleum exploration targets. It is concluded here that canyon fill, coarse-grained turbidites may comprise thick successions of potentially high-quality reservoirs. It is also shown that thick successions of coarse-grained turbidite reservoirs can likely accumulate in passive margin basins even during long-term trends of sea level rise, as long as intense tectonic activity takes place at the basin margin and adjacent hinterland.

(19) Detailed models of internal architecture and reservoir geometry of two very distinct types of turbidite reservoirs were developed in this study. Carapeba/Pargo reservoirs are typically widespread, non-channelized (tabular or lobate) sandstone bodies. On the other hand, Lagoa Parda reservoirs are relatively restricted channel fills that show

variable width, thickness, and orientation; as a result of the common amalgamation of many channel fills and the partial preservation of levee deposits between channel fills, Lagoa Parda channel complexes show a complicated, multi-storied sand body geometry.

(20) Finally, it is concluded that these Brazilian turbidite successions differ from most of the well-known turbidite systems. Therefore, this study provides important models to guide oil exploration and production in turbidites accumulated in tectonically-active passive margin basins, during long-term sea level rise. These models can be applied not only to the Brazilian marginal basins, but also to other passive margin basins, as in particular the basins of the western African margin.

# REFERENCES

Abrahão, D., and J.E. Warme, 1990, Lacustrine and associated deposits in a rifted continental margin - Lower Cretaceous Lagoa Feia Formation, Campos Basin, offshore Brazil, *in* B.J. Katz, ed., Lacustrine basin exploration: case studies and modern analogs: The American Association of Petroleum Geologists Memoir 50, p.287-305.

Abreu, C.J., and P.E. Potter, 1990, Tipos e distribuição de porosidade nos arenitos do Membro Maceió, Cretáceo da Bacia Sergipe-Alagoas, NE do Brasil: Boletim de Geociências da PETROBRÁS, v.4, p.315-336.

Adams, J., 1989, Turbidites off the Oregon-Washington margin record paleoearthquakes on the Cascadia subduction zone: Geological Survey of Canada Paper 89-1F, p.37-43.

Allen, J.R.L., 1986, Earthquake magnitude-frequency, epicentral distance, and soft-sediment deformation in sedimentary basins: Sedimentary Geology, v.46, p.67-75.

Almeida, F.F.M., 1983, Relações tectônicas das rochas alcalinas Mezosóicas da região meridional da plataforma Sul-Americana: Revista Brasileira de Geociências, v.13, p.139-158.

Alves, J.B., V.Q. Lima, and J.H.C. Negreiros, 1990, Revisão geológica do Campo de Fazenda Cedro, *in* Proceedings of the 4th Seminar on Development and Reservoir Geology, PETROBRÁS, Natal, Brazil, p.104-112.

Anjos, S.M.C., and A.V. Carozzi, 1988, Depositional and diagenetic factors in the generation of the Santiago arenite reservoirs (Lower Cretaceous): Araçás oil field, Recôncavo Basin, Brazil: Journal of South American Earth Sciences, v.1, p.3-19.

Anjos, S.M.C., C.R.F. Carvalho, and R.M. Mencarelli, 1991, Mineralogia total e de argilas dos folhelhos marinhos na área dos campos de Carapeba (Bacia de Campos) e Lagoa Parda (Bacia do Espírito Santo): Rio de Janeiro, PETROBRÁS Internal Report, 17p.

Antunes, R.L., 1984, Geohistória do paleocanyon de Fazenda Cedro, Bacia do Espírito Santo, Brasil, segundo dados bioestratigráficos, *in* Proceedings of the 33rd Brazilian Geological Congress, Sociedade Brasileira de Geologia, Rio de Janeiro, v.1, p.670-684.

Antunes, R.L., 1990a, Contribuição ao conhecimento geológico do Paleocânion de Regência (Bacia do Espírito Santo, Brasil): um estudo com base na bioestratigrafia dos nanofósseis calcários: unpublished M.Sc. Thesis, Universidade Federal do Rio de Janeiro, Rio de Janeiro, Brazil, 71p.

Antunes, R.L., 1990b, Eventos erosivos na seção terciária do

paleocânion de Regência (Bacia do Espírito Santo, Brasil): um estudo com base na bioestratigrafia dos nanofósseis calcários, *in* Proceedings of the 36th Brazilian Geological Congress, Sociedade Brasileira de Geologia, Natal, v.1, p.455-469.

Antunes, R.L., N.T. Sonoki, and M. Carminatti, 1988, The Enchova paleocanyon (Campos basin - Brazil): its Oligocene-Miocene history based on calcareous nannoplankton biostratigraphy and seismostratigraphy: Revista Brasileira de Geociências, v.18, p.283-290.

Appi, C.J., R.O. Kowsmann, R.D. Flood, P.L. Manley, and C. Pirmez, 1988, Evolução Quaternária pós-glacial do cone submarine do Amazonas: um modelo retrogradante, *in* Proceedings of the 35th Brazilian Geological Congress, Sociedade Brasileira de Geologia, Belém, v.2, p.451-465.

Arai, M., A.T. Hashimoto, and N. Uesugui, 1989, Significado cronoestratigráfico da associação microflorística do Cretáceo Inferior do Brasil: Boletim de Geociências da PETROBRÁS, v.3, p.87-103.

Asmus, H.E., and P.R. Baisch, 1983, Geological evolution of the Brazilian continental margin: Episodes, v.6, p.3-9.

Asmus, H.E., and F.C. Ponte, 1973, The Brazilian marginal basins, *in* A.E.M. Nairn and F.G. Stehli, eds., The ocean basins and margins, v.1 - The South Atlantic, New York, Plenum Press, p.87-133.

Asmus, H.E., and R. Porto, 1972, Classificação das bacias

sedimentares brasileiras segundo a tectônica de placas, *in* Proceedings of the 26th Brazilian Geological Congress, Sociedade Brasileira de Geologia, Belém, v.2, p.67-90.

Asmus, H.E., and R. Porto, 1980, Diferenças nos estágios iniciais da evolução tectônica da margem continental leste brasileira: possíveis causas e implicações, *in* Proceedings of the 31st Brazilian Geological Congress, Sociedade Brasileira de Geologia, Camboriú, Brazil, v.1, p.225-239.

Austin, J.A., and E. Uchupi, 1982, Continental-oceanic crustal transition off southwest Africa: The American Association of Petroleum Geologists Bulletin, v.66, p.1328-1347.

Azambuja, N.C., 1990, The Oligo-Miocene turbidites and associated facies of the Campos basin, offshore Brazil: unpublished Ph.D. Thesis, Imperial College, London, 456p.

Azambuja, N.C., C.J. Abreu, P.M. Horschutz, A. Cândido, and E.M. Ramos, 1980, Estudo sedimentológico, faciológico e diagenético dos conglomerados do campo petrolífero de Carmópolis, *in* Proceedings of the 31st Brazilian Geological Congress, Sociedade Brasileira de Geologia, Camboriú, v.1, p.240-253.

Azevedo, R.L.M., 1985, Estudos paleoecológicos da Bacia do Espírito Santo, Brasil, com base em foraminíferos, *in* Coletânea de Trabalhos Paleontológicos, Departamento Nacional de Produção Mineral, Brasília, Brazil, p.261-271.

Azevedo, R.L.M., J. Gomide, and M.C. Viviers, 1987a, Geo-história da Bacia de Campos: do Albiano ao Maastrichtiano: Revista Brasileira de Geociências, v.17, p.139-146.

Azevedo, R.L.M., J. Gomide, M.C. Viviers, and A.T. Hashimoto, 1987b, Bioestratigrafia do Cretáceo marinho da Bacia de Campos, Brasil: Revista Brasileira de Geociências, v.17, p.147-153.

Babinski, N.A., and R.C.R. Santos, 1987, Origem e classificação dos hidrocarbonetos da Bacia Sergipe-Alagoas: caracterização geoquímica: Boletim de Geociências da PETROBRÁS, v.1, p.87-95.

Bagnold, 1956, The flow of cohesionless grains in fluids: Royal Society of London Phylosophical Transactions, Series A, v.249, p.235-297.

Bagnoli, E., 1984, Petrografia, modelo deposicional e diagênese dos reservatórios eocênicos do Campo de Lagoa Parda, Bacia do Espírito Santo: unpublished M.Sc. Thesis, Universidade Federal de Ouro Preto, Ouro Preto, Brazil, 195p.

Barron, E.J., 1983, A warm, equable Cretaceous: the nature of the problem: Earth Science Reviews, v.19, p.305-338.

Basham, P., and J. Adams, 1983, Earthquakes on the continental margin of eastern Canada: need future large events be confined to the locations of large historical events ?, *in* The 1866 Charleston earthquake and its implication for

today: U.S. Geological Survey Open-File Report 83-842, p.456-467.

Basu, A., 1985, Influence of climate and relief on compositions of sands released at source areas, *in* G.G. Zuffa, eds., Provenance of arenites: Dordrecht, D. Reidel Publishing Company, p.1-18.

Becker, M.R., L.M. Arienti, L. Bonet, C.C.M. Branco, E.A. Campagnolo, F.P. Campozana, and C.V. Stank, 1988, Caracterização geológica e petrofísica do reservatório principal (Membro Carapebus Cretácico) do Campo de Pargo, Bacia de Campos, *in* Proceedings of the 2nd Latin American Congress on Hydrocarbons, ARPEL, Rio de Janeiro, TT-193, 18p.

Beltrami, C.V., J.L. Caldeira, and R.W. Freitas, 1989, Análise sismoestratigráfica dos sedimentos Oligo/Miocênicos da Bacia do Ceará - Águas profundas, *in* Proceedings of the 1st Seminar on Exploratory Interpretation, Rio de Janeiro, PETROBRÁS, p.185-194.

Berggren, W.A., D.V. Kent, J.J. Flynn, and J.A. Van Couvering, 1985, Cenozoic geochronology: Geological Society of America Bulletin, v.96, p.1407-1418.

Bertani, R.T., and A.V. Carozzi, 1985a, Lagoa Feia Formation (Lower Cretaceous), Campos Basin, offshore Brazil - Rift valley stage lacustrine carbonate reservoirs, I: Journal of Petroleum Geology, v.8, p.37-58.

Bertani, R.T., and A.V. Carozzi, 1985b, Lagoa Feia Formation

(Lower Cretaceous), Campos Basin, offshore Brazil - Rift valley stage lacustrine carbonate reservoirs, II: Journal of Petroleum Geology, v.8, p.199-220.

Beurlen, G., 1982, Bioestratigrafia e geohistória da seção marinha da Margem Continental Brasileira: Boletim Técnico da PETROBRÁS, v.25, p.77-83.

Blair, T.C., and W.L. Bilodeau, 1988, Development of tectonic cyclothems in rift, pull-apart, and foreland basins: sedimentary response to episodic tectonism: Geology, v.16, p.517-520.

Boles, J.R., and S.G. Franks, 1979, Clay diagenesis in Willcox sandstones of southwest Texas: implications of smectite diagenesis on sandstone cementation: Journal of Sedimentary Petrology, v.49, p.55-70.

Bouma, A.H., 1962, Sedimentology of some flysch deposits: a graphic approach to facies interpretation: Amsterdam, Elsevier, 168p.

Bouma, A.H., 1990, Clastic depositional styles and reservoir potential of Mediterranean basins: The American Association of Petroleum Geologists Bulletin, v.74, p.532-546.

Bouma, A.H., and J.M. Coleman, 1985, Peira-Cava turbidite system, France, *in* A.H. Bouma, W.R. Normark, and N.E. Barnes, eds., Submarine fans and related turbidite systems: New York, Springer-Verlag, p.217-222.

Bouma, A.H., W.R. Normark, and N.E. Barnes, eds., 1985a,

Submarine fans and related turbidite systems: New York, Springer-Verlag, 351p.

Bouma, A.H., C.E. Stelting, and J.M. Coleman, 1985b, Mississippi fan, Gulf of Mexico, *in* A.H. Bouma, W.R. Normark, and N.E. Barnes, eds., Submarine fans and related turbidite systems: New York, Springer-Verlag, p.143-150.

Bouma, A.H., J.M. Coleman, C.E. Stelting, and B. Kohl, 1989, Influence of relative sea level changes on the construction of the Mississippi fan: Geo-Marine Letters, v.9, p.161-170.

Bowen, A.J., W.R. Normark, and D.J.W. Piper, 1984, Modelling of turbidity currents on Navy submarine fan, California continental borderland: Sedimentology, v.31, p.169-185.

Bromley, R.G., 1990, Trace fossils: biology and taphonomy: London, Unwin Hyman, 280p.

Bromley, R.G., and A.A. Ekdale, 1986, Composite ichnofabrics and tiering of burrows: Geological Magazine, v.123, p.59-65.

Brown, G.C., D.S. Gorsline, and W.J. Schweller, eds., 1990, Deep-marine sedimentation: depositional models and case histories in hydrocarbon exploration & development: Society of Economic Paleontologists and Mineralogists, Pacific Section, Short Course Volume No. 66, 326p.

Bruhn, C.H.L., 1985, Sedimentação e evolução diagenética dos turbiditos eocretácicos do Membro Gomo, Formação

Candeias, no Compartimento Nordeste da Bacia do Recôncavo, Bahia: unpublished M.Sc. Thesis, Universidade Federal de Ouro Preto, Ouro Preto, Brazil, 203p.

Bruhn, C.H.L., 1990, Reservatórios profundos no Brasil: a próxima fronteira exploratória ?: Boletim de Geociências da PETROBRÁS, v.4, p.349-386.

Bruhn, C.H.L., and L.F. De Ros, 1987, Formação Sergi: evolução de conceitos e tendências na geologia de reservatórios: Boletim de Geociências da PETROBRÁS, v.1, p.25-40.

Bruhn, C.H.L., and M.A.S. Moraes, 1988, Turbiditos brasileiros: caracterização geométrica e faciológica, *in* Proceedings of the 35th Brazilian Geological Congress, Sociedade Brasileira de Geologia, Belém, v.2, p.824-838.

Bruhn, C.H.L., and M.A.S. Moraes, 1989, Turbiditos da Formação Urucutuca na Bacia de Almada, Bahia: um laboratório de campo para estudo de reservatórios canalizados: Boletim de Geociências da PETROBRÁS, v.3, p.235-267.

Bruhn, C.H.L., C. Cainelli, and R.M.D. Matos, 1988, Habitat do petróleo e fronteiras exploratórias nos rifts brasileiros: Boletim de Geociências da PETROBRÁS, v.2, p.217-253.

Bruhn, C.H.L., J.M. Caixeta, and J.C. Scarton, 1985, Sublacustrine fan reservoirs of Riacho da Barra field, Recôncavo rift basin, Brazil: The American Association of Petroleum Geologists Bulletin, v.69, p.241(abstract).

Bueno, G.V., 1988, Modelo evolutivo para um paleo-canyon

situado em uma bacia do tipo rift intracontinental, Bacia do Recôncavo, Brasil, *in* Proceedings of the 35th Brazilian Geological Congress, Sociedade Brasileira de Geologia, Belém, Brazil, v.2, p.854-868.

Burton, R., C.G.St.C. Kendall, and I. Lerche, 1987, Out of our depth: on the impossibility of fathoming eustasy from the stratigraphic record: Earth Science Reviews, v.24, p.237-277.

Cainelli, C., 1992, Sequence stratigraphy, canyons, and gravity mass-flow deposits in the Piaçabuçu Formation, Sergipe-Alagoas basin, Brazil: unpublished Ph.D. Thesis, University of Texas, Austin, 233p.

Caixeta, J.M., 1988, Estudo faciológico e características de reservatório dos arenitos produtores de gás do Campo de Jacuípe (Cretáceo Inferior), Bacia do Recôncavo, Brasil: unpublished M.Sc. Thesis, Universidade Federal de Ouro Preto, Ouro Preto, Brazil.

Cândido, A., 1990a, Características de reservatório do Campo de Carapeba: Boletim de Geociências da PETROBRÁS, v.4, p.165-173.

Cândido, A., 1990b, Desenvolvimento e estratégia de produção do Campo de Albacora: Boletim de Geociências da PETROBRÁS, v.4, p.175-181.

Cândido, A., and N.C. Wardlaw, 1985, Reservoir geology of the Carmópolis oil field, Brazil: Bulletin of Canadian Petroleum Geology, v.33, p.379-395.

Carlson, P.R., and H.A. Karl, 1988, Development of large submarine canyons in the Bering Sea, indicated by morphologic, seismic, and sedimentologic characteristics: Geological Society of America Bulletin, v.100, p.1594-1615.

Carminatti, M., and J.C. Scarton, 1991, Sequence stratigraphy of the Oligocene turbidite complex of the Campos Basin, offshore Brazil: an overview, *in* P. Weimer and M.H. Link, eds., Seismic facies and sedimentary processes of submarine fans and turbidite systems: New York, Springer-Verlag, p.241-246.

Caron, M., 1985, Cretaceous planktic foraminifera, *in* H.M. Bolli, J.B. Saunders, and K. Perch-Nielsen, eds. Plankton stratigraphy: Cambridge University Press, Cambridge, p.17-86.

Carozzi, A.V., and J.R. Fonseca, 1989, A new technique of locating turbidite fans: Candeias Formation (Lower Cretaceous), Recôncavo Basin, Brazil: Journal of South American Earth Sciences, v.2, p.277-293.

Carozzi, A.V., M.B. Araújo, P. Cesero, J.R. Fonseca, and V.J.L. Silva, 1976, Formação Salvador: um modelo de deposição gravitacional subaquosa: Boletim Técnico da PETROBRÁS, v.19, p.47-79.

Carter, R.M., 1988, The nature and evolution of deep-sea channel systems: Basin Research, v.1, p.41-54.

Carter, L., and R.M. Carter, 1988, Late Quaternary development

of left-bank-dominant levees in the Bounty trough, New Zealand: Marine Geology, v.78, p.185-197.

Carvalho, M.D., U.M. Praça, J.J. Moraes, Jr., and A.R. Spadini, 1990, Reservatórios carbonáticos profundos do Eo/Mesoalbiano da Bacia de Campos: Boletim de Geociências da PETROBRÁS, v.4, p.429-450.

Chan, M.A., and R.H. Dott, Jr., 1983, Shelf and deep sea sedimentation in Eocene forearc basin, western Oregon - fan or non fan ?: The American Association of Petroleum Geologists Bulletin, v.67, p.2100-2116.

Chang, H.K., and R.O. Kowsmann, 1987, Interpretação genética das seqüências estratigráficas das bacias da margem continental brasileira: Revista Brasileira de Geociências, v.17, p.74-80.

Chang, H.K., R.O. Kowsmann, and A.M.F. Figueiredo, 1988, New concepts on the development of East Brazilian marginal basins: Episodes, v.11, p.194-202.

Chang, H.K., R.O. Kowsmann, A.M.F. Figueiredo, and A.A. Bender, 1992, Tectonics and stratigraphy of the east Brazil rift system: an overview: Tectonophysics, v.213, p.97-138.

Chough, S., and R. Hesse, 1976, Submarine meandering thalweg and turbidity currents flowing for 4,000 km in the Northwest Atlantic Mid-Ocean Channel, Labrador Sea: Geology, v.4, p.529-533.

Christie-Blick, N., 1991, Onlap, offlap, and the origin of

unconformity-bounded depositional sequences: Marine Geology, v.97, p.35-56.

Cohen, A.S., 1990, Tectono-stratigraphic model for sedimentation in Lake Tanganyika, Africa, *in* B.J. Katz, ed., Lacustrine basin exploration - case studies and modern analogs: The American Association of Petroleum Geologists Memoir 50, p.137-150.

Cohen, Z., 1976, Early Cretaceous buried canyon: influence on accumulation of hydrocarbons in Helez oil field, Israel: The American Association of Petroleum Geologists Bulletin, v.60, p.108-114.

Conceição, J.C.J., P.V. Zalán, and S. Wolff, 1988, Mecanismo, evolução e cronologia do rift Sul-Atlântico: Boletim de Geociências da PETROBRÁS, v.2, p.255-265.

Coleman, J.M., D.B. Prior, and J.F. Lindsay, 1983, Deltaic influences on shelfedge instability processes, *in* D.J. Stanley and G.T. Moore, eds., The shelfbreak: critical interface on continental margins: Society of Economic Paleontologists and Mineralogists Special Publication No.33, p.121-137.

Coleman, J.M., A.H. Bouma, H.H. Roberts, P.A. Thayer, and DSDP Leg 96 Scientific Party, 1985, *in* A.H. Bouma, W.R. Normark, and N.E. Barnes, eds., Submarine fans and related turbidite systems: New York, Springer-Verlag, p.311-318.

Coleman, M.L., 1985, Geochemistry of diagenetic non-silicate:

kinetic considerations: Philosophical Transactions of the Royal Society of London, v.315A, p.39-56.

Cordani, U.G., B.B. Brito Neves, R. Fuck, R. Porto, A. Thomaz Filho, and F.M.B. Cunha, 1984, Estudo preliminar de integração do Pré-Cambriano com os eventos tectônicos das bacias sedimentares brasileiras: Série Ciência-Técnica-Petróleo, Seção Exploração de Petróleo, PETROBRÁS, Rio de Janeiro, v.15, 70p.

Cosmo, C.A., and A. Palhares, Jr., 1988, Estratégia explotatória do Campo de Fazenda Queimadas, Bacia do Espírito Santo, in Proceedings of the 3rd Seminar on Development and Reservoir Geology, PETROBRÁS, Salvador, Brazil, p.65-75.

Cosmo, C.A., A. Palhares, Jr., H.D. Rangel, B. Wolff, and A.M.F. Figueiredo, 1991, Lagoa Parda Field - Brazil: Espírito Santo Basin, southeastern Brazil, in N.H. Foster, and E.A. Beaumont, eds., Stratigraphic traps II: The American Association of Petroleum Geologists Treatise of Petroleum Geology, Atlas of oil and gas fields, p.349-360.

Costa, L.A.R., 1988, Análise termomecânica da porção offshore da Bacia do Espírito Santo: unpublished M.Sc. Thesis, Universidade Federal de Ouro Preto, Ouro Preto, Brazil, 142p.

Cremer, M., 1983, Approches sedimentologique et geophysique des accumulations turbiditiques: l'eventail profond du

Cap-Ferret (Golfe de Gascogne), la serie des Gres D'Annot (Alpes de Haute Provence): unpublished Ph.D. Thesis, L'Universite de Bordeaux I, France, 344p.

Cremer, M., P. Orsolini, and C. Ravenne, 1985, Cap-Ferret fan, Atlantic Ocean, *in* A.H. Bouma, W.R. Normark, and N.E. Barnes, eds., Submarine fans and related turbidite systems: New York, Springer-Verlag, p.113-120.

Crowley, T.J., 1983, The geologic record of climatic change: Reviews of Geophysics and Space Physics, v.21, p.828-877.

Curtis, C., 1987, Mineralogical consequences of organic matter degradation in sediments: inorganic/organic diagenesis, *in* J.K. Leggett, and G.G. Zuffa, eds., Marine clastic sedimentology: concepts and case studies: Dordrecht, Graham & Trotman, p.108-123.

D'Alessandro, A., A.A. Ekdale, and M. Sonnino, 1986, Sedimentologic significance of turbidite ichnofacies in the Saraceno Formation (Eocene), southern Italy: Journal of Sedimentary Petrology, v.56, p.294-306.

Damuth, J.E., and Embley, R.W., 1981, Mass-transport processes on Amazon cone, western equatorial Atlantic: The American Association of Petroleum Geologists Bulletin, v.65, p.629-643.

Damuth, J.E., V. Kolla, R.D. Flood, R.O. Kowsmann, M.C. Monteiro, M.A. Gorini, J.J.C. Palma, and R.H. Belderson, 1983a, Distributary channel meandering and bifurcation patterns on the Amazon deep-sea fan as revealed by long-

range side-scan sonar (GLORIA): Geology, v.11, p.94-98.

Damuth, J.E., R.O. Kowsmann, R.D. Flood, R.H. Belderson, and M.A. Gorini, 1983b, Age relationships of distributary channels on Amazon deep-sea fan: implications for fan growth pattern: Geology, v.11, p.470-473.

Damuth, J.E., R.D. Flood, R.O. Kowsmann, R.H. Belderson, and M.A. Gorini, 1988, Anatomy and growth pattern of Amazon deep-sea fan as revealed by long-range side-scan sonar (GLORIA) and high-resolution seismic studies: The American Association of Petroleum Geologists Bulletin, v.72, p.885-911.

Dauzacker, M.V., 1981, Basin analysis of evaporitic and post-evaporitic depositional systems, Espírito Santo Basin, Brazil, South America: unpublished PhD thesis, University of Texas, Austin.

Dengler, A.T., P. Wilde, E.K. Noda, and W.R. Normark, 1984, Turbidity currents generated by Hurricane Iwa: Geo-Marine Letters, v.4, p.5-11.

Dias, J.L., J.Q. Oliveira, and J.C. Vieira, 1988, Sedimentological and stratigraphic analysis of the Lagoa Feia formation, rift phase of Campos Basin, offshore Brazil: Revista Brasileira de Geociências, v.18, p.252-260.

Dias, J.L., J.C. Scarton, F.R. Esteves, M. Carminatti, L.R. Guardado, 1990, Aspectos da evolução tectono-sedimentar e a ocorrência de hidrocarbonetos na Bacia de Campos, *in*

G.P. Raja Gabaglia, and E.J. Milani, eds., Origem e evolução de bacias sedimentares: Rio de Janeiro, PETROBRÁS, p.333-360.

Dias-Brito, D., 1987, A Bacia de Campos no Mesocretáceo: uma contribuição à paleoceanografia do Atlântico Sul primitivo: Revista Brasileira de Geociências, v.17, p.162-167.

Dickas, A.B., and J.L. Payne, 1967, Upper Paleocene buried channel in Sacramento Valley, California: The American Association of Petroleum Geologists Bulletin, v.51, p.873-882.

Dickinson, W.R., and C.A. Suczek, 1979, Plate tectonics and sandstone composition: The American Association of Petroleum Geologists, v.63, p.2164-2182.

Droz, L., and G. Bellaiche, 1985, Rhone deep-sea fan: morphostructure and growth pattern: The American Association of Petroleum Geologists Bulletin, v.69, p.460-479.

Droz, L., and D. Mougenot, 1987, Mozambique upper fan: origin of depositional units: The American Association of Petroleum Geologists Bulletin, v.71, p.1355-1365.

Duarte, R.L.B., Winter, W.R., and M. Calderon, 1990, Aspectos geológicos e de produção na recuperação secundária do Campo de Cherne, Bacia de Campos, *in* Proceedings of the 4th Seminar on Development and Reservoir Geology, PETROBRÁS, Natal, Brazil, p.149-162.

Einsele, G., 1992, Sedimentary basins: evolution, facies, and sediment budget: Berlin, Springer-Verlag, 628p.

Ekdale, A.A., 1977, Abyssal trace fossils in worlwide Deep Sea Drilling Project cores, *in* T.P. Crimes, and J.C. Harper, eds., Trace fossils 2, Geological Journal Special Issues 9, p.163-182.

Ekdale, A.A., 1985, Paleoecology of the marine endobenthos: Palaeogeography, Palaeoclimatology, Palaeoecology, v.50, p.63-81.

Ekdale, A.A., 1988, Pitfalls of paleobathymetric interpretations based on trace fossil assemblages: Palaios, v.3, p.464-472.

Ekdale, A.A., and D.W. Lewis, 1991, The New Zealand *Zoophycos* revisited: morphology, ethology, and paleoecology: Ichnos, v.1, p.183-194.

Ekdale, A.A., and T.R. Mason, 1988, Characteristic trace-fossil associations in oxygen-poor sedimentary environments: Geology, v.16, p.720-723.

Elmore, R.D., O.H. Pilkey, W.J. Cleary, and H. Allen Curran, 1979, Black shell turbidite, Hatteras abyssal plain, western Atlantic Ocean: Geological Society of America Bulletin, v.90, p.1165-1176.

Esteves, F.R., A.R. Spadini, and M. Saito, 1987, A sedimentação albo-turoniana (Formação Macaé) da Bacia de Campos, *in* Proceedings of the 1st Simposium on the Geology of the Rio da Janeiro and Espírito Santo States,

Sociedade Brasileira de Geologia, Rio de Janeiro, Brazil, p.27-42.

Estrella, G., M.R. Mello, P.C. Gaglianone, R.L.M. Azevedo, K. Tsubone, E. Rossetti, J. Concha, and I.M.R.A. Brüning, 1984, The Espírito Santo Basin (Brazil) source rock characterization and petroleum habitat, *in* G. Demaison, and R.J. Murris, eds., Petroleum Geochemistry and basin evaluation: The American Association of Petroleum Geologists Memoir 35, p.253-271.

Eyles, N., and C.H. Eyles, 1992, Glacial depositional systems, *in* R.G. Walker and N.P. James, eds., Facies models: response to sea level change, Geological Association of Canada, p.73-100.

Farre, J.A., B.A. McGregor, W.B.F. Ryan, and J.M. Robb, 1983, Breaching the shelbreak: passage from youthful to mature phase in submarine canyon evolution, *in* D.J. Stanley and G.T. Moore, eds., The shelbreak: critical interface on continental margins: Society of Economic Paleontologists and Mineralogists Special Publication No. 33, p.25-39.

Feeley, M.H., T.C. Moore, Jr., T.S. Loutit, and W.R. Bryant, 1990, Sequence stratigraphy of Mississippi fan related to oxygen isotope sea level index: The American Association of Petroleum Geologists Bulletin, v.74, p.407-424.

Figueiredo, A.M.F., 1981, Depositional systems in the Lower Cretaceous Morro do Chaves and Coqueiro Seco formations and their relationship to petroleum accumulations: middle

rift sequence, Sergipe-Alagoas Basin, Brazil: unpublished Ph.D. Thesis, University of Texas, Austin, 302p.

Figueiredo, A.M.F., and C.C. Martins, 1990, 20 Anos de exploração da Bacia de Campos e o sucesso nas águas profundas: Boletim de Geociências da PETROBRÁS, v.4, p.105-123.

Figueiredo, A.M.F., and W.U. Mohriak, 1984, A tectônica salífera e as acumulações de petróleo da Bacia de Campos, *in* Proceedings of the 33rd Brazilian Geological Congress, Sociedade Brasileira de Geologia, Rio de Janeiro, v.3, p.1380-1394.

Figueiredo, A.M.F., J.A.E. Braga, H.M.C. Zabalaga, J.J. Oliveira, G.A. Aguiar, O.B. Silva, and L.F. Mato, 1993, Recôncavo basin, Brazil: a prolific intracontinental rift basin, *in* J.C. Harms, S.M. Landon, and M. Steckler, eds., Interior rift basins: The American Association of Petroleum Geologists Memoir, in press.

Fischer, A.G., 1991, Orbital cyclicity in Mesozoic strata, *in* G. Einsele, W. Ricken, and A. Seilacher, eds., Cycles and events in stratigraphy: Springer-Verlag, New York, p.48-62.

Flood, R.D., and J.E. Damuth, 1987, Quantitative characteristics of sinuous distributary channels on the Amazon deep-sea fan: Geological Society of America Bulletin, v.98, p.728-738.

Flood, R.D., P.L. Manley, R.O. Kowsmann, C.J. Appi, and C.

Pirmez, 1991, Seismic facies and late Quaternary growth of Amazon submarine fan, *in* P. Weimer, and M.H. Link, eds., Seismic facies and sedimentary processes of submarine fans and turbidite systems: New York, Springer-Verlag, p.415-433.

Fodor, R.V., E.H. McKee, and H.E. Asmus, 1983, K-Ar ages and the opening of the South Atlantic Ocean: basaltic rock from the Brazilian margin: Marine Geology, v.54, p.M1-M8.

Folk, R.L., 1974, Petrology of sedimentary rocks: Austin, Hemphill Publishing Company, 182p.

Folk, R.L., and W.C. Ward, 1957, Brazos river bar: a study in the significance of grain size parameters: Journal of Sedimentary Petrology, v.27, p.3-27.

Fondecave-Wallez, M.-J., P. Souquet, and Y. Gourinard, 1990, Sequence stratigraphy and grade-dating in the Senonian series from the South-Pyrenees (Spain), the sedimentary record of eustacy and tectonics, *in* R.N. Ginsburg and B. Beaudoin, eds., Cretaceous resources, events and rhythms: background and plans for research: Dordrecht, Kluwer Academic Publishers, p.63-74.

Forel, F.A., 1885, Les ravins sous-lacustres des fleuves glaciaires: Comptes Randus de l'Academie des Sciences, Paris, v.101, p.725-728.

Forel, F.A., 1892, Le Léman, v.1, 543p.

Frakes, L.A., and J.E. Francis, 1990, Cretaceous paleoclimates, *in* R.N. Ginsburg and B. Beaudoin, eds.,

Cretaceous resources, events and rhythms: background and plans for research: Dordrecht, Kluwer Academic Publishers, p.273-287.

Freitas, L.C.S., 1987, Estudo de reservatório do Membro Carapebus (Cretáceo) no Campo de Carapeba, Bacia de Campos, Estado do Rio de Janeiro, Brasil: unpublished M.Sc. Thesis, Universidade Federal de Ouro Preto, Ouro Preto, Brazil, 135p.

Frey, R.W., and A. Seilacher, 1980, Uniformity in marine invertebrate ichnology: Lethaia, v.13, p.183-207.

Fukushima, Y., G. Parker, and H.M. Pantin, 1985, Prediction of ignitive turbidity currents in Scripps submarine canyon: Marine Geology, v.67, p.55-81.

Galloway, W.E., W.F. Dingus, and R.E. Paige, 1991, Seismic and depositional facies of Paleocene-Eocene Wilcox Group submarine canyon fills, northwest Gulf Coast, U.S.A., *in* P. Weimer, and M.H. Link, eds., Seismic facies and sedimentary processes of submarine fans and turbidite systems: New York, Springer-Verlag, p.247-271.

Gamboa, L.A.P., F.P. Esteves, S. Shimabukuro, M. Carminatti, W.E. Peres, and C.E. Souza Cruz, 1986, Evidências de variações de nível do mar durante o Oligoceno e suas implicações faciológicas, *in* Proceedings of the 34th Brazilian Geological Congress, Sociedade Brasileira de Geologia, Goiânia, v.1, p.8-22.

Garcia, A.J.V., L.F. De Ros, R.S. Souza, and C.H.L. Bruhn,

1990, Potencial de reservatórios profundos na Formação Serraria, Bacia de Sergipe-Alagoas: Boletim de Geociências da PETROBRÁS, v.4, p.467-488.

Ghibaudo, G., 1980, Deep-sea fan deposits in the Macigno Formation (middle-upper Oligocene) of the Gordana Valley, northern Apennines, Italy: Journal of Sedimentary Petrology, v.50, p.723-742.

Gomes, J.B. et al., 1988, Revisão geológica regional da Bacia do Espírito Santo: Rio de Janeiro, PETROBRÁS Internal Report.

Goodwin, R.H., and D.B. Prior, 1989, Geometry and depositional sequences of the Mississippi canyon, Gulf of Mexico: Journal of Sedimentary Petrology, v.59, p.318-329.

Graham, S.A., and S.B. Bachman, 1983, Structural controls on submarine-fan geometry and internal architecture: upper La Jolla fan system, offshore southern California: The American Association of Petroleum Geologists Bulletin, v.67, p.83-96.

Guardado, L.R., L.A.P. Gamboa, and C.F. Lucchesi, 1990, Petroleum geology of the Campos Basin, Brazil: a model for a producing Atlantic-type basin, in J.D. Edwards and P.A. Santogrossi, eds., Divergent/passive margin basins: The American Association of Petroleum Geologists Memoir 48, p.3-79.

Guimarães, P.T.M., E.M. Ribeiro, and S.R.P. Silva, 1989, Interpretação sismoestratigráfica em águas profundas na

Bacia Pará-Maranhão, *in* Proceedings of the 1st Seminar on Exploratory Interpretation, Rio de Janeiro, PETROBRÁS, p.171-183.

Haq, B.U., 1991, Sequence stratigraphy, sea-level change, and significance for the deep sea, *in* D.I.M. McDonald, ed., Sedimentation, tectonics and eustasy: sea-level changes at active margins: International Association of Sedimentologists Special Publication 12, p.3-39.

Haq, B.U., J. Hardenbol, and P.R. Vail, 1987, Chronology of fluctuating sea levels since the Triassic: Science, v.235, p.1156-1167.

Haq. B.U., J. Hardenbol, and P.R. Vail, 1988, Mesozoic and Cenozoic chronostratigraphy and cycles of sea-level change, *in* C.K. Wilgus, B.S. Hastings, C.G.St.C. Kendall, H.W. Posamentier, C.A. Ross, and J.C. Van Wagoner, eds., Sea-level changes: an integrated approach: Society of Economic Paleontologists and Mineralogists Special Publication No.42, p.71-108.

Harland, W.B., A.V. Cox, P.G. Llewellyn, C.A.G. Pickton, A.G. Smith, and R. Walters, 1982, A geologic time scale: Cambridge, Cambridge University Press, 131p.

Harland, W.B., R.L. Armstrong, A.V. Cox, L.E. Craig, A.G. Smith, and D.G. Smith, 1990, A geologic time scale, 1989: Cambridge, Cambridge University Press, 263.

Harms, J.C., and R.K. Fahnestock, 1965, Stratification, bed forms and flow phenomena (with an example from the Rio

Grande), *in* G.V. Middleton, ed., Primary sedimentary structures and their hydrodynamic interpretation: Society of Economic Paleontologists and Mineralogists Special Publication No.12, p.84-115.

Harris, P.M., S.H. Frost, G.A. Seiglie, and N. Schneidermann, 1984, Regional unconformities and depositional cycles, Cretaceous of the Arabian Peninsula, *in* J.S. Schlee, ed., Interregional unconformities and hydrocarbon accumulation: The American Association of Petroleum Geologists Memoir 36, p.67-80.

Hayward, B.W., 1976, Lower Miocene bathyal and submarine canyon ichnocoenoses from Northland, New Zealand: Lethaia, v.9, p.149-162.

Heezen, B.C., and M. Ewing, 1952, Turbidity currents and submarine slumps and the 1929 Grand Banks earthquake: American Journal of Science, v.250, p.849-873.

Hein, F.J., 1982, Depositional mechanisms of deep-sea coarse clastic sediments, Cap Enragé Formation, Québec: Canadian Journal of Earth Sciences, v.19, p.267-287.

Heller, P.L., and W.R. Dickinson, 1985, Submarine ramp facies model for delta-fed, sand-rich turbidite systems: The American Association of Petroleum Geologists Bulletin, v.69, p.960-976.

Hess, G.R., and W.R. Normark, 1976, Holocene sedimentation history of the major fan valleys of Monterey fan: Marine Geology, v.22, p.233-251.

Hiscott, R.N., 1981, Deep-sea fan deposits in the Macigno Formation (middle-upper Oligocene) of the Gordana Valley, northern Apennines, Italy - Discussion: Journal of Sedimentary Petrology, v.51, p.1015-1021.

Horschutz, P.M.C., J.C. Della Fávera, and L.J. Passos, 1973, Sedimentação deltaica das seqüências Santiago e Cambuqui, Formação Pojuca, Bacia do Recôncavo, *in* Proceedings of the 27th Brazilian Geological Congress, Sociedade Brasileira de Geologia, Aracaju, p.315-338.

Horschutz, P.M.C, L.C.S. Freitas, C.V. Stank, A.S. Barroso, and W.M. Cruz, 1992, The Linguado, Carapeba, Vermelho, and Marimbá giant oil fields, Campos basin, offshore Brazil, *in* M.T. Halbouty, ed., Giant oil and gas fields of the decade 1978 - 1988: The American Association of Petroleum Geologists Memoir 54, p.137-153.

Hower, J., E.V. Eslinger, M.E. Hower, and E.A. Perry, Jr., 1976, Mechanism of burial metamorphism of argillaceous sediment: 1. Mineralogical and chemical evidence: Geological Society of America Bulletin, v.87, p.725-737.

Hoyt, W.V., 1959, Erosional channel in the middle Wilcox near Yoakum, Lavaca County, Texas: Transactions of the Gulf Coast Association of Geological Societies, v.9, p.41-50.

Hsü, K.J., K. Kelts, and J.W. Valentine, 1980, Resedimented facies in Ventura basin, California, and model of longitudinal transport of turbidity currents: The American Association of Petroleum Geologists Bulletin,

v.64, p.1034-1051.

Hubbard, R.J., 1988, Age and significance of sequence boundaries on Jurassic and Early Cretaceous rifted continental margins: The American Association of Petroleum Geologists Bulletin, v.72, p.49-72.

Imbrie, J., and J.Z. Imbrie, 1980, Modeling the climatic response to orbital variations: Science, v.207, p.943-953.

Inman, D.L., C.E. Nordstrom, and R.E. Flick, 1976, Currents in submarine canyons: an air-sea-land interaction: Annual Review of Fluid Mechanics, p.275-310.

Jervey, M.T., 1988, Quantitative geological modelling of siliciclastic rock sequences and their seismic expression, *in* C.K. Wilgus, B.S. Hastings, C.G.St.C. Kendall, H.W. Posamentier, C.A. Ross, and J. C. Van Wagoner, eds., Sea-level changes: an integrated approach: Society of Economic Paleontologists and Mineralogists Special Publication No. 42, p.47-68.

Kastens, K.A., 1984, Earthquakes as triggering mechanism for debris flows and turbidites on the Calabrian ridge: Marine Geology, v.55, p.13-33.

Keen, C.E., 1985 The dynamics of rifting: deformation of the lithosphere by active and passive driving forces: Geophysical Journal of the Royal Astronomical Society, v.80, p.95-120.

Kendall, A.C., 1984, Evaporites, *in* R.G. Walker, ed., Facies

Models: Toronto, Geological Association of Canada, Geoscience Canada Reprint Series 1, 2nd edition, p.259-296.

Kendall, A.C., 1992, Evaporites, *in* R.G. Walker and N.P. James, eds., Facies models: response to sea level change: Geological Association of Canada, p.375-409.

Kenyon, N.H., R.H. Belderson, and A.H. Stride, 1978, Channels, canyons and slump folds on the continental slope between south-west Ireland and Spain: Oceanologica Acta, v.1, p.369-380.

Kern, J.P., and J.E. Warme, 1974, Trace fossils and bathymetry of the Upper Cretaceous Point Loma Formation, San Diego, California: Geological Society of America Bulletin, v.85, p.893-900.

Klein, D. de V, Melo, U., and J.C. Della Fávera, 1972, Subaqueous gravity processes on the front of Cretaceous deltas, Recôncavo Basin, Brazil: Bulletin of the Geological Society of America, v.83, p.1469-1492.

Klemme, H.D., 1980, Petroleum basins - classification and characteristics: Journal of Petroleum Geology, v.3, p.187-207.

Kolla, V., and F. Coumes, 1987, Morphology, internal structure, seismic stratigraphy, and sedimentation of Indus fan: The American Association of Petroleum Geologists Bulletin, v.71, p.650-677.

Kolla, V., R.T. Buffler, and J.W. Ladd, 1984, Seismic

stratigraphy and sedimentation of Magdalena fan, southern Colombian basin, Caribbean Sea: The American Association of Petroleum Geologists Bulletin, v.68, p.316-332.

Komar, P.D., 1973, Continuity of turbidity current flow and systematic variations in deep-sea channel morphology: Geological Society of America Bulletin, v.84, p.3329-3338.

Komar, P.D., 1977, Computer simulation of turbidity current flow and the study of deep-sea channels and fan sedimentation, *in* E.D. Goldberg, ed., The sea: ideas and observations on progress in the study of the sea: Wiley, New York, p.603-621.

Koutsoukos, E.A.M., and M.B. Hart, 1990, Cretaceous foraminiferal morphogroup distribuition patterns, paleocommunities and trophic structures: a case study from the Sergipe Basin, Brazil: Transactions of the Royal Society of Edinburgh: Earth Sciences, v.81, p.221-246.

Koutsoukos, E.A.M., M.R. Mello, N.C. Azambuja, M.B. Hart, and J.R. Maxwell, 1991, The upper Aptian-Albian succession of the Sergipe basin, Brazil: an integrated paleoenvironmental assessment: The American Association of Petroleum Geologists Bulletin, v.75, p.479-498.

Kuenen, Ph.H., and C.I. Migliorini, 1950, Turbidity currents as a cause of graded bedding: The Journal of Geology, v.58, p.91-127.

Larson, R.L., and J.W. Ladd, 1973, Evidence for the opening of

the South Atlantic in the Early Cretaceous: Nature, v.246, p.209-212.

Lee, H.J., and B.E. Edwards, 1986, Regional method to assess offshore slope stability: Journal of Geotechnical Engineering, v.112, p.489-509.

Leonard, J.E., B. Cameron, O.H. Pilkey, and G.M. Friedman, 1981, Evaluation of cold-water carbonates as a possible paleoclimate indicator: Sedimentary Geology, v.28, p.1-28.

Leyden, R., H.E. Asmus, S. Zembruscki, and G. Bryan, 1976, South Atlantic diapiric structures: The American Association of Petroleum Geologists Bulletin, v.60, p.196-212.

Lima, M.R., 1983, Paleoclimatic reconstruction of the Brazilian Cretaceous based on palynological data: Revista Brasileira de Geociências, v.13, p.223-228.

Link, M.H., and T.H. Nilsen, 1980, The Rocks Sandstone, an Eocene sand-rich deep-sea fan deposit, northern Santa Lucia Range, California: Journal of Sedimentary Petrology, v.50, p.583-601.

Link, M.H., and J.E. Welton, 1982, Sedimentology and reservoir potential of Matilija sandstone: an Eocene sand-rich deep-sea fan and shallow-marine complex, California: The American Association of Petroleum Geologists Bulletin, v.66, p.1514-1534.

Lowe, D.R., 1975, Water escape structures in coarse-grained

sediments: Sedimentology, v.22, p.157-204.

Lowe, D.R., 1982, Sediment gravity flows: II. Depositional models with special reference to the deposits of high-density turbidity currents: Journal of Sedimentary Petrology, v.52, p.279-297.

Lowe, D.R., and R.D. LoPiccolo, 1974, The characteristics and origins of dish and pillar structures: Journal of Sedimentary Petrology, v.44, p.484-501.

Macedo, J.M., 1987, Evolução estrutural da Bacia de Santos e áreas continentais adjacentes: unpublished M.Sc. Thesis, Universidade Federal de Ouro Preto, Brazil, 165p.

Malinverno, A., W.B.F. Ryan, G. Auffret, and G. Pautot, 1988, Sonar images of the path of recent failure events on the continental margin off Nice, France, *in* H.E. Clifton, ed., Sedimentological consequences of convulsive geological events: Geological Society of America Special Paper 229, p.59-75.

Manley, P.L., and R.D. Flood, 1988, Cyclic sediment deposition within Amazon deep-sea fan: The American Association of Petroleum Geologists Bulletin, v.72, p.912-925.

Marintsch, E.J., and R.M. Finks, 1982, Lower Devonian ichnofacies at Highland Mills, New York, and their gradual replacement across environmental gradients: Journal of Paleontology, v.56, p.1050-1078.

Marques, A., 1990, Evolução tectono-sedimentar e perspectivas exploratórias da Bacia de Taubaté, São Paulo, Brasil:

Boletim de Geociências da PETROBRÁS, v.4, p.253-262.

Martin, B.D., 1963, Rosedale channel - evidence for late Miocene submarine erosion in Great Valley of California: The American Association of Petroleum Geologists Bulletin, v.47, p.441-456.

Martini, E., 1971, Standard Tertiary and Quaternary calcareous nannoplankton zonation, *in* A. Farinacci, ed., Proceedings of the 2nd Planktonic Conference, Rome, Edizioni Tecnoscienza, v.2, p.739-785.

Martins, F.A.L., A.R.E. Sad, J.C. Scarton, J.Q. Oliveira, and J.L.P. Moreira, 1990, Mapeamento regional dos turbiditos da Bacia de Campos: do neo-Albiano ao Mioceno, *in* Proceedings of the 4th Brazilian Petroleum Congress, Instituto Brasileiro do Petróleo, Rio de Janeiro, TT-208, 9p.

Masson, D.G., J.V. Gardner, L.M. Parson, and M.E. Field, 1985, Morphology of upper Laurentian fan using GLORIA long-range side-scan sonar: The American Association of Petroleum Geologists Bulletin, v.69, p.950-959.

May, J.A., J.E. Warme, and R.A. Slater, 1983, Role of submarine canyons on shelfbreak erosion and sedimentation: modern and ancient examples, *in* D.J. Stanley, and G.T. Moore, eds., The shelfbreak: critical interface on continental margins: Society of Economic Paleontologists and Mineralogists Special Publication No.33, p.315-332.

McBride, E.F., 1963, A classification of common sandstones: Journal of Sedimentary Petrology, v.33, p.664-669.

McHargue, T.R., 1991, Seismic facies, processes, and evolution of Miocene inner fan channels, Indus submarine fan, *in* P. Weimer, and M.H. Link, eds., Seismic facies and sedimentary processes of submarine fans and turbidite systems: New York, Springer-Verlag, p.403-413.

McHargue, T.R., and Webb, J.E., 1986, Internal geometry, seismic facies, and petroleum potential of canyons and inner fan channels of the Indus submarine fan: The American Association of Petroleum Geologists Bulletin, v.70, p.161-180.

McKenzie, D.P., 1978, Some remarks on the development of sedimentary basins: Earth and Planetary Science Letters, v.40, p.25-32.

Mear, J., 1984, Sequences et unites sedimentaires du glacis rhodanien (Mediterranee Occidentale): unpublished Ph.D. Thesis, University of Perpignan, Perpignan, France, 218p.

Mello, M.R., and J.R. Maxwell, 1990, Organic geochemical and biological marker characterization of source rocks and oils derived from lacustrine environments in the Brazilian continental margin, *in* B.J. Katz, ed., Lacustrine basin exploration: case studies and modern analogs: The American Association of Petroleum Geologists Memoir 50, p.77-97.

Melo, M.S., C. Riccomini, Y. Hasui, F.F.M. Almeida, and A.M.

Coimbra, 1985, Geologia e evolução do sistema de bacias tafrogênicas continentais do sudeste do Brasil: Revista Brasileira de Geociências, v.15, p.193-201.

Menard, H.W., 1964, Marine geology of the Pacific: McGraw-Hill, New York, 271p.

Miall, A.D., 1991, Stratigraphic sequences and their chronostratigraphic correlation: Journal of Sedimentary Petrology, v.61, p.497-505.

Miall, A.D., 1992, Exxon global cycle chart: an event for every occasion ?: Geology, v.20, p.787-790.

Middleton, G.V., 1966a, Experiments on density and turbidity currents: I. Motion of the head: Canadian Journal of Earth Sciences, v.3, p.523-546.

Middleton, G.V., 1966b, Experiments on density and turbidity currents: II. Uniform flow of density currents: Canadian Journal of Earth Sciences, v.3, p.627-637.

Middleton, G.V., 1967, Experiments on density and turbidity currents: III. Deposition of sediment: Canadian Journal of Earth Sciences, v.4, p.475-505.

Middleton, G.V., 1970, Experimental studies related to problems of flysch sedimentation, *in* J. Lajoie, ed., Flysch sedimentology in North America: Geological Association of Canada Special Paper 7, p.253-272.

Middleton, G.V., 1982, A brief guide to the sedimentology of the Hamilton area: Department of Geology, McMaster University Technical Memoir 82-1, 26p.

Middleton, G.V., and M.A. Hampton, 1973, Sediment gravity flows: mechanics of flow and deposition, *in* G.V. Middleton, and A.H. Bouma, eds., Turbidites and deep water sedimentation: Society of Economic Paleontologists and Mineralogists, Pacific Section, Short Course, p.1-38.

Middleton, G.V., and W.J. Neal, 1989, Experiments on the thickness of beds deposited by turbidity currents: Journal of Sedimentary Petrology, v.59, p.297-307.

Milani, E.J., M.C. Lana, and P. Szatmari, 1988, Mesozoic rift basins around the northeast Brazilian microplate (Recôncavo-Tucano-Jatobá, Sergipe-Alagoas), *in* W. Manspeizer, ed., Triassic-Jurassic rifting:continental breakup and the origin of the Atlantic Ocean and passive margins, part B, Developments in Geotectonics 22, New York, Elsevier, p.833-858.

Miller, K.G., R.G. Fairbanks, and G.S. Mountain, 1987, Tertiary oxygen isotope synthesis, sea level history, and continental margin erosion: Paleoceanography, v.2, p.1-19.

Mitchum, R.M., Jr., 1977, Seismic stratigraphy and global changes of sea level, Part 11: Glossary of terms used in seismic stratigraphy, *in* C.E. Payton, ed., Seismic stratigraphy - applications to hydrocarbon exploration: The American Association of Petroleum Geologists Memoir 26, p.205-212.

Mitchum, R.M., Jr., 1985, Seismic stratigraphic expression of

submarine fans, *in* O.R. Berg and D.G. Woolverton, eds., Seismic stratigraphy II; an integrated approach to hydrocarbon exploration: The American Association of Petroleum Geologists Memoir 39, p.117-136.

Mizusaki, A.M.P., 1986, Rochas ígneas básicas do Neocomiano da Bacia de Campos: características e comportamento como reservatório de hidrocarbonetos: unpublished M.Sc. Thesis, Universidade Federal do Rio de Janeiro, Brazil, 104p.

Mohriak, W.U., M.R. Mello, J.F. Dewey, and J.R. Maxwell, 1990, Petroleum geology of the Campos Basin, offshore Brazil, *in* J. Brooks, ed., Classic petroleum provinces: The Geological Society of London Special Publication No. 50, p.119-141.

Moraes, M.A.S., 1985, Petrologia dos arenitos turbidíticos Cretácicos e Terciários da Bacia de Campos, Rio de Janeiro, Brasil: unpublished M.Sc. Thesis, Universidade Federal de Ouro Preto, Ouro Preto, Brazil, 112p.

Moraes, M.A.S., 1989, Diagenetic evolution of Cretaceous-Tertiary turbidite reservoirs, Campos basin, Brazil: The American Association of Petroleum Geologists Bulletin, v.73, p.598-612.

Morris, W., and C. Busby-Spera, 1988, Sedimentologic evolution of a submarine canyon in a forearc basin, Upper Cretaceous Rosario Formation, San Carlos Mexico: The American Association of Petroleum Geologists Bulletin,

v.72, p.717-737.

Morris, W., and C. Busby-Spera, 1990, A submarine-fan valley-levee complex in the Upper Cretaceous Rosario Formation: implication for turbidite facies models: Geological Society of America Bulletin, v.102, p.900-914.

Moura, J.A., 1987, Biocronoestratigrafia da seqüência não-marinha do Cretáceo Inferior da Bacia de Campos, Brasil, *in* Proceedings of the 10th Paleontology Brazilian Congress, Sociedade Brasileira de Paleontologia, Rio de Janeiro, v.2, p.717-731.

Mutti, E., 1977, Distinctive thin-bedded turbidite facies and related depositional environments in the Eocene Hecho Group (south-central Pyrennes, Spain): Sedimentology, v.24, p.107-131.

Mutti, E., 1979, Turbidites et cones sous-marins profonds, *in* P. Homewood, ed., Sedimentation detritique (fluviatile, littorale et marine): Institut de Geologie, Université de Fribourg, Fribourg, Switzerland, p.353-419.

Mutti, E., 1985, Turbidite systems and their relations to depositional sequences, *in* G.G. Zuffa, ed., Provenance of arenites: Dordrecht, D. Reidel Publishing Company, p.65-93.

Mutti, E., 1992, Turbidite sandstones: Milan, Agip, 275p.

Mutti, E., and G. Ghibaudo, 1972, Un esempio di torbiditi di conoide sottomarina esterna: le arenarie di San Salvatore (Formazione di Bobbio, Micene) nell'Appennino di

Piacenza: Memorie dell'Accademia delle Scienze di Torino, Classe di Scienze Fisiche, Matematiche e Naturali, Serie 4, n.16, 40p.

Mutti, E., and W.R. Normark, 1987, Comparing examples of modern and ancient turbidite systems: problems and concepts, *in* J.R. Leggett, and G.G. Zuffa, eds., Marine clastic sedimentology: concepts and case studies: London, Graham and Trotman, p.1-38.

Mutti, E., and W.R. Normark, 1991, An integrated approach to the study of turbidite systems, *in* P. Weimer and M.H. Link, eds., Seismic facies and sedimentary processes of submarine fans and turbidite systems: New York, Springer-Verlag, p.75-106.

Mutti, E., and F. Ricci Lucchi, 1972, Le torbiditi dell' Appennino settentrionale: introduzione all' analisi di facies: Memorie della Società Geologica Italiana, v.11, p.161-199.

Mutti, E., and F. Ricci Lucchi, 1974, La signification de certaines unités séquentielles dans les séries à turbidites: Bulletin Societé Géologique de France, v.7, p.577-582.

Mutti, E., and F. Ricci Lucchi, 1975, Turbidite facies and facies associations, *in* E. Mutti, F. Ricci Lucchi, M. Sagri, G. Zanzucchi, G. Ghibaudo, and S. Iaccarino, eds., Examples of turbidite facies and facies associations from selected formations of the Northern Apennines:

International Association of Sedimentologists, Guidebook to Field Trip A-11, 9th International Congress of Sedimentology (Nice, 1975), p.21-36.

Mutti, E., and M. Sonnino, 1981, Compensation cycles: a diagnostic feature of turbidite sandstone lobes, *in* International Association of Sedimentologists, 2nd European Regional Meeting, Bologna, Italy, Abstracts Volume, p.120-123.

Mutti, E., F. Ricci Lucchi, M. Seguret, and G. Zanzucchi, 1984, Seismoturbidites: a new group of resedimented deposits: Marine Geology, v.55, p.103-116.

Natland, M.L., and Ph.H. Kuenen, 1951, Sedimentary history of the Ventura Basin, California, and the action of turbidity currents, *in* J.L. Hough, ed., Turbidity currents and the transportation of coarse sediment into deep water: Society of Economic Paleontologists and Mineralogists Special Publication No.2, p.76-107.

Negreiros, J.H.C., 1990, Arenitos da Formação Itaparica no extremo nordeste da Bacia do Recôncavo: sedimentação, evolução diagenética e características de reservatórios: Boletim de Geociências da PETROBRÁS, v.4, p.137-154.

Nelson, C.H., 1990, Estimated post-Messinian sediment supply and sedimentation rates on the Ebro continental margin, Spain: Marine Geology, v.95, p.395-418.

Nelson, C.H., and A. Maldonado, 1988, Factors controlling depositional patterns of Ebro turbidite systems,

Mediterranean Sea: The American Association of Petroleum Geologists Bulletin, v.72, p.698-716.

Nelson, C.H., and A. Maldonado, 1990, Factors controlling late Cenozoic continental margin growth from the Ebro Delta to the western Mediterranean deep sea: Marine Geology, v.95, p.419-440.

Nelson, C.H., and T.H. Nilsen, 1984, Modern and ancient deep-sea fan sedimentation: Society of Economic Paleontologists and Mineralogists Short Course 14, 404p.

Nelson, C.H., A. Maldonado, J.H. Barber, and B. Alonso, 1991, Modern sand-rich and mud-rich siliciclastic aprons: alternative base-of-slope turbidite systems to submarine fans, in P. Weimer, and M.H. Link, eds., Seismic facies and sedimentary processes of submarine fans and turbidite systems: New York, Springer-Verlag, p.171-190.

Nelson, C.H., D.C. Twichell, W.C. Schwab, H.J. Lee, and N.H. Kenyon, 1992, Upper Pleistocene turbidite sand beds and chaotic silt beds in the channelized, distal, outer-fan lobes of the Mississippi fan: Geology, v.20, p.693-696.

Netto, A.S.T., 1974, Petroleum and reservoir potentialities of the Água Grande member (Cretaceous), Recôncavo basin, Brazil: unpublished M.Sc. Thesis, University of Texas, Austin, 148p.

Netto, A.S.T., 1978, A implantação da fase rift na Bacia do Recôncavo, in Proccedings of the 30th Brazilian Geological Congress, Sociedade Brasileira de Geologia,

Recife, v.1, p.506-517.

Nilsen, T.H., 1980, Modern and ancient submarine fans: discussion of papers by R.G. Walker and W.R. Normark: The American Association of Petroleum Geologists Bulletin, v.64, p.1094-1112.

Noguti, I., and J.F. Santos, 1972, Zoneamento preliminar por foraminíferos planctônicos do Aptiano ao Mioceno na Plataforma Continental do Brasil: Boletim Técnico da PETROBRÁS, v.15, p.265-283.

Normark, W.R., 1970, Growth patterns of deep-sea fans: The American Association of Petroleum Geologists Bulletin, v.54, p.2170-2195.

Normark, W.R., 1978, Fan valleys, channels, and depositional lobes on modern submarine fans: characters for recognition of sandy turbidite environments: The American Association of Petroleum Geologists Bulletin, v.62, p.912-931.

Normark, W.R., and D.J. Piper, 1991, Initiation processes and flow evolution of turbidity currents: implications for the depositional record, *in* R.H. Osborne, ed., From shoreline to abyss: contributions in marine geology in honor of Francis Parker Shepard: Society of Economic Paleontologists and Mineralogists Special Publication 46, p.207-230.

Normark, W.R., D.J. Piper, and G.R. Hess, 1979, Distributary channels, sand lobes, and mesotopography of Navy

submarine fan, California Borderland, with applications to ancient fan sediments: Sedimentology, v.26, p.749-774.

Normark, W.R., D.J. Piper, and D.A.V. Stow, 1983, Quaternary development of channels, levees, and lobes on middle Laurentian fan: The American Association of Petroleum Geologists Bulletin, v.67, p.1400-1409.

O'Connell, S., C.E. Stelting, A.H. Bouma, J.M. Coleman, M. Cremer, L. Droz, A.A. Meyer-Wright, W.R. Normark, K.T. Pickering, D.A.V. Stow, and DSDP Leg 96 Shipboard Scientists, 1985, Drilling results on the Lower Mississippi Fan, *in* A.H. Bouma, W.R. Normark, and N.E. Barnes, eds., Submarine fans and related turbidite systems: New York, Springer-Verlag, p.291-298.

O'Connell, S., W.R. Normark, W.B.F. Ryan, and N.H. Kenyon, 1991, An entrenched thalweg channel on the Rhone fan: interpretation from a SeaBeam and SeaMARC I survey, *in* R.H. Osborne, ed., From shoreline to abyss: contributions in marine geology in honor of Francis Parker Shepard: Society of Economic Paleontologists and Mineralogists Special Publication 46, p.259-270.

Ojeda, H.A.O., 1982, Structural framework, stratigraphy, and evolution of Brazilian marginal basins: The American Association of Petroleum Geologists Bulletin, v.66, p.732-749.

Okada, H., and D. Bukry, 1980, Supplementary modification and introduction of code numbers to the low-latitude

coccolith biostratigraphic zonation (Bukry, 1973; 1975):
Marine Micropaleontology, v.5, p.321-325.

Oliveira, F.R.B., V.L. Beraldo, and Heinerici, J., 1985,
Análise exploratória do Paleocanyon de Regência, Bacia do
Espírito Santo: Macaé, PETROBRÁS Internal Report, 32p.

Olsson, R.K., 1991, Cretaceous to Eocene sea-level
fluctuations on the New Jersey margin: Sedimentary
Geology, v.70, p.195-208.

Osgood, R.G., Jr., and E.J. Szmuc, 1972, The trace fossil
*Zoophycos* as an indicator of water depth: Bulletins of
American Paleontology, v.62, p.1-22.

Parker, G., 1982, Conditions for the ignition of
catastrophically erosive turbidity currents: Marine
Geology, v.46, p.307-327.

Parrish, J.T., and Curtis, R.L., 1982, Atmospheric
circulation, upwelling and organic-rich rocks in the
Mezosoic and Cenozoic eras: Palaeogeography,
Palaeoclimatology and Palaeoecology, v.40, p.31-66.

Parrish, J.T., A.M. Ziegler, and C.R. Scotese, 1982, Rainfall
patterns and the distribution of coals and evaporites in
the Mesozoic and Cenozoic: Palaeogeography,
Palaeoclimatology, Palaeoecology, v.40, p.67-101.

Payton, C.E., ed., 1977, Seismic stratigraphy - applications
to hydrocarbon exploration: The American Association of
Petroleum Geologists Memoir 26, 516p.

Pemberton, S.G., J.A. MacEachern, and R.W. Frey, 1992, Trace

fossil facies models: environmental and allostratigraphic significance, *in* R.G. Walker and N.P. James, eds., Facies models: response to sea level change: Geological Association of Canada, p.47-72.

Pereira, M.J., C.M. Barbosa, J. Agra, J.B. Gomes, M. Saito, M.A. Ramos, M.D. Carvalho, M. Stamato, and O. Bagni, 1986, Estratigrafia da Bacia de Santos: análise das seqüências, sistemas deposicionais e revisão litoestratigráfica, *in* Proceedings of the 34th Brazilian Geological Congress, Sociedade Brasileira de Geologia, Goiânia, Brazil, v.1, p.65-79.

Peres, W.E., 1993, Shelf-fed turbidite system model and its application to the Oligocene deposits of the Campos basin, Brazil: The American Association of Petroleum Geologists Bulletin, v.77, p.81-101.

Pickering, K.T., R.N. Hiscott, and F.J. Hein, 1989, Deep marine environments: clastic sedimentation and tectonics: London, Unwin Hyman, 416p.

Pierson, T.C., 1981, Dominant particle support mechanisms in debris flows at Mt. Thomas, New Zealand, and implications for flow mobility: Sedimentology, v.28, p.49-60.

Piper, D.J.W., and W.R. Normark, 1983, Turbidite depositional patterns and flow characteristics, Navy submarine fan, California borderland: Sedimentology, v.30, p.681-694.

Piper, D.J.W., A.N. Shor, and J.E. Hughes Clarke, 1988, The 1929 "Grand Banks" earthquake, slump, and turbidity

current, *in* H.E. Clifton, ed., Sedimentological consequences of convulsive geological events: Geological Society of America Special Paper 229, p.77-92.

Pitman, III, W.C., 1978, The relationship between eustacy and stratigraphic sequences of passive margins: Geological Society of America Bulletin, v.89, p.1389-1403.

Pitman, III, W.C., and X. Golovchenko, 1983, The effect of sealevel change on the shelfedge and slope of passive margins, *in* D.J. Stanley and G.T. Moore, eds., The shelfbreak: critical interface on continental margins: Society of Economic Paleontologists and Mineralogists Special Publication No.33, p.41-58.

Poag, C.W., and J.S. Schlee, 1984, Depositional sequences and stratigraphic gaps on submerged United States Atlantic Margin, *in* J.S. Schlee, ed., Interregional unconformities and hydrocarbon accumulation: The American Association of Petroleum Geologists Memoir 36, p.165-182.

Ponte, F.C., and H.E. Asmus, 1978, Geological framework of the Brazilian continental margin: Geologische Rundschau, v.67, p.201-235.

Ponte, F.C., J.R. Fonseca, and A.V. Carozzi, 1980, Petroleum habitats in the Mesozoic-Cenozoic of the continental margin of Brazil, *in* A.D. Miall, ed., Facts and principles of world petroleum occurrence: Canadian Society of Petroleum Geologists Memoir 6, p.857-886.

Posamentier, H.W., and R.D. Erskine, 1991, Seismic expression

and recognition criteria of ancient submarine fans, *in* P. Weimer, and M.H. Link, eds., Seismic facies and sedimentary processes of submarine fans and turbidite systems: New York, Springer-Verlag, p.197-222.

Posamentier, H.W., and P.R. Vail, 1988, Eustatic controls on clastic deposition: II - Sequence and systems tract models, *in* C.K. Wilgus, B.S. Hastings, C.G.St.C. Kendall, H.W. Posamentier, C.A. Ross, and J.C. Van Wagoner, eds., Sea-level changes: an integrated approach: Society of Economic Paleontologists and Mineralogists Special Publication No. 42, p.125-154.

Posamentier, H.W., R.D. Erskine, and R.M. Mitchum, Jr., 1991, Models for submarine-fan deposition within a sequence-stratigraphic framework, *in* P. Weimer and M.H. Link, eds., Seismic facies and sedimentary processes of submarine fans and turbidite systems: New York, Springer-Verlag, p.127-136.

Posamentier, H.W., M.T. Jervey, and P.R. Vail, 1988, Eustatic controls on clastic deposition: I - Conceptual framework, *in* C.K. Wilgus, B.S. Hastings, C.G.St.C. Kendall, H.W. Posamentier, C.A. Ross, and J.C. Van Wagoner, eds., Sea-level changes: an integrated approach: Society of Economic Palaleontologists and Mineralogists Special Publication No. 42, p.109-124.

Powers, M.C., 1953, A new roundness scale for sedimentary particles: Journal of Sedimentary Petrology, v.23, p.117-

119.

Prentice, M.L., and R.K. Matthews, 1988, Cenozoic ice-volume history: development of a composite oxygen isotope record: Geology, v.16, p.963-966.

Prosser, S., 1993, Rift-related linked depositional systems and their seismic expression, *in* G.D. Williams, and A. Dobb, eds., Tectonics and seismic sequence stratigraphy: Geological Society of London Special Publication, in press.

Quadros, L.P., and J. Gomide, 1972, Nanofósseis calcários na Plataforma Continental Brasileira: Boletim Técnico da PETROBRÁS, v.15, p.339-354.

Rabinowitz, P.D., and J. La Brecque, 1979, The Mesozoic South Atlantic Ocean and evolution of its continental margins: Journal of Geophysical Research, v.84, p.5973-6002.

Raja Gabaglia, G.P., 1991, Paleossismicidade e sedimentação: evidências no compartimento sul da Bacia do Recôncavo, Bahia: Boletim de Geociências da PETROBRÁS, v.5, p.39-68.

Rangel, H.D., 1984, Geologic evolution of Fazenda Cedro paleosubmarine canyon, Espírito Santo basin, Brazil: unpublished Ph.D. Thesis, University of Texas, Austin, 176p.

Regali, M.S.P., 1966, Zoneamento palinológico e paleoclima da Bacia do Recôncavo e do Tucano, *in* Proceedings of the 20th Brazilian Geological Congress, Sociedade Brasileira de Geologia, Vitória.

Regali, M.S.P., and C.F. Viana, 1989, Late Jurassic - Early Cretaceous in Brazilian sedimentary basins: correlation with the international standard scale: PETROBRÁS Special Publication, Rio de Janeiro, Brazil, 95p.

Regali, M.S.P., N. Uesugui, and A.S. Santos, 1974a, Palinologia dos sedimentos Meso-Cenozóicos do Brasil (I): Boletim Técnico da PETROBRÁS, v.17, p.177-191.

Regali, M.S.P., N. Uesugui, and A.S. Santos, 1974b, Palinologia dos sedimentos Meso-Cenozóicos do Brasil (II): Boletim Técnico da PETROBRÁS, v.17, p.236-301.

Rehim, H.A.A.A., A.M.P. Mizusaki, M.D. Carvalho, and M. Monteiro, 1986, Talco e estivensita na Formação Lagoa Feia da Bacia de Campos - possíveis implicações no ambiente deposicional, in Proceedings of the 34th Brazilian Geological Congress, Sociedade Brasileira de Geologia, Goiânia, v.1, p.416-425.

Revelle, R., ed., 1990, Sea-level change: National Research Council, Studies in Geophysics, Washington, D.C., National Academy Press, 234p.

Ricci Lucchi, F., and E. Valmori, 1980, Basin-wide turbidites in a Miocene, over-supplied deep-sea plain: a geometrical analysis: Sedimentology, v.27, p.241-270.

Richter, A.J., 1987, Subafloramento das discordâncias Turoniana e Campaniana no sul da Bacia de Campos: Revista Brasileira de Geociências, v.17, p.173-176.

Rodrigues, R., and T. Takaki, 1987, O Cretáceo inferior nas

bacias sedimentares da costa sudeste do Brasil: análise isotópica e suas implicações paleoambientais: Revista Brasileira de Geociências, v.17, p.177-179.

Savin, S.M., 1977, The history of the Earth's surface temperature during the past 100 million years: Annual Review of Earth and Planetary Science Letters, v.5, p.319-355.

Savrda, C.E., and D.J. Bottjer, 1986, Trace-fossil model for reconstruction of paleo-oxygenation in bottom waters: Geology, v.14, p.3-6.

Schaller, H., 1969, Revisão estratigráfica da Bacia Sergipe-Alagoas: Boletim Técnico da PETROBRÁS, v.12, p.21-86.

Scheibnevorá, V., 1981, Paleogeographical implication of Cretaceous benthic foraminifers recovered by the Deep Sea Drilling Project in the Western South Atlantic Ocean: Cretaceous Research, v.2, p.1-18.

Scotese, C.R., L.M. Gahagan, and R.L. Larson, 1988, Plate tectonic reconstructions of the Cretaceous and Cenozoic ocean basins: Tectonophysics, v.155, p.27-48.

Sclater, J.G., R.N. Anderson, and M.L. Bell, 1971, Elevation of ridges and evolution of the central eastern Pacific: Journal of Geophysical Research, v.76, p.7882-7915.

Seguret, M., P. Labaume, and R. Madariaga, 1984, Eocene seismicity in the Pyrenees from megaturbidites of the South Pyrenean basin (Spain): Marine Geology, v.55, p.117-131.

Seiglie, G.A., and M.B. Baker, 1984, Relative sea-level changes during the middle and late Cretaceous from Zaire to Cameroon (Central West Africa), *in* J.S. Schlee, ed., Interregional unconformities and hydrocarbon accumulation: The American Association of Petroleum Geologists Memoir 36, p.81-88.

Seilacher, A., 1964, Biogenic sedimentary structures, *in* Imbrie, J., and N.D. Newell, eds., Approaches to paleoecology: New York, Wiley, p.296-316.

Seilacher, A., 1967, Bathymetry of trace fossils: Marine Geology, v.5, p.413-428.

Shackleton, N., and A. Boersma, 1981, The climate of the Eocene ocean: Journal of the Geological Society of London, v.138, p.153-157.

Shanmugam, G., and R.J. Moiola, 1985, Submarine fan models: problems and solutions, *in* A.H. Bouma, W.R. Normark, and N.E. Barnes, eds., Submarine fans and related turbidite systems: New York, Springer-Verlag, p.29-34.

Shanmugam, G., and R.J. Moiola, 1988, Submarine fans: characteristics, models, classification, and reservoir potential: Earth-Science Reviews, v.24, p.383-428.

Shepard, F.P., 1981, Submarine canyons: multiple causes and long-time persistence: The American Association of Petroleum Geologists Bulletin, v.65, p.1062-1077.

Shepard, F.P., and R.F. Dill, 1966, Submarine canyons and other sea valleys: Rand McNally, Chicago, 460p.

Shimabukuro, S., A.J. Richter, and J. Gomide, 1985, Nanofósseis calcários: bioestratigrafia do Mioceno ao Pleistoceno na Plataforma Continental Brasileira: Coletânea de Trabalhos Paleontológicos, Série Geologia, Departamento Nacional da Produção Mineral, Brazil, No.27, p.491-502.

Siegenthaler, Ch., and J. Buehler, 1986, The reconstruction of the paleo-slope of turbidity currents, based on simple hydromechanical parameters of the deposit: Acta Mechanica, v.63, p.235-244.

Silva, H.T.F., 1993, Flooding surfaces, depositional elements, and accumulation rates - characteristics of the lower Cretaceous tectonosequence in the Recôncavo basin, northeast Brazil: unpublished Ph.D. Thesis, University of Texas, Austin.

Silva, H.T.F., and A.T. Picarelli, 1990, Variações da linha de costa do lago do Recôncavo e taxas de acumulação durante o Andar Rio da Serra, fase rift: Boletim de Geociências da PETROBRÁS, v.4, p.205-216.

Sissingh, W., 1977, Biostratigraphy of Cretaceous calcareous nannoplankton: Geologie en Mijnbouw, v.56, p.37-65.

Sloss, L.L., 1988, Fourty years of sequence stratigraphy: Geological Society of America Bulletin, v.100, p.1661-1665.

Souza Cruz, C.E., S.L.S. Barrocas, and C.J. Appi, 1987, Modelo deposicional dos reservatórios turbidíticos

Oligocênicos/Eomiocênicos do Campo de Albacora, Bacia de Campos, Brasil: Boletim de Geociências da PETROBRÁS, v.1, p.215-223.

Spadini, A.R., F.R. Esteves, D. Dias-Brito, R.L.M. Azevedo, and R. Rodrigues, 1988, The Macaé Formation, Campos Basin, Brazil: its evolution in the context of the initial history of the South Atlantic: Revista Brasileira de Geociências, v.18, p.261-272.

Stanley, D.J., 1967, Comparing patterns of sedimentation in some modern and ancient submarine canyons: Earth and Planetary Science Letters, v.3, p.371-380.

Stanley, D.J., H.D. Palmer, and R.F. Dill, 1978, Coarse sediment transport by mass flow and turbidity current processes and downslope transformations in Annot sandstone canyon-fan valley systems, *in* D.J. Stanley, and G. Kelling, eds., Sedimentation in submarine canyons, fans, and trenches: Stroudsburg, Dowden, Hutchinson & Ross, p.85-115.

Stelting, C.E., K.T. Pickering, A.H. Bouma, J.M. Coleman, M. Cremer, L. Droz, A.A. Meyer-Wright,, W.R. Normark, S. O'Connell, D.A.V. Stow, and DSDP Leg 96 Shipboard Scientists, 1985a, Drilling results on the Middle Mississippi Fan, *in* A.H. Bouma, W.R. Normark, and N.E. Barnes, eds., Submarine fans and related turbidite systems: New York, Springer-Verlag, p.275-282.

Stelting, C.E., and DSDP Leg 96 Shipboard Scientists, 1985b,

Migratory characteristics of a mid-fan meander belt, Mississippi fan, *in* A.H. Bouma, W.R. Normark, and N.E. Barnes, eds., Submarine fans and related turbidite systems: New York, Springer-Verlag, p.283-290.

Stow, D.A.V., and A.J. Bowen, 1980, A physical model for the transport and sorting of fine grained sediment by turbidity currents: Sedimentology, v.27, p.31-46.

Stow, D.A.V., C.D. Bishop, and S.J. Mills, 1982, Sedimentology of the Brae oilfield, North Sea: fan models and controls: Journal of Petroleum Geology, v.5, p.129-148.

Stow, D.A.V., D.G. Howell, and C.H. Nelson, 1985, Sedimentary, tectonic, and sea-level controls, *in* A.H. Bouma, W.R. Normark, and N.E. Barnes, eds., Submarine fans and related turbidite systems: New York, Springer-Verlag, p.15-22.

Stow, D.A.V., M. Cremer, L. Droz, W.R. Normark, S. O'Connell, K.T. Pickering, C.E. Stelting, A.A. Meyer-Wright, and DSDP Leg 96 Shipboard Scientists, 1985b, Mississipi fan sedimentary facies, composition, and texture, *in* A.H. Bouma, W.R. Normark, and N.E. Barnes, eds., Submarine fans and related turbidite systems: New York, Springer-Verlag, p.259-266.

Straw, A., 1968, Late Pleistocene glacial erosion along the Niagara escarpment of southern Ontario: Geological Society of America Bulletin, v.79, p.889-910.

Stubblefield, W.L., B.A. McGregor, E.B. Forde, D.N. Lambert,

and G.F. Merril, 1982, Reconnaissance in DSRV Alvin of a "fluvial-like" meander system in Wilmington Canyon and slump features in South Wilmington Canyon: Geology, v.10, p.31-36.

Suter, J.R., and H.L. Berryhill, Jr., 1985, Late Quaternary shelf-margin deltas, northwest Gulf of Mexico: The American Association of Petroleum Geologists Bulletin, v.69, p.77-91.

Szatmari, P., R.S. Carvalho, and I.A. Simões, 1979, A comparison of evaporite facies in the Late Paleozoic Amazon and the Middle Cretaceous South Atlantic salt basins: Economic Geology, v.74, p.432-447.

Szatmari, P., E. Milani, M. Lana, J. Conceição, and A. Lobo, 1985, How South Atlantic rifting affects Brazilian oil reserves distribution: Oil & Gas Journal, v.83, p.107-114.

Teisserenc, P., and J. Villemin, 1990, Sedimentary basin of Gabon - Geology and oil systems, *in* J.D. Edwards and P.A. Santogrossi, eds., Divergent/passive margin basins: The American Association of Petroleum Geologists Memoir 48, p.117-199.

Tigre, C.A., A. Cândido, C.V. Stank, and A.S. Barroso, 1988, O pólo nordeste da Bacia de Campos, *in* Proceedings of the 2nd Latin American Congress on Hydrocarbons, ARPEL, Rio de Janeiro, TT-246, 13p.

Tölderer-Farmer, M., J.C. Coimbra, J.A. Moura, and H.N.

Gilson, 1989, Reconstrução paleoambiental da Bacia do Recôncavo com base em ostracodes - um estudo preliminar: Rio de Janeiro, PETROBRÁS Internal Report, 111p.

Troelsen, J.C., and L.P. Quadros, 1971, Distribuição bioestratigráfica dos nanofósseis em sedimentos marinhos (Aptiano-Mioceno) do Brasil: Anais da Academia Brasileira de Ciências, v.43, p.577-609.

Twichell, D.C., and D.G. Roberts, 1982, Morphology, distribution, and development of submarine canyons on the United States Atlantic continental slope between Hudson and Baltimore canyons: Geology, v.10, p.408-412.

Twichell, D.C., N.H. Kenyon, L.M. Parson, and B.A. McGregor, 1991, Depositional patterns of the Mississippi fan surface: evidence from GLORIA II and high-resolution seismic profiles, *in* P. Weimer, and M.H. Link, eds., Seismic facies and sedimentary processes of submarine fans and turbidite systems: New York, Springer-Verlag, p.349-363.

Vail, P.R., 1987, Seismic stratigraphy interpretation using sequence stratigraphy. Part I: Seismic stratigraphy interpretation procedure, *in* A.W. Bally, ed., Atlas of Seismic Stratigraphy: The American Association of Petroleum Geologists, Studies in Geology No.27, v.1, p.1-10.

Vail, P.R., R.M. Mitchum, Jr., and S. Thompson, III, 1977, Seismic stratigraphy and global changes of sea level,

part 4: Global cycles of relative changes of sea level, *in* C.E. Payton, ed., Seismic stratigraphy - applications to hydrocarbon exploration: The American Association of Petroleum Geologists Memoir 26, p.83-97.

Vail, P.R., F. Audemard, S.A. Bowman, P.N. Eisner, and C. Perez-Cruz, 1991, The stratigraphic signatures of tectonics, eustasy and sedimentology - an overview, *in* G. Einsele, W. Ricken, and A. Seilacher, eds., Cycles and events in stratigraphy: Berlin, Springer-Verlag, p.617-659.

Van Wagoner, J.C., H.W. Posamentier, R.M. Mitchum, P.R. Vail, J.F. Sarg, T.S. Loutit, and J. Hardenbol, 1988, An overview of the fundamentals of sequence stratigraphy and key definitions, *in* C.K. Wilgus, B.S. Hastings, C.G.St.C. Kendall, H.W. Posamentier, C.A. Ross, and J.C. Van Wagoner, eds., Sea-level changes: an integrated approach: Society of Economic Paleontologists and Mineralogists Special Publication No.42, p.39-45.

Van Wagoner, J.C., R.M. Mitchum, K.M. Campion, and V.D. Rahmanian, 1990, Siliciclastic sequence stratigraphy in well logs, cores, and outcrops: concepts for high-resolution correlation of time and facies: The American Association of Petroleum Geologists Methods in Exploration Series No.7, 55p.

Viana, A.R., D.D. Castro, and R.O. Kowsmann, 1990, A discordância do Mioceno Médio Superior: um marco regional

no talude da Bacia de Campos, *in* Proceedings of the 36th Brazilian Geological Congress, Sociedade Brasileira de Geologia, Natal, Brazil, v.1, p.313-323.

Viana, C.F., E.G. Gama, Jr., I.A. Simões, J.A. Moura, J.R. Fonseca, and J.R. Alves, 1971, Revisão estratigráfica da Bacia do Recôncavo/ Tucano: Boletim Técnico da PETROBRÁS, v.14, p.157-192.

Waldron, J.W.F., 1987, A statistical test for significance of thinning- and thickening-upwards cycles in turbidites: Sedimentary Geology, v.54, p.137-146.

Walker, R.G., 1965, The origin and significance of the internal sedimentary structures of turbidites: Proceedings of the Yorkshire Geological Society: v.35, p.1-32.

Walker, R.G., 1978, Deep-water sandstone facies and ancient submarine fans: models for exploration for stratigraphic traps: The American Association of Petroleum Geologists Bulletin, v.62, p.932-966.

Walker, R.G., 1980, Modern and ancient submarine fans: reply: The American Association of Petroleum Geologists Bulletin, v.64, p.1101-1108.

Walker, R.G., 1984, Turbidites and associated coarse clastic deposits, *in* R.G. Walker, ed., Facies models: Geological Association of Canada, Geoscience Canada, Reprint Series 1, 2nd ed., p.171-188.

Walker, R.G., 1985, Mudstones and thin-bedded turbidites

associated with the Upper Cretaceous Wheeler Gorge conglomerates, California: a possible channel-levee complex: Journal of Sedimentary Petrology, v.55, p.279-290.

Walker, R.G., 1992, Turbidites and submarine fans, *in* R.G. Walker and N.E. James, eds., Facies models: response to sea level change: Geological Association of Canada, p.239-263.

Walker, R.G., and N.E. James, eds., 1992, Facies models: response to sea level change: Geological Association of Canada, 409p.

Walker, R.G., and E. Mutti, 1973, Turbidite facies and facies associations, *in* G.V. Middleton and A.H. Bouma, eds., Turbidites and deep water sedimentation: Society of Economic Paleontologists and Mineralogists, Pacific Section, Short Course, p.119-157.

Weimer, P., 1989, Sequence stratigraphy of the Mississippi fan (Plio-Pleistocene), Gulf of Mexico: Geo-Marine Letters, v.9, p.185-272.

Weimer, P., 1990, Sequence stratigraphy, facies geometries, and depositional history of the Mississippi fan, Gulf of Mexico: The American Association of Petroleum Geologists Bulletin, v.74, p.425-453.

Weimer, P., 1991, Seismic facies, characteristics, and variations in channel evolution, Mississippi fan (Plio-Pleistocene), Gulf of Mexico, *in* P. Weimer, and M.H.

Link, eds., Seismic facies and sedimentary processes of submarine fans and turbidite systems: New York, Springer-Verlag, p.323-347.

Weimer, P., and R.T. Buffler, 1988, Distribution and seismic facies of the Mississippi fan channels: Geology, v.16, p.900-903.

Weimer, P., and M.H. Link, eds., 1991a, Seismic facies and sedimentary processes of submarine fans and turbidite systems: New York, Springer-Verlag, 447p.

Weimer, P., and M.H. Link, 1991b, Global petroleum occurrences in submarine fans and turbidite systems, *in* P. Weimer, and M.H. Link, eds., Seismic facies and sedimentary processes of submarine fans and turbidite systems: New York, Springer-Verlag, p.9-67.

Weimer, R.J., 1984, Relation of unconformities, tectonics, and sea-level changes, Cretaceous of Western Interior, U.S.A., *in* J.S. Schlee, ed., Interregional unconformities and hydrocarbon accumulation: The American Association of Petroleum Geologists Memoir 36, p.7-35.

Wetzel, A., and F. Werner, 1981, Morphology and ecological significance of *Zoophycos* in deep-sea sediments off NW Africa: Palaeogeography, Palaeoclimatology, Palaeoecology, v.32, p.185-212.

Wilgus, C.K., B.S. Hastings, C.G.St.C. Kendall, H.W. Posamentier, C.A. Ross, and J.C. Van Wagoner, eds., 1988, Sea-level changes: an integrated approach: Society of

Economic Paleontologists and Mineralogists Special
Publication No.42, 407p.

Winker, C.D., 1982, Cenozoic shelf margins, northwestern Gulf
of Mexico: Transactions of the Gulf Coast Association of
Geological Societies, v.32, p.427-448.

Winn, R.D., Jr., and R.H. Dott, Jr., 1979, Deep-water fan-
channel conglomerates of Late Cretaceous age, southern
Chile: Sedimentology, v.26, p.203-228.